# Genetic manipulation of fermentative metabolism in *Chlamydomonas reinhardtii*

**Hussein Haji Taha**

**Thesis submitted for the Degree of Doctor of Philosophy of Imperial College London**

**Department of Life Sciences**
**Faculty of Natural Sciences**
**Imperial College London**

**2015**

**Copyright declaration**



**Declaration of originality**

I hereby declare that this thesis, submitted in fulfilment of the requirements for the degree of Doctor of Philosophy of Imperial College London, represents my own work and has not been previously submitted to this or any other institute for any degree, diploma or other qualification.

Much of this thesis is written in the first person plural. This was done to acknowledge that thoughts and inputs of collaborators, all of whom are listed, towards the ideas presented here. Nonetheless, I made substantial contributions to all the original ideas presented and conducted all the experiments either solely or in conjuction with one or more collaborators.

---

Hussein Haji Taha

## Abstract

Photobiological hydrogen production by green algae, such as *Chlamydomonas reinhardtii* is an attractive approach to generate renewable energy, but is currently not economically viable. It has been suggested that hydrogen yields could potentially be improved by eliminating or down-regulating competing fermentative pathways. However, at present fermentative metabolism is not completely understood in *C. reinhardtii*, such as the nature of the ill-defined D-lactate dehydrogenase (D-LDH) activity responsible for the production of D-lactate.

To characterise the D-LDH activity, a bioinformatics analysis identified a candidate nucleus-encoded *D-LDH* in the *C. reinhardtii* genome (Phytozome v9.1 ID: Cre07.g324550), which was predicted to be localised to the chloroplast. The putative protein without its predicted chloroplast transit peptide was overexpressed in *Escherichia coli* as a C-terminal $His_6$-tagged protein to confirm its function and assess its structure. Enzyme assays confirmed that the protein was an $NAD^+$-dependent D-LDH, favouring the reduction of pyruvate to D-lactate with an estimated $K_m$ value of 1.85 ± 0.05 mM and $k_{cat}$ value of 415 ± 18 $s^{-1}$. Size-exclusion chromatography suggests the holoenzyme was tetrameric with a molecular mass of about 202 kDa. Artificial microRNA technology was used to reduce the amount of D-LDH protein to less than 20% of WT levels. D-lactate was still produced in the mutant either from residual D-LDH activity or from other routes such as from methylglyoxal. Both NMR and HPLC confirmed that the knockdown did not have any substantial impact on dark anaerobic metabolite production except in slightly increasing the pyruvate levels. Additionally, the knockdown did not improve hydrogen yields under sulphur-deprived conditions.

To assess the impact of eliminating fermentative pathways on metabolism, a series of mutants was isolated through cell mating, targeting the enzymes D-LDH, pyruvate decarboxylase (PDC3), pyruvate formate lyase (PFL1) and a bifunctional acetaldehyde/alcohol dehydrogenase (ADH1). Dark anaerobic metabolite production in the quadruple mutant confirmed the re-routing of metabolic flux from ethanol and formate towards glycerol and D-lactate. There was also a reduced flux towards acetate production. Pyruvate and glucose levels were found to be elevated in this mutant. Gas chromatography analysis suggested that downregulation of the fermentative pathways did not improve hydrogen production under sulphur-deprived conditions, in part because of reduced cell viability. These mutants are promising tools for future studies probing the metabolism of *C. reinhardtii*.

**Acknowledgments**

A big thank you to my supervisor, Prof. Peter J. Nixon for kindly willing to take me as his PhD student when my previous supervisor was made redundant, and for his endless guidance and strong support throughout my PhD. Thank you also to my mentor, Dr. Steven J. Burgess for his guidance and support throughout my PhD, and without him I would be lost. Thank you to all of my colleagues in the Photosynthesis Group especially Dr. Jiangfeng Yu, Oksana Iamshanova and Eirini Vlachaki, who all had provided help and moral support especially during the difficult times. I also would like to express my gratitude towards my family in the UK i.e. Azimin Ibrahim, Nigel Kitchen and Martyn Pickering for their moral support and for always being there for me through my ups and downs, and without them, I would not survive these four years of PhD. A special thank you, also, to my family in Brunei Darussalam for their support, encouragement and understanding. I am also very grateful to Associate Prof. Zohrah Sulaiman who supported me and without whom I would not be doing this PhD. Thank you also to the Government of Brunei Darussalam for giving me a scholarship to pursue my PhD.

## Table of contents

## List of figures

## List of tables

## List of abbreviations

A - absorbance

ACK – acetate kinase

ADH – alcohol dehydrogenase

ADH1 – *C. reinhardtii* bifunctional acetaldehyde/ alcohol dehydrogenase

ADHE – *E. coli* bifunctional acetaldehyde/ alcohol dehydrogenase

ADP – adenosine diphosphate

AIB – anaerobic induction buffer

ALAT – alanine aminotransferase

ALDH – aldehyde dehydrogenase

APS – ammonium persulphate

ATP – adenosine triphosphate

b – base

bp – base pair

BSA – bovine serum albumin

cDNA – complementary DNA

CFU – colony forming unit

$CO_2$ – carbon dioxide

CoA – coenzyme A

$Cytb_6f$ – cytochrome $b_6f$

Da – Dalton

DHAP – dihydroxyacetone phosphate

DNA – deoxyribonucleic acid

FDX – ferredoxin

E – Einstein

EST – expressed sequence tag

Eq – equation

Fe – iron

GC – gas chromatography

FHL – formate hydrogen lyase

FMR – fumarate reductase

FUM – fumarase

G3P – glyceraldehyde 3-phosphate

GK – glycerol kinase

GLO – glyoxalase

GPD – *sn*-glycerol-3- phosphate dehydrogenase

GPP – *sn*-glycerol-3-phosphate phosphatase

h – hour

$H_2$ – hydrogen gas

HP – sodium hypophosphite

HPLC – high pressure liquid chromatography

HSM – High salt medium

HYDA – hydrogenase

kb – kilobases

$k_{cat}$ – the turnover number

$k_{cat}/K_m$ – a measure of enzyme efficiency

KD – knockdown

$K_m$ – Michaelis constant

LB – Lysogeny broth

$LB_{amp100}$ – LB containing 100 µg/ml of ampicillin

LDH – lactate dehydrogenase

MDH – malate dehydrogenase

min – minute

MME4 – malic enzyme

mRNA – messenger ribonucleic acid

$mt^+$ – mating type *plus*

$mt^-$ – mating type *minus*

$NAD^+$ – nicotinamide adenine dinucleotide (oxidised form)

NADH – nicotinamide adenine dinucleotide (reduced form)

$NADP^+$ – nicotinamide adenine dinucleotide phosphate (oxidised form)

NADPH – nicotinamide adenine dinucleotide phosphate (reduced form)

Ni – nickel

NMR – nuclear magnetic resonance spectroscopy

OD – optical density

$P_i$ – inorganic phosphate

PAGE – polyacrylamide gel electrophoresis

PAT – phosphotransacetylase

PBS – phosphate buffered saline

PBS-T – phosphate buffered saline Tween 20

PC - plastocyanin

PCR – polymerase chain reaction

PDC3 – pyruvate decarboxylase

PDH – pyruvate dehydrogenase complex

PFL1- pyruvate formate lyase

PFOR – pyruvate:ferredoxin oxidoreductase

PQ – plastoquinone

PVDF – polyvinylidene fluoride

qRT-PCR – quantitative reverse transcription polymerase chain reaction

PSI – photosystem I

PSII – photosystem II

RNA – ribonucleic acid

RPL10a – RNA polymerase subunit L10a

rpm – revolutions per minute

s – second

SD – standard deviation

SDS – sodium dodecyl sulphate

SE – standard error

TAP – Tris acetate phosphate

$TAP_{P10}$ – TAP containing 10 µg/ml of paromomycin

$TAP_{P10 + lactate}$ – TAP containing 10 µg/ml of paromomycin and 1mM DL-lactate

TAP-N – nitrogen-deficient TAP

TAP-S – sulphur-deficient TAP

TCA – tricarboxylic acid cycle

TEMED – tetramethylethylenediamine

Tris – 2-amino-2-hydroxy-methylpropane-1,3-diol

UV – ultraviolet

$V_{max}$ – enzyme maximum rate

v/v – volume per volume

w/v – weight per volume

WT – wild type

# Chapter 1: Introduction

## 1.1 The green alga *Chlamydomonas reinhardtii*

*C. reinhardtii*, as described by Harris (2009), is a unicellular, motile, biflagellate, photosynthetic, green alga (Figure 1.1). This oval-shaped alga is approximately 10 µm in diameter and thus visible under a light microscope. It possesses a distinct cell wall, a nucleus, multiple mitochondria and a large cup-shaped chloroplast containing a large pyrenoid and a light-sensitive eyespot. The alga can grow photoautotrophically, mixotrophically and heterotrophically with a fast cell doubling time. The standard wild type (WT) strains of this alga designated as 137c strains, which are now used in many laboratories, were originally collected as a soil sample in 1945 from a potato field near Amherst, Massachusetts (Harris, 2009; Proschold *et al*., 2005). *C. reinhardtii* has become a well-known model organism for photosynthesis (Grossman, 2000) and also for hydrogen photoproduction (Rupprecht, 2009). The ability of many species of green algae to produce hydrogen has been observed for several decades (Gaffron, 1939; Gaffron and Rubin, 1942) but *C. reinhardtii* has been shown to have the highest rates of algal hydrogen production so far (Timmins *et al*., 2009a).

**(A)** **(B)**

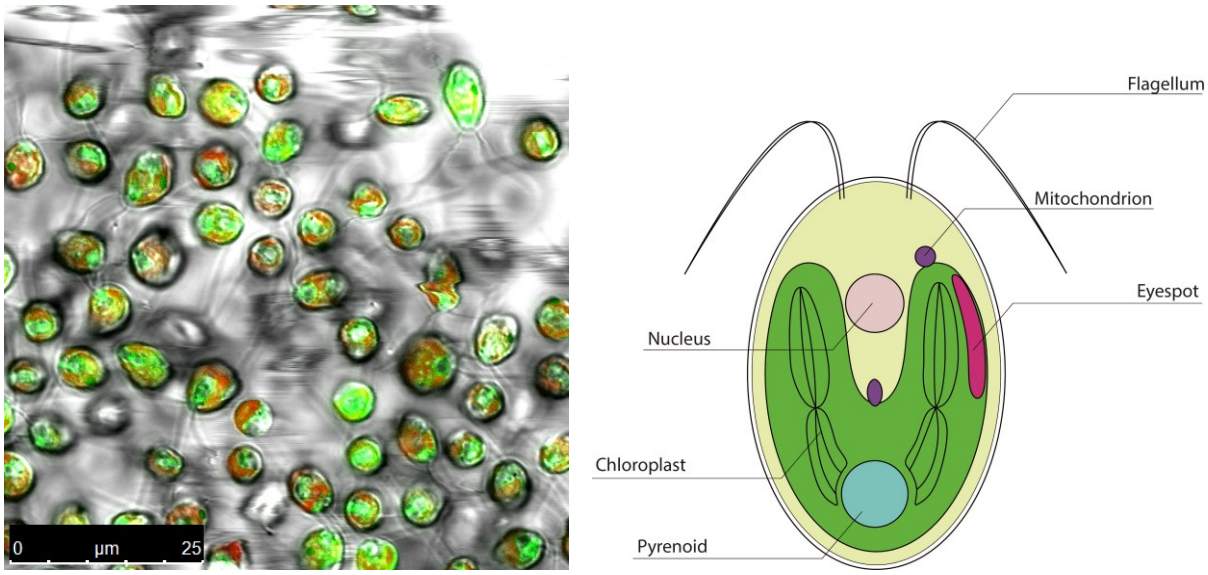


**Figure 1.1 *Chlamydomonas reinhardtii*.**

(A) Micrograph of *C. reinhardtii* cells with flagella. The chloroplast is shown in red and the cytoplasm is shown in green. The photo is courtesy of Prof. Conrad Mullineaux (Queen Mary London) and Ms. Marin Sawa (Central Saint Martins College of Art and Design). (B) Schematic representation of *C. reinhardtii* cell, kindly drawn by Ms. Marin Sawa.

*C. reinhardtii* is widely used as a model organism due to the availability of its fully sequenced mitochondrial genome (Vahrenholz *et al*., 1993), chloroplast genome (Maul *et al*., 2002) and nuclear genome (Merchant *et al*., 2007). In addition, microarrays (Toepel *et al*., 2011) and expressed sequence tags, ESTs (Shrager *et al.*, 2003; Asamizu *et al*., 2004) are also available. The genomes are transformable by various techniques such as microprojectile particle bombardment (Boynton *et al*., 1988), glass bead agitation (Kindle, 1990) or electroporation (Shimogawara *et al*., 1998). The vegetative cell of this alga is haploid and this makes any introduced mutation to be immediately expressed. Moreover, algal strains can exist either as mating type *plus* ($mt^+$) or *minus* ($mt^-$), allowing sexual reproduction between these opposite types (Harris, 2009).

Numerous molecular tools have been developed to aid molecular genetic analysis. For example, artificial micro-ribonucleic acid (microRNA) has been developed to target a particular gene (Molnar *et al*., 2009). Moreover, several selectable markers are available to aid in the selection of transformants (Debuchy e*t al*., 1989; Goldschmidt-Clermont, 1991; Nelson *et al*., 1994, Lumbreras *et al*., 1998, Sizova *et al*., 2001), and many promoters are also available to allow overexpression or controlled expression of an introduced gene in the algal cell (Lumbreras *et al*., 1998; Schroda *et al.*, 2000; Fischer and Rochaix, 2001). Reporter genes with optimized codon usage have also been developed for *C. reinhardtii* to help with monitoring nuclear gene expression or with protein localisation (Fuhrmann *et al*., 1999; Fuhrmann *et al*., 2004).

Genetic transformation through homologous recombination is possible for both the chloroplast and mitochondrion (Boynton *et al.*, 1988; Randolph-Anderson *et al*., 1993). However, the integration of introduced deoxyribonucleic acid (DNA) into the nuclear genome does not occur efficiently through homologous recombination (Sodeinde & Kindle, 1993; Zorin *et al*., 2005; Zorin *et al*., 2009). Therefore, the direct disruption of a targeted nuclear gene is not yet achievable. Knockout mutants for reverse and forward genetic analysis have been isolated from insertional mutagenesis library by PCR screening (Pootakham *et al*., 2010; Gonzalez-Ballester *et al*., 2011; Zhang *et al*., 2014) or phenotypic screening (Dent *et al*., 2005; Posewitz *et al*., 2005; Gonzalez-Ballester *et al*., 2005; Pollock *et al*., 2005) but these approaches are labour intensive and time consuming. Another reverse genetic approach is TILLING (Targeting Induced Local Lesions In Genomes) whereby mutants are generated through a chemically-induced point mutations, but similarly this process is time consuming and has some weaknesses (Gilchrist & Haughn, 2010; Gonzalez-Ballester *et al*., 2011). Knockdown mutants can also be isolated through RNA silencing

techniques. This strategy has been shown to successfully downregulate protein expression in *C. reinhardtii* (Schroda, 2006; Zhao *et al*., 2009; Molnar *et al*., 2009; Godman *et al*., 2010; Burgess *et al*., 2012).

Excitingly, a project to generate a library of tagged *C. reinhardtii* mutants has recently been announced in 2014 with a pilot collection that covers ~10% of all genes so far generated (Jonikas Lab, Carnegie Institution for Science), which will be made publicly available soon via the *Chlamydomonas* Resource Centre (University of Minnesota).

### 1.2 Artificial microRNAs

Many eukaryotes including *C. reinhardtii* have developed mechanisms to regulate gene expression. One of the mechanisms is RNA interference (RNAi), whereby a gene is silenced through RNA-RNA interaction. This post-transcriptional regulation of gene expression is mediated by silencing RNAs such as microRNA. This molecule, as described by Jones-Rhoades *et al*. (2006), is a small nucleic acid about 20 to 30 bases in length, single-stranded and encoded by non-coding nuclear DNA. Transcription of the genomic DNA produces RNA transcript that folds back to form double-stranded pre-microRNA with short hairpin loops. This pre-microRNA is then processed by an RNase-like enzyme called Dicer. The enzyme cuts this microRNA precursor to form a partially double-stranded, shorter RNA. This RNA duplex has to undergo a selection process, whereby only one of the double strands is selected as the microRNA. Together with the argonaute protein, the microRNA forms an RNA-induced silencing complex (RISC). In the selection process, the strand with the lower thermodynamic stability is recruited while the non-selected strand, which is known as passenger strand, will normally be degraded.

To regulate gene expression, the RISC binds targeted messenger RNA (mRNA) to activate gene silencing. This involves either translational inhibition or cleavage of target mRNA (Bartel, 2004; Jones-Rhoades *et al*., 2006). If there is only a partial complementarity between the mRNA and its microRNA, translational repression will occur. However, if there is a complete or nearly complete complementarity between those two RNAs, it will lead to the cleavage and subsequent degradation of the target mRNA. Plant microRNAs including those of *C. reinhardtii* generally activate transcript cleavage rather than translational inhibition (Schwab *et al*., 2005; Jones-Rhoades *et al*., 2006).

Efforts have been made to downregulate protein expression in *C. reinhardtii* (Schroda, 2006), and a novel artificial microRNA technology has been developed (Ossowski *et al*., 2008; Molnar *et al*., 2009). It involves the replacement of native microRNA with a

novel artificial microRNA sequence to target the mRNA of a gene of interest. The technology has been shown to successfully down regulate target genes in *C. reinhardtii* (Molnar *et al*., 2009, Zhao *et al*., 2009, Godman *et al*., 2010; Burgess *et al*., 2012) although this technique has its limitations (Nakayashiki 2005). Our research project aimed to use artificial microRNAs to manipulate *C. reinhardtii* fermentative metabolism.

**1.3 Fuels**

Fossil fuels are undeniably the most important energy sources in the world. According to the International Energy Agency (IEA, 2014), it was estimated that 66% of the global energy consumption in 2012 could be accounted for by fossil fuels (oil, natural gas and coal) whereas consumption accounted by other sectors, such as electricity (18.1%) and biofuels/waste (12.4%), were much lower. The total energy consumption in this particular year was estimated to be 8979 Mtoe (equivalent to ~12TW or 376 EJ per year), and this was higher than in the previous years (IEA, 2013; IEA, 2012; IEA, 2011), indicating an increasing trend of energy consumption with an increase of ~7% between 2009 and 2012.

There is an urgent need to move away from these non-renewable fuels. One of the main reasons is due to the pressures of climate change. The burning of fossil fuels is the major contributor to the emission of carbon dioxide into the air. An alarming increase of this greenhouse gas in the last few decades is predicted to bring global warming. It is predicted that by 2040 there would be a 46% increase in the global energy-related carbon dioxide emission relative to the emission in 2010 (EIA, 2013). Alarmingly, the current levels of greenhouse gases, which are above 450 ppm $CO_2$-e (e = equivalent contribution of all greenhouse gases), are already at a dangerously high level (Schenk *et al*., 2008). An increase of just a few degrees Celsius in the global average temperature could lead to catastrophic damage such as destructive changes to physical and biological systems (IPCC, 2007) and these could drastically affect global economies (Stern, 2006). Therefore, it is very important to avoid this climate change by reducing global carbon emissions and by finding alternative fuels that have zero net carbon dioxide emission. A 50 to 85% reduction in the total carbon dioxide emission is required by 2050 (IPCC, 2007; Schenk *et al*., 2008) and this is a tough global challenge.

The dramatic increase in the world population and also the rapidly emerging new economies, such as China and India, which will demand ever-increasing amounts of energy is another reason to move away from fossil fuels (Dorian *et al*., 2006). It is predicted by 2040 there would be a rise by 56% in the global energy consumption relative to 2010 (EIA, 2013).

The non-sustainable nature of the fossil fuels will not be able to meet this global energy demand. Oil production from oil fields will come to a peak, whereby the rate of production cannot increase anymore and will eventually decline with time. Thus, new oil fields need to be discovered to meet the rapidly increasing world energy requirements, but the discovery of new oil fields has been unsatisfactory (Hirsch *et al*., 2005; Dorian *et al*., 2006). Moreover, depletion of fuel reserves could cause a big strain in fuel production which can also lead to higher fuel prices.

Many alternatives to fossil fuels have been considered. One of them is the controversial nuclear power that uses nuclear fission to generate energy. Although it does not contribute to carbon dioxide emissions, it poses massive global security and environmental threats (BERR, 2008). Also, this technology is not accessible to many countries. Other alternatives are solar energy, wind power, hydropower and geothermal energy. These are all renewable sources of energy but their availabilities are dependent on geographical locations. Renewable energy is one of the rapidly growing energy sources with an increase of 2.5% per year (EIA, 2013), suggesting the increasing demand for energy renewability. An estimated 21.7% of global energy electricity generated in 2012 came from renewable energy sources (REN21, 2013). The most abundant, easily accessible and promising renewable energy source to feed the world is solar energy with the incident solar power estimated to be 178,000 TW per year (Miyamoto, 1997; Kruse *et al*., 2005b). Electricity can be generated by harnessing the sun's energy through solar energy technologies such as photovoltaic panels and concentrated solar power. However, these technologies have their own drawbacks. For example, photovoltaic panels are still relatively costly (IEA, 2008).

Photosynthetic organisms can provide a promising solution to the global energy problem as they are able to convert solar energy into chemical energy or biofuel through photosynthesis. Apart from providing biofuels, the conversion of atmospheric carbon dioxide into storable compounds such as starch, cellulose and oil will help in reducing the levels of carbon dioxide in the air. However, one of the major challenges in utilising photosynthesis for biofuel production is that the conversion efficiency of solar energy to stored chemical energy by photosynthetic organisms is still low due to energy losses from photoprotection and due to a network of competing metabolic pathways (Kruse *et al*., 2005b).

Biofuels are any fuels that are generated from biomass. They can be classified into primary and secondary biofuels. Primary biofuels refer to fuels that do not need to be processed. For example, wood chips that can be burned for cooking. Secondary biofuels refer to fuels that are generated through biomass processing. These are further classified into three

categories according to their sources (Bringezu *et al*., 2009; Nigam & Singh, 2011). First generation biofuels, also known as conventional biofuels, are fuels derived from crops that are also used as human or animal foods (such as sugar cane and corn). These crops provide sugars, starch or vegetable oils that can be converted to fuels through conventional methods. Second generation biofuels, also known as advanced biofuels, are fuels derived from crops that are not used for food purposes (such as grasses) and also from waste biomass (such as non-edible plant parts). However, these two categories of biofuels have their own issues. For example, a large area of arable land is needed to grow them and this could lead to deforestation to provide more space. Third generation biofuels are fuels produced by microalgae. This should also include cyanobacteria. Microalgae can solve the issue of land competition because they can simply be cultivated in bioreactors, on non-agricultural lands or in aquatic environments such as the sea.

Microalgae can be used to produce a range of biofuels such as diesel, ethanol, methane and hydrogen (Schenk *et al*., 2008; Scott *et al*., 2010; Wijffels & Barbosa, 2010). Microalgae can efficiently accumulate oils when faced with nutrient stress, and these oils can be extracted for conversion into diesel by transesterification (Mata *et al*., 2010). Ethanol can be produced from microalgae as a product of dark fermentation metabolism, and the algae can also accumulate substantial amounts of biomass in the form of starch or cellulose, which can be converted to ethanol by microbial fermentation (John *et al*., 2011). The microbial fermentation of algal biomass can also produce methane (Singh & Gu, 2010). Some microalgae can produce hydrogen under certain conditions (Benemann, 2000). Hydrogen is a particularly attractive fuel because its combustion does not produce carbon dioxide but only water. Other biofuels that can be derived from microalgae are hydrocarbons (Banerjee *et al*., 2002) and butanol (Nigam & Singh, 2011). Additionally, the production of biofuels by microalgae can also be coupled to the production of other commercial products. For example, (1) human food supplements or animal feed due to the high nutritional content, (2) use as highly valuable products such as polyunsaturated fatty acids oils and pigments, and (3) use in cosmetics (Spolaore *et al*., 2006).

### 1.4 Biological hydrogen production

In recent years, there has been a growing interest in using hydrogen fuel as this gas is considered to be a cleaner or greener fuel. Moreover, hydrogen fuel can also be used for other applications, such as for producing other fuels and organic chemicals, for producing fertilizers, and for hydrogenation of oils and fats (Ramachandran & Menon, 1998).

Unfortunately, the current sources of hydrogen fuel mostly come from fossil fuels such as natural gas and coal because the alternative routes for producing hydrogen fuel, such as nuclear, solar and wind energy are considered to be less economical due to their high estimated costs of production. Nevertheless, the increasing costs of fossil fuels and significant improvement in technologies could potentially lower these costs in the future (Bartels *et al*., 2010).

Various efforts that have been attempted to produce hydrogen fuel by alternative routes, involving water splitting to produce hydrogen gas. This can either be carried out through thermal (Pregger *et al*., 2009), electrochemical (de Souza *et al*., 2007) or photochemical processes (Balzani *et al*., 2008; Hambourger *et al*., 2009). The photochemical approach is more attractive because it utilises solar energy to drive water splitting. However, one of the major drawbacks of the electrochemical or photochemical approach is the lack of cheaper and easily available chemical catalysts to reduce protons into hydrogen fuel. Therefore, a biological catalyst i.e. hydrogenase enzyme has been introduced into these systems. For example, hydrogen gas was successfully produced from a hybrid nanoparticle system containing hydrogenase (Reisner *et al*., 2009), or from an electrochemical system containing hydrogenases immobilized onto the electrodes (Noda *et al*., 1998). Hydrogenases could also be further linked to photosystem complexes for hydrogen production (Lubner *et al*., 2010), whereby the photosystems are used to capture light energy and transmit electrons to the hydrogenases. Although all these biological inspired technologies are promising, they still have their own limitations and more effort is needed to turn them into a feasible means of producing hydrogen. One of the limitations is the requirement of an oxygen-tolerant hydrogenase. Oxygen can reversibly inactivate the catalytic site of the enzyme by binding to it. Random or site-directed mutagenesis could be applied to improve the oxygen tolerance of hydrogenase (Esper *et al*, 2006), and the structure of the enzyme could be genetically manipulated, which could be based on an existing available structure of an oxygen tolerant hydrogenase but unfortunately, this has lower hydrogen activity (Buhrke *et al*., 2005; Esper *et al*, 2006). There is still a long way to go before an ideal enzyme could be isolated.

To overcome issues with biological-inspired technologies, microbial production of hydrogen fuel could instead be adopted (Meher Kotay & Das, 2008). Under certain conditions, microorganisms such as bacteria and algae can evolve hydrogen gas. Microbial production of hydrogen is catalysed by either nitrogenase or hydrogenase enzymes, depending on the species of the microorganisms (Tamagnini *et al*, 2002; Ghirardi *et al*., 2007). The problem with utilising nitrogenase for hydrogen production is the process requires

higher amount of adenosine triphosphate (ATP) compared to hydrogenase (Benemann, 1996). Hydrogenases are further classified into three families according to the structures of the active sites (Vignais and Billoud, 2007), containing either an iron (Fe) complex or iron with nickel (Ni) complex. Firstly, [Fe]-hydrogenases, which are formerly known as metal-free hydrogenases, contain one iron atom and can be found in methanogenic archaea. Secondly, [FeFe]-hydrogenases, which are formerly known as iron-only hydrogenases, contain a binuclear iron centre, and can mostly be found in green algae and anaerobic bacteria but can also be found in fungi and protists. Thirdly, [NiFe]-hydrogenases contain a Ni-Fe complex, and these enzymes are widely distributed and occur in all bacterial classes. Generally, [NiFe]-hydrogenases are more tolerant to oxygen compared to the other hydrogenases. However, the [FeFe]-hydrogenases are generally more involved in hydrogen production while the [NiFe]-hydrogenases are, in general, more involved in hydrogen oxidation (Lubitz *et al*., 2008).

Microbial hydrogen production can occur by light-dependent processes namely biophotolysis (either direct or indirect) and photofermentation, or by light-independent process namely dark fermentation (Benemann, 1996; Hallenbeck & Benemann, 2002).

In direct biophotolysis, photosynthetic water splitting produces reductant (electrons) and also oxygen. The reductant can be directly transferred to the hydrogenase via reduced ferredoxin generated by the photosynthetic electron transport chain (Benemann, 1996). However, the co-produced oxygen can strongly inhibit hydrogenase activity. Therefore, it is essential for the oxygen levels to be lowered in order to make hydrogen production possible. Microorganisms overcome this problem by separating the hydrogen and oxygen production temporally or spatially. For example, in filamentous cyanobacteria *Anabaena cylindrica*, hydrogen production occurs in a specialised cell called the heterocyst while oxygen production occurs in vegetative cells (Benemann & Weare, 1974). This nitrogen-fixing cell creates an anaerobic environment for the hydrogen-producing enzyme which in this case is an oxygen-sensitive nitrogenase. The main advantage of hydrogen production by direct biophotolysis is the abundance of solar energy and water. However, the problem with this type of production, apart from the oxygen-sensitive hydrogenase, is that the conversion efficiencies of light to hydrogen gas are still low (Hallenbeck & Ghosh, 2009). In indirect biophotolysis, instead of the photosynthetic water splitting, another alternative source for providing electrons to the hydrogenase or nitrogenase is made possible by NAD(P)H that is generated from catabolic metabolism. The generated NAD(P)H transfers electrons to the hydrogenase or nitrogenase via ferredoxin for light-dependent hydrogen production. Direct

and indirect biophotolysis can possibly occur together to supply reductant for hydrogen production.

Hydrogen production can also occur via photofermentation (Benemann, 1996), and this method is adopted by photosynthetic bacteria. Organic substrates, like acetic acid, can be converted by these bacteria into hydrogen gas. The energy required by these conversion processes is provided by anoxygenic photosynthesis which does not contribute to oxygen production. For example, in purple non-sulphur bacteria, the photosystem is not able to split water to generate electrons. Instead, electrons are introduced into the photosystem from the breakdown of organic substrate. This anoxygenic photosynthesis generated electrons that can be donated to the nitrogenase via ferredoxin for the ATP-dependent production of hydrogen gas (Akkerman *et al*., 2002). This method of hydrogen production is interesting because there is a complete conversion of organic acid wastes to hydrogen gas and carbon dioxide, and thus, it has the potential for waste treatment. However, the high energy demand by nitrogenase coupled to the low light conversion efficiencies are rather discouraging (Hallenbeck & Ghosh, 2009).

In dark fermentation, carbohydrate-rich substrates are broken down enzymatically to provide electrons for generating hydrogen gas, whereby the reductants are transferred directly to ferredoxin and then to hydrogenase (Benemann, 1996). A variety of organic substrates for fermentative hydrogen production have been reported such as glucose (Logan *et al*., 2002), sucrose (Chang & Lin, 2004), starch (Zhang *et al*., 2003), cellulose (Liu *et al*., 2003), municipal solid waste (Lay *et al*., 1999) and waste water (Yu et al., 2003). Apart from the hydrogen gas, other fermentative products such as organic acids and alcohols can also be co-produced. Dark-fermentative hydrogen production can occur in strict and facultative anaerobic bacteria by utilising organic substrates. In the case of photosynthetic microorganisms such as unicellular algae, organic substrate can be produced and accumulated through photosynthesis coupled with carbon dioxide fixation. The dark fermentation has to occur in the dark when there is no light-dependent oxygen production and so there is no issue with oxygen-modulated inhibition of hydrogenase. However, the yields of hydrogen gas generated from dark fermentation are very low (Hallenbeck & Ghosh, 2009). For example, according to Hallenbeck (2005), enteric bacteria such as *E. coli* could only theoretically produce a maximum yield of 2 moles of hydrogen gas per mole of glucose, but in practice, the amount of hydrogen gas produced is normally lower than 2 moles. This is because the degradation of formate by the formate hydrogen lyase (FHL) complex (Axley *et al*., 1990) is normally incomplete, leading to less production of hydrogen. Moreover, instead of being

converted to formate, the pyruvate can also be converted to lactate especially under acidic conditions leading to a lower production of hydrogen (Hallenbeck, 2005). Similarly, anaerobic bacteria, such as *Clostridium*, which carry out acetate fermentation, could theoretically produce 4 moles of hydrogen gas per mole of glucose but in general the yields are around 2 moles. This is because of the reduction of ferredoxin by the reduced form of nicotinamide adenine dinucleotide, NADH, (to produce theoretically 2 moles of hydrogen gas) is not an energetically favourable reaction. Ferredoxin is favourably reduced by pyruvate ferredoxin:oxidoreductase (PFOR), which in turn can transfer the electrons to hydrogenase for hydrogen production (Hallenbeck, 2005).

### 1.5 Improving biological hydrogen production

Various approaches have been attempted to improve the yields of hydrogen gas from dark fermentation. Because an increase in hydrogen partial pressure can inhibit hydrogen production, one of the approaches is to reduce hydrogen partial pressure in the liquid phase of the culture by sparging with inert gases or steam (Mizuno *et al*., 2000; Van Groenestijna, 2002). However, this would dilute the hydrogen gas, making it expensive to recover this fuel (Hallenbeck, 2005).

Another approach is to exploit a two-stage hydrogen production. Apart from hydrogen gas, fermentation can also produce organic acids and alcohols. These products, especially acetate, can be further converted to hydrogen by using a two-stage production process. The first stage refers to the hydrogen production by the microorganism of interest by dark fermentation, which will also produce unfavourable products. These unfavourable products can be further converted into hydrogen gas in the second stage, utilising photosynthetic bacteria (for example, *Rhodobacter capsulatus* and *R. sphaeroides*) that carry out photofermentation. The overall hydrogen yields of the two-step hydrogen production processes have been shown to be higher than from the single step dark fermentation (Nath *et al*., 2008; Ozgur *et al*., 2010). Alternatively, the unfavourable products can also be converted to methane (Chu *et al*., 2008; Zhu *et al*., 2008; Wang & Zhao, 2009; Park *et al*., 2010). A two-stage anaerobic digestion process involves a first stage of hydrogen production and a second stage of methane production. The second stage could employ methanogens such as the hydrotrophic bacterium, *Methanobacterium beijingense* and the acetrotrophic bacterium, *Methanothrix soehngenii* (Park *et al*., 2010).

Many other approaches have also been attempted (Hallenbeck & Ghosh, 2009) but the one approach that is considered to be important is hydrogen enhancement by metabolic

engineering. Metabolic engineering has also been carried out to improve hydrogen production by fermentation (Vardar-Schara *et al*., 2008; Hallenbeck & Ghosh, 2009). Much of the research on the genetic manipulation of fermentative metabolism has focussed on *E. coli*. The limitation of dark fermentative hydrogen production is the yield of hydrogen per sugar molecule consumed. As pyruvate serves as the main fuel for several fermentative pathways, this important substrate can be unequally shared between these pathways. Since not all pyruvate will be converted to hydrogen gas, the yields obtained will be lowered than the maximum possible yields. By removing these competing pathways, the metabolic flux can potentially be re-directed towards the hydrogen-producing pathway for improved hydrogen yields. The elimination of competing lactate dehydrogenase pathway in *E. coli*, which involves the bacterial lactate dehydrogenase gene, *ldhA*, resulted in a small increase in hydrogen production (Sode *et al*., 1999; Bisaillon *et al*., 2006), as more pyruvate was re-channelled to the hydrogen-producing pathway. These studies demonstrate the possibility of achieving a high efficiency of bacterial hydrogen production from glucose by removing a competing pathway. Other pathways competing for pyruvate in *E. coli* are the pyruvate dehydrogenase (encoded by *aceE*) pathway, and the acetate-producing pathway which is catalysed by pyruvate oxidase (encoded by *poxB*) (Figure 1.2).

Fermentative hydrogen production in *E. coli* can be further enhanced by eliminating more than one of the competing pathways. As described above, pyruvate can be directed towards the competing lactate production pathway instead of the hydrogen production pathway. Pyruvate is obtained from the degradation of glucose through a multi-step process called glycolysis. In the last step, the intermediate phosphoenolpyruvate is formed and can be further converted to pyruvate to activate many fermentative pathways. However, not all of this intermediate will be converted to the fermentative substrate as it can also be directed towards succinate production. Therefore, this pathway is also competing with the hydrogen-generating pathway. Genetically manipulated *E. coli* with blocked lactate production (created by deletion of *ldhA*) and blocked succinate production (created by deletion of fumarate reductase which is encoded by *frdBC*) showed a 1.4x increase in hydrogen production rate compared to the WT (Yoshida *et al*., 2006).

For the production of hydrogen, pyruvate is firstly converted to formate which is then degraded to carbon dioxide and hydrogen gas. Alternatively, formate can also be oxidised by formate dehydrogenases, FDH-O and FDH-N (Vardar-Schara *et al*., 2008). The hydrogen-generating pathway is catalysed by the FHL complex, and this system contains two enzymatic components i.e. formate dehydrogenase, FDH-H and hydrogenase (Axley *et al*.,

1990). FHL system can be activated by FHL activator (encoded by *fhlA*) and inactivated by FHL repressor (encoded by *hycA*). Therefore, enhancement of hydrogen production could potentially be carried out by increasing or deactivating the expression of the enzymes involved in this hydrogen-producing pathway. Bisaillon *et al*. (2006) and Penfold *et al*. (2003) genetically produced *E. coli* strains with overexpressed *fhlA* and inactivated *hycA*, respectively, and the studies showed there was a 1.1x increase in yield (Bisaillon *et al*., 2006) and a 2x increase in production rate (Penfold *et al*., 2003), respectively. Similarly, Yoshida *et al*. (2005) also produced *E. coli* strains with inactivated *hycA* and/or overexpressed *fhlA*. This study found the mutants had higher hydrogen production compared to the WT with the double mutant having the highest improvement with a 2.8x increase in production rate. However, when the overexpression of *fhlA* and inactivation of *hycA* were coupled with the deletion of *ldhA* and *frdBC*, the hydrogen yield was not significantly further improved (Yoshida *et al*., 2006).

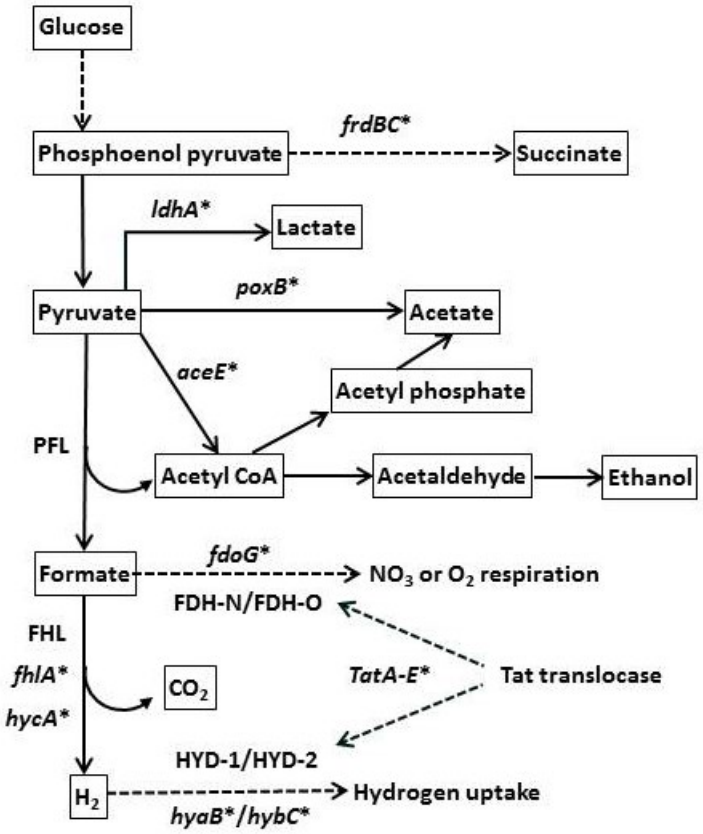


**Figure 1.2 Genetic manipulation of fermentative metabolism in *E. coli*.**

The map is adapted from Vardar-Schara *et al*. (2008). The asterisk indicates genetic manipulation had been carried out on the specified gene to improve hydrogen production. For convenience, some

pathways are simplified (dash lines). Abbreviations: *aceE* (pyruvate dehydrogenase), FDH (formate dehydrogenase), *fdoG* (formate dehydrogenase-O), FHL (formate hydrogen lyase), *fhlA* (FHL activator), *frdBC* (fumarate reductase), *hyaB* (hydrogenase-1), *hybC* (hydrogenase-2), *hycA* (FHL repressor), HYD (hydrogenase), *ldhA* (lactate dehydrogenase), PFL (pyruvate formate lyase), *poxB* (pyruvate oxidase), and *TatA-E* (twin-arginine translocation system).

Another genetic manipulation approach to improve hydrogen production is to knock out the genes for uptake hydrogenases as the enzymes can oxidise the hydrogen gas produced, leading to lower yields of hydrogen due to their competing activities. There are two uptake hydrogenases that can be targeted for deletion in *E.coli*. These are hydrogenase-1 (HYD-1) and hydrogenase-2 (HYD-2), encoded by *hya* and *hyb*, respectively. On the other hand, hydrogenase-3 (HYD-3) is a component of the FHL complex, involved in hydrogen production (Vardar-Schara *et al*., 2008). An *E. coli* strain with both uptake hydrogenases deleted showed a 1.4x increase in hydrogen production rate compared to the WT, and the yield was further improved when the deletion was coupled with *ldhA* deletion and *fhlA* overexpression (Bisaillon *et al*., 2006). Interestingly, this study also found the hydrogen yields approached 2 moles per mole of glucose consumed when the cells were incubated at low glucose concentrations, indicating the effect of nutrient limitation on hydrogen yields (Bisaillon *et al*., 2006). To block the uptake hydrogenase activities, the twin-arginine translocation (Tat) system could also be manipulated. The Tat system is responsible for the transport of HYD-1 and HYD-2 and can also transport FDH-O and FDH-N (Vardar-Schara *et al*., 2008). The elimination of the Tat system, either by deletion of *tatABCDE* or only *tatC*, caused a 2x increase in the hydrogen production rate (Penfold *et al*., 2006).

Introducing an increasing number of mutations can increase the possibility of maximising the hydrogen yield to the maximum theoretical yield. This is as demonstrated by Maeda *et al*. (2007; 2008), whereby various mutations were introduced into *E. coli*. It was found the maximum theoretical hydrogen yield of 1 mole hydrogen per mole of formate was achieved by producing a quintuple mutant. This mutant had uptake HYD-1 and HYD-2 removed (by the deletion of *hyaB* and *hybB*, respectively), overexpressed *fhlA*, inactivated *hycA*, and inactivated FDH-O (by the deletion of *fdoG*) (Maeda *et al*., 2008). To increase the hydrogen yield per mole of glucose, further mutations were added that included the removal of *ldhA*, *frdBC*, *poxB* and *ace*. It was found a septuple mutant, which had seven mutations i.e. *hyaB*, *hybC*, *hycA*, *fdoG*, *frdC*, *ldhA* and *ace*, had the highest hydrogen production rate (4.6x

higher than the WT) with a yield of 1.3 mole of hydrogen per mole of glucose (Maeda *et al*., 2007).

Apart from *E. coli*, attempts had also been made to enhance fermentative hydrogen yields in other microorganisms by genetic or metabolic engineering. To increase hydrogen yields in *Clostridium paraputrificum*, Morimoto *et al*. (2005) overexpressed the hydrogenase gene that is involved in hydrogen production. They showed hydrogen yield successfully increased compared to the WT, and they found it also increased acetate production and stopped lactate production. Liu *et al*. (2006) inactivated the acetate-producing pathway in *C. tyrobutyricum* in order to enhance butyric acid production, and apparently, this also led to the enhancement of hydrogen production from glucose.

Another successful example of metabolic engineering to improve hydrogen production was carried out in *Enterobacter cloacae*. The hydrogenases of this facultatively anaerobic bacterium can receive electrons from the electron carrier, NADH, for hydrogen production. However, NADH, which is produced from glycolysis, can also be used in the metabolic conversion of pyruvate to ethanol, butanediol, lactate and butryric acid, whereby it is oxidised to the oxidised form of nicrotinamide adenine dinucleotide, $NAD^+$. By isolating mutants through the use of the allyl alcohol method (Durre *et al*., 1986) and the proton suicide method (Winkelman & Clark, 1984), the hydrogen yields were successfully improved by blocking the formation of alcohol and some organic acids (Kumar *et al*., 2001). Similarly, when the approaches were applied to *E. aerogenes* in order to block the NADH-mediated metabolic pathways that produced ethanol, butanediol and lactate, hydrogen yields were improved (Rachman *et al*., 1997).

As described above, the genetic manipulation of fermentative metabolism to improve hydrogen yields in *E. coli* and other species has demonstrated the feasibility of improving hydrogen production in *C. reinhardtii*. Indeed it has been previously proposed that hydrogen yields could potentially be improved by targeting the algal fermentative pathways under the assumption that the genetic manipulation would re-direct metabolic flux to the algal hydrogenases (Burgess *et al*., 2011). This approach is the focus of my research project described here. Apart from targeting the *C. reinhardtii* fermentative metabolism, various other approaches have also been suggested and previously reported, and this has been extensively reviewed by Burgess *et al*. (2011). Several genetic approaches have been reported to improve photobiological hydrogen production in *C. reinhardtii*. These previous approaches are (1) by targeting the cyclic electron flow (Kruse *et al*., 2005a; Doebbe *et al*., 2007; Tolleter *et al*., 2011; Burgess & Nixon, unpublished); (2) by modifying the photosynthetic apparatus

such as decreasing the light-harvesting antennae to increase the light to hydrogen conversion efficiency (Kosourov *et al*., 2011) and downregulating the PSII activity to reduce oxygen evolution (Torzillo *et al*., 2009; Faraloni & Torzillo, 2010); and (3) by reducing the intracellular oxygen levels through the expression of oxygen-scavenging proteins (Wu *et al*., 2010; Wu *et al*., 2011).

### 1.6 Hydrogen production in *C. reinhardtii*

Hydrogen consumption and production in green algae was discovered more than 70 years ago (Gaffron, 1939; Gaffron & Rubin, 1942). This discovery led to numerous studies on algal hydrogen production with much research focusing on *C. reinhardtii*. Hydrogen production in *C. reinhardtii* is carried out by direct and indirect biophotolysis and also by dark fermentation (Figure 1.3; Posewitz *et al*., 2009). However, the amount of hydrogen gas produced by dark fermentation alone is much lower compared to the light-driven photosynthetic processes. Therefore, for viable hydrogen production, a combination of all these processes has to be considered.

Firstly, direct biophotolysis, also known as photosystem II (PSII)-dependent pathway, refers to production of hydrogen gas that is initiated when light energy is absorbed by PSII. The light energy is used by the cell to split water molecules into oxygen gas, protons and electrons (Equation 1). The generated electrons are transferred from PSII to photosystem I (PSI) through a series of electron carriers that form the chloroplast photosynthetic electron transport chain. These electron carriers are plastoquinone (PQ), cytochrome $b_6f$ complex ($Cytb_6f$) and plastocyanin (PC). From PSI, absorption of light energy by this photosystem leads to the transfer of electrons to ferredoxin molecules. The reduced ferredoxin molecules subsequently transfer the electrons to hydrogenase enzymes, whereby protons are reduced to hydrogen gas (Equation 2). Therefore, two molecules of water can be converted to two molecules of hydrogen gas and one molecule of oxygen gas (Equation 3). However, hydrogen gas can only be produced by this light-dependent method when the cellular levels of oxygen gas are low because hydrogenases are sensitive to oxygen.

$2H_2O \rightarrow 4H^+ + O_2 + 4e^-$ (Eq. 1)

$2H^+ + 2e^- \rightarrow H_2$ (Eq. 2)

$2H_2O \rightarrow 2H_2 + O_2$ (Eq. 3)

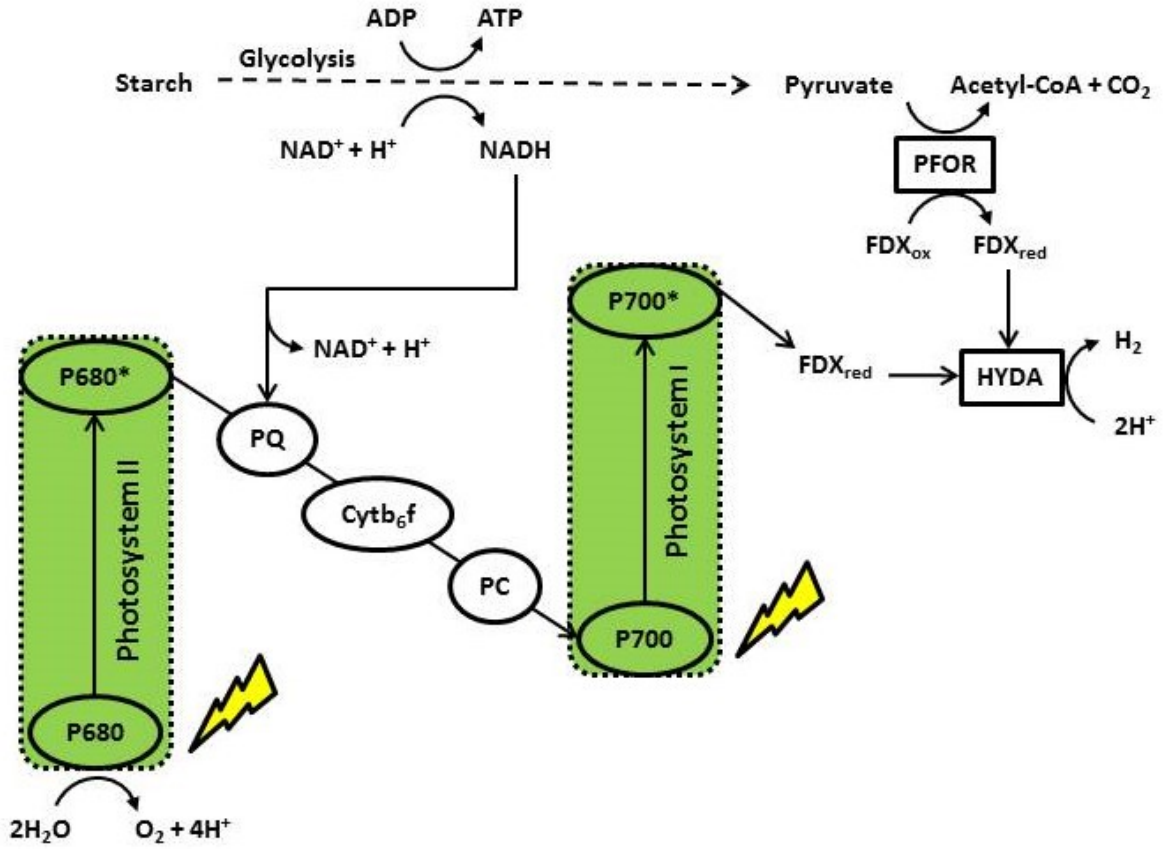


**Figure 1.3 Metabolic pathways for hydrogen production in *C. reinhardtii*.**

The simplified illustration is adapted from Posewitz *et al*. (2009). For simplicity, the glycolysis pathways (dash line) are not described. Abbreviations: ADP (adenosine diphosphate), ATP (adenosine triphosphate), $CO_2$ (carbon dioxide), $Cytb_6f$ (cytochrome $b_6f$ complex), $FDX_{ox}$ (oxidised ferredoxin), $FDX_{red}$ (reduced ferredoxin), $H^+$ (hydrogen positive ion), $H_2$ (hydrogen gas), HYDA (hydrogenase), $NAD^+$ (oxidised nicotinamide adenine dinucleotide), NADH (reduced nicotinamide adenine dinucleotide), PC (plastocyanin), PFOR (pyruvate:ferredoxin oxidoreductase), and PQ (plastoquinone).

Secondly, in indirect biophotolysis, also known as the PSII-independent pathway, electrons do not come from the splitting of water but from catabolic metabolism such as the breakdown of starch and glucose by glycolysis. The electrons are fed into the photosynthetic electron transport chain at the plastoquinone pool. This non-photochemical reduction of plastoquinone is mediated by NAD(P)H. This transfer is catalysed by a chloroplastic NADH dehydrogenase belonging to a family of type II dehydrogenases (Jans *et al*., 2008). Like in the PSII-dependent pathway, the electrons are then transferred through the photosynthetic electron chain to reach PSI. This is where electrons are further transferred one at a time to

ferredoxin, a process requiring the absorption of a photon of light by this photosystem. The reduced ferredoxin molecules subsequently transfer the electrons to hydrogenases for hydrogen production, thereby re-oxidising ferredoxin so it will be able to transport more electrons. Similarly, for this pathway to work, the cellular oxygen levels have to be reduced to prevent the inhibition of hydrogenases.

Thirdly, in dark fermentation, which is another PSII-independent pathway for producing hydrogen gas, the electrons required by hydrogenases come from the breakdown of starch that is produced and accumulated by photosynthetic activity. Through glycolysis, pyruvate is generated which can then be oxidised by pyruvate:ferredoxin oxidoreductase (PFOR) to produce acetyl-CoA and carbon dioxide. This enzymatic reaction consequently reduces ferredoxin which can subsequently transfer its electron to hydrogenases. *C. reinhardtii* encodes six differently regulated ferredoxins i.e. FDX1 (also known as PETF) and FDX2-FDX6 (Terauchi *et al*., 2009; Peden *et al*., 2013) with the transcript levels of FDX2 and especially FDX5 showing a moderate increase upon acclimation to dark anaerobic conditions (Mus *et al*., 2007). FDX1 has been reported to function as the primary electron donor for hydrogen photoproduction (Peden *et al*., 2013).

The hydrogenase enzyme has been isolated from *C. reinhardtii* (Happe & Naber, 1993) and was found to be located in the chloroplasts (Happe *et al*., 1994). Two similar monomeric reversible [FeFe]-hydrogenases of approximately 49 kDa in size have been identified from a *C. reinhardtii* cDNA library, and designated as HYDA1 and HYDA2 (Happe & Kaminski, 2002; Forestier *et al*., 2003). A third protein, HYD3 with homology to [FeFe]-hydrogenases was also found in the *C. reinhardtii* genome but it is thought not to possess hydrogenase activity (Posewitz *et al*., 2009). By using artificial microRNA technology, it was shown that the silencing of HYD3 did not affect hydrogen production but this protein was shown to be involved in biogenesis or maintenance of cytosolic Fe-S proteins (Godman *et al*., 2010). Genetically engineered knockout mutants lacking either HYDA1 or HYDA2 have been shown to produce hydrogen gas, indicating both proteins play a role in algal hydrogen production, with HYDA1 found to contribute more to hydrogen production than HYDA2 under the conditions tested (i.e. hydrogen production mediated by methyl viologen as electron donor) (Godman *et al*., 2010; Meuser *et al*., 2012). Similarly, the same trend was observed for hydrogen photoproduction but not observed for dark fermentative hydrogen production in which the levels of hydrogen production for both single mutants were similar to the WT (Meuser *et al*., 2012), suggesting both hydrogenases contributed equally to hydrogen production under this condition.

The oxygen-sensitive nature of the hydrogenase makes it difficult to induce hydrogen production in the green algae when grown or incubated under light. For viable production of hydrogen gas, light is required but it will cause photosynthetic production of oxygen. No hydrogen production will occur under aerobic conditions as hydrogenase transcript levels were only found to be significantly increased under anoxic conditions and not under aerobic conditions (Happe & Kaminski, 2002; Forestier *et al*., 2003; Mus *et al*., 2007; Posewitz *et al*., 2009), and the enzymes are irreversibly deactivated within minutes by exposure to atmospheric oxygen (Happe & Nabber, 1993; Ghirardi *et al*., 1997). Nevertheless, the enzyme has been found to have a high specific activity for hydrogen production (Happe and Naber, 1993). Therefore, to overcome this problem a novel approach has been described (Melis *et al*., 2000), which has opened the door to sustained hydrogen photoproduction by the green alga.

The novel approach of inducing hydrogen photoproduction (Melis *et al*., 2000) involves re-suspending *C. reinhardtii* cells in a sulphur-deficient, acetate-containing medium. Sulphur deprivation in the light causes a reduction in the photosynthetic activity of the chloroplasts but does not affect the respiratory activity of the mitochondria at the early stage of the incubation (Melis *et al*., 2000; Zhang & Melis, 2002). Consequently, with reduced production of oxygen from the photosynthetic activity of PSII and continuous consumption of oxygen by cellular oxidative respiration, a sealed algal culture becomes anaerobic. This condition induces hydrogenase expression and enzymatic activity, leading to hydrogen evolution. The hydrogen photoproduction can last for 4 to 5 days (Melis *et al*., 2000; Melis 2007). At the end of the incubation period, the hydrogen production slows down and eventually comes to a stop. As the energy reserves are not yet fully depleted, cessation of hydrogen production is most likely due to the loss of key cellular functions or due to the accumulation of toxic fermentative products (Timmins *et al*., 2009b).

Photosynthetic activity is gradually reduced under sulphur starvation because lack of sulphur interferes with the biosynthesis of the D1 protein of the PSII complex, leading to less photosynthetic production of oxygen. During photosynthesis, the D1 protein becomes damaged by the light energy especially when it is exposed to high light intensities. Therefore, the photodamaged protein needs to be frequently replaced with a new D1 protein to allow normal functioning of PSII (Nixon *et al*., 2010; Komenda *et al*., 2012). When the cells are starved of sulphur, the D1 protein turnover rate is impaired, and this leads to a more than 50% reduction in the light-saturated PSII activity but no effect on the light-saturated PSI activity (Wykoff *et al*., 1998). Since PSI activity is not affected, it allows the light-driven

reduction of ferredoxin which can transfer its electron to the hydrogenases for hydrogen production. Acetate, which is present in the sulphur-deprived medium, also has been shown by Melis *et al*. (2000) to play an important role in enhancing cellular respiration for the establishment of anaerobiosis. It acts as the main substrate for respiration during the early stage of the incubation but not at the later stage when acetate is no longer consumed. It does not act as an electron donor for hydrogen production (Melis *et al*., 2000). The electrons needed by hydrogenases come from the photosynthetic water splitting, which is the primary source of electrons, and endogenous substrate catabolism, such as the starch, protein and probably lipid catabolism, which is the secondary source of electrons (Melis, 2007).

The incubation of *C. reinhardtii* in sulphur-deficient medium promotes the accumulation of starch and also triacylglycerides during the initial stage of incubation, from 0 to 24 hours (Timmins *et al*., 2009b), as this is a common response to nutrient starvation. This is accompanied by the degradation of Rubisco, an enzyme involved in carbon fixation (Zhang & Melis, 2002). This is further followed by starch degradation (Timmins *et al*., 2009b). The starch acts as an electron donor to hydrogenases via the PSII-independent pathways. Moreover, starch catabolism provides NADH to the mitochondria for the maintenance of oxidative respiration (Melis, 2007). By doing so, it also sustains anaerobiosis which is necessary for sustained hydrogen production. Although starch catabolism is not the main contributor of electrons (Chochois *et al*., 2009), it has been shown to still contribute considerably to the algal hydrogen production through the PSII-independent pathway (Chochois *et al*., 2009). A range of values have been previously reported for the contribution of the PSII-dependent pathway in hydrogen production (Burgess *et al*., 2011), which suggest ~10% of electrons come from starch catabolism. The isolation of *C. reinhardtii* mutants affected in their starch metabolism showed there was a reduction or delay in their hydrogen photoproduction (Chochois *et al*., 2010), indicating the important role of starch in algal hydrogen production. This is also supported by the isolation of Rubisco-less mutant that had reduced levels of hydrogen under sulphur-deprived conditions. This mutant failed to accumulate starch during the initial stage of sulphur starvation and consequently, it failed to produce hydrogen gas (White & Melis, 2006). Additionally, the over-accumulation of starch in the *stm6* mutant has been linked with the increased hydrogen production exhibited by this mutant (Kruse *et al*., 2005a), as the enhanced level of starch could provide increased amounts of reductant for hydrogen production and also for sustaining oxidative respiration (Posewitz *et al*., 2009).

## 1.7 Fermentative metabolism

Fermentative metabolism is activated when cells experience hypoxia (low levels of oxygen) or anoxia (absence of oxygen) as a means of generating energy in the form of ATP and maintaining redox balance. Under this anaerobic stress, organisms such as green algae switch their metabolism from respiratory oxidative metabolism to fermentative metabolism. This allows any organisms to tolerate and inhabit any anaerobic conditions or environments. In the presence of oxygen, production of ATP is carried out through oxidative phosphorylation that involves a mitochondrial electron transport chain. However, in the absence of oxygen that acts as a terminal electron acceptor for aerobic respiration, living cells have to generate their energy currency through fermentation by carrying out substrate-level phosphorylation (Catalanotti *et al*., 2013). Alternatively, the cells can also activate anaerobic respiration whereby alternative terminal electron acceptors, such as sulphate and nitrate, have to be used but this is rather uncommon in eukaryotic algae (Catalanotti *et al*., 2013; Atteia *et al*., 2013).

Fermentation pathways can vary among different eukaryotes including different algal species (Catalanotti *et al*., 2013; Atteia *et al*., 2013). Information about algal dark fermentation mostly comes from several studies of *C. reinhardtii* (Gfeller & Gibbs, 1984; Kreuzberg, 1984; Ohta *et al*., 1987; Mus *et al*., 2007; Hemschemeier *et al*., 2008; Dubini *et al*., 2009; Philipps *et al*., 2011; Burgess *et al*., 2012; Catalanotti *et al*., 2012; Magneschi *et al*., 2012). Dark fermentative pathways in *C.reinhardtii* have been characterised to some degree (Figure 1.4) but more work is still needed to understand algal anoxic metabolism. The green alga is metabolically flexible as it is able to flexibly utilise the multiple metabolic pathways present in its fermentation metabolism (Catalanotti *et al*., 2013). During fermentation, starch, which is accumulated during photosynthetic fixation of carbon dioxide, is broken down into glucose by β-amylase activity, as indicated by the increased transcript levels of amylase (Mus *et al*., 2007; Dubini *et al*., 2009). The sugar is further metabolised to pyruvate through glycolysis, a multi-step metabolic process that involves several enzymes and metabolic intermediates. The overall reaction is summarised in Equation 4 below, showing the net production of two molecules of ATP and two molecules of NADH from one molecule of glucose.

$$\text{Glucose} + 2NAD^+ + 2ADP + 2P_i \rightarrow 2\ \text{Pyruvate} + 2NADH + 2ATP + 2H_2O + 2H^+ \qquad \text{(Eq. 4)}$$

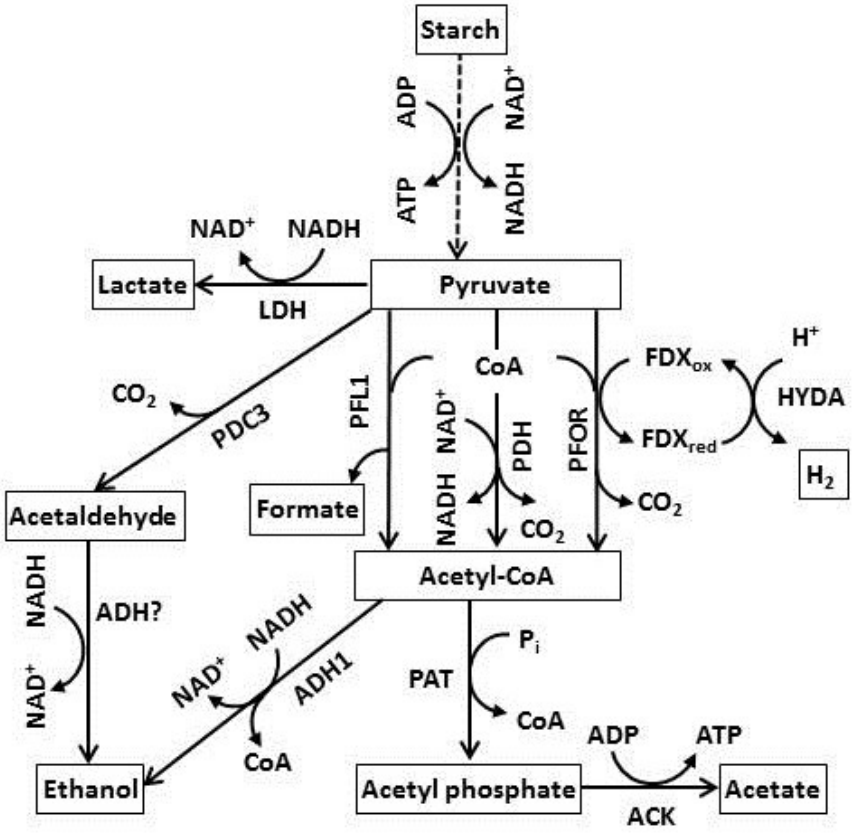


**Figure 1.4 Fermentative pathways in *C. reinhardtii*.**

The map of the *C. reinhardtii* putative fermentative pathways is adapted from Grossman *et al*. (2007). For simplicity, glycolysis pathway (dash line) is not described. Abbreviations: ACK (acetate kinase), ADH (alcohol dehydrogenase), ADH1 (bifunctional acetaldehyde/alcohol dehydrogenase 1), ADP (adenosine diphosphate), ALAT (alanine aminotransferase), ATP (adenosine triphosphate), $CO_2$ (carbon dioxide), CoA (coenzyme A), $FDX_{ox}$ (oxidised ferredoxin), $FDX_{red}$ (reduced ferredoxin), $H^+$ (hydrogen positive ion), $H_2$ (hydrogen gas), HYDA (hydrogenase), LDH (D-lactate dehydrogenase), $NAD^+$ (oxidised nicotinamide adenine dinucleotide), NADH (reduced nicotinamide adenine dinucleotide), $P_i$ (inorganic phosphate), PAT (phosphotransacetylase), PDC3 (pyruvate decarboxylase 3), PDH (pyruvate dehydrogenase complex), PFL1 (pyruvate formate lyase 1), PFOR (pyruvate:ferredoxin oxidoreductase).

Pyruvate serves as the main substrate for fermentation. Due to the existence of multiple fermentative pathways, which can be interconnected to each other, this three-carbon compound can be converted to a variety of end products. This allows for the regeneration of $NAD^+$ to sustain glycolytic flow, and it can also help in increasing the amounts of ATP produced through substrate-level phosphorylation. Fermentation patterns among different species of algae have been reported to vary. For examples, no formate is observed in *C.*

*moewusii* (Klein & Betz, 1978) while in *C. minutum*, acetate, glycerol and carbon dioxide are the main fermentative products (Ohta *et al*., 1987). In *C. reinhardtii*, formate, acetate and ethanol are the major products of dark fermentation, and it has been reported these organic acids are produced in the ratio of 2:1:1, respectively (Gfeller and Gibbs, 1984; Kreuzberg, 1984). However, alternative ratio of 2:2:1 has also been reported (Ohta *et al*., 1987; Mus *et al*., 2007). These different ratios could reflect the use of different conditions or different laboratory strains (Posewitz *et al*., 2009), and as reported by Ohta *et al*. (1987), changes in the concentration of sodium chloride or ammonium chloride in the incubation medium could alter the fermentation pattern of a marine green alga, *Chlamydomonas* MGA 161. Hydrogen and carbon dioxide are also emitted by *C. reinhardtii* but the amounts are only minor, and similarly, minor amounts of lactate, glycerol and malate have also been observed (Gfeller & Gibbs, 1984; Kreuzberg, 1984; Ohta *et al*., 1987; Mus *et al*., 2007).

Three metabolic pathways are thought to exist in *C. reinhardtii* for converting pyruvate to acetyl-CoA, indicating the diversity of metabolic pathways available in this green alga (Hemschemeier & Happe, 2005; Atteia *et al*., 2006; Grossman *et al*., 2007; Mus *et al*., 2007).

Pyruvate can be converted to acetyl-CoA and a one-carbon compound, formate, by pyruvate formate lyase (PFL1) (Equation 5). Based on an immunoblot analysis, this enzyme is present in both the chloroplast and mitochondria of aerobically grown *C. reinhardtii* (Atteia *et al*., 2006). This is in accordance with the proteomic analysis by Terashima *et al*. (2010). In *E. coli*, this enzyme is activated by PFL activating enzyme (PFL-AE), which belongs to the radical S-adenosyl methionine (SAM) protein superfamily, and is deactivated by PFL deactivating enzyme (PFL-DA), which in *E. coli* is performed by a bifunctional acetaldehyde/alcohol dehydrogenase (ADHE). In *E. coli*, to activate pyruvate formate lyase, PFL1-AE generates an amino acid radical in the PFL1 enzyme by stereospecific abstraction of a hydrogen atom from glycine-734 (Wagner *et al*., 1992). This reaction is strictly dependent on the co-substrate *S*-adenosyl L-methionine (AdoMet) (Broderick *et al*., 2000). However, this activation of PFL1 also causes it to become highly sensitive to oxygen, leading to cleavage into two fragments (Wagner *et al*., 1992; Zhang *et al*., 2007). On the other hand, *E. coli* ADHE deactivates the enzyme by quenching the glycyl radical of the activated enzyme (Kessler *et al*., 1992). Similarly, the ADHE enzyme of the ruminal bacterium *Streptococcus bovis* also has PFL-deactivating activity (Asanuma *et al*., 2004) but this deactivating activity is not always present in ADHE, for example in *Lactococcus lactis* (Melchiorsen *et al*., 2000). In *C. reinhardtii*, the transcript of PFL-AE (also called PFLA)

was detected although at similar levels in both aerobic and anaerobic conditions, establishing the possible occurrence of a PFL activating system in this green alga (Atteia *et al*., 2006; Mus *et al*., 2007). The PFL1 transcript was also detected and the levels increased significantly under dark anaerobic conditions compared to aerobic conditions (Atteia *et al*., 2006; Mus *et al*., 2007). However, surprisingly, the increase in the PFL1 transcript levels was not reflected in the protein level, as the protein levels were found not to be further increased by the dark anaerobiosis (Atteia *et al*., 2006).

Alternatively, pyruvate can be oxidised by decarboxylation with the help of pyruvate:ferredoxin oxidoreductase (PFOR; sometimes referred as PFR) to acetyl-CoA and carbon dioxide, and this enzymatic reaction results in the reduction of oxidised ferredoxin (Equation 6). The generated reduced ferredoxin can be re-oxidised by [FeFe]-hydrogenases, causing production of hydrogen gas. A proteomic analysis only identified PFOR being present in the chloroplast sample and not in the mitochondria sample, indicating its specific subcellular location, and that the protein level was induced under anaerobic conditions (Terashima *et al*., 2010). Noth *et al*. (2013) has shown that PFOR is able to transfer electrons from pyruvate to hydrogenase, using ferredoxins as electron carriers. Therefore, this provides evidence of a link between hydrogen production and the PFOR pathway.

Pyruvate can also undergo oxidative decarboxylation by the pyruvate dehydrogenase (PDH) complex, which involves the removal of a carboxyl group, to release carbon dioxide and formation of acetyl-CoA and NADH (Equation 7). However, this pathway is thought to be active only under aerobic conditions (Grossman *et al*., 2007). Moreover, as this enzymatic reaction produces NADH instead of $NAD^+$, which is needed to sustain glycolysis, it is assumed this pathway is the least favoured pathway compared to the PFL1 and PFOR pathways for converting pyruvate to acetyl-CoA under anaerobic conditions (Catalanotti *et al*., 2013).

$$\text{Pyruvate} + \text{CoA} \rightarrow \text{Acetyl-CoA} + \text{Formate} \quad \text{(Eq. 5)}$$

$$\text{Pyruvate} + \text{CoA} + 2\ \text{Ferredoxin}_{ox} \rightarrow \text{Acetyl-CoA} + CO_2 + 2\ \text{Ferredoxin}_{red} + 2H^+ \quad \text{(Eq. 6)}$$

$$\text{Pyruvate} + \text{CoA} + NAD^+ \rightarrow \text{Acetyl-CoA} + \text{NADH} + H^+ + CO_2 \quad \text{(Eq. 7)}$$

The generated acetyl-CoA can be further converted to ethanol or acetate (Hemschemeier & Happe, 2005; Atteia *et al*., 2006; Grossman *et al*., 2007; Mus *et al*., 2007).

For the production of ethanol, the acetyl-CoA is reduced to ethanol via acetaldehyde. This two-step enzymatic reaction has to be catalysed by a bifunctional acetaldehyde

dehydrogenase/alcohol dehydrogenase. The first step is the conversion of acetyl-CoA to acetaldehyde, a reaction that releases coenzyme A (CoA; sometimes referred as CoASH) and oxidises one molecule of NADH per molecule of acetyl-CoA (Equation 8). The second step refers to the subsequent conversion of acetaldehyde to ethanol, oxidising another one molecule of NADH (Equation 9). Therefore, this two-step enzymatic reaction generates two molecules of $NAD^+$ that can be used for sustaining glycolysis. This bifunctional enzyme is designated as ADHE in *E. coli* to distinguish it from the monofunctional alcohol dehydrogenase that cannot perform the acetaldehyde dehydrogenase activity (Posewitz *et al*., 2009). However, in *C. reinhardtii*, the orthologue of the *E. coli* ADHE enzyme is designated as ADH1. The conversion of acetyl-CoA to ethanol is likely being carried out in the green alga by this bifunctional enzyme (Hemschemeier & Happe, 2005; Atteia *et al*., 2006; Grossman *et al*., 2007; Mus *et al*., 2007).

Proteomic surveys indicated the ADH1 enzyme is only found in the chloroplast (Terashima *et al*., 2010) and not in the mitochondrion (Atteia *et al*., 2009) but its cytoplasmic location could not be ruled out (Burgess, 2011). This is completely different compared to the *C. reinhardtii* relative*, Polytomella* sp., whereby the enzyme was located in the mitochondria (Atteia *et al*., 2003). There was a small increase in the protein level when exposed to anaerobic conditions (Terashima *et al*., 2010). This is in accordance with the increase in the *ADH1* transcript levels upon exposure to anoxic conditions (Mus *et al*., 2007; Magneschi *et al*., 2012). The enzyme was also detected at the transcript and protein levels under aerobic conditions (Whitney *et al*., 2011; Magneschi *et al*., 2012) but its enzymatic capability under oxic conditions has yet to be confirmed (Magneschi *et al*., 2012).

Apart from ADH1, there are two other putative alcohol dehydrogenases, which belong to the iron-containing alcohol dehydrogenase family, found in the *C. reinhardtii* genome (Posewitz *et al*., 2009), designated as ADH2 and ADH3 by Magneschi *et al*. (2012). However, protein sequence analysis of the enzymes suggests ADH2 could also be a bifunctional acetaldehyde dehydrogenase/alcohol dehydrogenase but ADH3 is probably not since it only has the alcohol dehydrogenase domain (Magneschi *et al*., 2012).

$$\text{Acetyl-CoA} + \text{NADH} + H^+ \rightarrow \text{Acetaldehyde} + NAD^+ + \text{CoA} \qquad \text{(Eq. 8)}$$

$$\text{Acetaldehyde} + \text{NADH} + H^+ \rightarrow \text{Ethanol} + NAD^+ \qquad \text{(Eq. 9)}$$

Apart from ethanol, the generated acetyl-CoA from pyruvate can also be further converted to acetate (Hemschemeier & Happe, 2005; Atteia *et al*., 2006; Grossman *et al*.,

2007; Mus *et al*., 2007). Two metabolic pathways, which are catalysed by two different enzymes, are involved in acetate production. The first enzymatic reaction is catalysed by phosphotransacetylase (PAT), and this reaction involves the transfer of an acetyl group from acetyl-CoA to inorganic phosphate ($P_i$; sometimes called orthophosphate), which consequently produces acetyl-phosphate (acetyl-P) and releases coenzyme A (Equation 10). The generated acetyl-phosphate can be further converted in a second enzymatic reaction to acetate by acetate kinase (ACK). This enzymatic reaction involves substrate-level phosphorylation, whereby phosphate is transfered from acetyl-phosphate to adenosine diphosphate (ADP), and this generates one molecule of ATP (Equation 11). *C. reinhardtii* has two copies of PAT and ACK, and based on proteomic analyses, PAT1 and ACK2 were found to be localised to the mitochondria (Atteia *et al*., 2006; Atteia *et al*., 2009; Terashima *et al*., 2010) while PAT2 and ACK1 were found to be localised to the chloroplast (Terashima *et al*., 2010). By expressing the *PAT* and *ACK* genes in *C. reinhardtii* as Venus fusion proteins, a recent study (Yang *et al*., 2014) provided support to the previous proteomic analyses. The genes for mitochondrial PAT1 and ACK2, although not contiguous, are found on the same chromosome while the genes for chloroplast PAT2 and ACK1 are contiguous (Catalanotti *et al*., 2013) and are also adjacent to the gene encoding the chloroplast HYDA2 (Atteia *et al*., 2006).

$$\text{Acetyl-CoA} + P_i \rightarrow \text{CoA} + \text{Acetyl-phosphate} \qquad \text{(Eq. 10)}$$

$$\text{Acetyl-phosphate} + \text{ADP} \rightarrow \text{Acetate} + \text{ATP} \qquad \text{(Eq. 11)}$$

Pyruvate can also be decarboxylated by pyruvate decarboxylase to acetaldehyde and carbon dioxide (Equation 12). A homologue of this enzyme has been found in the *C. reinhardtii* genome, which is annotated as PDC3. The generated acetaldehyde could potentially be further converted, as describe above, to ethanol by an alcohol dehydrogenase. The alcohol dehydrogenase could be the bifunctional ADH1 and/or the other iron-containing alcohol dehydrogenases (ADH2 and ADH3) (Magneschi *et al*., 2012) which are yet to be validated. The conversion of acetaldehyde to ethanol would regenerate one molecule of NADH per molecule of acetaldehyde. However, the production of ethanol through the PDC3 pathway has not been validated yet. Nevertheless, Burgess (2011) showed the gene was expressed under anaerobic conditions, indicating it might be involved in dark fermentation. However, its role in the *C. reinhardtii* fermentative pathways is currently not very well understood.

Pyruvate → Acetaldehyde + $CO_2$ (Eq. 12)

Pyruvate can be reduced to lactate by lactate dehydrogenase (LDH). This enzymatic reaction involves the transfer of hydride from NADH to pyruvate, and this reduces the substrate to lactate and re-generates $NAD^+$ (Equation 13). Lactate can exist as either D- or L-lactate. It has been previously reported that *C. reinhardtii* can produce and oxidise D-lactate (Husic & Tolbert, 1985; Husic & Tolbert, 1987), suggesting the occurrence of D-LDH. Lactate has only been observed as the minor end product of fermentation (Gfeller & Gibbs, 1984; Kreuzberg, 1984; Ohta *et al*., 1987) but its production has been found to increase when PFL1 was inhibited (Kreuzberg, 1984; Hemschemeier *et al*., 2008). However, the enzyme responsible for the D-lactate formation has not been confirmed or characterised. Therefore, this will be the subject of Chapter 3.

Pyruvate + NADH + $H^+$ → Lactate + $NAD^+$ (Eq. 13)

**1.8 Aims of the project**

Biological photoproduction of hydrogen fuel from *C. reinhardtii* is an attractive approach to generate renewable and clean energy. Currently, algal hydrogen production is not economically feasible due to low hydrogen yields which are caused by low light-to-hydrogen-gas conversion efficiency. A number of competing metabolic pathways have been proposed to contribute to this low conversion efficiency, and these include the various proposed fermentative pathways of the green alga, competing with the hydrogen-producing pathways. Metabolic engineering provides an easier approach to eliminate these competing pathways. However, at present, the fermentative metabolism of *C. reinhardtii* is still not fully understood. Therefore, the aims of this research project are:

- To identify and characterise the D-LDH activity responsible for D-lactate production in *C. reinhardtii*.

- To generate a quadruple *C. reinhardtii* mutant affected in fermentation, targeting the enzymes D-LDH, PDC3, PFL1 and ADH1, and to assess the impact of these mutations on metabolism and physiology.

# Chapter 2: Materials and Methods

## 2.1 Chemicals

Chemicals used for preparing solutions and growth media were purchased from Sigma-Aldrich, UK and Melford Laboratories, UK. Solutions and media used for growing organisms were sterilised before use by autoclaving at 120ºC for 25 minutes but for thermolabile solutions, the solutions were filter-sterilised using 0.2 µm Acrodisc Syringe Filters with Supor Membrane (Pall Life Sciences, USA).

## 2.2 *C. reinhardtii* strains and growth conditions

*C. reinhardtii* strains used in this work are described in Table 2.1. The wild type strains were bought from the *Chlamydomonas* Resource Centre (University of Minnesota). The knockdown mutant, *PDC3*-KD was isolated in our lab while the double mutant, *pfl1-1-adh1* was kindly given to us by Prof Arthur R. Grossman (Carnegie Institution for Science, Stanford).

*C. reinhardtii* was usually grown mixotrophically in Tris-acetate-phosphate (TAP) medium (Gorman & Levine, 1965) at 28°C (in a temperature-controlled growth room, Imperial College London) at a light intensity of ~30 $\mu Em^{-2}s^{-1}$ (cool white fluorescent tubes F18W/29 T8; Philips, UK) and constantly shaken at 100 rpm (Lab Companion SK-300 Shaker; Jeio Tech, Korea). For photoautotrophic growth, cells were cultivated in high salt medium (HSM) (Sueoka, 1960) instead of TAP. Corning cell culture flasks (25 or 75 $cm^2$) were used for cell cultivation. For growing cells on a plate, 2% agar (w/v) plates containing either TAP or HSM were used. If appropriate, antibiotic paromomycin was added into the agar plate at a standard concentration of 10 µg/ml. For long term storage, cells were grown on 2% TAP agar plates at lower temperature (25°C) (LMS Cooled Incubator, Jencons Scientific Ltd, UK) and lower light intensity (~10 $\mu Em^{-2}s^{-1}$; cool white fluorescent light, Philips, UK), and cells were transferred to fresh agar plates once a month. Inoculation of cultures was conducted in a laminar flow cabinet (Microflow Advanced Biosafety Cabinet Class II, Bioquell, UK) to avoid biological contamination.

| Strain | Description | Reference |
|---|---|---|
| **CC-124** | Wild type strain; mating type *minus* (*mt*$^-$); carries *nit1* & *nit2* mutations and *agg1* allele. | *Chlamydomonas* Resource Centre |
| **CC-125** | Wild type strain; mating type *plus* (*mt*$^+$); carries *nit1* & *nit2* mutations and *agg1*+ allele. | *Chlamydomonas* Resource Centre |
| **D66** | CC-4425 wild type strain; carries cell wall mutation *cw15*; *mt*$^+$. | *Chlamydomonas* Resource Centre |
| ***ldh*-KD** | CC-124 was transformed with artificial microRNA that targeted *D-LDH* transcript; Four strains were isolated i.e. *ldh*-KD1, *ldh*-KD2, *ldh*-KD3 and *ldh*-KD4; paromomycin resistant; *mt*$^-$. | This work |
| ***pdc3-KD*** | CC-124 was transformed with artificial microRNA that targeted *PDC3* transcript; paromomycin resistant; *mt*$^-$. | Burgess (2011) |
| ***pdc3*-1st** | First backcross of *pdc3*-KD; *mt*$^+$. | This work |
| ***pdc3*-2nd** | Second backcross of *pdc3*-KD; *mt*$^-$. | This work |
| ***pdc3*-3rd** | Third backcross of *pdc3*-KD; *mt*$^+$. | This work |
| ***pdc3*** | Fourth backcross of *pdc3*-KD; *mt*$^-$. | This work |
| ***pfl1-1-adh1*** | Double mutant with *PFL1* and *ADH1* knockout mutation; paromomycin resistant; hereafter known as *pfl-adh1*; *mt*–. | Catalanotti *et al*. (2012) |
| ***pfl1*** | *pfl1-adh1* was crossed with CC-125. | This work |
| ***adh1*** | *pfl1-adh1* was crossed with CC-125. | This work |
| **Triple** | *pfl1-adh1* was crossed with *pdc3*-1st to obtain *pdc3-pfl1-adh1* (re-named as triple); *mt*$^+$. | This work |
| ***pdc3-pfl1*** | *pfl1-adh1* was crossed with *pdc3*-1st. | This work |
| ***pdc3-adh1*** | *pfl1-adh1* was crossed with *pdc3*-1st. | This work |
| **Quadruple** | Triple mutant was crossed with *ldh*-KD1 to obtain *ldh-pdc3-pfl1-adh1* (re-named as quadruple). | This work |
| ***ldh-pdc3-pfl1*** | Triple mutant was crossed with *ldh*-KD1. | This work |
| ***ldh-pdc3-adh1*** | Triple mutant was crossed with *ldh*-KD1. | This work |
| ***ldh-pfl1-adh1*** | Triple mutant was crossed with *ldh*-KD1. | This work |

**Table 2.1. *C. reinhardtii* strains used in this work.**

TAP medium (Gorman & Levine, 1965) and HSM (Seuoka, 1960) were prepared according to the protocol shown in the *Chlamydomonas* Connection, a database of resources for *C. reinhardtii* research (http://www.chlamy.org/media). For 1 litre (L), TAP medium pH 7.2 contains 2.42 g Tris, 0.375 g $NH_4Cl$, 0.1 g $MgSO_4.7H_2O$, 0.05 g $CaCl_2.2H_2O$, 0.1 g $K_2HPO_4$, 0.05 g $KH_2PO_4$, 1 ml glacial acetic acid, and 1 ml Hutner's trace elements. For 1 L, HSM pH 6.8 contains 0.5 g $NH_4Cl$, 0.246 g $MgSO_4.7H_2O$, 0.01 g $CaCl_2.2H_2O$, 1.44 g $K_2HPO_4$, 0.72 g $KH_2PO_4$, and 1 ml Hutner's trace elements. A solution of Hutner's trace elements (Hutner *et al*., 1950) was also prepared according to the protocol shown in the *Chlamydomonas* Connection. For 1 L, Hutner's trace elements solution contains 50 g NaEDTA, 22 g $ZnSO_4.7H_2O$, 11.4 g $H_3BO_3$, 5.06 g $MnCl_2.4H_2O$, 1.61 g $CoCl_2.6H_2O$, 1.57 g $CuSO_4.5H_2O$, 1.1 g $(NH_4)_6Mo_7O_{24}.4H_2O$, and 4.99 g $FeSO_4.7H_2O$.

Sulphur-deficient TAP medium (TAP-S) was prepared in a similar manner to TAP medium except magnesium sulphate was replaced with its chloride derivative (0.08 g/L $MgCl_2.6H_2O$), and a solution of sulphur-free Hutner's trace elements was used instead. To prepare this modified Hutner's trace elements, the sulphate salts were simply replaced with an equimolar amount of their chloride derivatives (10 g $ZnCl_2$, 1 g $CuCl_2.2H_2O$, and 3.6 g $FeCl_2.4H_2O$ per litre of Hutner's trace elements). This medium was used to induce *C. rienhardtii* hydrogen photoproduction.

Nitrogen-deficient TAP medium (TAP-N) was also prepared in a similar manner to TAP medium except ammonium chloride was replaced with potassium chloride. This medium was used to induce cell mating in *C. reinhardtii*.

### 2.3 *E. coli* strains and growth conditions

Two *E. coli* strains were used: 10-β and KRX competent cells. These self-prepared competent cells were used for cloning and protein expression, respectively. To maintain the cell stocks and prepare these competent cells for their intended purposes, we followed the protocol of Promega (1996). This protocol requires a starting inoculum to start a bacterial culture that would later be prepared to make it competent for transformation. Therefore, we used a small amounts of commercially available competent cells either 10-β competent cells (New England Biolabs, USA) or KRX competent cells (Promega, USA) as inoculum. The prepared competent cells were stored at -80ºC.

*E. coli* was grown in a sterile Lysogeny Broth (LB) medium containing 10 g/l tryptone, 5 g/l yeast extract and 10 g/l sodium chloride. The culture was incubated at 37ºC (Raven Benchtop Incubator; LTE Scientific, UK) and was constantly shaken at 200 rpm

(Stuart Orbital Shaker SSL1, Jencons-PLS, UK). For large-scale cultivation of *E. coli*, a larger incubator was used (Innova 43 Incubator Shaker; New Brunswick Scientific, USA). To grow *E. coli* on a plate, we used LB 1.5% agar (w/v) to which was added an appropriate antibiotic, if applicable, at standard concentrations i.e. 50 µg/ml ampicillin, 50 µg/ml carbenicillin and 50 µg/ml kanamycin. All preparations for growing cells were conducted in a laminar flow cabinet (Microflow Advanced Biosafety Cabinet Class II, Bioquell, UK) to avoid biological contamination.

**2.4 Measurement of chlorophyll concentration**

Chlorophyll concentration was measured according to the method of Porra *et al*. (1989). A cell culture (1 ml) was harvested by centrifugation (16000 g, 5 minutes; AccuSpin Microcentrifuge, Fisher Scientific, USA). To extract the chlorophylls, the cells were re-suspended in 1 ml methanol, and vortexed vigorously (Vortex-Genie 2, Scientific Industries, USA) for 30 seconds. The supernatant, which contained the chlorophylls, was collected by centrifugation (16000 g, 5 minutes; AccuSpin Microcentrifug, Fisher Scientific, USA). The absorbance values for chlorophyll a and b was measured at 652 and 665 nm, respectively, by using a spectrophotometer (UV-1601 UV-Visible Spectrophotometer; Shimadzu Europa, UK). If the cell sample was too concentrated, appropriate dilution was made. The concentration of the total chlorophylls (µg/ml) was estimated by using this formula:

$$\text{Chlorophyll concentration} = [22.12\ (A_{652}) + 2.71\ (A_{665})] \times \text{Dilution factor}$$

**2.5 Determination of cell optical density (OD)**

Optical density (OD) of cells was measured by using a spectrophotometer (UV-1601 UV-Visible Spectrophotometer; Shimadzu Europa, UK) and also a disposable cuvette with an optical path length of 1 cm (VWR International, UK). The optical density was measured at 750 nm and 600 nm for *C. reinhardtii* and *E. coli*, respectively.

**2.6 Cell counting**

*C. reinhardtii* cells were counted by using a hemocytometer (Improve Neubauer; Hawksley, UK) according to the method described by Harris (1989). The cells were viewed with a compound microscope (Kyowa Medilux-12; Finlay Microvision, UK).

## 2.7 Measurement of DNA or RNA concentration

DNA or RNA concentration was measured using a Nanodrop 1000 (Thermo Fisher Scientific, USA) according to the manufacturer's instructions.

## 2.8 Measurement of protein concentration

Protein concentration was measured using the DC Protein Assay (Bio-Rad Laboratories, USA) according to the manufacturer's instructions. This involved measuring a series of protein standards every time a sample was measured. We used bovine serum albumin (BSA; New England Biolabs, USA) in different concentrations as our protein standards (a representative standard curve is given in Appendix 1). The measurements involved measuring the absorbance of the sample at 750 nm using a spectrophotometer (UV-1601 UV-Visible Spectrophotometer; Shimadzu Europa, UK).

## 2.9 DNA restriction digests

Restriction digest was performed with commercially available restriction enzymes (New England Biolabs, USA) according to the manufacturer's instructions. A typical 50 µl reaction consisted of 1 µg of DNA, 5 µl of appropriate 10x buffer, 0.5 µl of 10x bovine serum albumin (if applicable), and 10 units of restriction enzyme(s). Enzymatic digestion was normally performed for 1 hour at 37°C (Raven Benchtop Incubator, LTE Scientific, UK) with constant shaking (200 rpm; Stuart Orbital Shaker SSL1, Jencons-PLS, UK). Heat inactivation of the enzyme(s), if applicable, was carried out by heating the sample for 20 minutes at the manufacturer's recommended temperature. Heating was carried out using a heating block system (QBA1 Dry Block Heating System, Grant, UK). To visualize the digested DNA sample, agarose gel electrophoresis was performed.

## 2.10 Polymerase chain reaction (PCR)

PCR was employed to amplify DNA samples. A typical 50 µl reaction consisted of roughly 5 ng of template DNA, 0.5 µM forward primer, 0.5 µM reverse primer, 1.25 units of DNA Polymerase and 25 µl of 2x FailSafe PCR PreMix G (Epicentre Biotechnologies, USA). All of our primers were synthesized by Invitrogen (UK). PCR was performed using a PeqStar 96 gradient thermocycler (Peqlab Biotechnologies, Germany) with the lid heated at 110°C throughout the reaction. A typical PCR program consisted of an initial denaturation step (98°C for 30 seconds or longer if the template was genomic DNA), followed by 30 cycles of denaturation (98°C for 30 seconds), primer annealing (variable temperature,

depending on the melting temperatures of primers, for 20 seconds) and primer extension (72°C for 30 seconds per kb of expected DNA fragment), and ended with a final extension step (72°C for 5 minutes).

For amplification of DNA to be used for cloning, PCR was carried out using a high-fidelity DNA polymerase i.e. Phusion High Fidelity DNA Polymerase (New England Biolabs, USA). For amplification of DNA to be used for other purposes such as for colony PCR screening, a cheaper *Taq* DNA polymerase (New England Biolabs, USA) was used instead.

### 2.11 Extraction of plasmid from *E. coli*

For a small-scale extraction of plasmid (known as mini preparation) from *E. coli*, a culture had to be prepared. A single colony of *E. coli* was toothpicked and grown overnight in a 3 ml LB medium containing the appropriate antibiotic at 37 °C (Raven Benchtop Incubator, LTE Scientific, UK) and constantly shaken at 200 rpm (Stuart Orbital Shaker SSL1, Jencons-PLS, UK). Commercially available P1, P2 and P3 solutions of QIAMidi Kit (Qiagen, Germany) were used for plasmid extraction. The grown cells (2 ml) were harvested by centrifugation (16000 g, 5 minutes; AccuSpin Microcentrifuge, Fisher Scientific, USA) and re-suspended in 100 µl of the suspension buffer, P1. The cell suspension was mixed with 100 µl of P2 (lysis solution) by inverting the microcentrifuge tube several times, and left for 5 minutes. Neutralization buffer, P3 (100 µl) was subsequently added, and mixed together by inverting the tube a few times. The suspension was incubated on ice for 5 minutes, and subsequently centrifuged at a maximum speed (16000 g; AccuSpin Microcentrifuge, Fisher Scientific, USA). The supernatant was transferred to a new microcentrifuge tube, and centrifuged again to completely remove cell debris. The supernatant was transferred to a new microcentrifuge tube containing 1 ml of absolute ethanol, mixed by inverting the tube several times and left for 5 minutes. A DNA pellet should be seen after spinning down the sample at the maximum speed (16000 g; AccuSpin Microcentrifuge, Fisher Scientific, USA) for 10 minutes. After discarding the supernatant, the pellet was washed with 200 µl of 70% ethanol and centrifuged again to discard the ethanol. The pellet was left to dry before re-suspending it with 50 µl of sterile distilled water or in Tris-EDTA (TE) buffer (10 mM Tris pH 8.0, and 1 mM EDTA), and stored at -20ºC. Agarose gel electrophoresis was normally performed to check the quality of the prepared plasmid.

For a large-scale extraction of plasmid (known as midi preparation) from *E. coli* culture (100 ml), QIAMidi Kit (Qiagen, Germany) was used according to the manufacturer's

instructions. Agarose gel electrophoresis was normally performed to check the quality of the extracted plasmid.

### 2.12 *E. coli* transformation

DNA (~50 ng of plasmid) was mixed with 50 µl of appropriate competent cells (10-β or KRX competent cells) in a microcentrifuge tube, and incubated on ice for 30 minutes. To insert the plasmid into the cells, heat shock transformation was performed. This was carried out by quickly transferring the cell suspension from the ice into a heating block system (QBA1 Dry Block Heating System, Grant, UK) set at 42°C for 45 seconds, and this was followed by incubation on ice again for 2 minutes. These transformed cells were incubated with 500 µl Super Optimal Broth with Catabolite repression (SOC) medium [2% (w/v) tryptone, 0.5% (w/v)) yeast extract, 10 mM sodium chloride, 2.5 mM potassium chloride, 20 mM glucose, 10 mM magnesium chloride and 10 mM magnesium sulphate] at 37°C (Raven Benchtop Incubator, LTE Scientific, UK) for 1 hour with continuous shaking (200 rpm; Stuart Orbital Shaker SSL1, Jencons-PLS, UK). The cells were plated onto an LB 1.5% (w/v) agar plate containing appropriate antibiotic, and incubated again at 37°C (Raven Benchtop Incubator, LTE Scientific, UK) overnight.

### 2.13 Nuclear transformation of *C. reinhardtii*

Three different methods for transforming the nuclear genome of *C. reinhardtii* were tested. These were the electroporation method, the biolistic particle delivery method (also known as the gene gun method) and the glass bead method. It was later decided to use only the electroporation method as a means of transforming *C. reinhardtii* as it was found to be the most effective method for nuclear transformation.

For nuclear transformation by electroporation, *C. reinhardtii* was grown to exponential mid log phase ($OD_{750}$ was ~0.5 and hemocytomer cell count was ~$10^7$ cells/ml). The cells were harvested by centrifugation (1000g, 10 minutes; Allegra 6R Centrifuge, Beckman Coulter, UK) and re-suspended and concentrated in TAP medium, which was supplemented with 40 mM sucrose, to a final concentration of $3x10^8$ cells/ml. In a pre-cooled 4-mm gap electroporation cuvette (Bio-Rad Laboratories, USA), 250 µl of the cells and 1 µg DNA plasmid were mixed together, and the cuvette was put on ice before electroporation. An exponential electric pulse (2000 V/cm) was applied to the sample by using an electroporator (Gene Pulser Xcell Total System, Bio-Rad Laboratories, USA) with the voltage set at 800 V, capacitance at 25 µF and no shunt resistor was used ($R = \infty$). These settings should give a

pulse time of 10 to 13 milliseconds (ms) for CC-124 under the specified conditions. Following electroporation, the cuvette was put back on ice until the cells were ready to be re-suspended in 10 ml TAP medium that was supplemented with 40 mM sucrose. To allow the cells to recover, the cells were incubated overnight at 28ºC with gentle shaking (50 rpm; Lab Companion SK-300 Shaker, Jeio Tech, Korea). The cells were gently harvested by centrifugation (1000g, 10 minutes; Allegra 6R Centrifuge, Beckman Coulter, UK), and plated onto TAP 2% agar (w/v) plates containing the appropriate antibiotic. Colonies of transformants normally appeared after a week.

For transformation using the biolistic particle delivery system, *C. reinhardtii* was similarly grown to exponential mid log phase. A total of $2x10^8$ cells were harvested by centrifugation (1000g, 10 minutes; Allegra 6R Centrifuge, Beckman Coulter, UK), plated onto an TAP 2% agar (w/v) plate containing the appropriate antibiotic, and left to dry in a laminar flow cabinet (Microflow Advanced Biosafety Cabinet Class II, Bioquell, UK). DNA plasmid (1 µg) was precipitated onto gold particles (S550d Gold Carrier Particles; Bio-Rad Laboratories, USA) according to the manufacturer's instructions. DNA-coated gold particles were then immobilized onto a microcarrier disc (Bio-Rad Laboratories, USA), and injected into the green alga by using a biolistic particle delivery system (PDS-1000/He, Bio-Rad Laboratories, USA) that was fitted with a 1350 psi rupture disc and connected to a compressed helium cylinder (BOC, UK).

For transformation by using glass beads, a cell-wall less strain had to be used. *C. reinhardtii* D66 strain grown to exponential mid log phase was harvested by centrifugation (1000g, 10 minutes; Allegra 6R Centrifuge, Beckman Coulter, UK). The cells were re-suspended and concentrated with fresh TAP medium to a final density of $3x10^8$ cells/ml. Plasmid DNA (1 µg) was mixed with 330 µl of the cell suspension in a sterile microcentrifuge tube containing 0.3 g of sterile glass beads (Sigma Aldrich, UK). The mixture was vortexed vigorously at a maximum setting (Vortex-Genie 2, Scientific Industries, USA) for 15 seconds. The resulting cell suspension was further diluted with 300 µl of TAP medium before being plated gently onto TAP 2% agar (w/v) plates containing the appropriate antibiotic.

### 2.14 Cell mating

*C. reinhardtii* cells can be mated together if two algal strains are of the opposite mating types, mating type *plus* (*mt*+) and *minus* (*mt*-). To check for the mating type of a

particular strain, the unknown strain could be mated with other algal strains of known mating type, such as CC-124 (*mt*-) and CC-125 (*mt*+).

To induce mating in *C. reinhardtii*, cells were grown to mid-log phase in TAP medium. The cells were harvested by centrifugation (1000g, 5 minutes; Allegra 6R Centrifuge, Beckman Coulter, UK), and re-suspended in the same volume with TAP-N. The cells were incubated in this nitrogen-deprived medium for 3 to 4 days at 28ºC, ~30 $\mu Em^{-2}s^{-1}$ (cool white fluorescent light, Philips, UK) and with constant shaking (100 rpm, Lab Companion SK-300 Shaker; Jeio Tech, Korea). Two algal strains were directly mixed together in equal volumes, and the cell mixture was left under a strong light ~150 $\mu Em^{-2}s^{-1}$ (cool white fluorescent light, Philips, UK) without shaking or stirring. After 3 to 4 hours, 4 x 100 µl of the cell mixture were gently collected and spotted onto a 3% (w/v) TAP agar plate containing the appropriate antibiotic. The cell spots were left to dry in a laminar flow cabinet (Microflow Advanced Biosafety Cabinet Class II, Bioquell, UK). Once dried, the plate was left overnight under a medium light ~30 $\mu Em^{-2}s^{-1}$ (cool white fluorescent light, Philips, UK). The next day the plate was covered with aluminium foil and left for one to two weeks to allow the zygotes to mature. The remaining cell mixture was also left overnight to determine the efficiency of mating. On the following day, if the mating was successful, the cells would form a big clump that normally adhered to the container. When shaken, the clump would not resuspend. However, if mating was not successful, the cells would not stick to the container and would resuspend easily when shaken.

After a week, the cell spot was gently scraped with a sharp blade. This would remove most of the vegetative cells but the zygotes would attach tightly onto the 3% (w/v) TAP agar. By using a compound microscope (Kyowa Medilux-12; Finlay Microvision, UK), the zygotes were observed and would appear larger than the vegetative cells, yellowish in colour, and had blackish cell wall. The plate was treated for 60 seconds with chloroform vapour to kill the vegetative cells. The spot was cut with a blade to produce a small agar block containing the zygotes. The small agar block was transferred into a tube containing 2 ml of TAP medium, and exposed to a high light again (~150 $\mu Em^{-2}s^{-1}$; cool white fluorescent light, Philips, UK) without shaking the medium. This was to allow the zygotes to germinate. A control was also set up, whereby another agar block was left on an agar plate and was similarly exposed to the high light. After 24 to 48 hours, when the control agar block was observed to already have germinated zygotes, the tube was vigorously vortexed (Vortex-Genie 2, Scientific Industries, USA) for 1 minute. The cell suspension (100 µl) was subsequently plated onto 2% (w/v) TAP

agar plate containing the appropriate antibiotic. Colonies of daughter cells would normally appear after a week.

### 2.15 Agarose gel electrophoresis

Analysis of DNA samples was performed by agarose gel electrophoresis. Depending on the sizes of DNA fragments to be analysed, 1 or 2% (w/v) agarose gel was prepared. This was carried out by dissolving agarose in Tris-acetate-EDTA (TAE) buffer containing 40 mM Tris pH 8.0, 20mM acetic acid and 1 mM EDTA. To dissolve it, the solution was boiled for a few minutes by using a conventional microwave (Daewoo Electronics, UK). Once dissolved, the solution was cooled down under a running tap water. SYBR Safe (Invitrogen Life Technologies, USA) was added into the solution (1 µl SYBR Safe in 20 ml solution). The agarose gel was moulded by using PerfectBlue Minigel System (PeqLab, UK).

A DNA sample (5 µl) to be electrophoresed was mixed with 6x loading dye (1 µl) that contained 0.25% (w/v) Orange G dye (or xylene cyanol dye) and 40% (w/v) sucrose. The mixture was loaded into the well of the agarose gel. To approximate the DNA size, 5µl of DNA ladder (2-Log DNA Ladder, New England Biolabs, USA) was also loaded into an adjacent well. The gel was run by using PerfectBlue Minigel System (PeqLab, UK) for 10 to 20 minutes at a constant voltage (120 V) (PowerPac Basic Power Supply; Bio-Rad Laboratories, USA) in TAE buffer. After electrophoresis, the DNA was visualized and photographed using a GelDoc-It Imaging System (UVP, USA).

Analysis of RNA samples, for checking the quality of extracted RNA, was also performed by agarose gel electrophoresis. The procedure was similar to the analysis of DNA samples. However, when mixing a RNA sample with the 6x loading dye, formaldehyde (1 µl) was also added into the mixture.

To prepare a working solution of DNA ladder, 5 µl of 2-Log DNA Ladder stock solution (1000 µg/ml; New England Biolabs, USA) was mixed with 20 µl of the 6x loading dye and 125 µl of distilled water.

### 2.16 Protein gel electrophoresis

For protein analysis by sodium dodecyl sulphate polyacrylamide gel electrophoresis (SDS-PAGE), a denatured protein sample had to be initially prepared. In this work, the protein samples were obtained either from *C. reinhardtii* whole cell extract or from *E. coli* overexpressed protein. To prepare whole cell extracts from *C. reinhardtii*, 1 ml of cell culture ($OD_{750}$ 1.0) was harvested by centrifugation (16000 g, 5 minutes; AccuSpin Microcentrifug,

Fisher Scientific, USA), and the cells were re-suspended in 100 µl of 1x SDS protein sample buffer that contains 62.5 mM Tris pH 6.8, 10% (v/v) glycerol, 2% (w/v) SDS, 0.05% (w/v) bromophenol blue dye, and fresh 10% (v/v) β-mercaptoethanol. The cell suspension was quickly boiled (100°C; QBA1 Dry Block Heating System, Grant, UK) for 10 minutes, and stored at -20ºC for future use. To prepare protein sample from *E. coli* overexpressed protein, protein sample was mixed with an equal volume of 2x sample buffer (similar as above but 2x concentrated), and as above, boiled for 10 minutes and stored at -20ºC before being used for SDS-PAGE.

A SDS-polyacrylamide gel is composed of two parts: a stacking gel (the top layer) and a resolving gel (the bottom layer). To prepare the gel, stock solutions had to be prepared and mixed together (Table 2.2). To cast the gel, two glass plates (0.75mm spacer), casting stand, and casting clamp (Mini Protean System, Bio-Rad Laboratories, USA) were used. The resolving gel was cast first by pouring the mixture into the glass mold. To allow the gel to solidify, isopropanol was poured on top of the resolving gel. Once solidified, the isopropanol was washed away with distilled water, and the excess water was removed by absorption with Whatman filter paper. The stacking gel was subsequently poured on top of the solidified resolving gel, and 15-well comb (Mini Protean, Bio-Rad Laboratories, USA) was quickly inserted into the gel to create wells. Once solidified, the gel could be stored at 4ºC by wrapping it with moisten blue roll and plastic wrap (to prevent dehydration) for up to one week.

To run protein samples using the gel, each well was carefully loaded with 10 µl (maximum volume) of the prepared protein sample. To approximately determine protein size, a well was also loaded with 3 µl of protein ladder. We used either Low Molecular Weight SDS Calibration Kit for SDS Electrophoresis (GE Healthcare Life Sciences, USA), which was prepared according to the manufacturer's instruction, or Precision Plus Protein Standards (Bio-Rad Laboratories, USA). The gel was run in a electrophoresis cell (Mini Protean, Bio-Rad Laboratories, USA) by using Tris-glycine running buffer, which contains 25 mM Tris pH 8.3, 190 mM glycine, and 0.1% (w/v) SDS, at constant voltages, 100-120 V (PowerPac Basic Power Supply; Bio-Rad Laboratories, USA). It was run until the bromophenol blue dye, which could be found in the prepared protein sample, had reached the bottom of the resolving gel. After electrophoresis, the gel was used either for Coomassie Brilliant Blue staining or immunoblotting.

| | 5% Stacking gel | 10% Resolving gel | 12.5% Resolving gel |
|---|---|---|---|
| **40% (w/v) Acrylamide-bis (37.5:1)** | 1.35 ml | 6.25 ml | 7.8 ml |
| **3M Tris pH 8.9** | - | 5 ml | 5 ml |
| **1M Tris pH 6.8** | 1.2 ml | - | - |
| **Urea** | - | 9 g | 9 g |
| **10% (w/v) SDS** | 100 µl | 300 µl | 300 µl |
| **TEMED** | 8 µl | 5 µl | 5 µl |
| **Fresh 10% (w/v) APS** | 80 µl | 150 µl | 150 µl |
| **Total volume** | 10 ml | 25 ml | 25 ml |

**Table 2.2. Composition of SDS polyacrylamide gel.**

The volumes for this recipe are for the preparation of six mini gels. After addition of urea, the pH must be re-adjusted. TEMED and APS should be added last for polymerisation, and 10% (w/v) APS solution has to be freshly prepared for every gel casting. The final acrylamide concentrations (10 or 12.5%) for the resolving gel depend on the sizes of proteins to be analysed.

### 2.17 Coomassie Brilliant Blue staining

For Coomassie Brilliant Blue staining, the SDS-polyacrylamide gel was stained with Coomassie staining solution, which contains 40% (v/v) ethanol, 10% (v/v) acetic acid, and 0.2% (w/v) Coomassie brilliant blue R250, for at least an hour with a constant gentle swirling (Stuart Gyro Rocker SSL3, Scientific Laboratory Supplies, UK). After staining, the gel was de-stained overnight with 10% acetic acid solution also with gentle swirling (20 rpm). A picture of the de-stained gel was taken using a GelDoc-It Imaging System (UVP, USA).

### 2.18 Immunoblotting

For immunoblotting, the proteins from the gel were transferred onto 0.2 µm nitrocellulose membrane (Bio-Rad Laboratories, USA) or polyvinylidene difluoride (PVDF; Life Technologies, UK), either by using a dry or a semi-dry blotting method. For the dry blotting method, iBlot Dry Blotting System (Invitrogen Life Technologies, USA) and iBlot Gel Transfer Stacks PVDF (Life Technologies, UK) were used according to the manufacturer's instructions. For the semi-dry blotting method, transfer of proteins was carried out in Mini Trans-Blot Electrophoretic Transfer Cell (Bio-Rad Laboratories, USA) with a transfer buffer, which contains 3 mM sodium carbonate, 10 mM sodium bicarbonate and 20% (v/v) methanol, at constant voltage (55 V) and 4ºC.

The membrane was blocked with a blocking solution for an hour at room temperature with gentle swirling (Stuart Gyro Rocker SSL3, Scientific Laboratory Supplies, UK). A blocking solution contains 5% (w/v) dried skimmed milk dissolved in phosphate buffered saline Tween (PBS-T) solution, which contains 145 mM sodium chloride, 7.5 mM disodium hydrogen phosphate, 2.5 mM sodium dihydrogen phosphate and 0.1% (v/v) Tween 20. The blocked membrane was rinsed with PBS-T solution. The rinsed membrane was subsequently incubated overnight with 10ml of PBS-T solution containing diluted primary antibody (Table 2.3) at 4ºC and with gentle swirling (Stuart Gyro Rocker SSL3, Scientific Laboratory Supplies, UK). The membrane was washed three times with PBS-T for 20 minutes per wash. It was incubated again for an hour at room temperature with 10 ml of PBS-T solution containing 1:10,000 diluted secondary antibody (ECL Anti-Rabbit IgG Horseradish Peroxidase Linked Whole Antibody; Amersham, UK). The membrane was washed three times with PBS-T solution for 10 minutes per wash, and washed one time with PBS solution (similar to PBS-T solution but without Tween 20) for 10 minutes.

| Antibody | Working dilution (antibody: PBS-T) | Target protein | Expected size (kDa) |
|---|---|---|---|
| **αADH1** | 1:2000 | ADH1 | 102 |
| **αPFL1** | 1:3000 | PFL1 | 91 |
| **αPDC3** | 1:2000 | PDC3 | 61 |
| **αHYDA** | 1:5000 | HYDA1 & HYDA2 | 53 |
| **αLDH** | 1:5000 | LDH | 45 |
| **αPDC1** | 1:10000 | PDC1 (PDH) | 43 |
| **αPDC2** | 1:10000 | PDC2 (PDH) | 43 |
| **αD1** | 1:5000 | D1 | 30 |
| **αPSAD** | 1:5000 | PSAD | 20 |

**Table 2.3. Polyclonal antibodies used.**

All antibodies were prepared in our lab by Burgess (2011) except for αD1 which was prepared by Prof. Peter J. Nixon (Imperial College London) and αPSAD which was kindly provided by Prof. Jean-David Rochaix, University of Geneva). All antibodies were raised in rabbits.

To develop the membrane, an enhanced chemiluminescence (ECL) method was used. The membrane was incubated for 30 seconds with 5 ml of ECL Solution A (100 mM Tris pH 8.5, 0.4 mM p-coumaric acid and 2.5 mM luminol) and 5 ml of ECL Solution B (100 mM

Tris pH 8.5 and 100 mM hydrogen peroxide). After draining the excess ECL solutions off the membrane, a transparent plastic sheet was put on top of the membrane and this was followed by a sheet of X-ray film (SLS Laboratories, UK). The X-ray was exposed to the membrane in a dark room (with red light) for a short duration of time. The exposed X-ray film was developed using Curix60 Table Top Processor (AGFA Healthcare, Belgium). The picture of the developed X-ray film was taken using a GelDoc-It Imaging System (UVP, USA). Alternatively, after incubating the membrane with ECL solutions, the membrane was simply developed and viewed with Fujifilm LAS-3000 (Raytek Scientific, UK).

**2.19 Transcript analysis**

*C. reinhardtii* was grown to late log phase ($OD_{750}$ ~1.0), and 5 ml of culture was harvested by centrifugation (1000g, 10 minutes; Allegra 6R Centrifuge, Beckman Coulter, UK). For RNA extraction, RNeasy Plant Mini Kit (Qiagen, Germany) was used according to the manufacturer's instructions. The extraction also included DNase treatment of the extracted RNA sample by using RNase-free DNase Set (Qiagen, Germany). To check the quality of the extracted RNA sample, agarose gel electrophoresis was carried out.

The extracted RNA sample (125 ng) was converted to complementary DNA (cDNA) using a High-Capacity cDNA Reverse Transcription Kit (Applied Biosystems, USA) according to the manufacturer's protocol.

To relatively quantify the transcript levels, quantitative real time PCR (qRT-PCR) was chosen. Taqman Gene Expression Assay System (Applied Biosystems, USA) was used for this purpose, whereby a single 10 µl reaction consisted of 1 µl of 1:5 diluted cDNA, 5 µl of Taqman Fast Universal PCR Master Mix, and 0.5 µl of Taqman Gene Expression Assay which consisted of designed probe and primers (Table 2.4). The qRT-PCR was carried out by using ABI 7500 Fast Real Time PCR machine (Applied Biosystems, USA) according to the manufacturer's protocol. Following the instructions of the manufacturer (Applied Biosystems, USA), the data obtained from the qRT-PCR were analysed by using a standard curve method, and the data were normalised with the reference transcript which was *RPL10A*. This transcript encodes 60S ribosomal protein L10a.

| Transcript | Primers and probe | Sequence |
|---|---|---|
| ***PDC3*** | *PDC3* forward | GGACCAGCTGCTCAAGCA |
| | *PDC3* reverse | CGCATTCAGCTCGTTGCA |
| | *PDC3* probe | ACCAGGGACAGCTCG |
| ***LDH*** | *LDH* forward | GCAGTGCTGTTCGTGAATGAC |
| | *LDH* reverse | ACCCGCCTTGGCTAACTC |
| | *LDH* probe | ATGCGTCGGTGATCAA |
| ***RPL10A*** | *RPL10A* forward | CCTGCTCCTATCAACAAGAACCT |
| | *RPL10A* reverse | GAACTTGATGCTGCACTTGGT |
| | *RPL10A* probe | CCAGCACCATCTCCTC |

**Table 2.4. Taqman Gene Expression Assay.**

The primers were kindly provided by Dr. Steven J. Burgess.

### 2.20 Gas measurements

For determination of hydrogen gas and carbon dioxide produced under the condition of sulphur deprivation, *C. reinhardtii* was grown to late log phase ($OD_{750}$ ~1.0) in TAP medium. The cells (225 ml) were harvested by centrifugation (1000g, 10 minutes; Allegra 6R Centrifuge, Beckman Coulter, UK), and washed once with TAP-S medium. The cells were re-suspended in 325 ml TAP-S medium, and transferred to a custom-made mini bioreactor (Figure 2; Cambridge Glassblowing, UK) which was designed to be air tight.

Cell samples were taken from the culture sampling port using a syringe, which was fitted with a needle, to be used for SDS-PAGE protein sample and also for chlorophyll measurement. Data were normalised to the chlorophyll amount. Typically, the chlorophyll concentrations would be in the range of 15 to 20 µg/ml. The cells were incubated at 28°C, continuously stirred (RO 10 Power Magnetic Stirrer; IKA, UK) and illuminated with high light intensity (150 $\mu Em^{-2}s^{-1}$; cool white fluorescent light, Philips, UK).

The volume of gases evolved was determined by a water displacement method. The gases produced by the cells would enter the inner tubing of the gas collection tube, and this would displace the distilled water found in the outer tubing of the gas collection tube. For this mini bioreactor, as determined, 0.8 cm of water displaced in the outer tubing would equal to a volume of 1 ml. The total volume of water displaced by the gases would represent the total volume of gas evolved by the algal cells. To calculate the no. of moles of gas based on the gas volume, the ideal gas equation was used, n = PV/RT, where n is the no.of moles of gas, P

is the pressure of the gas (1 atm), V is volume of gas, R is the gas constant (0.08206 L.atm/mol//K), and T is temperature of the gas (298 K).

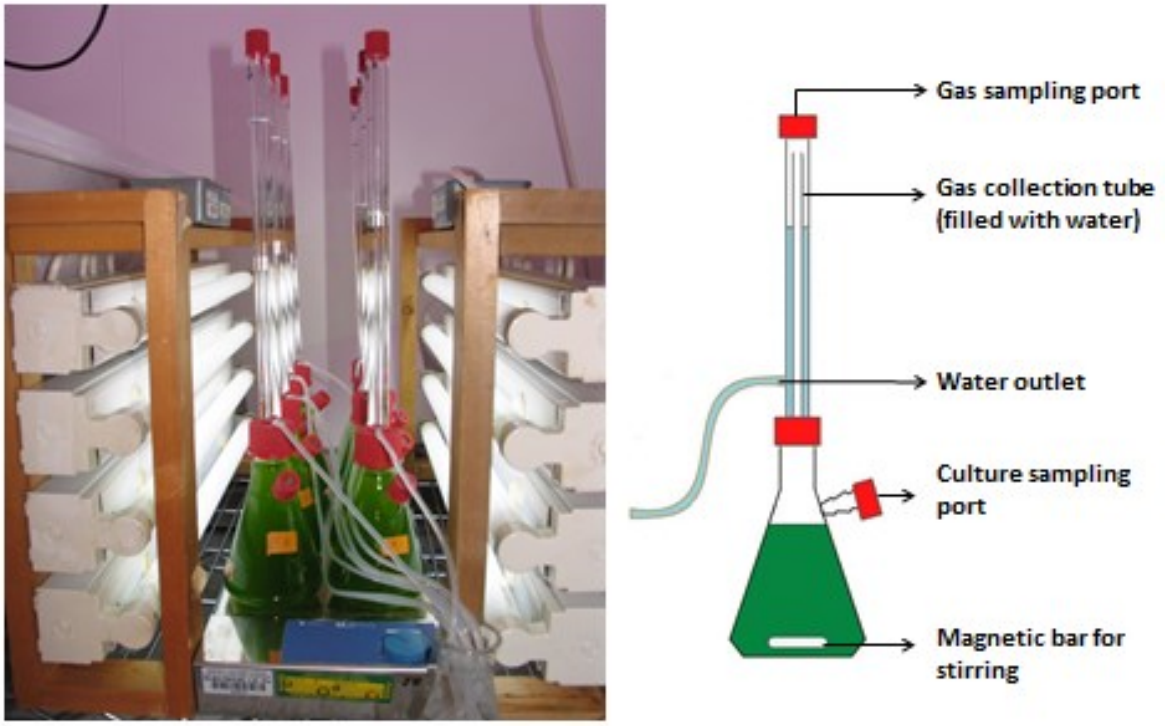


**Figure 2 Mini bioreactors for gas analysis.**

The schematic diagram of the mini bioreactor is kindly drawn by Mr. Marcos Perez (Imperial College London).

To determine the composition of the gases produced, a sample of the headspace gases was taken from the gas sampling port with an air-tight 1 ml Hamilton syringe (Hamilton, Switzerland), and injected immediately into a gas chromatograph (GC2014 model; Shimadzu, Japan). The gas composition was measured according to the manufacturer's instruction with the settings of 200 µl gas injection volume, 30 ml/min flow rate of the carrier gas (compressed helium research grade; BOC, UK), 35°C column (CTR1 concentric packed column 8700; Alltech, UK) and 110°C detector (thermal conductivity detector). The gas chromatograph would produce a chromatogram made up of peaks. Each peak represent different types of gas, and the area under the peak would be measured. To convert the peak area into the amount (%) of gas, the GC was calibrated with known amounts (%) of gases following the previous method by Burgess (2011). The GC was injected with either a gas mixture (10% $N_2$, 80.3% $H_2$ and 9.7% $CO_2$; BOC, UK) or a pure hydrogen gas (BOC, UK),

and the peak area for 1% of each gas was subsequently calculated from the total peak area generated by each gas.

### 2.21 Isolation of intracellular materials from *C. reinhardtii*

To extract the intracellular materials from *C. reinhardtii* for enzyme assays, the cells were grown to late log phase ($OD_{750}$ ~1.0) in TAP medium. The cells (50 ml) were harvested by centrifugation (1000g, 10 minutes; Allegra 6R Centrifuge, Beckman Coulter, UK) and washed once with buffer (25 mM sodium phosphate at pH 7.5, and 250 mM sodium chloride). This buffer was the same buffer used in the enzyme assays. The cells were concentrated 10x with the buffer. The cells were lysed using a sonicator (Vibra Cell Ultrasonic Processor; Sonics, USA) with the amplitude set to 50%, and the pulser set to 2 seconds. The total processing time was 5 minutes, and the cells were always kept on ice during the sonication. The cellular debris was removed from the cell lysate by centrifugation (21000g, 4ºC, Centrifuge 5424R; Eppendorf, UK). The supernatant was collected to be used for enzyme assays, protein concentration determination, and also SDS-PAGE analysis.

### 2.22 Excreted metabolite analysis

For dark anaerobic metabolite analysis, *C. reinhardtii* cells were grown to late log phase ($OD_{750}$ ~1.0) in TAP medium, harvested by centrifugation (1000g, 5 minutes; Allegra 6R Centrifuge, Beckman Coulter, UK), washed twice with HSM, and resuspended and concentrated 20x in HSM (chlorophyll concentration ~ 150 μg/ml). In air-tight vial (7 ml Bijou bottle fitted with 12.5 mm rubber stopper; VWR International, UK), 5 ml of cell suspension was purged with argon for 5 minutes. The vial was left in the dark at 28ºC and constantly shaken (100 rpm; Lab Companion SK-300 Shaker; Jeio Tech, Korea). After 4 or 8 hours of incubation, the cells were harvested in the dark by centrifugation (1000g, 5 minutes; Allegra 6R Centrifuge, Beckman Coulter, UK), and the supernatant was collected and filtered using 0.2 μm Acrodisc Syringe Filters with Supor Membrane (Pall, USA).

For metabolite analysis under sulphur-deprived conditions, 1 ml of cell sample was collected as described in Section 2.20. The sample was centrifuged (16000 g, 5 minutes; AccuSpin Microcentrifuge, Fisher Scientific, USA), and the resulting supernatant was collected. The collected supernatant was re-centrifuged to make sure all cells were completely removed, as no syringe filtration could be carried out due to the small sample volume.

All supernatant samples were stored at -20°C before being quantitatively analysed for excreted metabolites. The analysis was performed using two techniques i.e. proton nuclear magnetic resonance ($^1$H NMR) spectroscopy and high pressure liquid chromatography (HPLC).

For the $^1$H NMR analysis, the work was carried out in collaboration with Dr. Volker Behrends and Dr. Jacob Bundy (Imperial College London). To prepare the sample for $^1$H NMR spectroscopy, 480 µl of the supernatant was mixed with 120ul of NMR buffer (0.97mM DSS, 4.5mM sodium azide, 90% $D_2O$, and 50mM phosphate buffer pH7.2). The mixture was centrifuged (16000 g, 4ºC, 5 minutes, AccuSpin Microcentrifuge; Fisher Scientific, USA) to remove any potential precipitate, and only 550 µl of the resulting supernatant was poured into an NMR tube (VWR International, UK). The sample was analysed with a Bruker Avance DRX600 NMR spectrometer (Bruker BioSpin, Germany), and the generated data were processed with iNMR (Nucleomatica, Italy) and Chenomx NMR suite (Chenomx, Canada). The metabolites were quantified relative to the NMR standard (DSS).

For the HPLC analysis, the work was carried out in collaboration with Ms. Charlotte E. Ward (Imperial College London). The supernatant was directly injected into the HPLC system (Jasco, UK). This system consisted of a UV-2075 plus UV/Vis spectrophotometer (set at 210 nm) and a RI-2031 plus refractive index (RI) detector. The metabolites were separated using an Aminex HPX87H ion exclusion column (Bio-Rad Laboratories, UK) with 10 mM sulphuric acid (HPLC quality) as the mobile phase (flow rate 0.6 ml/min, 35ºC). The data obtained from the spectrophotometer and RI detector were processed with ChromPass software (Jasco, UK). The metabolites were quantified by using generated standard curves.

### 2.23 Construction of artificial microRNAs

Two pairs of single-stranded oligonucleotides (Table 2.5), which would be used for the construction of double-stranded artificial microRNAs, were kindly provided by Dr. Steven J. Burgess. The oligonucleotides were designed using Web microRNA designer according to Molnar *et al*. (2009) and would target the *C. reinhardtii D-LDH* transcript. The expression vector (named pChlamiRNA3int) that would be used to express the constructed artificial microRNAs was kindly provided by Dr. Attila Molnar (University of Cambridge).

The construction of a plasmid containing artificial microRNA was carried out according to the protocol by Molnar *et al*. (2009). Briefly, a pair of the single-stranded oligonucleotides (forward and reverse) were annealed together to form a double stranded

oligonucleotide which was then phosphorylated. The circular expression vector was linearized by restriction digest, and was then dephosphorylated. The phosphorylated double-stranded oligonucleotide was ligated to the dephosphorylated and linearized expression vector. The ligation mixture was used to transform 10-β competent *E. coli* cells in order to clone the constructed plasmid.

| Oligonucleotide | Sequence | Plasmid |
|---|---|---|
| **LDH3 Forward** | ctagtAGGCACCTTACGGATGGATAAtctcgctgatcggca ccatgggggtggtggtgatcagcgctaTTATGCATCCGTAAGG TGCCTg | pLDH3 |
| **LDH3 Reverse** | ctagcAGGCACCTTACGGATGCATAAtagcgctgatcacc accacccccatggtgccgatcagcgagaTTATCCATCCGTAAG GTGCCTa | |
| **LDH4 Forward** | ctagtGTGCTTGCCTATGACAACAAAtctcgctgatcggca ccatgggggtggtggtgatcagcgctaTTTGATGTCATAGGCA AGCACg | pLDH4 |
| **LDH4 Reverse** | ctagcGTGCTTGCCTATGACATCAAAtagcgctgatcacca ccacccccatggtgccgatcagcgagaTTTGTTGTCATAGGCA AGCACa | |

**Table 2.5. Oligonucleotides used for the construction of artificial microRNAs to target *D-LDH* transcript.**

Upper case refers to sequences complementary to *C. reinhardtii D-LDH* transcript.

Colony PCR screening was carried out according to Molnar *et al*. (2009) to screen for potential *E. coli* colonies containing the desired plasmid. Once the positive clones were identified, the plasmid was extracted by mini preparation. The extracted plasmids were sent for sequencing (Eurofins MWG Operon, UK) using the recommended sequencing primers i.e. forward (TATGGGTGTTGGGTCGGTG) and reverse (TAGCGCTGATCACCACCACCC) (Molnar *et al*., 2009). To check and compare the DNA sequences, we used a multiple sequence alignment program, ClustalW2 (http://www.ebi.ac.uk/Tools/msa/clustalw2/) (Thompson *et al*., 1994). Once the plasmids with the correct sequence and orientation were identified, the plasmid was prepared on a large scale by carrying out a midi preparation. The plasmid obtained from the midi preparation would be used for the nuclear transformation of

*C. reinhardtii*. A total of two plasmids were constructed and used, which were named as pLDH3 and pLDH4.

Graphic maps of the plasmids were drawn by using a software called A plasmid Editor (ApE) (http://biologylabs.utah.edu/jorgensen/wayned/ape/).

### 2.24 Construction of plasmids for *E. coli* protein expression

To synthesize the *LDH* gene from *C. reinhardtii* for protein expression in *E. coli*, the putative *LDH* gene sequence was first obtained from the *C. reinhardtii* database (Phytozome; http://www.phtoyzome.net/; Gene ID: Cre07.g324550). This gene sequence was subsequently sent to a company (Biomatik, Canada) to be synthesized. The manufacturer was requested to codon optimise the gene sequence for expression in *E. coli*, and the synthesized gene was also requested to be inserted into the manufacturer's standard vector (pBMH). This led to the production of a plasmid which we named as pBMH-LDH (Table 2.6).

| Plasmid | Description | Source |
|---|---|---|
| **pRSETA-thr** | Modified pRSETA vector (Invitrogen Life Technologies, USA), *E. coli* expression, and ampicillin resistant. | Dr. Ernesto Cota |
| **pRSETA-thr-LDH** | Mature *D-LDH* from *C. reinhardtii* inserted into pRSETA-thr. | This work |
| **pBMH-LDH** | Full length *D-LDH* from *C. reinhardtii* inserted into pBMH, and ampicillin resistant. | Biomatik, Canada |
| **pET28b** | *E.coli* expression vector, and kanamycin resistant. | Novagen, Germany |
| **pET28b-LDH** | Mature *D-LDH* from *C. reinhardtii* inserted into pET28b. | This work |

**Table 2.6. List of plasmids used.**

Mature gene means the putative chloroplast transit peptide was removed from the full length gene sequence. Dr Ernesto Cota (Imperial College London) kindly provided one of the plasmids.

The synthesized pBMH-LDH was used as a PCR template for the construction of two others plasmids named as pRSETA-thr-LDH and pET28b-LDH (Table 2.6). The putative D-LDH gene from the template plasmid would be copied by using PCR. However, the putative chloroplast transit peptide found on the gene sequence would not be copied, and this

modified *D-LDH* gene without the transit peptide was called the mature *D-LDH* gene. The putative chloroplast transit peptide was predicted using several programs i.e. TargetP (Emanuelsson *et al*., 2007), ChloroP (Emanuelsson *et al*., 1999), SignalP (Petersen *et al*., 2011), and MitoProt (Claros & Vincens, 1996). These online programs are available at http://www.cbs.dtu.dk/services/ and http://ihg.gsf.de/ihg/mitoprot.html. To construct the two other plasmids, the PCR fragment of the mature *LDH* gene would have to be inserted into an *E.coli* expression vector, either pRSETA-thr or pET28b (Table 2.6).

To do the above, we used the In-Fusion HD Cloning Kit (Clontech Laboratories, USA) according to the manufacturer's instructions. Briefly, primers were specifically designed for the generation of PCR fragment containing the mature *LDH* gene and also some bases complementary to the expression vector (Table 2.7). We used OligoCalc (Kibbe, 2007; http://www.basic.northwestern.edu/biotools/oligocalc.html) to predict the melting temperatures of the primers. The designed primers had to be first tested for their optimal PCR annealing temperature, and several annealing temperatures (50 to 70°C) were tested simultaneously by using gradient PCR (PeqStar 96 gradient thermocycler; Peqlab Biotechnologies, Germany). Once the optimal temperature was determined, the PCR fragment was generated and subsequently purified by gel extraction using QIAquick Gel Extraction Kit (Qiagen, Germany) according to the manufacturer's instructions. Alternatively, the generated PCR fragment could also be purified by using QIAquick PCR Purification Kit (Qiagen, Germany) according to the manufacturer's instructions. To generate a linearized vector, restriction digest was performed by using the appropriate restriction enzymes (New England Biolabs, USA) which were Bam-HI and XhoI for pRSETA-thr, and NcoI and XhoI for pET28b. The digested vector was also purified by gel extraction. The purified PCR fragment was fused to the purified and linearized vector by using the In-Fusion HD Enzyme Premix (In-Fusion HD Cloning Kit; Clontech Laboratories, USA) according to the manufacturer's instructions. The resulting In-Fusion reaction mixture (2.5 µl) was used to transform 50 µl of self-prepared 10-β *E. coli* competent cells by heat shock transformation.

Potential *E. coli* transformants were screened by using restriction digests. Plasmids were extracted by mini preparation, and subsequently digested with the appropriate restriction enzymes (New England Biolabs, USA). Once the desired plasmid was identified, the plasmid from the positive clone was prepared in large quantity by midi preparation. To further confirm we obtained the correct plasmid, the purified plasmid from the midi preparation was re-checked with restriction digests, and was also sent for DNA sequencing (Beckman Coulter Genomics, UK). The plasmid was sequenced by using two universal primers which were T7P

primer (forward primer; TAATACGACTCACTATAGGG) and also T7-REV primer (reverse primer; TAGTTATTGCTCAGCGGTGG) (Beckman Coulter Genomics, UK). Once the plasmid was confirmed, it was used to transform self-prepared *E. coli* KRX competent cells by heat shock transformation.

Graphic maps of the plasmids were drawn by using a software called A plasmid Editor (ApE) (http://biologylabs.utah.edu/jorgensen/wayned/ape/).

| Plasmid | Primer | Sequence |
|---|---|---|
| **pET28b-LDH** | F10 | AGGAGATATACCATGGCGCTGAACGTTGGTCCG |
| | R10 | GGTGGTGGTGCTCGAGAGTCTTGCCTGCCGGTGC |
| **pRSETA-thr-LDH** | F20 | GGTTCCGCGTGGATCCGCGCTGAACGTTGGTCCG |
| | R20 | AGCTGCAGATCTCGAGTTAAGTCTTGCCTGCCGGTG |

**Table 2.7. Primers for constructing plasmids.**

Underlined sequence refers to the bases which are complementary to the expression vector (either pET28b or pRSETA-thr) while the sequence, which is not underlined, refers to the bases complementary to the *LDH* gene. This is to allow for the amplification of the LDH gene by PCR and subsequently its fusion with with the vector. Primers are in pair, forward (F) and reverse (R).

### 2.25 Determination of *E. coli* protein overexpression and solubility

This work was carried out in collaboration with Dr. Justin A. Yeoman (Imperial College London). A single colony of freshly transformed *E. coli* KRX was toothpicked and grown in 5 ml LB medium containing the appropriate antibiotic at 37°C overnight (Raven Benchtop Incubator, LTE Scientific, UK) with continuous shaking (200 rpm; Stuart Orbital Shaker SSL1, Jencons-PLS, UK). This overnight culture was subsequently used as an inoculum, whereby 50 µl of the overnight culture was used to inoculate 5 ml LB. The 5 ml culture was similarly incubated at 37°C for a few hours until it reached $OD_{600}$ of ~0.5. Rhamnose was then added to a final concentration of either 0.1 or 0.01% (w/v) to induce protein expression. A control (un-induced sample) was also set up by not adding any rhamnose. The culture was transferred to a new incubator set at either 18 or 30°C (Innova 43 Incubator Shaker, New Brunswick Scientific, USA), and incubated overnight with continuous shaking (200 rpm).

The cells from the culture (2 ml) were harvested by centrifugation (16000 g, 5 minutes; AccuSpin Microcentrifuge, Fisher Scientific, USA) to be used for the determination of the *E. coli* protein overexpression and also to test the solubility of the overexpressed

protein if there was any. To do this, BugBuster Protein Extraction Reagent (Novagen, USA) was used according to the manufacturer's protocol. The kit was used to lyse the bacterial cells and separate the proteins into soluble and insoluble fractions. The protocol also included the purification of the insoluble fraction with lysozyme according to the manufacturer's instructions, and also the re-suspension of this purified inclusion bodies using the BugBuster reagent in the same volume used to obtain the soluble fraction. The soluble and insoluble protein fractions were analysed by SDS-PAGE and the resulting gel was stained with Coomassie Brilliant Blue stain.

**2.26 Large scale protein expression and purification**

This work was carried out in collaboration with Dr. Justin A. Yeoman (Imperial College London). A single colony of freshly transformed *E. coli* KRX was toothpicked and grown in 10 ml LB medium containing 50 µg/ml kanamycin at 37°C overnight (Raven Benchtop Incubator, LTE Scientific, UK) with continuous shaking (200 rpm; Stuart Orbital Shaker SSL1, Jencons-PLS, UK). This overnight culture (2 x 5 ml) was used to inoculate 2 x 500 ml of LB medium with 50 µg/ml kanamycin, and was grown for 2 to 3 hours at 37ºC with continuous shaking at 200 rpm (Innova 43 Incubator Shaker; New Brunswick Scientific, USA) until the $OD_{600}$ reached ~0.5. The culture was subsequently induced by the addition of rhamnose to a final concentration of 0.1% (w/v), and grown at 30ºC with continuous 200 rpm shaking (Innova 43 Incubator Shaker; New Brunswick Scientific, USA). The cells from the overnight culture were harvested by centrifugation (4500g, 4ºC, 10 minutes, Sorvall RC6+ Centrifuge; Thermo Scientific, UK), and the cell pellet could be stored at -80ºC before further use.

The cell pellet was re-suspended in 50 ml of buffer (25 mM sodium phosphate pH 7.5, 250 mM sodium chloride, and 25 mM imidazole), and the cell suspension was protected with one tablet of Roche complete EDTA-free Protease Inhibitor Cocktail (Roche, Germany). The cells were lysed on ice by using a sonicator (Vibra Cell Ultrasonic Processor; Sonics, USA) with the amplitude set to 50%, and the pulser set to 2 seconds. The total processing time was 5 minutes, and the cells were always kept on ice during the sonication. The cellular debris was removed by centrifugation (3000g, 4ºC, 30 minutes, Centrifuge 5810R; Eppendorf, UK) and the supernatant containing the overexpressed D-LDH protein was collected.

The overexpressed D-LDH protein was purified from the supernatant by using immobilised metal ion affinity chromatography. We used 2 ml of Generon Ni-Superflow Resin (Generon, UK) which was packed into a plastic column (S1014; MoBiTec GmbH,

Germany), and the resin was prepared according to the manufacturer's instructions. The collected supernatant was loaded into the prepared column, and was allowed to run through the column by gravity at 4ºC. The resulting flow-through was collected for SDS-PAGE analysis. The column was washed twice with 5 ml of buffer (as above) per wash, and the flow-through was also collected for SDS-PAGE analysis. The D-LDH protein was eluted from the column with 5 ml of elution buffer (25 mM sodium phosphate pH 7.5, 250 mM sodium chloride, and 400 mM imidazole). To remove imidazole from the eluted protein sample, the collected sample was immediately dialysed against 1 L of optimised dialysis buffer (25 mM sodium phosphate pH 7.5, 250 mM sodium chloride, and 1 mM EDTA) at 4ºC overnight. The resulting dialysed sample was either used immediately or stored at 4ºC for future use.

**2.27 Size exclusion chromatography**

To estimate the molecular size of *C. reinhardtii* D-LDH protein that was overexpressed in *E. coli*, size exclusion chromatography (SEC) was used. Two different instruments were used. This work was carried out in collaboration with Dr. Justin A. Yeoman and Dr. Wojciech J. Bialek (Imperial College London).

Firstly, size exclusion chromatography or gel filtration was carried out using an AKTA Protein Purification System (Aktapurifier; GE Healthcare Life Sciences, USA). A protein sample was concentrated by using a Vivaspin concentrator with a molecular weight cut-off (MWCO) of 10,000 (Generon, UK) according to the manufacturer's instructions. The concentrated sample was loaded onto a HiLoad 16/60 Superdex 200 column (GE Healthcare Life Sciences, UK), which had been equilibrated with a running buffer (25 mM Tris pH 7.5, and 250 mM NaCl). The protein sample was run with the running buffer at a flow rate of 1 ml/min at 4ºC. A single intense peak was observed at an elution volume of 60-70 ml, and the elution fraction relating to this peak was collected for future use. To estimate the protein molecular size, the elution volume was compared to the elution volumes of seven protein standards (Sigma-Aldrich, UK) that also had to be run using the column. These protein standards were cytochrome c (12.4 kDa), carbonic anhydrase from bovine erythrocytes (29 kDa), BSA (66 kDa), yeast alcohol dehydrogenase (150 kDa), β-amylase from sweet potato (200 kDa), apoferritin from horse spleen (443 kDa), and bovine thyroglobulin (669 kDa).

Secondly, size exclusion chromatography was carried out by using a SEC-s2000 column (Phenomenex, UK) attached to a HPLC system (Jasco, UK). This HPLC system was equipped with a diode array detector (MD-2015, Jasco, UK). The protein sample was run

with a buffer (25 mM sodium phosphate pH 7.5, 250 mM sodium chloride, and 1 mM EDTA) at a flow rate of 1 ml/min. The running buffer used was the same buffer used in the dialysis of the D-LDH protein. To estimate the molecular size of D-LDH protein, the column was calibrated with three molecular weight standard i.e. bovine serum albumin (66 kDa), yeast alcohol dehydrogenase (150 kDa) and β-amylase from sweet potato (200 kDa) (Sigma-Aldrich, UK).

**2.28 Enzyme assays**

For measuring enzymatic activity, a 1 ml reaction mixture was set up in a disposable cuvette with 1 cm optical path length (VWR International, UK). Unless stated otherwise, this mixture contained a buffer (25 mM sodium phosphate at pH 7.5, and 250 mM sodium chloride), an enzymatic substrate, and 300 μM of either NADH or $NAD^+$. The reaction was initiated by adding D-LDH enzyme into the reaction mixture, and the change in the absorbance at 340 nm was quickly measured at room temperature by using a spectrophotometer (UV-1601 UV-Visible Spectrophotometer; Shimadzu Europa, UK). The spectrophotometer was blanked with the reaction mixture containing only the buffer and the enzymatic substrate. All solutions of enzymatic substrates, NADH, $NAD^+$, and D-LDH enzymes were prepared by using the buffer.

**2.29 Protein crystallisation**

To obtain protein crystals for X-ray crystallography, crystal screening was carried out using commercial 96-well crystal screening plates. The plates tested were ICL1, ICL2, ICL3, ICL4, ICL8, ICL10 and ICL11 (Imperial College London, UK; http://www3.imperial.ac.uk/xraycrystallography/crystn/xtalscreens). The plates were set up using the Mosquito liquid handling robot (TTP Labtech, UK), in which a single minidrop was prepared in each well. The minidrop was prepared to contain 200 nl of purified D-LDH protein and 200 nl precipitant, purification of the protein was carried out using gel filtration chromatography (Aktapurifier; GE Healthcare Life Sciences, USA). The crystal screening plates were stored at 20ºC. Each plate was regularly checked for crystal formation. To determine the structure of a protein crystal, X-ray crystallography was carried out by our collaborators, Dr. James W. Murray and Mr. Charles Cotton (Imperial College London) at the Diamond Light Source (DLS), UK.

**2.30 Cell viability**

*C. reinhardtii* cells were first grown in TAP medium to late log phase, and then harvested by centrifugation (1000g, 5 minutes; Allegra 6R Centrifuge, Beckman Coulter, UK). The cells were either directly resuspended in TAP medium or washed first with TAP-S medium before being resuspended in the same medium. The test involved taking samples every 24 hours. In order to avoid introducing air into the culture during sampling, the culture was divided into four parafilm-sealed 1.5 ml microcentrifuge tubes for the four samplings (i.e. 24, 48, 72 and 96 hours). Each tube contained 1 ml of the cell sample with a final $OD_{750}$ of 1.0. The cells were incubated either in the dark (covered with aluminium foil) or under high light illumination (150μ$Em^{-2}s^{-1}$). For sampling, 5 μl of culture was spotted directly onto a TAP agar plate. Two serial 1:10 dilutions of the culture were also spotted. To quantify the number of viable cells, 5 μl of the 1:100 diluted cells was spread onto TAP agar plate. Before photos were taken and viable cell counting was performed, all plates were left to grow for 1-2 weeks at 28°C and ~30 μ$Em^{-2}s^{-1}$.

# Chapter 3: Identification of *D-LDH* and characterisation of *D-LDH* knockdown mutants

## 3.1 Introduction

Lactate dehydrogenase (LDH) is an enzyme that can be found in many organisms. For example, in many animals (Adams *et al*., 1973; White *et al*., 1976; Grau *et al*., 1981; Abad-Zapatero *et al*., 1987), in plants (Oba *et al*., 1977; Betche, 1981) and in various microbes (Buehner *et al*., 1974; Piontek *et al*., 1990; Wigley *et al*., 1992; Iwata *et al*., 1994; Auerbach *et al*., 1998; Razeto *et al*., 2002; Uchikoba *et al*., 2002; Shinoda *et al*., 2005; Antonyuk et al., 2009). The enzyme catalyses the interconversion of pyruvate and lactate with the concomitant interconversion of NADH and $NAD^+$, and the enzymatic activity can be determined spectrophotometrically at 340 nm by following either the oxidation of NADH with pyruvate or reduction of $NAD^+$ with lactate, resulting in either a decrease or increase in absorbance, respectively (Markert, 1984).

LDH enzymes can only act on either one of the two stereoisomers of lactate i.e. D- or L-lactate. Interestingly, D-LDHs and L-LDHs belong to evolutionarily unrelated families of enzymes (Cristescu *et al*., 2008). The D-LDHs belong to a member of the D-isomer-specific 2-hydroxyacid dehydrogenase family while the L-LDHs belong to the L-specific $NAD^+$-dependent dehydrogenase family (Taguchi & Ohta, 1991; Cristescu *et al*., 2008). Prokaryotes and invertebrates can produce either D- or L-lactate (Garvie, 1980; Long &Kaplan, 1968; Cristescu *et al*., 2008). Interestingly, some prokaryotes can produce both stereoisomers of lactate (Dennis & Kaplan, 1960; Gasser *et al*., 1970). Multiple isozymes of LDH have been observed in eukaryotes but each can only possess a single stereospecificity (Markert, 1984). *C. reinhardtii* has been shown to produce D-lactate (Husic & Tolbert, 1985) and therefore should possess a D-LDH. Various other green algae have also been shown to produce D-lactate (Hirt *et al*., 1971; Gruber *et al*., 1974).

Alternatively, there also exists a distinct class of LDH enzymes which are not dependent on NADH. These enzymes are known as $NAD^+$-independent, cytochrome-dependent LDH (also known as lactate ferricytochrome-c oxidoreductase). These enzymes catalyse the conversion of lactate to pyruvate with the subsequent conversion of ferricytochrome c to ferrocytochrome c, as the cytochrome c acts as an electron acceptor. The enzymatic reaction also requires a redox cofactor, flavin adenine dinucleotide (FAD) to aid in the chemical reaction. The enzyme has been characterised in many organisms such as yeasts

(Lodi & Ferrero, 1993; Lodi *et al*., 1994) and plants (Engqvist *et al*., 2009). The enzyme has been shown in *Arabidopsis thaliana* to participate in the last step of the methylglyoxal pathway, whereby the generated lactate is converted to pyruvate (Engqvist *et al*., 2009). *C. reinhardtii* has been shown to oxidise D-lactate, which was produced from dark anaerobic fermentation, to pyruvate but only under aerobic conditions, with this enzymatic reaction thought to be catalysed by a mitochondrion-located, cytochrome-dependent LDH (Husic & Tolbert, 1987). Glycolate dehydrogenase from *C. reinhardtii*, which has been found in mitochondria (Beezley *et al*., 1976), has also been shown to catalyse the oxidation of D-lactate (Nelson & Tolbert, 1970). Meanwhile, the oxidation of L-lactate can be catalysed by glycolate oxidase and not glycolate dehydrogenase (Gruber *et al*., 1974). However, both enzymes are capable to oxidise glycolate to glyoxylate and thus can be involved in the glycolate pathway (Bruin *et al*., 1970).

Although D-lactate is a minor end product of dark fermentation in *C. reinhardtii*, its production increased significantly when the PFL1 pathway was blocked (Philipps *et al*., 2011; Burgess *et al*., 2012; Catalanotti *et al*., 2012). As the PFL1 pathway was eliminated, formate production was significantly affected (Ohta *et al*., 1987; Philipps *et al*., 2011; Burgess *et al*., 2012; Catalanotti *et al*., 2012). The elimination also led to an increase in the production of carbon dioxide and ethanol but a decrease in acetate production (Philipps *et al*., 2011; Burgess *et al*., 2012; Catalanotti *et al*., 2012). Moreover, it also led to an increase in the intracellular production of malate, fumarate, succinate, indicating the activation of the reverse TCA reactions, and intracellular levels of amino acids and various sugars also increased, which could play a role in redox balancing and $NAD^+$ regeneration (Catalanotti *et al*., 2012). However, the effect of PFL1 elimination on dark fermentative hydrogen production is unclear as the observations from previous studies were conflicting which could be due to different culturing or induction conditions (Ohta *et al*., 1987; Philipps *et al*., 2011; Catalanotti *et al*., 2012). Similarly, when the ADH1 pathway or both the PFL1 and ADH1 pathways were eliminated, an accumulation of lactate was also observed (Magneschi *et al*., 2012; Catalanotti *et al*., 2012).

When *C. reinhardtii* was incubated under sulphur-deprived conditions, the elimination of the PFL1 pathway similarly caused a dramatic reduction in the amount of formate produced (Burgess *et al*., 2012; Hemschemeier *et al*., 2008) with the metabolic flux redirected in part from formate to lactate production (Burgess *et al*., 2012). The effects on ethanol accumulation and carbon dioxide evolution were unclear due to conflicting results but no effect was observed on the hydrogen photoproduction (Burgess *et al*., 2012;

Hemschemeier *et al*., 2008). Interestingly, under these conditions, 3-hydroxybutyrate was also produced in a *pfl1* knockdown mutant (Burgess *et al*., 2012).

In this chapter, I describe the identification and characterisation of the $NAD^+$-dependent D-LDH from *C. reinhardtii* and the isolation and characterisation of *D-LDH* knockdown mutants generated by artificial microRNA technology.

## 3.2 Results

### 3.2.1 Identification of the *D-LDH* in *C. reinhardtii*

#### 3.2.1.1 *In silico* identification of *LDH*

An earlier bioinformatic analysis by Burgess (2011) suggested the presence of one potential $NAD^+$-dependent D-LDH in *C. reinhardtii*. This is in agreement with Husic & Tolbert (1985) who showed the lactate produced by the alga *in vivo* was of D-configuration and was produced by an $NAD^+$-dependent enzyme. A recent version of the *C. reinhardtii* database, Phytozome v9.1 (Goodstein *et al*., 2012) became available recently and I, in collaboration with Dr. Steven J. Burgess (University of Cambridge), decided to repeat the bioinformatics analysis in order to identify candidate genes encoding potential LDH enzymes.

The Phytozome database was searched with the D- and L-LDHs from other species that already had their crystal structures determined. We used the sequences of $NAD^+$-dependent D-LDHs of *Aquifex aeolicus* (thermophilic Gram –ve bacterium; Antonyuk et al., 2009), *Lactobacillus pentosus* (Gram +ve bacterium; Razeto *et al*., 2002) and *L. delbrueckii* (Gram +ve bacterium; Shinoda *et al*., 2005), and the sequences of $NAD^+$-dependent L-LDH of *Sus scrofa* (pig; Grau *et al*., 1981), *Squalus acanthias* (dogfish; Adams *et al*., 1973; White *et al*., 1976; Abad-Zapatero *et al*., 1987), *Bifidobacterium longum* (Gram +ve bacterium; Iwata *et al*., 1994), *Thermotoga maritima* (thermophilic Gram -ve bacterium; Auerbach *et al*., 1998), *L. pentosus* (Gram +ve bacterium; Uchikoba *et al*., 2002), *L. casei* (Gram +ve bacterium; Buehner *et al*., 1974) and *Bacillus stearothermophilus* (thermophilic Gram +ve bacterium; Piontek *et al*., 1990; Wigley *et al*., 1992). We also searched the database with the cytochrome-dependent/FAD-dependent LDHs from other species that had been experimentally investigated with enzyme assays i.e. *Kluyveromyces lactis* (yeast; Lodi *et al*., 1994), *Saccharomyces cerevisiae* (yeast; Lodi & Ferrero, 1993) and *A. thaliana* (flowering plant; Engqvist *et al*., 2009).

All protein sequences were checked for their potential subcellular location using TargetP (Emanuelsson *et al*., 2007), and their putative transit peptide using ChloroP (Emanuelsson *et al*., 1999), SignalP (Petersen *et al*., 2011) and MitoProt (Claros & Vincens, 1996). Prior to the protein alignment and generation of phylogenetic trees, putative transit peptides were removed. The protein sequences were aligned by using MergeAlign (Collingridge & Kelly, 2012). The phylogenetic tree was generated by using EPoS software (Griebel *et al*., 2008). We used the Neighbour Joining method with midpoint rooting and 1000 bootstrap replicates.

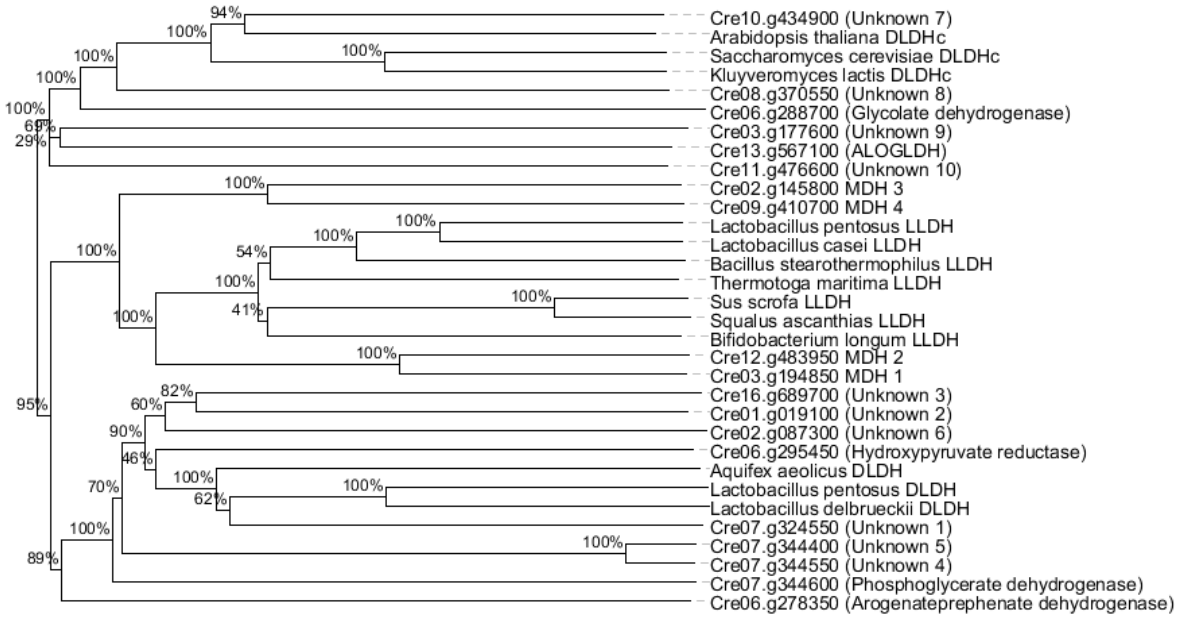


**Figure 3.1 Phylogenetic analysis of LDHs with *C. reinhardtii* candidate genes.**

The numbers at the nodes are bootstrap values. *C. reinhardtii* candidate genes are compared to the $NAD^+$-dependent D- and L-LDHs (labelled as DLHD and LLDH, respectively) and cytochrome-dependent D-LDHs (labelled as DLDHc). The following sequences are included: *Aquifex aeolicus* (NP_213499.1), *Lactobacillus pentosus* (D-LDH: P26298.1; L-LDH: P56511.1), *L. delbrueckii* (P26297.3), *Sus scrofa* (NP_001165834.1), *Squalus acanthias* (AAA91038.1), *Bifidobacterium longum* (AAA22900.1), *Thermotoga maritima* (1a5z), *L. casei* (P00343.3), *Bacillus stearothermophilus* (P00344.1), *Kluyveromyces lactis* (CAA50635.1), *Saccharomyces cerevisiae* (NP_010107.1) and *Arabidopsis thaliana* (AED91037). Protein accessions are given according to the NCBI database except for *T. maritima* which is given according to the RCSB Protein Data Bank, and for *C. reinhardtii* which are given according to the Phytozome. MDH: malate dehydrogenase. ALOGLDH: arabinono lactone oxidase/galactono-lactone dehydrogenase.

The phylogenetic tree (Figure 3.1) revealed six potential *C. reinhardtii* genes that could possess $NAD^+$-dependent D-LDH activity: Cre07.g324550, Cre01.g019100, Cre16.g689700, Cre07.g344550, Cre07.g344400 and Cre02.g087300 (labelled here as Unknown 1, 2, 3, 4, 5 and 6, respectively). However, when we checked for the presence of the $NAD^+$-binding domain ($GXGX_2GX_{17}D$), the conserved histidine (for catalysis), arginine (for substrate binding) and glutamic acid residues (for modulating pH dependence) (Lapierre *et al*., 1999) in these unknown proteins, only Cre07.g324550/Unknown 1, possessed all these features (Figure 3.2). This suggests that Cre07.g324550 could be the only $NAD^+$-dependent D-LDH in *C. reinhardtii*. In addition, the phylogenetic tree also revealed two potential genes that could possess cytochrome-dependent/FAD-dependent LDH activity: Cre10.g434900 and Cre08.g370550 (labelled here as Unknown 7 and 8, respectively). However, this type of LDH presumably only converts lactate to pyruvate instead of reducing pyruvate to lactate (Lodi & Ferrero, 1993; Lodi *et al*., 1994; Engqvist *et al*., 2009).

```
L. delbrueckii  ----------------------------------------------------------------------------MTKIFAYAIREDEKPFLKEWEDAH 24
L. pentosus     ----------------------------------------------------------------------------MKIIAYAVRDDERPFFDTWMKEN 23
C. reinhardtii  MMLLSSTQSHCLTASKANQRNVVAKPGIIARGRGLVQHRAYRVAALNVGPGGGSPVSTVEDTGRVELTPQEAAKVATTRCICYSTTQYVKDFLAGPMQK- 99
A. aeolicus     ----------------------------------------------------------------------------MNVLFTSVPQEDVPFYQEALKD- 22
                                                                                              . :  :  :    *     .

L. delbrueckii  KDVEVEYTDKLLTPETVALAKGADGVVVYQQLDYTAETLQALADNGITKMSLRNVGVDNIDMAKAKELGFQITNVPVYSPNAIAEHAAIQAARILRQDKA 124
L. pentosus     PDVEVKLVPELLTEDNVDLAKGFDGADVYQQKDYTAEVLNKLADEGVKNISLRNVGVDNLDVPTVKARGLNISNVPAYSPNAIAELSVTQLMQLLRQTPM 123
C. reinhardtii  VFTDTYFVEPPLDKDTAQLARGYDVAVLFVNDRADASVIKELAKAGVKLIALRCAGFDRVDLHACAEHGVRVVRVPTYSPESVAEHAVALIFALNRHLTD 199
A. aeolicus     --LSLKIYTTDVSKVPENELKKAELISVFVYDKLTEELLSKMPR--LKLIHTRSVGFDHIDLDYCKKKGILVTHIPAYSPESVAEHTFAMILTLVKRLKR 118
                   .       :        :  :   ::       . :. :.   :. :  * .*.*.:*:      *. : .:*.***:::** :      : ::

                                      GXGXXGXXXXXXXXXXXXXXXD
L. delbrueckii  MDEKVARHDLRWAP-TIGREVRDQVVGVIGTGHIGQVFMQIMEGFGAKVIAYDIFRNPELEKKGYYVDSLDDLYKQADVISLHVPDVPANVHMINDESIA 223
L. pentosus     FNKKLAKQDFRWAP-DIAKELNTMTVGVIGTGRIGRAAIDIFKGFGAKVIGYDVYRNAELEKEGMYVDTLDELYAQADVITLHVPALKDNYHMLNADAFS 222
C. reinhardtii  AYIRVRMGNYSLSG-LVGVEMRHKVVGVVGTGAIGQQAARILKGIGCKVFAYDIKPNPAVEAMGIPYVSLDELLAMSDIVTLHCPLLPSTRQLINKESIQ 298
A. aeolicus     IEDRVKKLNFSQDSEILARELNRLTLGVIGTGRIGSRVAMYGLAFGMKVLCYDVVKREDLKEKGCVYTSLDELLKESDVISLHVPYTKETHHMINEERIS 218
                   ::   :       :. *:.  .:**:*** **        .:* **: **:  .  ::  *    :**:*   :*:::** *    . :::* : :

                            R                             E                                H
L. delbrueckii  KMKQDVVIVNVSRGPLVDTDAVIRGLDSGKIFGYAMDVYEGEVGIFNEDWEGKE------FPDARLADLIARPNVLVTPHTAFYTTHAVRNMVVKAFDNN 317
L. pentosus     KMKDGAYILNFARGTLIDSEDLIKALDSGKVAGAALVTYEYETKIFNKDLEGQT------IDDKVFMNLFNRDNVLITPHTAFYTETAVHNMVHVSMNSN 316
C. reinhardtii  KMKKGVMLINVSRGGLIDSAALFDALESGQIGALGLDVYENEGGLFFVDHTKFDPSVRMQKWDRQFRTLLSYPQVLVTPHTAFLTEEALNNICTTTIQNI 398
A. aeolicus     LMKDGVYLINTARGKVVDTDALYRAYQRGKFSGLGLDVFEDEEILILKKYTEGKAT----DKNLKILELACKDNVIITPHIAYYTDKSLERIREETVKVV 314
                 **... ::* :** ::*:  :  . : *:. . .: .:* *  ::  . :             :  *    :*::*** *: *  ::..:   :..


L. delbrueckii  LELVEGKEAETPVKVG------- 333
L. pentosus     KQFIETGKADTQVKFD------- 332
C. reinhardtii  ADYVLDRPLGNEVKAQPAPAGKT 421
A. aeolicus     KAFVKGDLEQIKGNFVVGPS--- 334
                   :        :
```

**Figure 3.2 Multiple sequence alignment of putative *C. reinhardtii* D-LDH with $NAD^+$-dependent D-LDHs.**

The putative *C. reinhardtii* D-LDH (Cre07.g324550) is aligned by using ClustalW2 with the following sequences: *Aquifex aeolicus* (NP_213499.1), *Lactobacillus pentosus* (P26298.1) and *L. delbrueckii* (P26297.3). Protein accessions are given according to the NCBI database except for *C. reinhardtii* which refers to the Phytozome. The sequence in grey box is the putative chloroplast transit

peptide. Black boxes show the locations of the $NAD^+$-binding domain ($GXGX_2GX_{17}D$) and the conserved arginine, glutamic acid and histidine residues.

### 3.2.1.2 Construction of plasmid for *D-LDH* expression

Our bioinformatic analysis suggested there was only a single $NAD^+$-dependent D-LDH in *C. reinhardtii* (Phytozome ID: Cre07.g324550) which was predicted to be located in the chloroplast. We were interested to confirm the enzymatic function of this putative *D-LDH* gene by enzyme assays. To do this, plasmids that could over-express this putative gene in *E. coli* were constructed.

The putative *D-LDH* gene sequence was sent to a company (Biomatik, Canada) to be synthesized. The *C. reinhardtii* sequence was codon-optimised for expression in *E. coli*, and the synthesised DNA fragment was cloned into the company's vector to produce pBMH-LDH. The next step was to transfer the mature *D-LDH* (without the predicted chloroplast transit peptide sequence) from pBMH-LDH into two different expression vectors. Our strategy was to express the same protein in two forms i.e. one with an N-terminal $His_6$ tag and another one with a C-terminal $His_6$ tag. This was because the position of the $His_6$ tag might affect the solubility of the expressed protein. It was important for *E. coli* to over-express soluble D-LDH protein which could be used for future enzyme assays. We used expression vectors pRSETA-thr (courtesy of Dr. Ernesto Cota, Imperial College London) and pET28b (Novagen, Germany) in order to generate the N- and C-terminal $His_6$ tag derivatives, respectively.

To verify the constructed plasmids, diagnostic restriction digests were carried out. The digests using a number of restriction enzymes produced the expected results (Figure 3.3). The plasmids were also sent for sequencing, and the gene of interest was sequenced in both forward and reverse directions. The sequencing results confirmed that the *D-LDH* gene was correctly inserted into the two vectors, and no point mutation or other mutations were observed (data not shown).

**(A) pRSETA-thr-LDH**

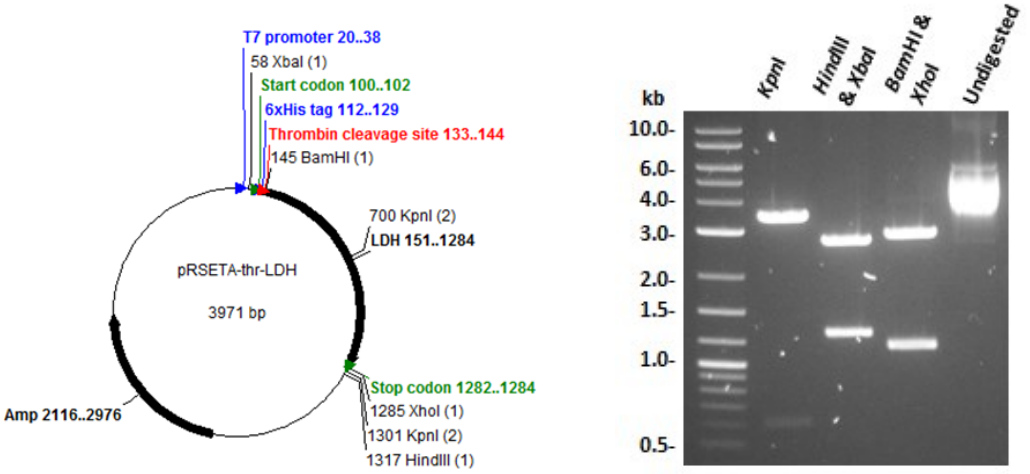


**(B) pET28b-LDH**

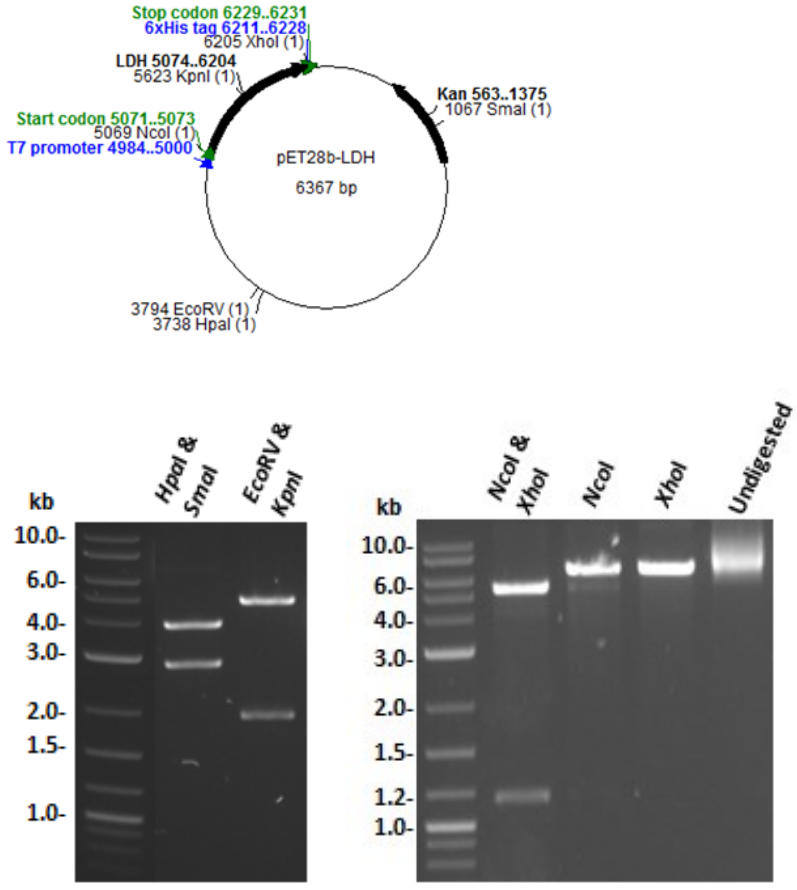


**Figure 3.3 Restriction analyses of constructed D-LDH expression plasmids.**

Expected sizes of digests: KpnI - 3370 & 601 bp; HindIII & XbaI - 2712 & 1259 bp; BamHI & XhoI - 2831 & 1140 bp; HpaI & SmaI - 3696 & 2671 bp; EcoRV & KpnI - 4538 & 1829 bp; NcoI & XhoI - 5231 & 1136 bp; NcoI - 6367 bp; XhoI - 6367 bp.

### 3.2.1.3. Optimisation of D-LDH expression in *E. coli*

One potential problem when expressing a foreign protein in *E. coli* is that the protein might not be expressed in a soluble form. As stated earlier, the location of the $His_6$ tag at the N- or C- terminus could affect the solubility of the protein since the tag could possibly affect the folding of the protein. This explained why we constructed the two plasmids. Another issue was that the conditions used for protein expression might not be suitable to produce soluble protein. Thus, before we produced the D-LDH protein on a large scale, we optimized the conditions for expression by performing a mini-scale protein expression trial using different *E. coli* incubation temperatures and different concentrations of rhamnose to induce protein expression in Single Step (KRX) *E. coli* cells. Rhamnose induces the expression of T7 RNA polymerase, which subsequently transcribes the gene of interest. This work was carried out in collaboration with Dr. Justin A. Yeoman (Imperial College London).

We transformed KRX *E. coli* cells with both pRSETA-thr-LDH and pET28b-LDH, and, for each plasmid, a representative colony was chosen and grown to mid-log phase ($O.D_{600}$ ~0.5), at which point the cultures were transferred to a lower incubation temperature overnight at either 18 or 30ºC, and were either induced with 0.1 or 0.01% rhamnose or left uninduced. The cells were harvested, and BugBuster Protein Extraction Reagent (Novagen, USA) was used to extract the soluble and purified insoluble proteins from the bacterial pellet. The soluble and insoluble fractions were analysed on a SDS-PAGE gel by loading and running equal proportion of the samples. However, it should be noted that it was difficult to resuspend and load the insoluble fractions, and hence, the amount of proteins loaded might not be equal.

For pRSETA-thr-LDH, the Coomassie-stained gel showed that a band corresponding to the predicted mass of D-LDH (~42 kDa) was induced in KRX cells but was mainly present in the insoluble fraction (Figure 3.4.A). On the other hand, for pET28b-LDH, the Coomassie-stained gel showed overexpression of soluble D-LDH (Figure 3.4.B). Although we also obtained insoluble D-LDH when using this plasmid, this was no longer considered a problem due to the high amount of soluble D-LDH being produced, which was sufficient for future work. The gel also showed there was no observable difference in the production of soluble D-LDH when using 0.1 or 0.01% (w/v) rhamnose. However, the incubation temperature of 30ºC produced a slightly higher amount of soluble D-LDH compared to 18ºC. Therefore, for future large-scale expression of D-LDH, 30ºC was the preferred temperature.

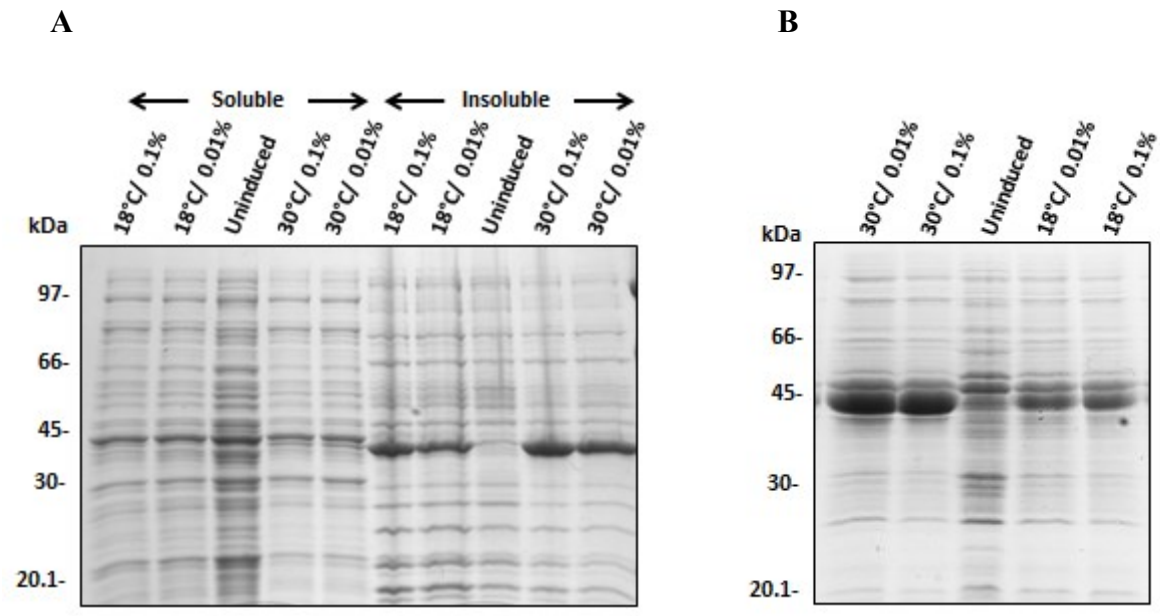


**Figure 3.4 Optimisation of D-LDH expression.**

D-LDH was over-expressed in *E. coli* by using either (A) pRSETA-thr-LDH or (B) pET28B-LDH. The bacteria were incubated at either 18 or 30°C, and were either induced with rhamnose (0.1 or 0.01%) or left uninduced. Soluble and insoluble fractions were collected and analysed by using protein gel electrophoresis. Visualisation of the protein bands was carried out by Coomassie staining. Only the soluble fractions are shown for pET28B-LDH.

### 3.2.1.4. Large-scale production of D-LDH

The production of D-LDH on large scale was carried out in collaboration with Dr. Justin A. Yeoman (Imperial College London). A fresh transformation of KRX *E. coli* competent cells with pET28b-LDH was performed. A colony was chosen and grown overnight to be used as a starting culture. The overnight culture was diluted 100-fold and grown to mid-log phase ($OD_{600}$ ~0.5) at which point they were transferred to a 30ºC incubation temperature and induced with 0.1% rhamnose. After the cells were allowed to grow overnight, they were harvested and we usually managed to obtain a total wet weight of ~5 g of cells from the 1 L of culture. The cells were broken using a sonicator, and then centrifuged in order to collect the supernatant containing the soluble D-LDH.

Immobilised metal ion affinity chromatography using Ni Superflow Resin (Generon, UK) was used to purify the $His_6$-tagged D-LDH protein from the collected supernatant. The supernatant was allowed to flow through a column containing the equilibrated resin, as this would make the $His_6$-tagged D-LDH bind to the resin while other untagged proteins would just pass through the column. The column flow-through was collected for SDS-PAGE

analysis. The resin was washed to further remove untagged proteins, and again the wash fractions were collected for analysis. The D-LDH was eluted with elution buffer that contained 400 mM imidazole. Imidazole was removed from the elution fraction by overnight dialysis. Our first dialysis attempt resulted in the D-LDH precipitating and becoming insoluble. Thus, we had to optimise the dialysis buffer to ensure the D-LDH remained soluble. We altered the pH of the buffer (pH 7.5 or 8.5), and the concentration of sodium chloride (150 or 250 mM), imidazole (none or 10 mM) and EDTA (none or 1 mM). Our results showed that 25 mM sodium phosphate at pH 7.5 containing 1 mM EDTA and 250 mM sodium chloride resulted in the removal of imidazole without protein precipitating. After dialysis, the protein was stored at 4ºC before further analyses.

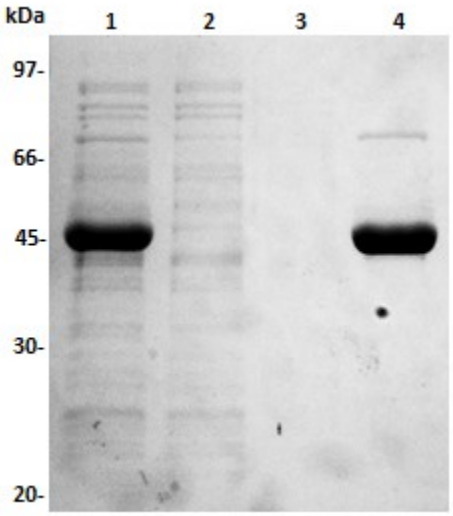


**Figure 3.5 D-LDH purification with immobilised metal ion affinity chromatography.**

1: Lysis soluble fraction (25 mM imidazole); 2: Flow-through from lysis soluble fraction (25 mM imidazole); 3: Flow-through from washing (25 mM imidazole); 4: Elution (400 mM imidazole).

To determine the efficiency of the purification, we examined the various fractions by SDS-PAGE. The Coomassie-stained gel in Figure 3.5 confirmed that the supernatant obtained after cell breakage contained high amounts of D-LDH protein, whereas the flow-through after loading the supernatant on the column did not show any significant D-LDH band, indicating that $His_6$-tagged D-LDH did successfully bind to the resin. Very little protein was eluted in the final washing step, whereas a major band of the expected size was detected in the fraction eluted with 400 mM imidazole. The lack of other protein bands observed in the gel suggested a high degree of purity. The faint band at around 80-90 kDa might represent an

aggregation product. Analysis of the protein concentration indicated a yield of approximately 5 mg per L of culture.

### 3.2.1.5. D-LDH enzyme assays

Enzymatic assays were performed to test the substrate specificity of the purified $His_6$-tagged D-LDH sample. The assays were performed in a 1-ml cuvette containing 25 mM sodium phosphate at pH 7.5 and 250 mM sodium chloride. Changes in NAD(P)H levels were measured by following the absorbance change at 340 nm (Markert, 1984). When we used pyruvate in the presence of NADH, we observed enzymatic activity. We used a range of pyruvate concentrations. As the concentration was increased the rate of catalysis also increased until it reached its maximum limit, indicating the enzyme became saturated with the substrate. Similarly, when we used D-lactate and $NAD^+$, we also observed enzymatic activity (Figure 3.6). When we changed from using NADH to NADPH for the reaction with pyruvate, we did not observe any activity. There was hardly any change in the absorbance value at 340 nm (Figure 3.7.A). This indicated that NADH was the specific co-enzyme used by the enzyme. When we tried to determine if the enzyme could also consume L-lactate in the presence of $NAD^+$, we did not observe any significant activity (Figure 3.7.B). This confirmed the D-LDH protein used lactate in the D-configuration. We were also interested to test if the D-LDH protein could also utilize other substrates of structural similarity to pyruvate. We tested phenylpyruvate in the presence of NADH but we did not observe any significant activity (Figure 3.7.C), indicating the protein did not consume this substrate. We also tested glyoxylate with NADH, and observed enzymatic activity, indicating the protein was able to utilize this substrate (Figure 3.6).

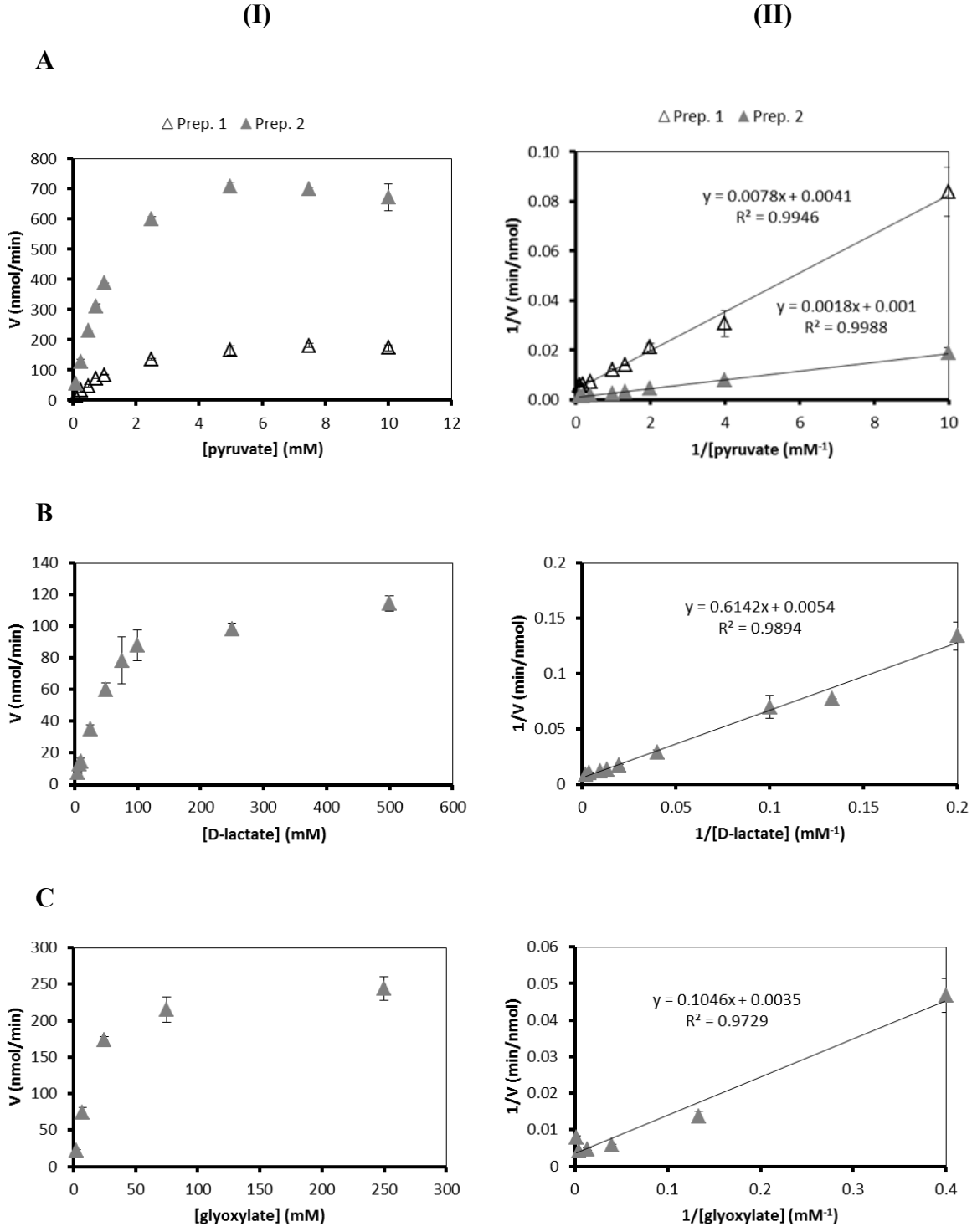


**Figure 3.6 Rates of D-LDH enzymatic activity.**

The enzymatic rates are shown as (I) Michaelis-Menten plot and (II) Lineweaver-Burk plot. Two independent preparations (each with two technical replicates, given as average ± SD) were carried out for pyruvate but only one preparation (with two technical replicates) for D-lactate and glyoxylate. The rates of enzymatic activity (V) were measured by using different concentrations of substrates.

Pyruvate and glyoxylate were assayed in the presence of 300 µM NADH while D-lactate was assayed with $NAD^+$ of similar concentration.

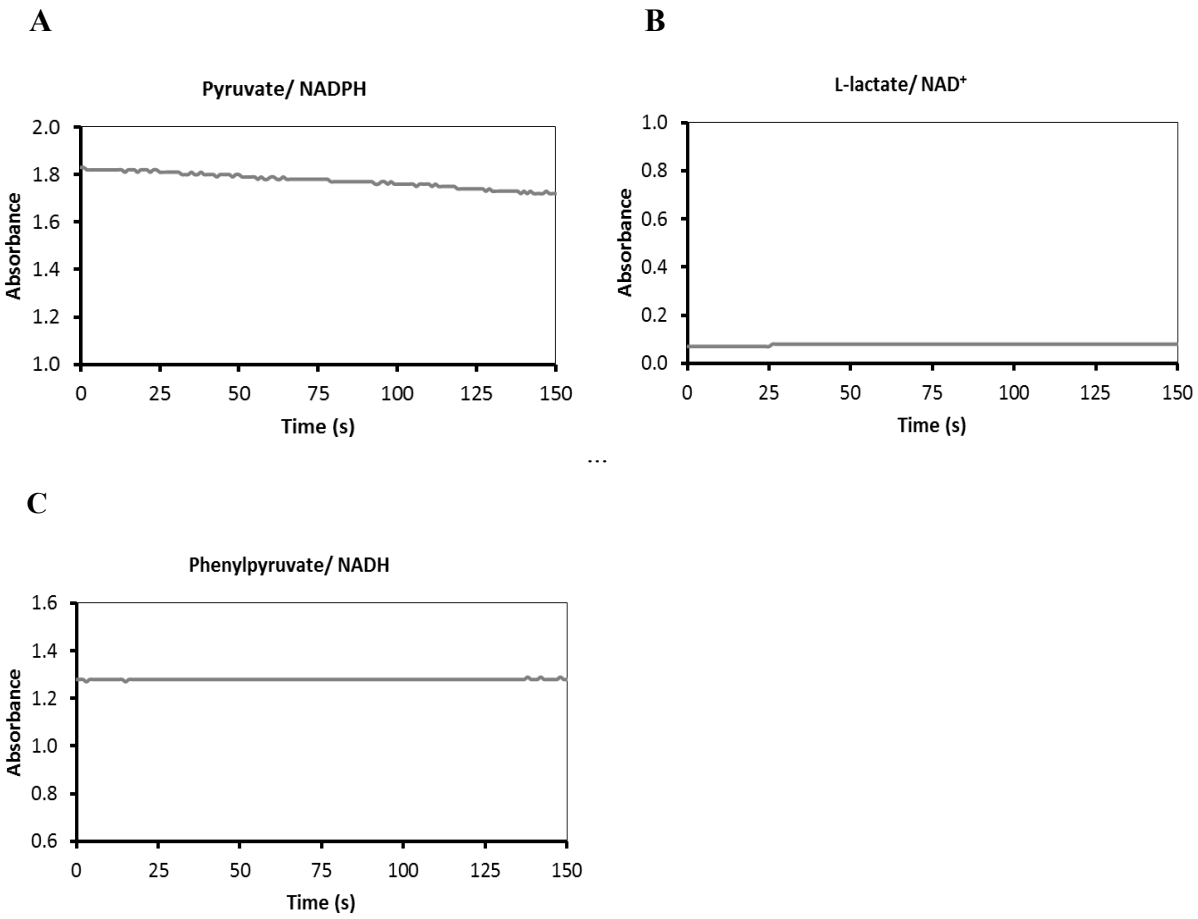


**Figure 3.7 D-LDH enzyme assays using alternative substrates.**

The absorbance at 340 nm was recorded at every 1-second interval for a total period of 150 seconds. Two technical replicates were carried out per assay, and only the representative results are shown. The assays were performed using (A) 10 mM pyruvate/ 300 µM NADPH , (B) 500 mM L-lactate/ 300 µM $NAD^+$, and (C) 7.5 mM phenylpyruvate/ 300 µM NADH.

To calculate the enzyme kinetics, we used the Lineweaver-Burk method (Table 3.1). The D-LDH enzyme had a lower $K_m$ value, a higher turnover number ($k_{cat}$) and a higher catalytic efficiency ($k_{cat}/K_m$) when pyruvate was used as a substrate compared to when D-lactate was used. These results indicate that the D-LDH from *C. reinhardtii* was a pyruvate reductase. The enzymatic reaction was in favour of the forward reaction whereby pyruvate was reduced to D-lactate instead of the backward reaction i.e. oxidation of D-lactate to pyruvate. The $K_m$ value for glyoxylate was higher relative to pyruvate. In comparison, the $K_m$ values for *L. bulgaricus* $NAD^+$-dependent D-LDH, which were determined in 50 mM HEPES

at pH 7.5, are 1.5 and 100 mM for pyruvate and glyoxylate, respectively (Kochhar *et al*., 1992).

| Substrate | $V_{max}$ (nmol/min) | $K_m$ (mM) | $k_{cat}$ ($s^{-1}$) | $k_{cat}/K_m$ ($M^{-1}s^{-1}$) |
|---|---|---|---|---|
| **Pyruvate** | 244; 1000 | 1.85 ± 0.07 | 415 ± 25 | $2.24 \pm 0.05 \times 10^5$ |
| **D-Lactate** | 185 | 114 | 15 | $1.3 \times 10^2$ |
| **Glyoxylate** | 286 | 30 | 28 | $9.3 \times 10^2$ |

**Table 3.1. Enzyme kinetics determined by the Lineweaver-Burk method.**

For pyruvate, the average values (±SD) were given for the two independent preparations except for $V_{max}$ where both values were shown due to its dependency on LDH concentrations, as different amounts were used from each preparation (i.e. 0.0094 and 0.042 nmol). Pyruvate and glyoxylate were assayed in the presence of NADH while D-lactate was assayed with $NAD^+$. As there was not enough protein, there was no replicate for D-lactate and glyoxylate. $V_{max}$ – enzyme maximum rate; $K_m$ – Michaelis constant (the concentration of substrate at which the rate of reaction is half of $V_{max}$); $k_{cat}$ – the turnover number i.e. the maximum number of reactions catalysed per second; $k_{cat}/K_m$ – a measure of enzyme efficiency.

### 3.2.1.6. Quaternary structure of D-LDH protein

Gel filtration chromatography (also known as size-exclusion chromatography, SEC) was used to determine the approximate size of D-LDH protein and hence its possible quaternary structure. This was carried out in collaboration with Dr. Justin A. Yeoman (Imperial College London). This type of chromatography was also used to further purify D-LDH from contaminating proteins of different sizes found in the sample. The over-expressed *C. reinhardtii* D-LDH protein was run and filtered using an equilibrated HiLoad 16/60 Superdex 200 column (GE Healthcare Life Sciences, UK), resulting in the protein being eluted and collected at an elution volume of 65.83 ml (Figure 3.8). This elution volume was compared to the elution volumes of seven gel-filtration protein standards (Sigma-Aldrich, UK) that were also run separately on the column (Appendix 1), which was carried out by Dr. Wojciech J. Bialek (Imperial College London). By comparison we found our D-LDH protein had a molecular mass of 202 kDa.

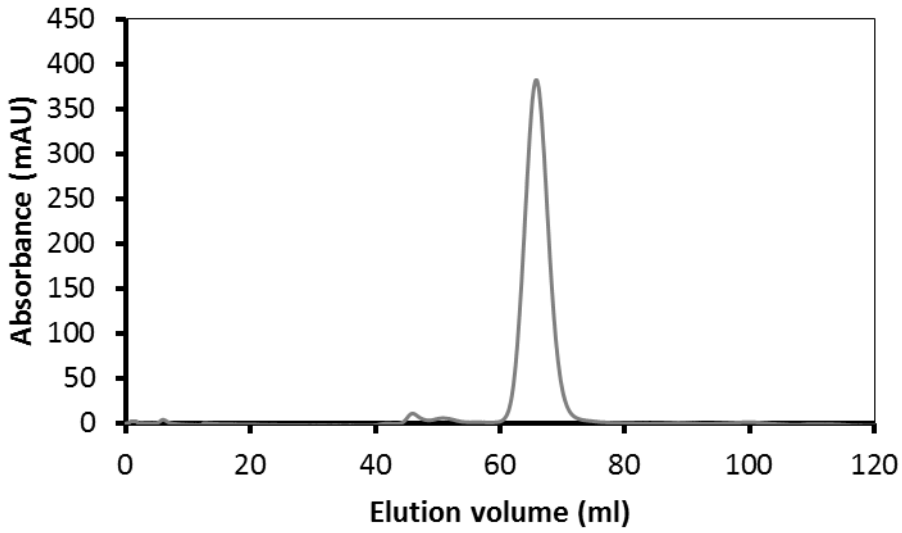


**Figure 3.8 D-LDH sample run using gel filtration chromatography.**

Protein sample was run and separated according to their different sizes. Different sizes of proteins would be eluted at different elution volumes which could be collected. The presence of proteins at different elution volumes was determined by measuring their absorbance at 280 nm.

Additionally, we also ran our D-LDH sample using the SEC-s2000 column (Phenomenex, UK) attached to a high-performance liquid chromatography (HPLC) instrument. Our D-LDH sample gave a retention time of 6.84 ± 0.08 (average ± SE was based on three technical replicates). This retention time was compared to a protein standard curve that we made with three protein markers (Appendix 1). We found the D-LDH to also have a size of 202 kDa. This is consistent with the result from the previous analysis.

Based on the two techniques that we used, the D-LDH protein had a molecular mass of 202 kDa. This size was approximately four times bigger than the predicted molecular mass of the D-LDH protein monomer of 45.6 kDa, which was consistent with its migration on denaturing SDS-PAGE gels (Figure 3.5). Overall these data suggest that the *C. reinhardtii* D-LDH forms a tetramer.

The purified D-LDH obtained from the gel filtration chromatography was further used for protein crystallisation. This was done in collaboration with Dr. Wojciech J. Bialek (Imperial College London). Numerous crystal screening conditions were used, and we managed to obtain several crystals under different conditions, an example is shown in Figure 3.9.A.

X-ray crystallography was carried out to determine the quaternary structure of *C. reinhardtii* D-LDH protein. This was carried out by Dr. James W. Murray and Mr. Charles

Cotton (Imperial College London). Several crystals were tested, an example is shown in Figure 3.9.B. To date, we are still in the process of refining the D-LDH structure obtained from a crystal with a resolution of 2.5 Å. Nevertheless, preliminary analysis suggests it is a tetramer.

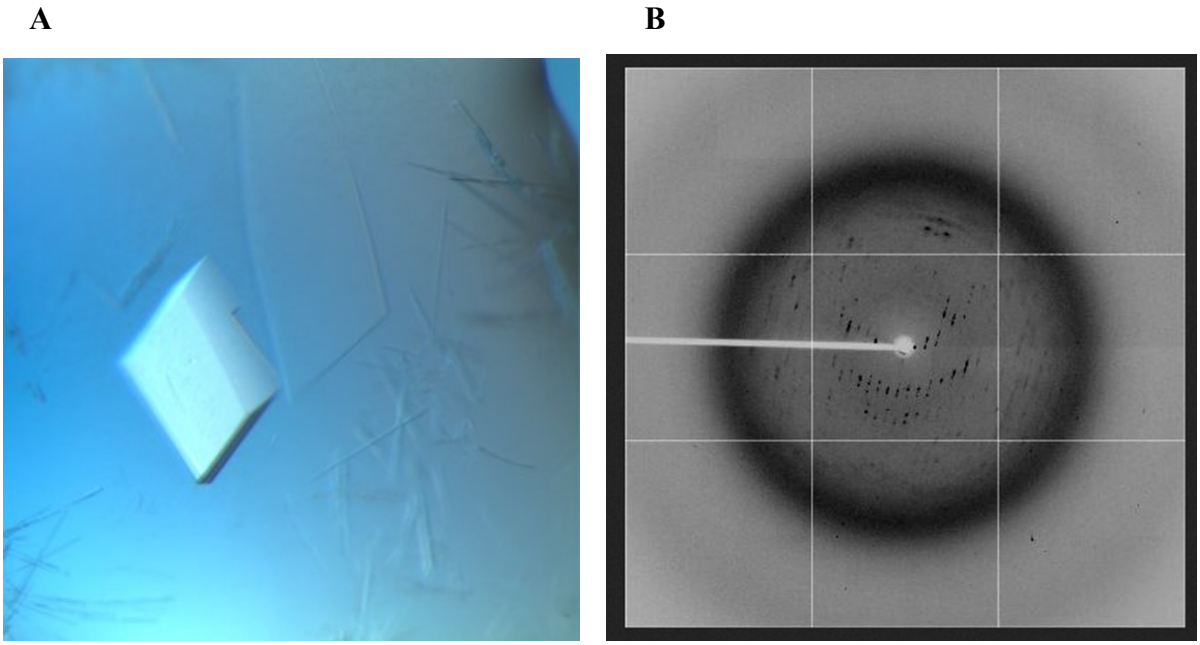


**Figure 3.9 Protein crystallisation and X-ray crystallography.**

(A) A crystal obtained from the D-LDH crystal screening. (B) An X-ray diffraction pattern of a crystal sample, which was obtained by X-ray crystallography.

### 3.2.2 Characterisation of *C. reinhardtii D-LDH* knockdown mutants

#### 3.2.2.1 Construction of artificial microRNAs

Artificial microRNAs were constructed according to Molnar *et al*. (2009). Oligonucleotides were designed using Web MicroRNA Designer version 3, WMD3 (Ossowski *et al*., 2008). Dr. Steven J. Burgess (University of Cambridge) had kindly designed and provided the oligonucleotides for this work. Two pairs of oligonucleotides, named as LDH3 and LDH4, were chosen to target two different regions of the 978 b *D-LDH* transcript. The target site for the former was at 295 to 315 b while the latter was at 451 to 471 b. For each pair, the single-stranded oligonucleotide was annealed to its complementary oligonucleotide to form a double-stranded 90 bp molecule. In order to confirm successful annealing, the molecule was digested with the restriction enzyme NcoI to give two ~40 bp

DNA fragments. This was checked by using agarose gel electrophoresis (data not shown). Once confirmed, the double-stranded molecule was then phosphorylated using T4 polynucleotide kinase. This was carried out in order to allow the subsequent ligation of the molecule to a dephosphorylated expression vector. The expression vector used for this work was pChlamiRNA3int and was provided by Dr. Attila Molnar (University of Cambridge). This vector contained a strong *PSAD* promoter to drive the nuclear expression of the inserted gene (Fischer & Rochaix, 2001), and also the *Streptomyces rimosus APHVIII* gene, which was controlled by both HSP70 and RBCS2 promoters, to allow the selection of transformants on the antibiotic paromomycin (Sizova *et al*., 2001). The circular vector was linearized by digestion with the restriction enzyme SpeI, and dephosphorylated with alkaline phosphatase to prevent self ligation. The vector was then ligated with each of the two phosphorylated microRNAs by using T4 ligase. The mixtures from the ligation reactions were then used to transform 10-β competent *E. coli* cells. Appropriate controls were also included. Non-transformed cells did not produce any colonies on the $LB_{amp100}$ agar plates as expected, indicating successful antibiotic selection. Transformation with only the dephosphorylated vector yielded no colonies, while the re-ligated non-dephosphorylated vector yielded ~300 colonies, indicative of successful dephosphorylation. Transformation with both the dephosphorylated vector and non-phosphorylated microRNA resulted in no colonies as expected. Transformation with the dephosphorylated vector and each of the two phosphorylated microRNAs yielded ~100 colonies.

Colony PCR was carried out following Molnar *et al*. (2009) to screen the *E. coli* colonies for the presence of the inserted DNA fragment encoding the artificial microRNA, using the recommended pair of primers that would bind to both the expression vector and DNA insert. A total of 8 colonies from each of the two microRNAs were tested. The PCR products were checked using agarose gel electrophoresis; two colonies from each microRNA were found to be positive (data not shown). A representative colony from each of the two microRNAs was selected for the preparation of purified plasmids. To further verify the plasmids, diagnostic restriction digests were carried out. The digests using BsmI, XbaI, NcoI and SmaI produced expected results (Figure 3.10). We also sent the plasmids for sequencing. The sequencing results (data not shown) showed that the microRNA constructs had the correct sequences with no unwanted point mutations and were also positioned in the correct orientation within the vector. Thus, we had successfully constructed two artificial microRNA encoding plasmids, pLDH3 and pLDH4, for the production of *C. reinhardtii D-LDH* knockdown mutants.

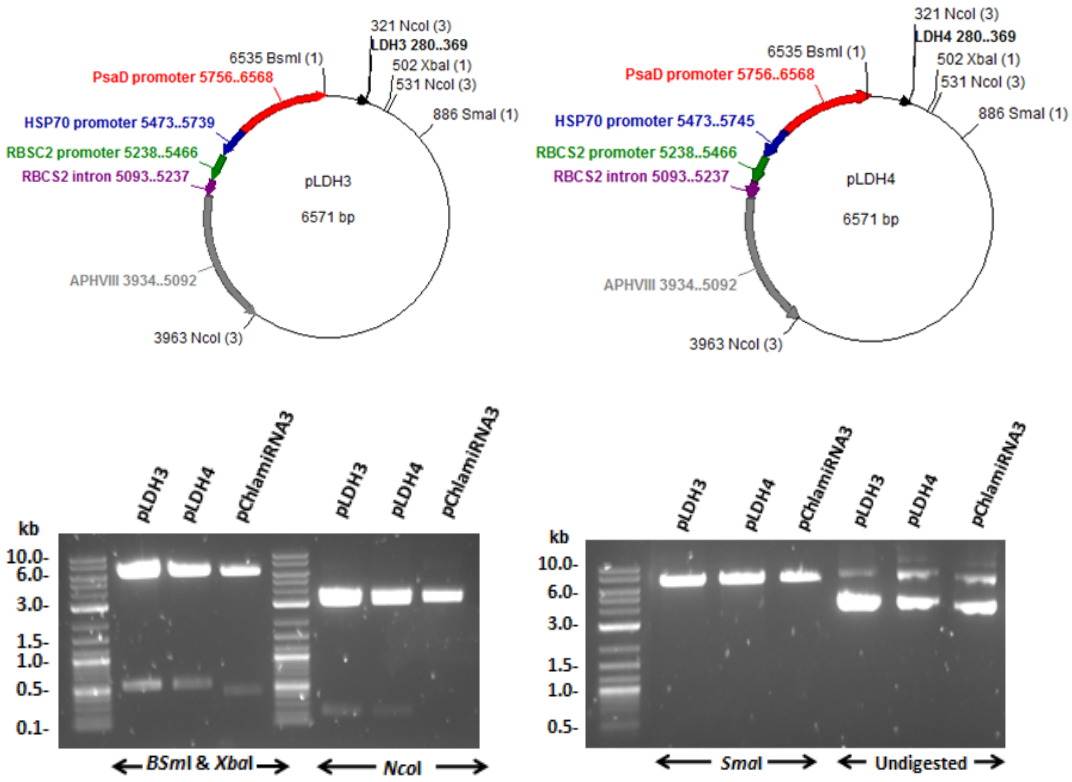


**Figure 3.10 Restriction analyses of constructed artificial microRNAs.**

Expected sizes of BsmI & XbaI digests: pLDH3 & pLDH4 (6033 & 538 bp) and pChlamiRNA3 (6033 & 448 bp). Expected sizes of NcoI digests: pLDH3 & pLDH4 (3432, 3048 & 210 bp) and pChlamiRNA3 (3432 & 3048 bp). Expected sizes of SmaI digests: pLDH3 & pLDH4 (6571 bp) and pChlamiRNA3 (6480 bp).

### 3.2.2.2 Optimisation of *C. reinhardtii* nuclear transformation

We were interested to determine the most efficient method for nuclear transformation. Three different methods were tested: electroporation, biolistic and glass bead method, using strains CC-124 and/or D66 (Section 2.13). Our pre-tests showed electroporation was a better method compared to the other two methods, and more transformants were obtained by using CC-124 than D66 (preliminary data not shown). We therefore decided to employ electroporation as our method for transforming *C. reinhardtii* strain CC-124.

We also tested different forms of DNA for transforming *C. reinhardtii*. For this purpose, we used a 4610 bp plasmid named pJet1.2PpsD-AphVIII (courtesy of Prof. Joerg Nickelsen, University of Munich) which contains an *APHVIII* cassette conferring resistance to paromomycin (Sizova *et al*., 2001). Three different forms of the *APHVIII* construct were tested: First, the cassette in its circular plasmid form; second, the cassette in its linearized form whereby the plasmid was double digested using HindIII and PstI to create a shorter

2255 bp linear fragment; and third, the cassette in the form of a linear PCR fragment in which the *APHVIII* cassette was amplified by PCR to create a shorter 1636 bp linear fragment. We transformed *C. reinhardtii* with 1 μg of purified DNA and found that the PCR fragment had the highest number of transformants followed by the linear fragment, while the circular form produced a lower number of colonies (Table 3.2). Our transformation controls (non-transformed cells) did not produce any transformants on the $TAP_{P10}$ agar plates as expected, indicating successful selection. Our results showed that shorter and linearized fragments produced better numbers of transformants compared to larger or circular fragments. However, we did not rule out the possibility that the unequal number of copies of DNA could also contribute to the differences observed in this work since all transformations were performed using 1 μg of DNA. Although using the PCR fragment yielded a higher number of transformants, we decided to use an enzyme-digested plasmid for future transformation due to the ease of its production and its lower cost.

| **DNA form and size** | **No. of DNA copies for 1 μg** | **Average no. of transformants (±SE)** |
|---|---|---|
| **Circular plasmid (4610 bp)** | $2.01 \times 10^{11}$ | 16 ± 1 |
| **Linear fragment (2255 bp)** | $4.11 \times 10^{11}$ | 352 ± 49 |
| **PCR fragment (1636 bp)** | $5.66 \times 10^{11}$ | 872 ± 27 |

**Table 3.2. Average no. of transformants obtained using different forms of DNA.**
Average value was based on a total of 4 replicates obtained from 2 independent experiments. Transformants were obtained by transforming ~$7.5 \times 10^7$ cells with 1 μg of DNA

Transforming *C. reinhardtii* by electroporation involved a high electric field strength (2000 V/cm) which could potentially kill the cells. We therefore determined the survival rate of *C. reinhardti*. We calculated the number of viable colony forming cells before and after electroporation by diluting the cells in a series of dilutions ($10^2$ to $10^5$ dilutions), plating and growing them on TAP agar plates. We found that only dilutions $10^4$ and $10^5$ gave readable counts. The results showed the viability of the cells was not drastically affected (Table 3.3).

| Dilution | Before electroporation | | After electroporation | |
|---|---|---|---|---|
| | Average no. of colonies | Colony forming units, CFU (cells/ml x $10^7$) | Average no. of colonies | Colony forming units, CFU (cells/ml x $10^7$) |
| $10^{-4}$ | 222 ± 18 | 2.2 ± 0.2 | 194 ± 32 | 1.9 ± 0.3 |
| $10^{-5}$ | 25 ± 1 | 2.5 ± 0.1 | 18 ± 4 | 1.8 ± 0.4 |
| | Average CFU | 2.2 ± 0.2 | Average CFU | 2.1 ± 0.2 |

**Table 3.3. No. of colony forming units before and after electroporation.**

Average value (±SE) was based on a total of 4 replicates obtained from 2 independent experiments.

### 3.2.2.3 Generation and isolation of *D-LDH* knockdown mutants

The generation of *D-LDH* knockdown mutants was carried out in collaboration with Ms. Oksana Iamshanova (Imperial College London). Plasmids pLDH3 and pLDH4 were inserted into *C. reinhardtii* by electroporation. We decided to transform the algal cells with either the circular or the purified linearized form of the plasmids. To linearize the plasmids, we firstly tested three different restriction enzymes: NaeI, SmaI and NotI. Both SmaI and NotI produced complete linearization of the DNA after 1 hour of digestion but NaeI showed incomplete digestion (agarose gel not shown). We therefore decided to use SmaI for plasmid linearization (Figure 3.10). As expected, we found that the linearized form of the plasmids produced more transformants on the $TAP_{P10}$ agar plates compared with the circular form (Table 3.4). We also used $TAP_{P10}$ agar plates supplemented with 1 mM DL-lactic acid. Our rationale was that the disruption of D-LDH pathway could affect the survival of potential mutants due to D-lactate not being produced and thus might require lactate supplementation. However, we later found out our transformants, which were selected on DL-lactate-supplemented medium, could also grow normally on the non-supplemented $TAP_{P10}$ medium. Hence, lactate supplementation was no longer necessary.

| Plasmid | pLDH3 | | pLDH4 | |
|---|---|---|---|---|
| | $TAP_{P10}$ | $TAP_{P10 + lactate}$ | $TAP_{P10}$ | $TAP_{P10 + lactate}$ |
| **Circular** | 172 ± 73 | 23 ± 2 | 90 ± 20 | 42 ± 9 |
| **Linearized** | 345 ± 84 | 293 ± 143 | 135 ± 65 | 125 ± 25 |

**Table 3.4. Average no. of transformants obtained with artificial microRNAs.**

Average values (±SE) were obtained from three replicates. Transformants were obtained by transforming ~7.5 x $10^7$ cells with 1 μg of DNA.

In order to get protein samples, we randomly selected more than 50 transformants from all of the different plates shown on Table 3.4 and cultivated them in TAP medium to late log phase ($OD_{750}$ ~1.0). The screening for *D-LDH* knockdown mutants was carried out by immunoblotting. In order to get a more reliable quantification, we carried out two technical replicates per biological sample. To make sure any results obtained were not due to the type of membrane being used, one set of the technical replicates was blotted onto nitrocellulose membrane while the other set was blotted onto PVDF membrane. We found no significant differences were observed between the two membranes (data not shown). To aid in the quantification of D-LDH protein, the WT protein sample was diluted in a series of dilutions (100% to 12.5%) which would later be compared to the mutants to get the approximate reduction in D-LDH. In this first round of screening, we identified a total of 28 potential knockdown mutants with at least 80% reduction in their D-LDH level relative to WT (data not shown). Our loading controls (Coomassie staining, αD1 and αPSAD) confirmed that we loaded an equal amount of proteins. We were also interested to see if transforming *C. reinhardtii* with the linearized plasmid was better at producing knockdown mutants compared to using the circular plasmid: we did not see any obvious difference in the number and degree of knockdowns produced by both types. Similarly, there was also no obvious difference between pLDH3 and pLDH4 (data not shown). Both artificial microRNAs could successfully reduce the D-LDH level, although they targeted separate sites on the *D-LDH* transcript.

We re-grew mixotrophically the 28 *D-LDH* knockdown mutants for a second round of screening. We re-identified a total of 14 mutants with at least 80% reduction in their D-LDH level while the other 14 mutants contained WT levels of D-LDH (Appendix 2). Our loading controls (Coomassie Brilliant Blue staining and αPSAD) confirmed equal loading of samples. The possible ability of *C. reinhardtii* mutants to revert back to WT is a potential drawback when using artificial microRNA knockdown approaches, and thus repetitive screenings were used to confirm that the knockdown mutation remained stable. Four knockdown mutants were chosen for future analyses: *L11-3*, *L11-13*, *c* and *54*. These were later re-named as *ldh*-KD1, *ldh*-KD2, *ldh*-KD3 and *ldh*-KD4, respectively. These four knockdown mutants remained stable throughout the research period.

### 3.2.2.4 Transcript and protein analyses of *ldh*-KD mutants

WT (CC-124) and the *ldh*-KD mutants (i.e. *ldh*-KD1, *ldh*-KD2, *ldh*-KD3 and *ldh*-KD4) were grown photoautotrophically in HSM, with air bubbling, to late log phase for protein and transcript analyses.

For transcript analyses, RNAs were extracted and the quality of the transcripts was confirmed by running them in an agarose gel (data not shown). The RNAs had to be converted to cDNA before quantitative real time PCR was performed. We amplified *D-LDH* and *RPL10A* transcripts using the Taqman Gene Expression Assay System (Applied Biosystems, USA). The *RPL10A* encodes the 60S ribosomal protein L10a, and served as our reference gene to normalise our *D-LDH* data because it has been reported that an accurate quantification of gene expression can be obtained by normalisation to transcripts encoding ribosomal proteins (Zhou *et al*., 2010). For the calculation and comparison of transcript levels, a relative efficiency plot had to be plotted first according to the manufacturer's instructions. To do this, we used the WT sample with three bioreplicates (each with two technical replicates). Our relative efficiency plot (Appendix 3) showed the amplification efficiencies of *D-LDH* and *RPL10A* were not similar (slope > 0.1). Therefore, the standard curve method had to be employed for this work, and hence, standard curves for *D-LDH* and *RPL10A* were also plotted (Appendix 3). Our results showed that our four *ldh*-KD mutants had significantly less *D-LDH* transcript compared to the WT with the mutants having less than 20% of the transcript (Figure 3.11.A). Thus, our artificial microRNAs had successfully reduced the transcript level up to 80%. Similarly, we also measured the *PDC3* transcript level of the WT and *ldh*-KD mutants. We found out the *PDC3* transcript levels were similar between the WT and the mutants, further confirming equal loading of samples (Appendix 3).

For protein analyses, proteins were extracted and immunoblotting was performed. Our results showed all the four *ldh*-KD mutants had reduced protein level up to 80% in comparison with the WT (Figure 3.11.B). This is in agreement with the transcript analyses. Our loading control ruled out the possibility that the observed reduction could be due to unequal loading of samples. Similarly, when we used TAP-grown samples, we also observed a decrease in the D-LDH level up to 80% relative to the WT for all four knockdowns (data not shown).

**A**

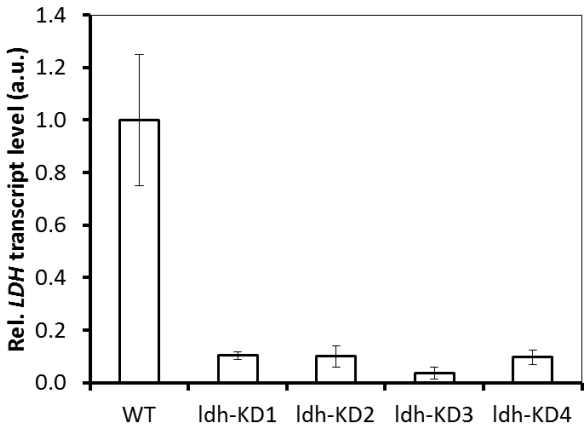


**B**

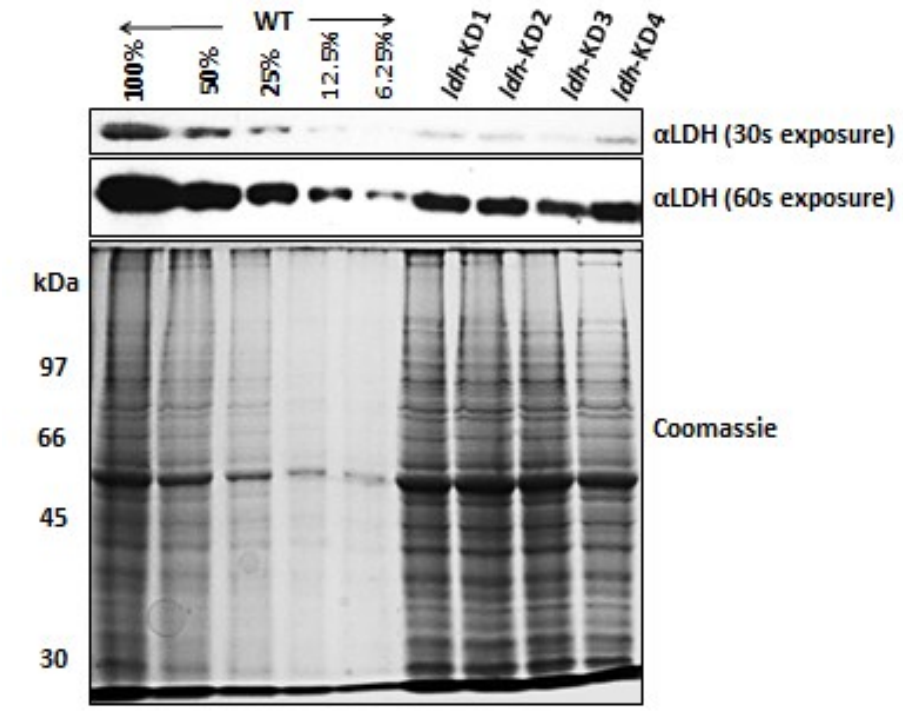


**Figure 3.11 *D-LDH* transcript and protein quantitative analyses for HSM-grown algae.**

A) Transcript levels measured by qRT-PCR. Average values (±SE) were based on three bioreplicates with two technical replicates each. B) Protein levels measured by immunoblotting. D-LDH bands were shown in two durations of X-ray exposure to aid in relative quantification of *D-LDH* knockdowns. Loading control was provided by Coomassie Brilliant Blue staining.

### 3.2.2.5 D-LDH activity analysis of *ldh*-KD mutants

The protein and transcript analyses showed the knockdown mutants had an approximate 80% reduction in the D-LDH level relative to the WT. To further confirm the D-LDH pathway was affected by this knockdown, we did an enzymatic activity assay using the intracellular materials extracted from the cells. The cells were grown in TAP medium to late log phase before being broken using an ultrasonicator. The cellular debris and unbroken cells were removed by centrifugation, and the supernatant containing the D-LDH enzyme was collected for the enzymatic activity assay. To confirm the knockdown mutants had not reverted to the WT phenotype and still had a knockdown level of D-LDH, we did immunoblotting with the collected supernatants. Our blots showed the knockdown mutants still had lower levels of D-LDH compared to the WT (Appendix 4). Protein concentrations were determined using the Bio-Rad Protein Assay (Bio-Rad, UK) according to the manufacturer's instructions, and the concentrations were normally found to be between 2 to 3 mg/ml. We used BSA to generate our protein standard curve, and as recommended the standards were re-run each time samples were measured (data not shown). The kinetic data obtained from the enzyme assay were normalized to the amount of total proteins used from the cell free extract.

$NAD^+$-dependent D-LDH activity was determined by measuring the initial changes in spectrophotometric absorbance at 340 nm. The enzymatic reaction was performed in a 1-ml assay mixture containing 25 mM sodium phosphate at pH 7.5, 250 mM sodium chloride, 300 µM NADH, 10 mM sodium pyruvate and 100 µl cell extract. When we tested 50 and 200 µl of cell extract, we observed as expected that calculated rates of enzymatic activity (in nmol/min) were roughly halved and doubled, respectively (data not shown). The D-LDH activity assays showed there was a faster decline in the absorbance values in the WT compared to the knockdown mutants when a similar amount of total protein was analysed (representative results are shown in Appendix 4).The decline in the absorbance was caused by the consumption of NADH by the D-LDH enzyme found in the cell extract. However, the cell extract should also contain many other proteins that could also utilize NADH. Therefore, we also measured the decrease in the absorbance in a control assay mixture containing all components except for the substrate pyruvate. The value obtained from this control assay was used to deduct any value obtained from its corresponding D-LDH activity assay, which was found to be ~20% of the D-LDH activity assay value based on CC-124 and CC-125. Our results showed the background rates of NADH oxidation were lower than in the presence of

added pyruvate (representative results are shown in Appendix 4). We also did a negative control assay where we did not add any cell extract into the 1-ml assay mixture, and our results showed there was no decrease in the absorbance as expected (data not shown).

Our D-LDH activity assays on cell extracts confirmed there was a reduction in the D-LDH enzymatic activity in the knockdown mutants (Figure 3.12). The D-LDH pathway was affected by the low level of D-LDH protein found in these mutants. On average, both *ldh*-KD1 and *ldh*-KD2 only showed 9% of D-LDH enzymatic activity relative to the WT. This means there was ~90% reduction in the enzymatic activity and this almost agrees with the ~80% reduction in the D-LDH protein and transcript level.

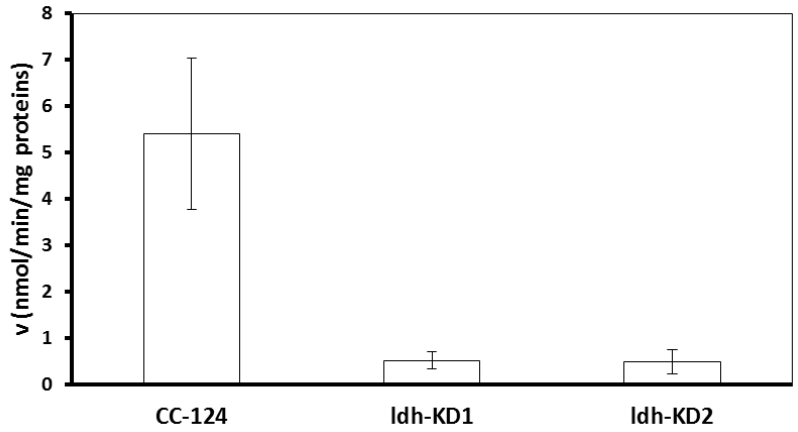


**Figure 3.12 Rates of NADH oxidized/ pyruvate reduced by *C. reinhardtii* D-LDH.**

Average values (±SE) were based on three biological replicates. The units of enzymatic activity (v) were calculated as nmol of NADH oxidized (or pyruvate reduced) per minute per mg of total protein assayed.

### 3.2.2.6 Assessing the physiological role of lactate

The physiological roles of the D-LDH pathway in *C. reinhardtii* are still not understood. When the algal cells experience dark anoxic conditions, glycolysis and fermentation would be activated. The D-LDH pathway would be active, and this would lead to the reduction of pyruvate to D-lactate and the oxidation of NADH to $NAD^+$. The generated $NAD^+$ could be used to sustain glycolysis. In light of this possibility, there is a good link between the D-LDH pathway and glycolysis. The reduction of the pyruvate by the D-LDH pathway could also limit any potentially damaging consequences of pyruvate accumulation in the cells due to the starch breakdown. Therefore, it is not surprising for the D-LDH pathway to be active under dark anoxic conditions. However, more interestingly the D-LDH pathway is also found to be active under light oxic conditions. Lactate was found to be produced by light-acclimated *C. reinhardtii* cultures (Davis *et al*., 2013). This was not surprising as the D-LDH protein was found to be expressed during mixotrophic and photoautotrophic growth, and the enzyme was thought to be active as revealed by the lactate being secreted during the growth (Burgess, 2011). This brings us to question the physiological roles of this novel pathway under the specified conditions.

To assess if *D-LDH* knockdown had an effect on the cell morphology and mobility, the cells were observed using a standard laboratory compound microscope with a magnification up to 400X. We assessed both TAP-grown and HSM-grown cells that were grown to late log phase. We found there were no obvious difference between the *ldh*-KD mutants and the WT (data not shown), suggesting the knockdown had no observable effect on the cellular appearance and swimming ability of the alga. It should be noted that under the compound microscope the cells, which were about 10 μm in diameter, still appeared small even with the highest magnification and hence minor morphological changes would not be easily detected.

To qualitatively assess if *D-LDH* knockdown had an effect on the cell growth or phenotype under high light, the knockdown mutants were grown on agar plates at three different light intensities (30, 150 and 500 $\mu Em^{-2}s^{-1}$). To carry out these tests, algal cells from TAP agar plates were grown in HSM overnight to an $OD_{750}$ of 0.05. TAP and HSM agar plates were spotted with 5 μl of the overnight cultures, and were continuously exposed to the different light intensities. For the light source, we used a cool white LED lamp (Deltech, UK). To qualitatively assess if *D-LDH* knockdown had an effect on the cell growth in the absence of light, we also grew the cells in the dark. When we did these qualitative assessments, we also tested the effect of adding acetate into the growth medium on the cell

growth. As expected, our results (Figure 3.13) showed that the cells grew better on the acetate-containing medium (TAP) compared to the medium without this carbon source (HSM) in all tested conditions. No cell growth was observed on the HSM plate incubated in the dark, indicating in the absence of light growth required the presence of acetate in the medium. When comparing the cell growth between the low and high light intensities, it was observed that the cells that were grown under the high light intensities appeared yellowish compared to the cells that were grown under the low light, which showed a healthy green colour.

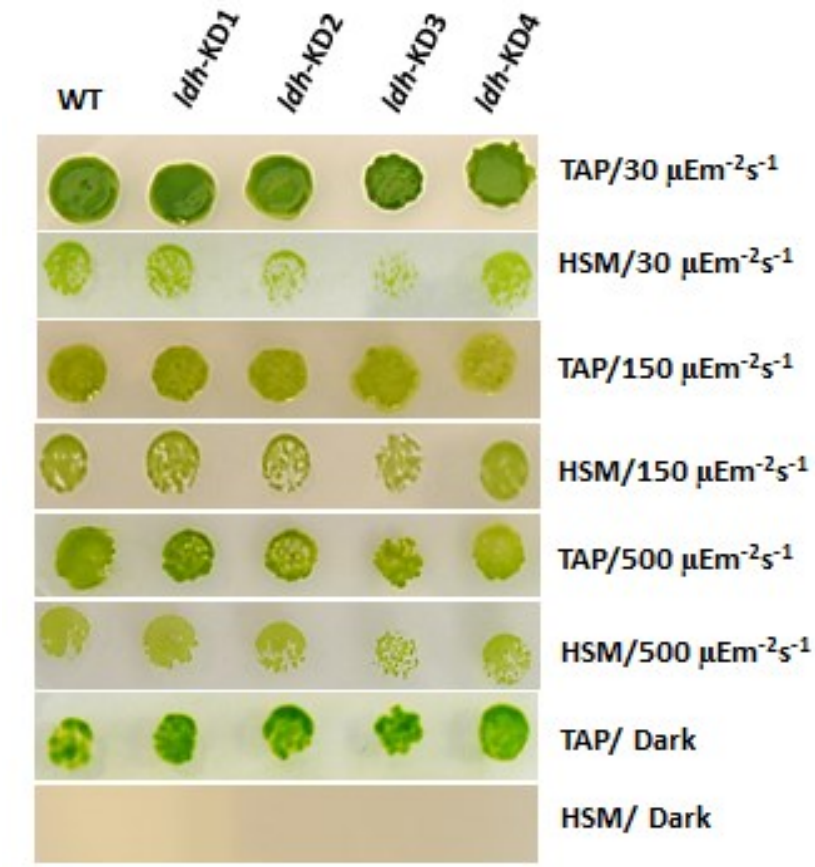


**Figure 3.13 Growth analysis of *ldh*-KD mutants under different light intensities.**

Equal amount of cells were spotted either on a TAP or HSM plate, and exposed continuously to different light intensities. Photos were taken after 1 to 2 weeks of growth. For each treatment, six bioreplicates were carried out and a representative result is shown.

The assessment of cell growth described above was carried out using agar plates that did not contain the paromomycin antibiotic used to select the *ldh*-KD mutants. This was carried out in order to allow the WT to grow on the same plate as the mutants. In order to rule

out the possibility of the mutants reverting back to the WT when grown in the absence of this selective pressure, we also tested the mutants using paromomycin-containing TAP and HSM agar plates. The WT was also tested concurrently with the mutants by using similar agar plates but without the antibiotic. The cells were only exposed to either 30 (control) or 150 $\mu Em^{-2}s^{-1}$. Similarly, we did not observe any significant difference between the *ldh*-KD mutants and the WT (data not shown).

Although the qualitative assessment of cell growth under high light intensity described above did not reveal any suggestive physiological role of the D-LDH pathway, we decided to carry out a quantitative assessment of *D-LDH* knockdown on cell growth under high light since it might be able to reveal minor effects. To carry out this assessment, algal cells were cultured and tested in HSM instead of TAP medium. This was because to rule out any potential effect acetate might have that could conceal or suppress any potential effect of *D-LDH* mutation. The cells were grown either under high light (150 $\mu Em^{-2}s^{-1}$) or low light (30 $\mu Em^{-2}s^{-1}$; as control). When grown in the HSM, both the low- and high-light grown cultures showed a healthy green colour without any clear distinction between the *ldh*-KD mutants and the WT (data not shown). To quantify the growth, the optical density of the culture was measured at specific time points. The loss of water due to evaporation was also quantified, and we found the total loss was 7.7 ± 0.5% (average ± SE was based on 3 replicates) of the initial volume employed. Our results (Figure 3.14) showed under low light all the four *ldh*-KD mutants had similar cell growth to the WT. Similarly, the growth under high light was also not distinctively different between the mutants and the WT. Although the average $OD_{750}$ values for the mutants were generally lower when compared to the WT, the overlapping standard error bars need to be taken into account with the exception of *ldh*-KD3. This particular line had a slightly lower $OD_{750}$ values when compared to the WT. This was because the cells tended to stick together and form clumps, which could result in an inaccurate determination of their optical density. Since this ability to form clumps was not observed on the other *ldh*-KD mutants, it is not associated with the *D-LDH* mutation. It could be due to another random mutation or it could just be a natural occurrence as according to Harris (2009), *C. reinhardtii* could sometimes form palmelloids (clumps of non-motile cells). The growth curves for the *ldh*-KD mutants shown in Figure 3.14 were very similar to the WT, with a doubling time of ~10 hours when grown under high light and ~25 hours when grown under low light.

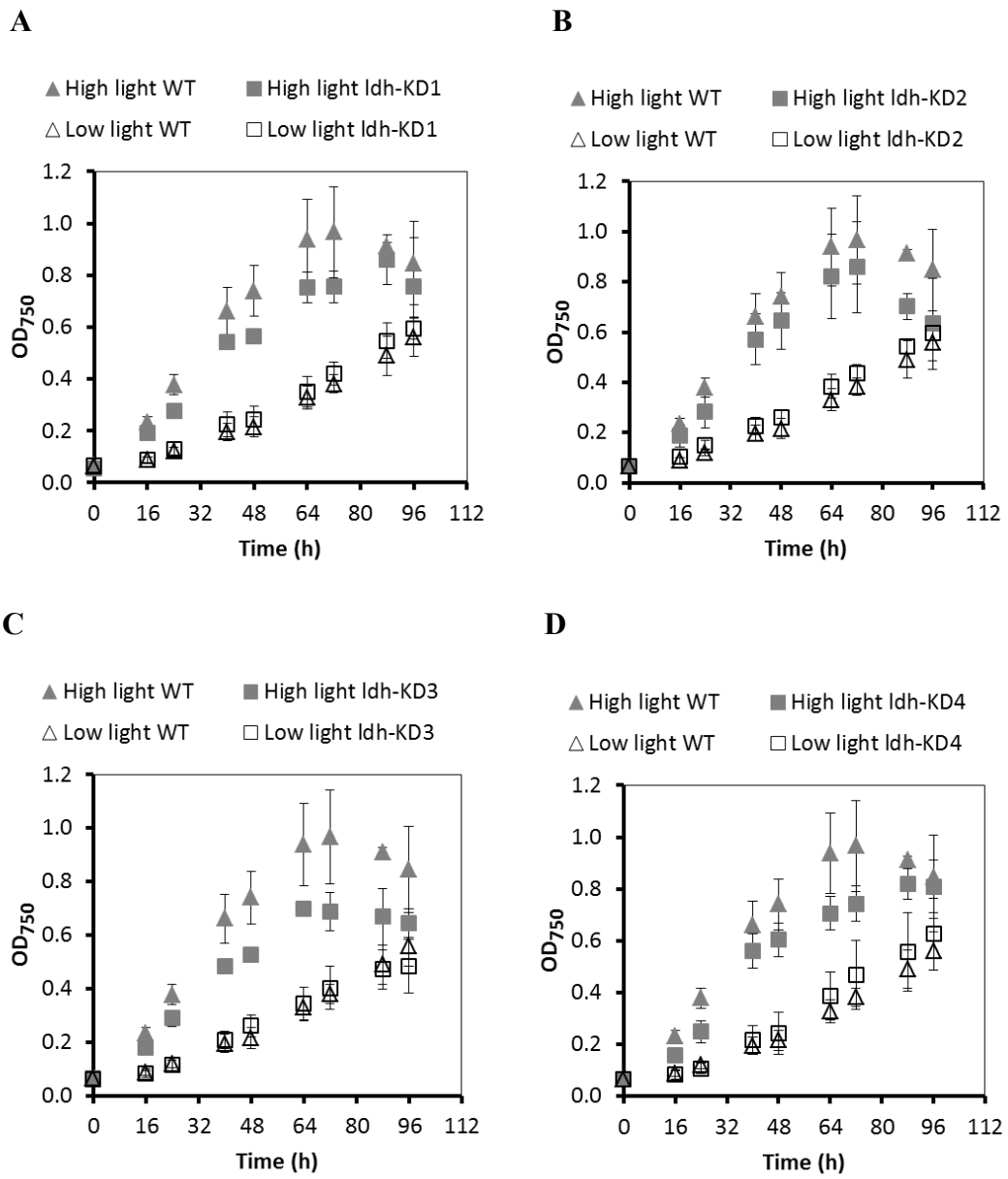


**Figure 3.14 Cell density analysis of *ldh*-KD mutants grown under high and low light.**

Cells were grown in HSM bubbled continuously with air, and exposed either to low (30 $\mu Em^{-2}s^{-1}$) or high light (150 $\mu Em^{-2}s^{-1}$). Optical density was measured at 750 nm ($OD_{750}$) using a spectrophotometer. Average values (±SE) were based on three independent replicates.

*C. reinhardtii* artificial microRNA mutants could potentially revert back to WT. To rule out this possibility, we collected the HSM-grown cells at the late log phase (at 64 hours after the start of the growth analysis; Figure 3.14) and quantified their D-LDH protein levels by immunoblotting. The blots confirmed that the four *ldh*-KD mutants had not reverted to WT. The mutants only had ~20% or less D-LDH protein relative to the WT, and our loading

controls confirmed the unequal D-LDH levels observed was not due to unequal loading (Appendix 5).

To assess if *D-LDH* knockdown had an effect on the sensitivity of photosynthesis to high light, we measured the amount of oxygen produced by the cells after being exposed to a physiologically-stressful high light intensity. The high-light treatment would damage the cell's photosynthetic apparatus, which would inhibit photosynthesis and lead to impaired oxygen production. However, photosynthetic organisms have evolved a number of regulatory systems to prevent or reduce this photoinhibition. If the D-LDH pathway was involved in this regulatory system, the knockdown of this pathway could cause the cell's photosynthetic efficiency to be more affected compared to the WT. One hypothesis, termed the 'lactate-valve hypothesis' has suggested that D-LDH could potentially operate as a valve to dispose of excess reducing equivalents in the chloroplast under anoxia and during photoautotrophic growth, similar to the malate valve (Gruber *et al*., 1974; Burgess, 2011).

Our preliminary analysis showed the initial photosynthetic efficiencies of the knockdown mutants and WT before the high light treatment were very similar. This was carried out by measuring the photosynthetic efficiency of photosystem II, also known as $F_V/F_M$ by using a PAM fluorometer (DUAL PAM 2000, Walz, Germany), and the preliminary analysis showed all the strains had a similar value of ~0.6. We did not measure the $F_V/F_M$ after the high light treatment because the oxygen measurement would be sufficient to directly inform us of the photosynthetic efficiency of the cells.

To carry out this assessment of oxygen production, the cells were grown in HSM with air bubbling to late log phase. After harvesting and resuspending in the same medium, the cells were exposed to a very high light intensity (500 $\mu Em^{-2}s^{-1}$) for a total period of 4 hours. Prior to this 500 $\mu Em^{-2}s^{-1}$ setting, an attempt was made to expose the cells to 1000 $\mu Em^{-2}s^{-1}$ but this setting was found to be unsuitable because after 1 hour of exposure all the cells became yellowish and the quantity of oxygen produced was negligible. It was suspected the heat from the light source could be mainly responsible for this issue. For oxygen measurements, we collected 1 ml samples at every 1 hour interval and used the Clark-type $O_2$ electrode (Hansatech, UK) to measure their light-saturated rate of oxygen evolution. To ensure it was a light-saturated rate, we used an optimised amount of chlorophyll for the measurements, which was 30-40 µg/ml (Appendix 6). The oxygen evolution was measured in the presence of 2,5-dichloro-1,4-benzoquinone (DCBQ; an artificial PSII electron acceptor) and potassium ferricyanide (for oxidation of DCBQ). Upon exposure to high light, the production of oxygen in the WT initially declined but after 1 hour the production gradually

improved (Figure 3.15). This should be due to the cell regulatory or repair system responsible in reducing the effect of photoinhibition. We also carried out a control whereby the cells were incubated with the antibiotic chloramphenicol which would inhibit chloroplast protein synthesis. If proteins were unable to be synthesized, the cells would not be able to perform any protein-dependent regulations or to repair themselves from the photodamage. Hence after 1 hour of high-light treatment, the oxygen evolution of the chloramphenicol-treated cells did not improve but continued to drop down. By comparing the oxygen evolution of the WT and *ldh*-KD mutants, no difference was observed. The *ldh*-KD mutants did not display any apparent vulnerability to photoinhibition. Our preliminary analysis of the cell's ability to produce oxygen in the absence of DCBQ and KFeCN also suggests there was no noticeable difference between the mutants and the WT (data not shown).

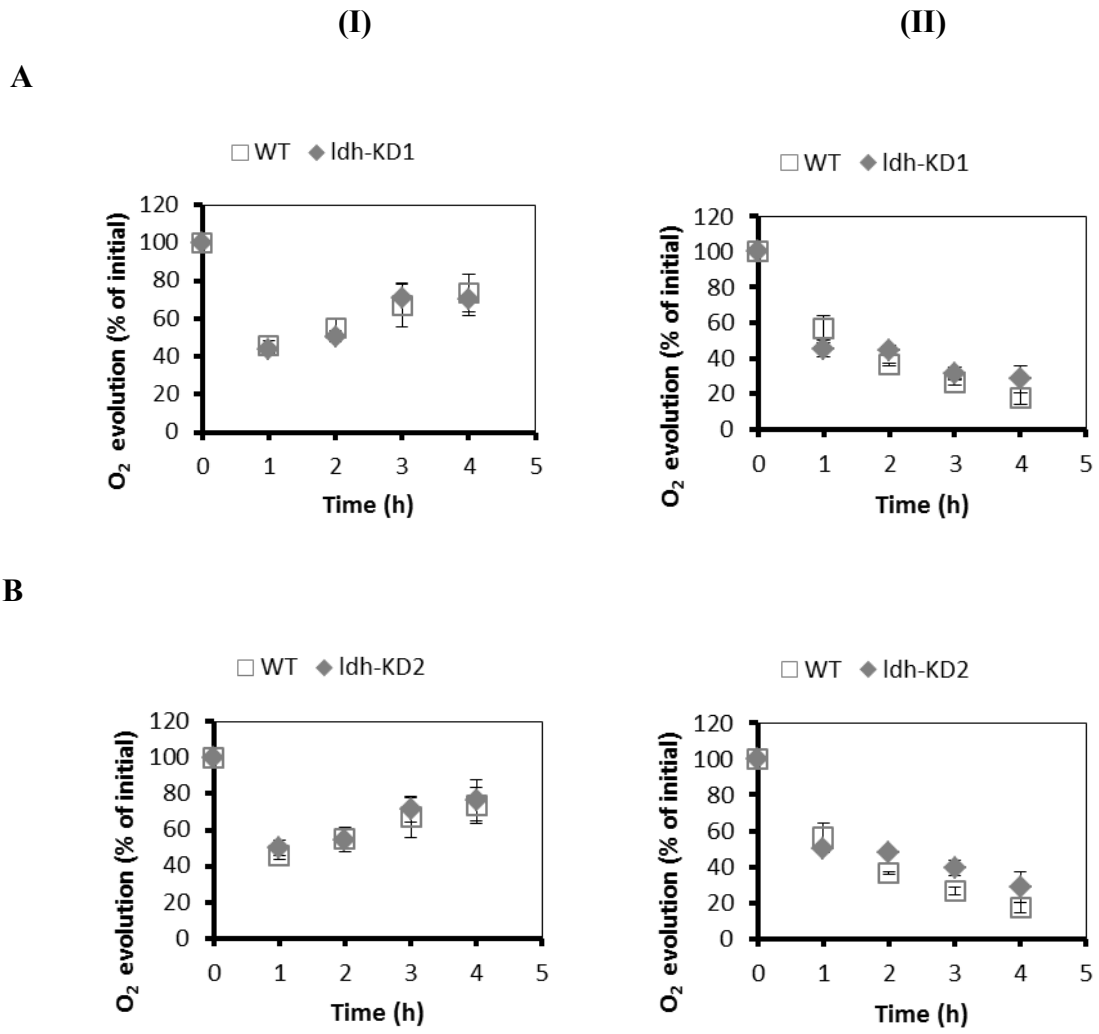

**C**

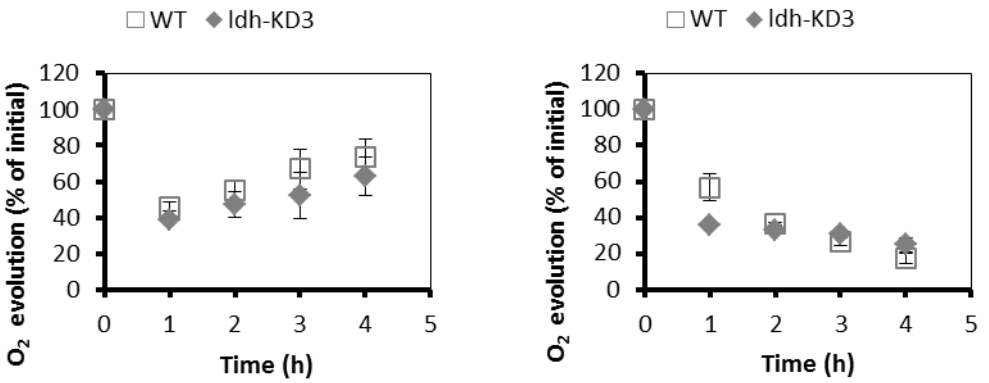


**D**

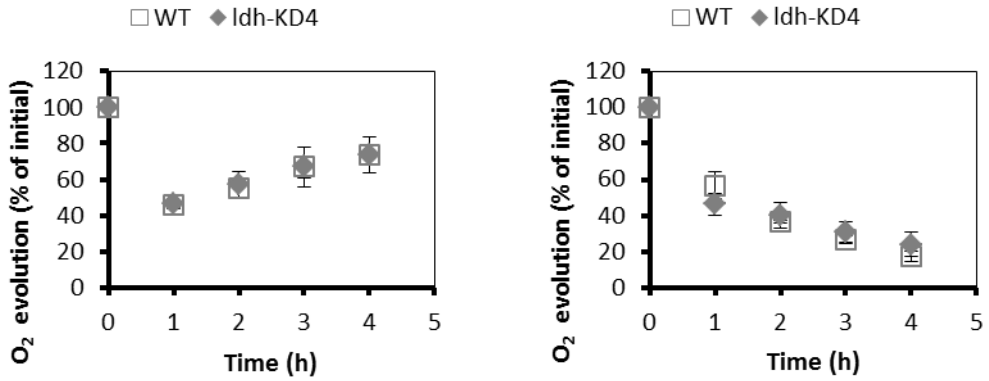


**Figure 3.15 Photoinhibition assays.**

Light-saturated rate of oxygen evolution from HSM-grown cells exposed to a very high light intensity (500 $\mu Em^{-2}s^{-1}$) for a duration of 0 to 4 hours. The cells were incubated either in the absence (I) or presence (II) of chloramphenicol. Oxygen evolution was measured in the presence of DCBQ and potassium ferricyanide. Average values (±SE) were based on three independent replicates, and were expressed as percentage of the initial values (40 to 60 µmole/h/mg chlorophyll).

### 3.2.2.7 Metabolite analysis of *ldh*-KD mutants under dark anaerobic condition

To assess if *D-LDH* knockdown had an effect on metabolites excreted in the dark under anaerobic conditions, we analysed the metabolites secreted by the algal cells after 4 hours of dark anaerobic incubation. The cells were first grown in TAP medium to late log phase and later re-suspended and concentrated 20 times in HSM to give a total chlorophyll concentration of ~150 µg/ml. The chlorophyll concentration was measured according to Porra *et al.* (1989). The reason for using HSM instead of TAP medium was to remove acetate from the analysed medium to allow for the measurement of excreted acetate. We did not re-suspend the cells in anaerobic induction buffer, AIB (50mM $KH_2PO_4$ pH 7.0, 3mM $MgCl_2$) (Mus *et al.*, 2007) as carried out by similar studies (Burgess et al., 2012; Catalanotti *et al.*, 2012; Magneschi *et al*., 2012). This was to avoid any potential effect on fermentation metabolism due to nutrient stress caused by some missing nutrients, as discussed by Burgess *et al*. (2012). Alternatively, instead of using HSM, a modified TAP medium (without adding acetate; known as Tris minimal medium) could have been used. However, we opted to use HSM as it lacks Tris which gives a strong signal in nuclear magnetic resonance (NMR) spectra.

Apart from assessing the effect of *D-LDH* knockdown, we were also interested to determine the effect of both *D-LDH* knockdown and PFL1 inhibition on the dark anaerobic metabolite production. To inhibit PFL1, the cells were incubated with sodium hypophosphite (HP) as carried out in previous studies (Ohta *et al*., 1987; Hemschemeier *et al*., 2008; Burgess *et al*., 2012). Hypophosphite is considered to be a formate analogue and acts as a competitive inhibitor of PFL1 (Knappe *et al*., 1984). It should be noted that when this test was carried out, we had not yet isolated an *ldh-pfl1* double mutant that had both *D-LDH* knockdown and *PFL1* knockout mutations (see Chapter 4) and hence, this explains the use of the PFL1 inhibitor. To establish anaerobic condition, the algal culture was initially purged with argon to remove dissolved oxygen and then incubated in the dark. After 4 hours, the sample was harvested by centrifugation. The supernatant was further filtered to remove any residual cells and then collected for metabolite analysis. A protein sample was also collected for protein immunoblot analysis. This was to confirm the *D-LDH* knockdown mutation was still stable. Our blots confirmed the lower levels of D-LDH protein (~20%) relative to the WT, and the blots also showed the cells were in anoxic condition as anticipated, indicated by the expression of oxygen-sensitive hydrogenases (Appendix 7).

We used NMR spectroscopy to analyse the metabolites excreted by the cells. This was carried out in collaboration with Dr. Volker Behrends and Dr. Jacob Bundy (Imperial College London). The NMR analysis showed that a number of metabolites were excreted and accumulated after 4 hours of dark anaerobic incubation (Figure 3.16). Their concentrations were quantified relative to the NMR standard that we used, which was 4,4-dimethyl-4-silapentane-1-sulfonic acid (DSS).

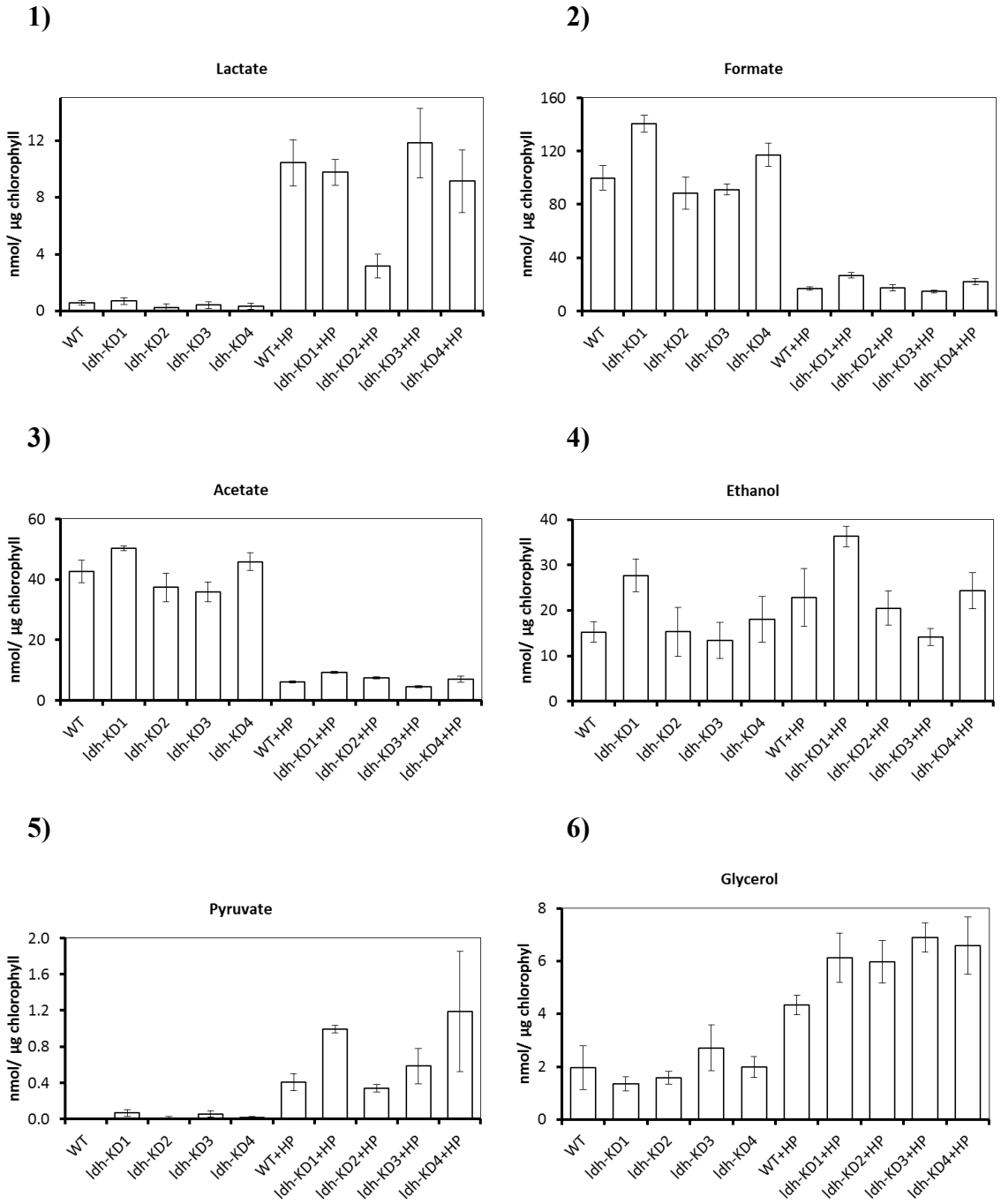

**7)**

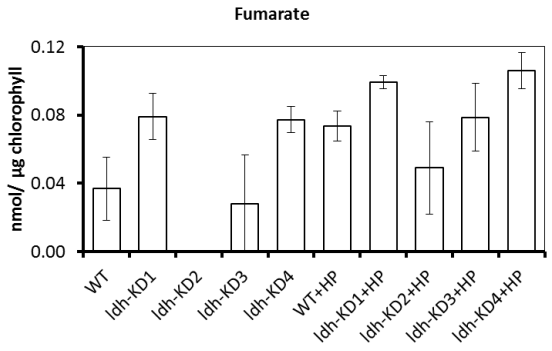


**8)**

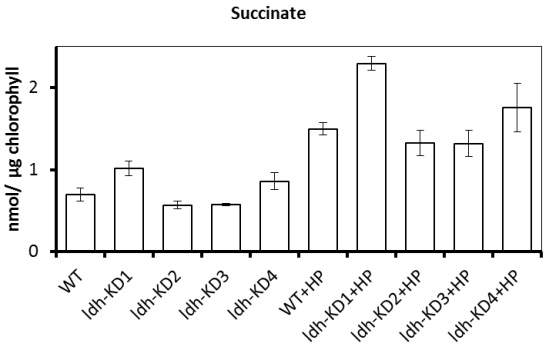


**9)**

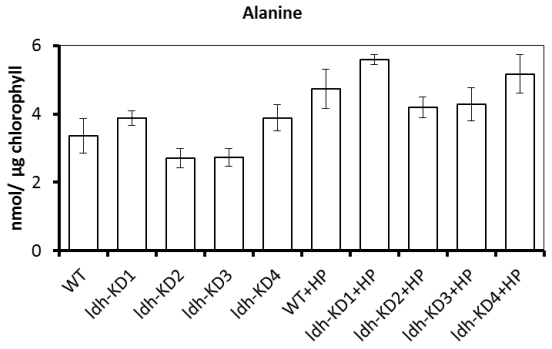


**10)**

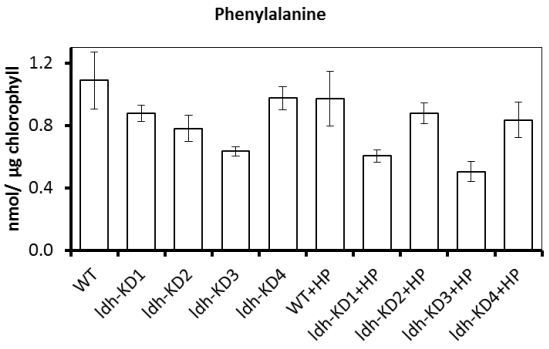


**11)**

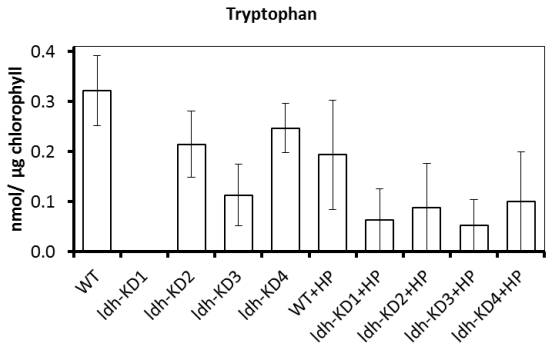


**12)**

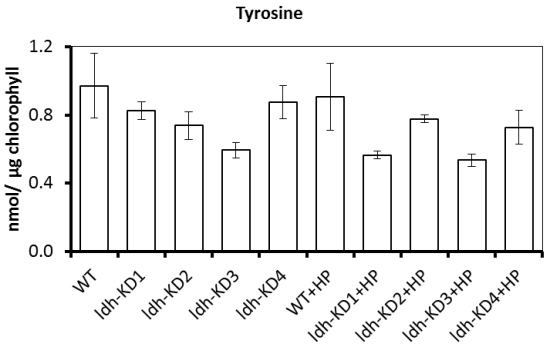


**13)**

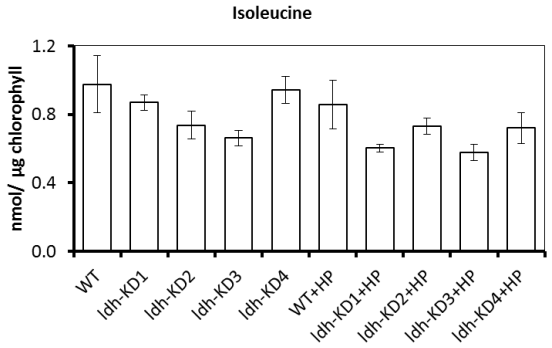


**14)**

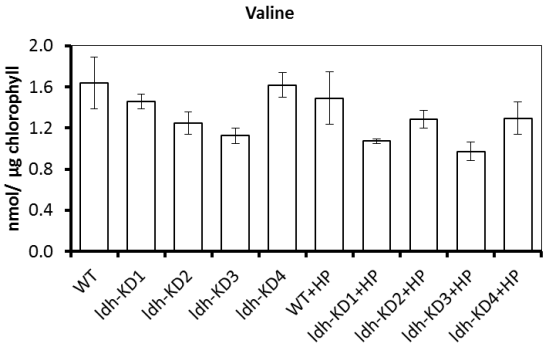

**15)**

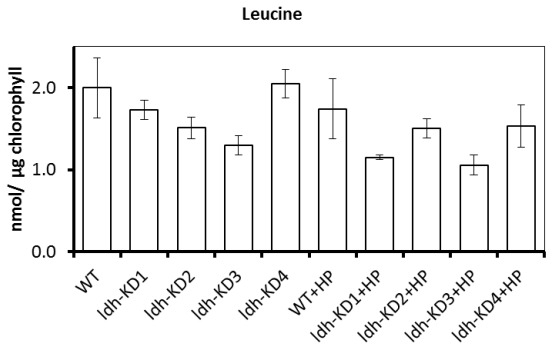


**16)**

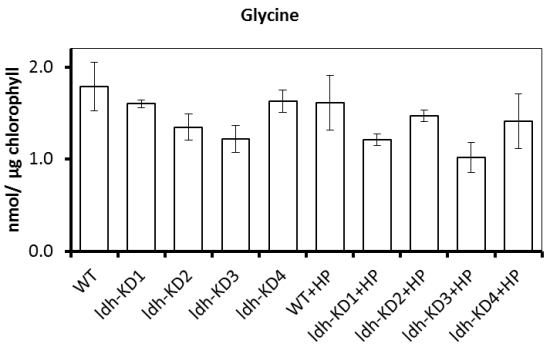


**17)**

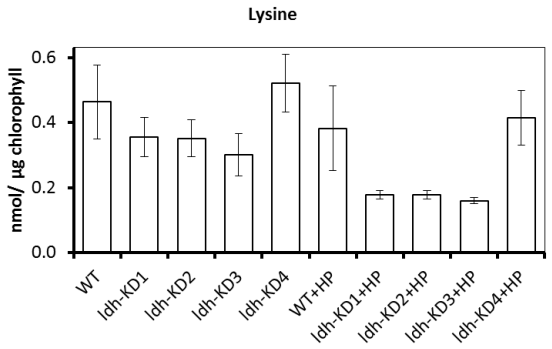


**18)**

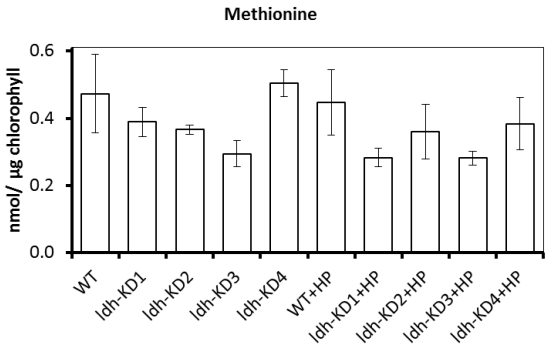


**19)**

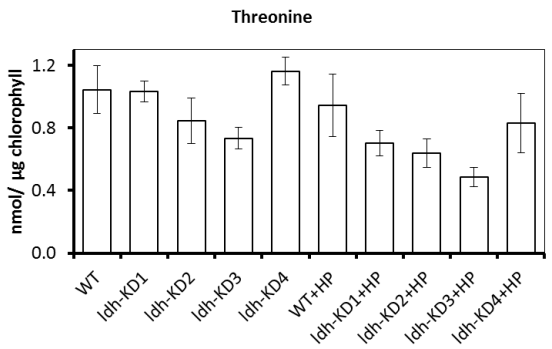


**20)**

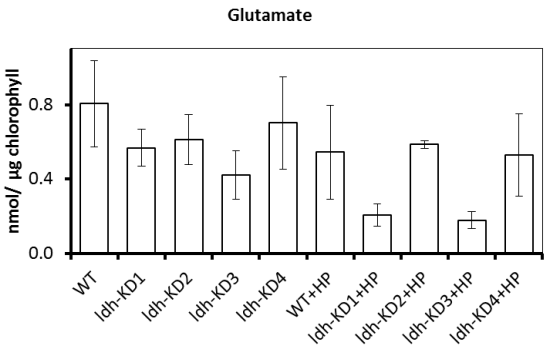


**21)**

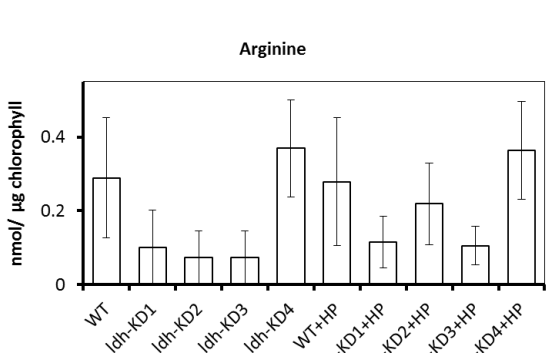


**22)**

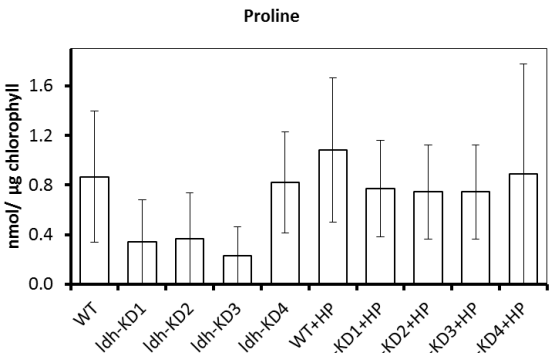

**23)** **24)**

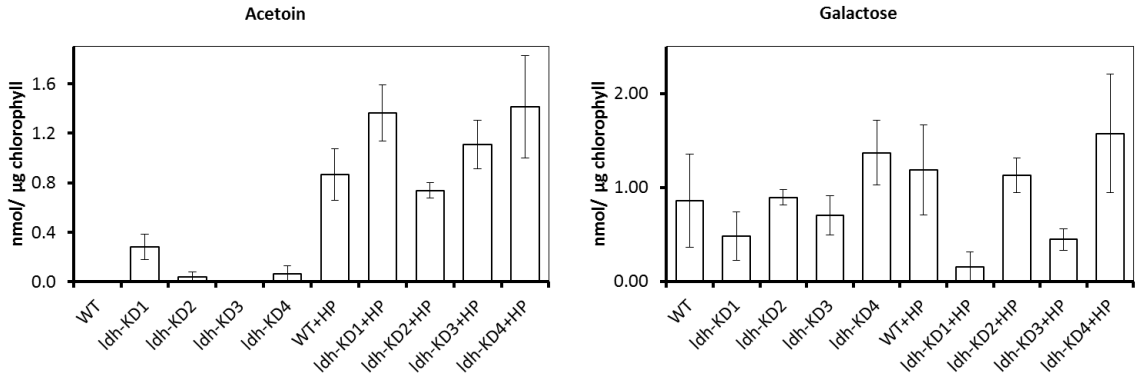


**Figure 3.16 NMR analysis of metabolite production under dark anaerobic condition.**

Excreted metabolites were analysed after 4 hours of dark anaerobic incubation in HSM. The metabolite concentrations were quantified relative to the NMR standard (DSS). Average values (±SE) were based on three biological replicates, and the values were normalised to the concentrations of chlorophyll (~150 µg/ml). Samples were also treated with 10 mM sodium hypophosphite (HP) to inhibit PFL1.

In order to confirm the metabolite results obtained from the NMR analysis, we also re-analysed the same samples using a different analytical technique. We used HPLC to quantify selected metabolites that were present in the samples. This was carried out in collaboration with Ms. Charlotte E. Ward (Imperial College London). The selected metabolites that we only managed to quantify were lactate, formate, acetate, pyruvate, ethanol, succinate and glycerol (Figure 3.17). To identify and quantify the selected metabolites, we determined the retention time of each metabolite using a standard and we generated a standard curve for each metabolite (Appendix 7). Our HPLC worked by separating the different components found in the sample using an Aminex HPX87H ion exclusion column (BioRad, Hemel Hempstead, UK), with the different components mostly eluted at different time points from the column. This is known as the retention time and is considered an identifying characteristic of a particular metabolite under a particular condition. The eluate from the column was automatically measured using a UV/Vis spectrophotometer and also a refractive index (RI) detector. We found that ethanol and glycerol could only be measured using the RI detector but not with the spectrophotometer. The organic acids could be measured with both techniques but we also found the spectrophotometer to be more sensitive compared to the RI detector. Therefore, it was decided to use only the measurements obtained with the spectrophotometer. However, we

later found out the chromatogram peak for acetate in many of our samples overlapped with another unknown peak. This caused its accurate quantification to be made impossible. Therefore, for acetate we had to use the data from the RI.

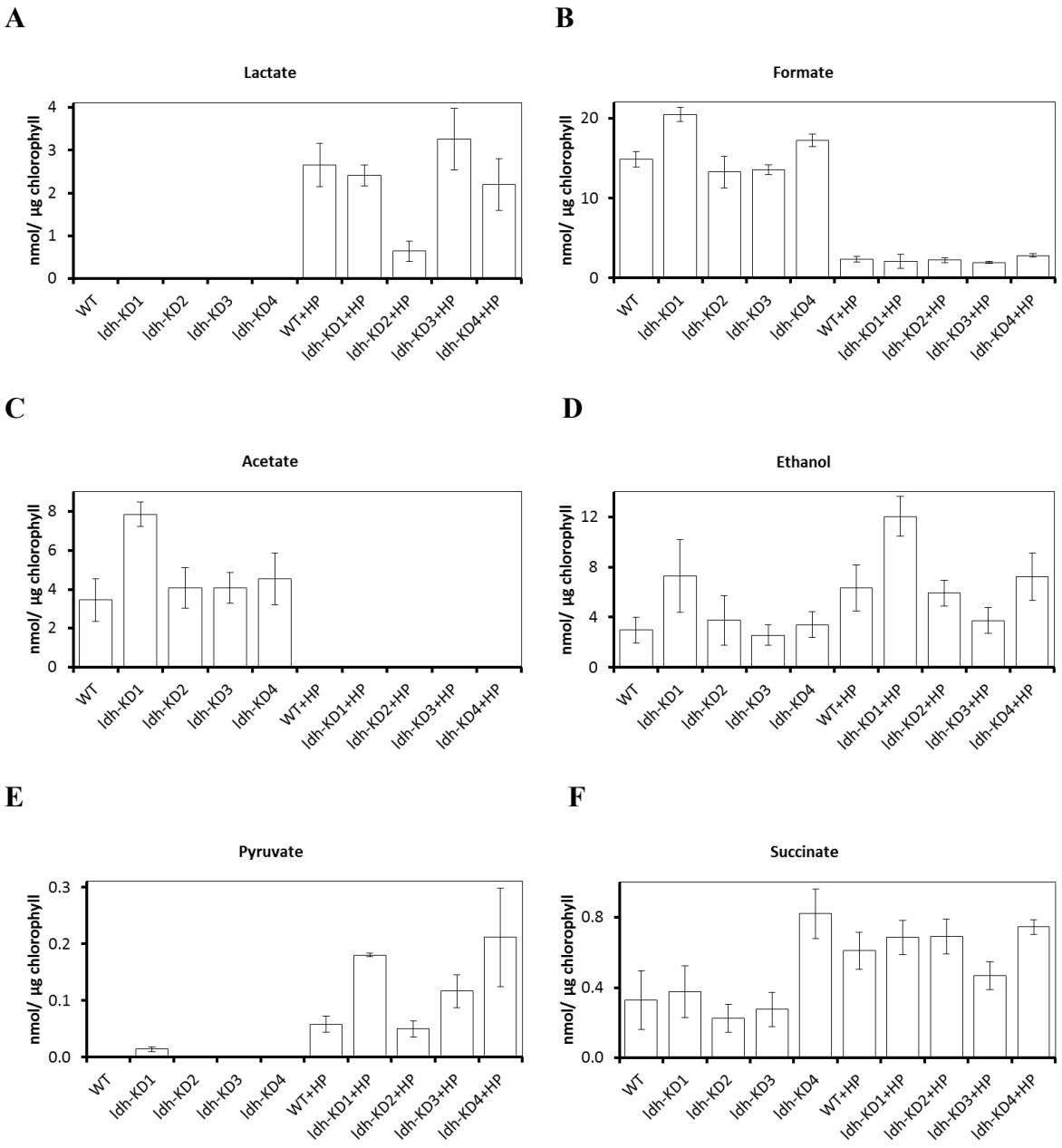


**Figure 3.17 HPLC analysis of metabolite production under dark anaerobic condition.**

HPLC analysis was carried out to re-confirm our NMR analysis on selected metabolites. The excreted metabolites were quantified after 4 hours of dark anaerobic incubation in HSM. Glycerol was undetected in the samples. Average values (±SE) were based on three biological replicates, and the values were normalized to the concentrations of chlorophyll (~150 µg/ml). Samples were also treated with 10 mM sodium hypophosphite (HP) to inhibit PFL1.

From the NMR analysis, the level of lactate (Figure 3.16.1) was found to be very low in the WT and *ldh*-KD mutants. This trace level of lactate was as expected in the WT as this metabolite is considered to be a minor fermentative product (Grossman *et al*., 2007). The similar levels of lactate observed in the *ldh*-KD mutants in comparison to the WT were surprising as the D-LDH levels and enzymatic activities had been shown to be reduced. When the cells were incubated with HP, the inhibition of the PFL1 pathway caused a dramatic increase in lactate production (~18x increase in the WT). This dramatic increase is in agreement with previous studies that used HP (Philipps *et al*., 2011; Burgess *et al*., 2012) or *PFL1* knockdown mutants (Burgess *et al*., 2012) and *PFL1* insertional mutants (Philipps *et al*., 2011; Catalanotti *et al*., 2012). The elevated levels of extracellular lactate displayed by the *PFL1* knockout mutant, *pfl1*, have been shown by Catalanotti *et al*. (2012) to correlate with a slightly higher internal level. However, the increase over WT was only ~2x, suggesting that lactate was favourably excreted. It was anticipated that lactate production would be affected in the *ldh*-KD mutants due to the knockdown level of D-LDH but surprisingly the levels of this metabolite were found to be similar to the WT except for *ldh*-KD2. Only this mutant line had a lower level of lactate when incubated with HP. Our immunoblot analysis ruled out the other lines of knockdown mutants had reverted to WT (Appendix 7).

For confirmation, the HPLC analysis showed no lactate was detected in the WT and *ldh*-KD mutants (Figure 3.17.A). The NMR analysis only revealed that very tiny amounts of lactate were excreted by the WT and *ldh*-KD mutants. Considering the lower sensitivity of this analysis compared to the NMR analysis, this was not surprising. Nevertheless, the HPLC analysis confirmed the NMR analysis by demonstrating lactate was a minor fermentative product. The HPLC analysis also confirmed the NMR analysis of cells treated with HP. A similar trend was observed with lactate production increasing dramatically with the inhibition of PFL1. Comparison of the total amount of lactate produced by the HP-treated WT with previous studies (Philipps *et al*., 2011; Burgess *et al*., 2012) revealed we had a slightly lower production (2.7 ± 0.5 nmol/µg chl) in contrast to the TAP-incubated and AIB-incubated cells that produced ~4 and ~3.5 nmol/µg chl, respectively. This again could be due to the different conditions being used or laboratory strain variability. Alternatively, the HPLC analysis using RI also suggested similar trend was observed but with less analytical sensitivity (Appendix 7).

The level of formate (Figure 3.16.2), which is considered to be the major fermentative product (Grossman *et al*., 2007), was found to be similar between the WT and *ldh*-KD

mutants except for *ldh*-KD1 whereby the level was higher. This could be due to biological variability. Incubation with HP lowered the production of formate by ~80% as shown with the WT. The addition of 10 mM HP would not completely inhibit formate production as it is a competitive inhibitor. As in previous studies (Ohta *et al*., 1987; Hemschemeier *et al*., 2008; Philipps *et al*., 2011; Burgess *et al*., 2012), it was expected for the formate to still be produced but at lower levels. In contrast, the knockout *PFL1* mutant (Catalanotti *et al*., 2012) did not show a detectable level of formate. However, the other knockout *PFL1* mutant, 48F5 (Philipps *et al*., 2011) still showed a detectable but very low level of the metabolite, similar to the level shown by the HP-treated WT. This indicates the effectiveness of the HP treatment to inhibit the PFL1 protein. Our *ldh*-KD mutants when treated with HP did not show any major change in formate production when compared to the corresponding WT.

The HPLC analysis also confirmed the NMR analysis with regard to formate production (Figure 3.17.B). The amount of formate produce by our WT (14.9 ± 0.9 nmol/µg chl) was higher in contrast to previous studies (~10 nmol/µg chl, Philipps *et al*. 2011; ~4.5 nmol/µg chl, Burgess *et al*., 2012). Similarly, the HP-treated WT also had higher formate (2.3 ± 0.3 nmol/µg chl) compared to the previous studies (~1 nmol/µg chl). These differences again could be due to different conditions used or laboratory strain variability. Alternatively, the HPLC analysis using RI also suggested similar trend was observed but with less analytical sensitivity (Appendix 7).

The level of acetate (Figure 3.16.3), which is also a major fermentative product (Grossman *et al*, 2007) was found to be similar between the WT and *ldh*-KD mutants. Incubation with HP decreased the level of acetate by ~80% as shown by the WT. The acetate reduction due to PFL1 inhibition is in agreement with previous studies (Philipps *et al*., 2011; Burgess *et al*., 2012; Catalanotti *et al*., 2012) although the decrease observed was only about 50 to 60% when using HP (Philipps *et al*., 2011; Burgess *et al*., 2012). This could be due to the different conditions being used in the experiments. For example, Philipps *et al*. (2011) used Tris minimal medium while Burgess *et al*. (2012) used AIB. Burgess (2011) did a comparison of dark anaerobic metabolite production between HSM and AIB, and it was found that when using HSM, the reduction of acetate due to HP was by ~80%. This is in agreement with the reduction observed in this work. When the *ldh*-KD mutants were treated with HP, there was no major change in acetate production when compared to the corresponding WT.

The NMR analysis of acetate production was confirmed by the HPLC analysis but with the acetate level to be below detection limit for the HP-treated cells (Figure 3.17.C). The

acetate level of our WT is in agreement with the previous studies (~4 nmol/µg chl; Philipps *et al*., 2011; Burgess *et al*., 2012). However, since the acetate results were based on the RI instead of the UV absorbance, caution needs to be taken when interpreting these similar amounts of acetate due to analytical sensitivity.

The level of the other major fermentative product, ethanol (Grossman *et al*., 2007), was found to follow a similar trend (Figure 3.16.4). The ethanol levels were similar between the WT and *ldh*-KD mutants except for *ldh*-KD1 which again showed a higher level. This could be due to biological variability. In the WT, the treatment of cells with HP did not cause a substantial increase in ethanol. This is in agreement with Burgess *et al*. (2012) but not with other studies (Philipps *et al*., 2011; Catalanotti *et al*., 2012) which found ethanol levels to increase significantly by ~2x. Similarly, when HSM was used, there was only a slight increase in the ethanol production (Burgess, 2011) which is almost in agreement when AIB was used (Burgess *et al*., 2012). Our lower levels of ethanol accumulation might be explained by the use of different conditions since Philipps *et al*. (2011) used, as an example, TAP medium for ethanol analysis. Moreover, it could also be explained by the presence of low level of functional PFL1 as indicated by the production of low level of formate in our HP-treated cultures, and the fact that Catalanotti *et al*. (2012) used an insertional mutant that had an undetectable level of formate suggests that the level of ethanol accumulation might be dependent on the degree of PFL1 inhibition.

The HPLC analysis confirmed the NMR analysis of ethanol production (Figure 3.17.D). In comparison with previous studies, our WT excreted a lower amount ethanol (2.98 ± 1.0 nmol/µg chl) which is in agreement with the ethanol level (~2.5 nmol/µg chl) observed by Burgess *et al*. (2012) but not by Philipps *et al*. (2011) (~7 nmol/µg chl). Similarly, our HP-treated WT had a lower ethanol level (6.4 ± 1.8 nmol/µg chl) compared to Philipps *et al*. (2011) (~13 nmol/µg chl) but slightly higher compared to Burgess *et al*. (2012) (~3.5 nmol/µg chl).

We also detected pyruvate being excreted by the cells. This metabolite has not been detected before in previous studies on dark anaerobic metabolite excretion, presumably due to limitations with analytical techniques. Moreover, pyruvate acts as a substrate of many fermentative pathways rather than a by-product like many of the metabolites being measured here. A possible reason for pyruvate excretion is to prevent the accumulation of this metabolite to a potentially toxic level which could cause cell death. Thus, it was interesting to determine if any fermentative mutation such as *D-LDH* knockdown could affect pyruvate accumulation and excretion. To show the likelihood of *C. reinhardtii* being able to excrete

pyruvate, we did a bioinformatics analysis. We searched the Phytozome database for potential pyruvate transporters using the amino acid sequence of a characterised *Trypanosoma brucei* pyruvate transporter (Sanchez, 2013) as a query sequence. We found one protein (Phytozome ID: Cre01.g039950) with 30.4% protein identity and 44.1% protein similarity that was functionally annotated as a monocarboxylate transporter but had not been experimentally proven.

The NMR analysis showed pyruvate (Figure 3.16.5) was not detected in the WT but interestingly, tiny amounts were detected in the *ldh*-KD mutants. When the cultures were treated with HP, there was a substantial increase in the relative amounts of excreted pyruvate. There seemed to be a tendency for higher excretion of pyruvate when both D-LDH and PFL1 pathways were blocked.

The HPLC analysis using UV spectrometer also confirmed the NMR analysis on the excretion of pyruvate (Figure 3.17.E). The metabolite was not detected from the non-treated cultures except for *ldh*-KD1, and was detected from all of the HP-treated cultures. The amounts of excreted pyruvate were very small in all cultures with less than 0.3 nmol/µg chl after 4 hours of dark anaerobic incubation. Alternatively, the HPLC analysis using RI detector could not detect any pyruvate due to the minor amounts of pyruvate present in the samples.

Glycerol was detected by the NMR spectrometer in all cultures (Figure 3.16.6). This metabolite was described to be an excreted product of dark anaerobic fermentation from *C. reinhardtii* mutants lacking ADH1 (Magneschi *et al*., 2012; Catalanotti *et al*., 2012). In these previous studies, glycerol was undetected from the WT based on their HPLC analyses. However, this was probably because of the lower sensitivity of HPLC analysis compared to NMR analysis. We managed to detect glycerol in the WT using NMR. Previous studies (Gfeller & Gibbs, 1984; Kreuzberg, 1984; Ohta *et al*., 1987) also managed to detect glycerol excreted by *C. reinhardtii* using an enzyme-based assay. The amount of glycerol excreted by our WT was similar to the *ldh*-KD mutants. Interestingly, HP treatment caused an increase in the production of glycerol. The WT had an increase of ~2x while the *ldh*-KD mutants had an increase of ~3-5x relative to their corresponding non-treated cultures. The *ldh*-KD mutants consistently showed higher amount of glycerol relative to the WT when treated with HP. Previous studies with HP treatment (Philipps *et al*., 2011; Burgess *et al*., 2012) did not report any excreted glycerol, presumably due to limitations with their analytical techniques.

Glycerol was undetected in our HPLC analysis. Since we detected this metabolite by using the NMR spectrometer, this indicated glycerol was present in the samples but the

amounts were too small to be detected by HPLC. This supported our assumption that the limitations with analytical techniques could explain the reason why glycerol was previously undetected in the WT (Magneschi *et al*., 2012; Catalanotti *et al*., 2012).

Fermentative succinate production had been reported in *C. reinhardtii* and the metabolic pathways for its production have also been proposed (Dubini *et al*., 2009). Reverse tricarboxylic acid (TCA) reactions were proposed for succinate production and a few intermediates would be involved i.e. oxaloacetate, malate and fumarate. Therefore, all these metabolites were analysed by NMR. However, we could not detect oxaloacetate and malate. This could mean that their levels were too small to be detected by the NMR spectrometer or it could also mean that these intermediates had been converted to fumarate or succinate. Alternatively, these metabolites might not be favourably excreted by the cells. However, Mus *et al*. (2007) have reported the accumulation of malate in the medium although at low levels (less than 1 mM). On the other hand, the other intermediate, fumarate, could be detected in most samples although at very low levels (Figure 3.16.7). However, there was no clear trend observed linking *D-LDH* knockdown with changes in fumarate production. This could be explained by the fact that this metabolite is an intermediate. There seemed to be an increase in fumarate when the cells were treated with HP, suggesting the potential effect of PFL1 inhibition on fermentative succinate production. The NMR analysis on succinate revealed the metabolite was detected (Figure 3.16.8) but there was no substantial difference in the excreted levels between the WT and *ldh*-KD mutants. The levels of succinate from the HP-treated cultures were higher compared to the non-treated ones with the WT having an increase of ~2x. This is in agreement with the fumarate analysis. This supports the effect of PFL1 inhibition in elevating succinate production. The extracellular analysis of fermentative succinate production due to PFL1 inhibition has not been reported yet, presumably due to limitations with analytical techniques. However, intracellular levels of malate, fumarate and succinate had been successfully determined by gas chromatography coupled to mass spectrometry, GC-MS (Catalanotti *et al*., 2012). It was found the internal levels of these metabolites were elevated in the knockout *PFL1* mutant with an increase of ~2x in succinate, ~4x in malate and undetectable levels of fumarate in the WT. This was in agreement with the results obtained in this work although we measured the excreted levels.

Succinate was successfully detected with the HPLC analysis (Figure 3.17.F), and the analysis confirmed the NMR analysis except for *ldh*-KD4. Here, this knockdown mutant had a relative higher amount of succinate whereas in the NMR analysis, it had a similar level to the WT. The inhibition of PFL1 pathway should increase the production of succinate

(Catalanotti *et al*., 2012) but this was not seen in this line of knockdown mutant based on the HPLC analysis. Considering this fact, we assumed the higher amount of succinate observed in *ldh*-KD4 was probably due to overlapping peaks. There could be a metabolite produced specifically by this mutant, which unfortunately shared a similar retention time with succinate. Thus, it was important to confirm any measurements with different analytical techniques. Alternatively, the HPLC analysis using RI detector could not detect any succinate due to the minor amounts of succinate present in our samples. The amounts of excreted succinate were small with less than 1.0 nmol/µg chl after 4 hours of dark anaerobic incubation.

The NMR spectrometer could also detect several amino acids excreted by *C. reinhardtii*. These amino acids were alanine, arginine, glutamate, glycine, isoleucine, leucine, lysine, methionine, phenylalanine, proline, threonine, tryptophan, tyrosine and valine (Figure 3.16). As far as we are aware of, there are no previous studies that have described the excretion of amino acids under dark anaerobic fermentative conditions. This could be due to the limitations imposed by analytical techniques such as HPLC and assay kits. However, Catalanotti *et al*. (2012) did intracellular analysis of amino acids by using a gas chromatography that was coupled to a mass spectrometer (GC-MS), and found many amino acids accumulated at higher levels in the *pfl1* mutant compared to the WT. The biosynthesis of many amino acids by *C. reinhardtii* has been proposed and described in detail by Vallon & Spalding (2009). We will not re-describe these biosynthesis pathways in this chapter but only a brief and essential description is provided, as most of the amino acids are produced through an extensive network of metabolic pathways. It is thought that amino acid biosynthesis mostly occurs in the *C. reinhardtii* plastid (Valon & Spalding, 2009).

It had been proposed that pyruvate can be converted to alanine through transamination. This involves the transfer of an amino ($-NH_2$) group from glutamate to pyruvate, producing alanine and α-ketoglutarate (Vallon & Spalding, 2009). Our analysis of alanine production (Figure 3.16.9) showed there was no difference in the alanine levels between the WT and *ldh*-KD mutants. However, there was a slight increase in the alanine production when the cells were treated with HP. Given that Catalanotti *et al*. (2012) only detected significant increases in the intracellular alanine level of the *pfl1* mutant after 24 hours, there potentially could be a further increase in alanine production if the period of dark anaerobic incubation with HP was made longer.

Phenylalanine, tryptophan and tyrosine are aromatic amino acids. According to Vallon & Spalding (2009), the biosynthesis of these amino acids could occur in *C. reinhardtii*

through the conversion of PEP, which can be produced through glycolysis, into chorismate in a series of enzymatic reactions. The generated chorismate could serve as the common precursor for the biosynthesis of the three aromatic amino acids, involving a series of metabolic pathways. Our analysis of these aromatic amino acids (Figure 3.16.10; Figure 3.16.11; Figure 3.16.12) showed there were no distinctive differences between the WT and *ldh*-KD mutants, either in the untreated or HP-treated samples. However phenylalanine and tyrosine showed similar patterns of accumulation. This is perhaps unsurprising as their productions are metabolically interrelated. However, this does not explain the different pattern of tryptophan accumulation, suggesting differential secretion of this amino acid.

Isoleucine, valine and leucine are branched-chain amino acids. Vallon & Spalding (2009) proposed valine could be produced from the conversion of pyruvate through a series of enzyme-catalysed pathways. Through parallel pathways, these same enzymes could also convert 2-ketobutyrate into isoleucine. Meanwhile, the biosynthesis of leucine could occur through the branching of the valine biosynthetic pathways. Our analysis of these branched-chain amino acids (Figure 3.16.13; Figure 3.16.14; Figure 3.16.15) showed they shared similar patterns of accumulation but there were no distinctive differences between the WT and *ldh*-KD mutants, either in the untreated or HP-treated samples.

Glycine can be produced through the conversion of 3-phosphoglycerate, which could come from either glycolysis or the photorespiratory glycolate pathway, into serine and then into glycine through a series of metabolic pathways (Vallon & Spalding, 2009). Our analysis of glycine (Figure 3.16.16) showed no distinctive differences between the WT and *ldh*-KD mutants, either in the untreated or HP-treated samples. However, the pattern of glycine accumulation was similar to the accumulation of the branched-chain amino acids described above, suggesting the production of this metabolite could be linked to the glycolytic pathway.

Lysine, methionine and threonine are aspartate-derived amino acids. In light of the *C. reinhardtii* fermentative pathways, the biosynthesis of these aspartate-derived amino acids could start with oxaloacetate, which could be produced through the fermentative reverse TCA reactions, and its transamination with glutamate to yield aspartate. The generated aspartate could then be converted to lysine, methionine and threonine, through a series of metabolic steps (Vallon & Spalding, 2009). Our analysis of these aspartate-derived amino acids (Figure 3.16.17; Figure 3.16.18; Figure 3.16.19) showed there were no distinctive differences between the WT and *ldh*-KD mutants, either in the untreated or HP-treated samples.

Glutamate, arginine and proline were also observed to be excreted by *C. reinhardtii* (Figure 3.16.20; Figure 3.16.21; Figure 3.16.22). However, the direct link between dark

fermentation and the biosynthesis of these amino acids is currently unclear. Vallon & Spalding (2009) proposed that glutamate could be produced through ammonia assimilation while arginine and proline could be derived from glutamate through a series of enzyme-catalysed reactions. Due to the unclear link between the biosynthesis of these amino acids and dark fermentation, it is perhaps unsurprising there were no distinctive differences between the WT and *ldh*-KD mutants, either in the untreated or HP-treated samples.

Acetoin was observed to be excreted by *C. reinhardtii* (Figure 3.16.23), and as far as we are aware of, this is the first report of the excretion of this organic compound under dark anaerobic fermentative conditions. Our analysis showed there was a tendency for the acetoin to be produced when the D-LDH pathway was affected. Interestingly, when PFL1 was inhibited, there was a marked accumulation of acetoin. However, when PFL1 inhibition was coupled to the *D-LDH* knockdown, no distinctive change was observed.

Galactose was observed to be secreted by *C. reinhardtii* (Figure 3.16.24). This is perhaps unsurprising as the green alga has been shown to be able to secrete a large amount of exopolysaccharide containing galactose, glucose and other sugars (Bafana, 2013). Catalanotti *et al*. (2012) did intracellular analysis of various sugars accumulated under dark anaerobic conditions but galactose was not analysed. Our analysis showed there were no distinctive differences in the galactose secretion between the WT and *ldh*-KD mutants, either in untreated cells or cells treated with the PFL1 inhibitor.

### 3.2.2.8 Gas analysis of *ldh*-KD mutants under dark anaerobic condition

We also tried to measure the amounts of hydrogen gas being produced under dark anaerobic conditions in order to understand the regulation of fermentation metabolism in *C. reinhardtii*. The gas was collected after 4 hours of dark anaerobic incubation, and was measured by gas chromatography (GC). Unfortunately, our attempts to detect hydrogen were unsuccessful, even when we increased the amount of cells and/or increased the incubation time. To reduce the possibility that the experimental condition was insufficiently anaerobic to induce expression of the hydrogenases, we repeated the experiment by putting the air-tight vials containing the cells in an anaerobic chamber (Glove Box, Belle Technology, UK), which was filled up with nitrogen gas, instead of putting them in an open air. We still could not detect any hydrogen gas. To rule out leakage of hydrogen gas from the airtight vials, we tested the vial by filling it with a volume of water and purging it with a commercially available hydrogen gas. The hydrogen gas was measured after 4 and 24 hours but we did not see any significant reduction of hydrogen gas compared to 0 hour, indicating the vials were airtight (data not shown). For measuring gases using the GC, an airtight syringe was used to collect gas sample from the vial headspace, and the gas sample was quickly injected into the GC for analysis. To rule out leakage of hydrogen gas from this syringe, we filled the syringe with hydrogen gas and left it for 15 and 30 minutes. We did not see any significant reduction of the gas compared to 0 minute (data not shown). Therefore, we suspected that the amount of hydrogen gas being produced by our algal samples was at undetectable levels. We roughly estimate that the injection of ~80 nmoles of hydrogen gas into the gas chamber would produce a very small peak that would be indistinguishable from the background noise or baseline (data not shown). From previous studies, after four hours of dark anaerobic incubation, the amounts of hydrogen produced by WTs were in the range of ~10-20 nmoles/L (Magneschi *et al*., 2012; Catalanotti *et al*., 2012) and the calculated rate of hydrogen production was ~0.1 nmol/µg chl/h (Philipps *et al*., 2011). These small amounts of hydrogen gas were not surprising, considering the gas is known as one of the minor products of dark fermentation. In the future, measurement of hydrogen could be carried out by using a membrane inlet mass spectrometry (MIMS) system (Tamburic *et al*., 2011). Alternatively, the analytical sensitivity of the GC could possibly be improved by increasing the GC injection loop volume bigger than the current setting of 200 µl.

### 3.2.2.9 Metabolite analysis of *ldh*-KD mutants under sulphur deprivation

To assess if *D-LDH* knockdown had an effect on metabolite produced under sulphur deprivation, we analysed the metabolites secreted by *C. reinhardtii*. The cells were first grown in TAP medium to late log phase and later re-suspended in TAP-S medium to give a total chlorophyll concentration in the range of 15 to 20 µg/ml. This sulphur-deprived medium contained ~16 mM of acetate as a carbon source. The culture was exposed to high light (150 $\mu Em^{-2}s^{-1}$) for a period of 96 hours. Every 24 hours, a 1-ml sample was collected and centrifuged to obtain the cells and supernatant. The cells were used for immunoblot analysis while the supernatant was used for metabolite analysis. The immunoblot analysis was carried out in order to confirm that the *D-LDH* knockdown mutation was still stable. Our blots confirmed the knockdown levels of D-LDH protein relative to the WT (Appendix 8).

The metabolite analysis was performed using NMR (Figure 3.18) and was carried out in collaboration with Dr. Volker Behrends and Dr. Jacob Bundy (Imperial College London). To confirm the NMR analysis, the same samples were also analysed by HPLC, done in collaboration with Charlotte E. Ward (Imperial College London). However, we could only confidently analyse two metabolites i.e. formate and acetate from the HPLC analysis (Figure 3.19). This was because of the difficulty in identifying and quantifying the other metabolites, as the generated peaks for these metabolites overlapped with many unknown peaks. This is perhaps not surprising as it was expected for more metabolites to be produced under sulphur-deprived conditions than dark fermentation. Our NMR analysis could only detect a total of 8 different metabolites: lactate, formate, acetate, ethanol, pyruvate, succinate, alanine and glycolate. This was probably due to the samples not being as concentrated as the samples derived from the dark fermentation analysis, and therefore minor metabolites would be present below the limits of detection.

**A**

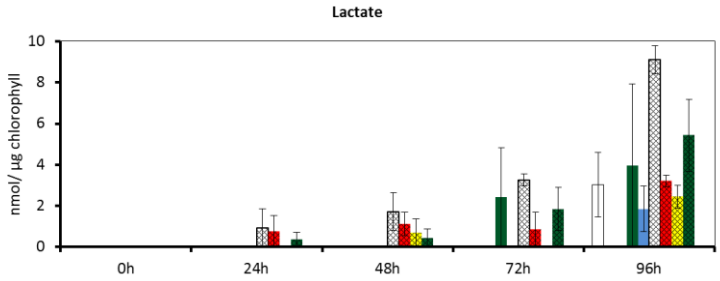

**B**

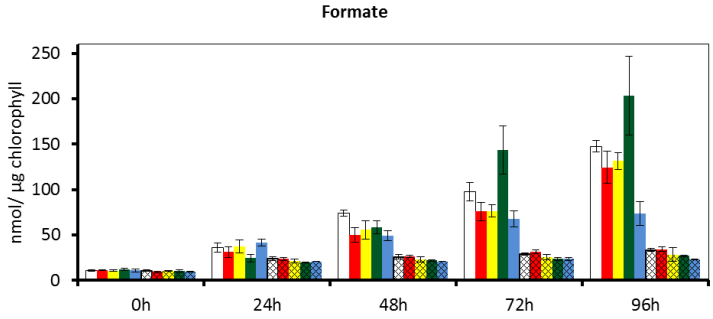
Formate
nmol/ µg chlorophyll
250
200
150
100
50
0
0h
24h
48h
72h
96h

**C**

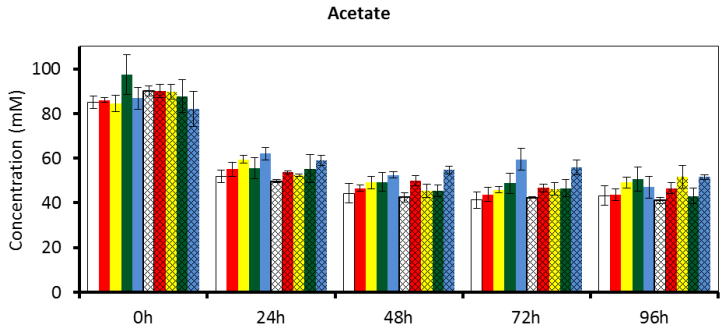
Acetate
Concentration (mM)
100
80
60
40
20
0
0h
24h
48h
72h
96h

**D**

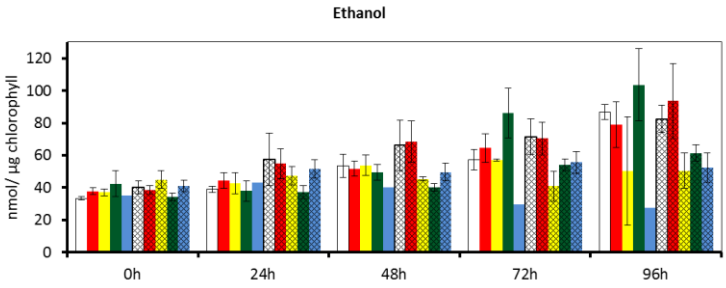
Ethanol
nmol/ µg chlorophyll
120
100
80
60
40
20
0
0h
24h
48h
72h
96h

**E**

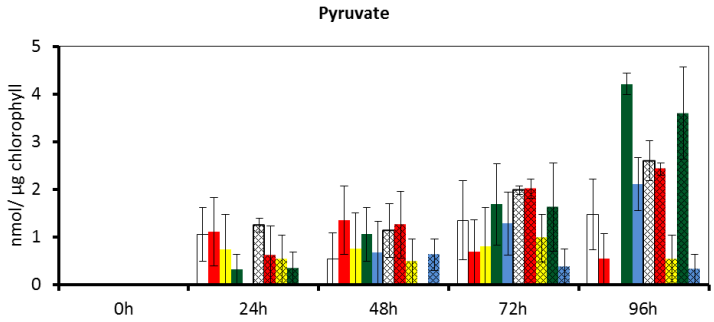
Pyruvate
nmol/ µg chlorophyll
5
4
3
2
1
0
0h
24h
48h
72h
96h

**F**

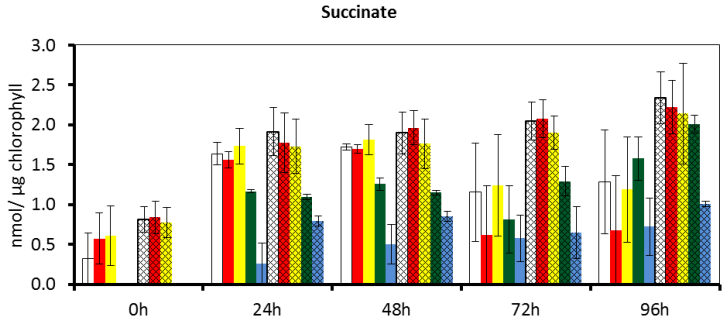


**G**

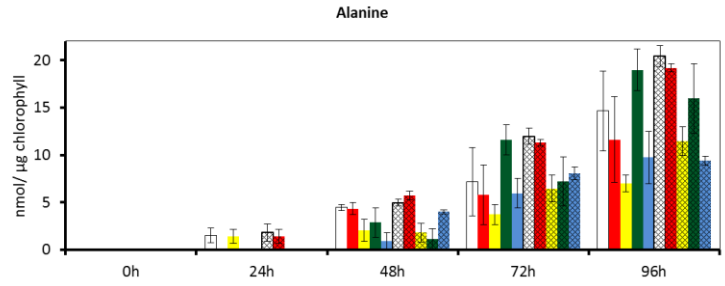


**H**

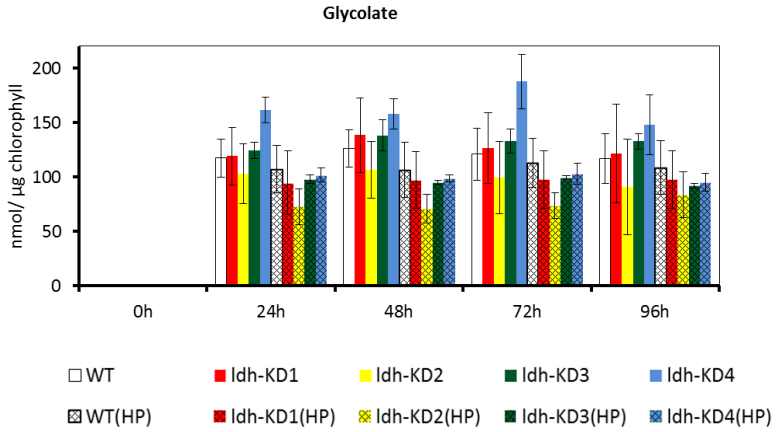


**Figure 3.18 NMR analysis of metabolite production under sulphur deprivation.**

The metabolite concentrations were quantified relative to the NMR standard (DSS). Average values (±SE) were based on three independent replicates, and the values were normalised to the concentrations of chlorophyll (~15 µg/ml) except for acetate. This is to show the consumption of acetate by the algal cells. Samples were also treated with 10 mM sodium hypophosphite (HP) to inhibit PFL1.

Lactate (Figure 3.18.A) was initially undetected but after 72 hours post-sulphur starvation some samples began to show lactate excretion. However after 96 hours, there was no distinctive difference in the total amounts of excreted lactate between the WT and *ldh*-KD mutants. On the other hand, when the PFL1 pathway was inhibited with sodium hypophosphite, lactate could already be detected in some samples after 24 hours post-sulphur starvation. Interestingly, when the PFL1 inhibition was coupled to the *D-LDH* knockdown, the total levels of lactate were lower compared to PFL1 inhibition alone.

Formate (Figure 3.18.B) was already detected at 0 hour but only in minor amounts. This could be due to the centrifugation effect that caused the cells to go anaerobic. As the incubation time was increased, the levels of formate also gradually increased but this was not observed from the samples treated with the PFL1 inhibitor, indicating successful enzyme inhibition. There was no distinguishing difference observed between the WT and *ldh*-KD mutants, either untreated or treated with the PFL1 inhibitor. There were some variations observed (i.e. *ldh*-KD3 and *ldh*-KD4) but these could simply be due to biological variations. The NMR results were confirmed by our HPLC analysis (Figure 3.19.A) although the HPLC measurements were not as sensitive as the NMR. All the results suggest that *D-LDH* knockdown had no significant effect on formate production.

The production of acetate could not be determined in this analysis as the medium contained ~16 mM acetate as the carbon source. Thus, only the net consumption of this organic compound could be analysed. Acetate was not accurately determined by the NMR analysis (Figure 3.18.C) as the initial concentration should be ~16 mM. As we were only interested in the relative comparison between the WT and the mutants, the absolute metabolite concentrations were perhaps unnecessary. Nevertheless, our HPLC analysis correctly determined the expected acetate concentration (Figure 3.19.B). Both NMR and HPLC analyses showed there were no distinctive differences observed between the WT and *ldh*-KD mutants, either untreated or treated with the PFL1 inhibitor. It seems acetate was no longer consumed after 24 hours post sulphur starvation. However, the cells could also produce and consume their own acetate.

Ethanol (Figure 3.18.D) was also observed at the start of sulphur starvation, which could be due to the centrifugation effect. As the incubation time was increased, the levels of ethanol also gradually increased but the increase was rather small. Caution should be taken when interpreting the total ethanol concentrations as firstly, the NMR analysis might not give an accurate value as demonstrated with the acetate concentration, and secondly, as ethanol is a volatile compound, some evaporative loss might also be encountered as the cultures were

constantly stirred at a high speed. Nevertheless, if this were true, this should still not affect any comparative analysis between the WT and *ldh*-KD mutants as the rates of evaporative loss were assumed to be similar in all samples. Moreover, the loss by evaporation, if there was any, should only be small as the experimental temperature was set at 28ºC, not high enough to cause any major evaporative loss. Our analysis showed there were no distinctive differences observed between the WT and *ldh*-KD mutants, either untreated or treated with the PFL1 inhibitor.

Pyruvate (Figure 3.18.E) was observed to be excreted by *C. reinhardtii* under sulphur-deprived conditions. As far as we are aware of, no previous studies have reported pyruvate excretion under these specified conditions, presumably due to limitations with analytical techniques. Pyruvate was detected as early as after 24 hours post-sulphur starvation. However, no obvious differences were observed between the WT and *ldh*-KD mutants, either untreated or treated with the PFL1 inhibitor.

Succinate (Figure 3.18.F) was detected at the start of sulphur starvation. This could be due to the anaerobic centrifugation effect. Alternatively, the observed succinate could come from a much earlier metabolic production (such as TCA cycle) when the cells were grown in TAP medium. Therefore, when the cells were re-suspended in TAP-S medium, the accumulated succinate was released into the medium by the cells. As the incubation time was increased, the levels of succinate also increased but only up to 24 hours. After this time period, the levels seemed not to increase any further, and there seemed to be a tendency for the HP-untreated samples to have a reduction in their succinate levels at the later stage of the post sulphur starvation. This suggests the cells might be able to consume back the succinate that was released earlier.

Alanine (Figure 3.18.G) was first detected after 24 hours post-sulphur starvation, and the levels increased gradually afterwards. However, there are no obvious differences observed between the WT and *ldh*-KD mutants, either untreated or treated with the PFL1 inhibitor.

Glycolate (Figure 3.18.H) was detected after 24 hours post-sulphur starvation with the levels remained more or less similar afterwards. There are no obvious differences observed between the WT and *ldh*-KD mutants, either untreated or treated with the PFL1 inhibitor.

**A**

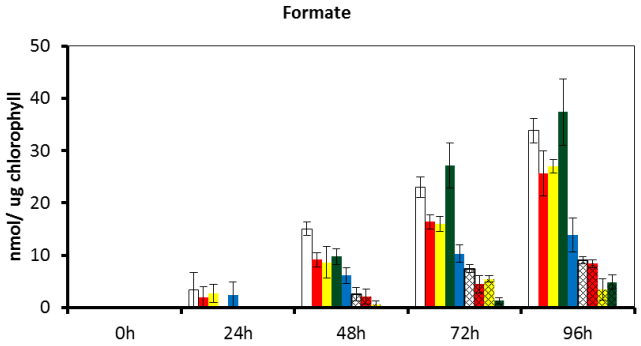


**B**

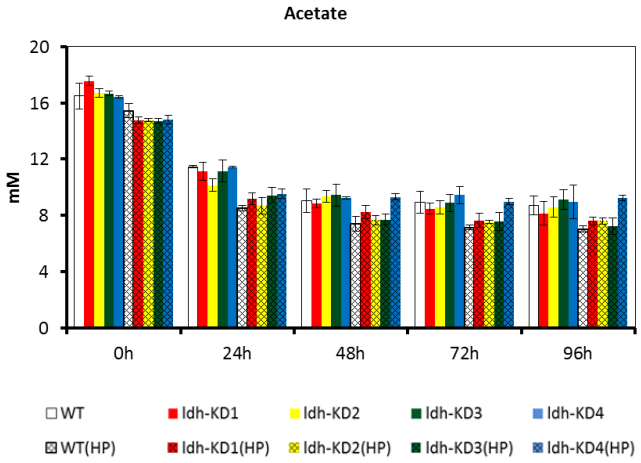


**Figure 3.19 HPLC analysis of metabolite production under sulphur deprivation.**

HPLC analysis was carried out to re-confirm our NMR analysis on selected metabolites. Average values (±SE) were based on three independent replicates, and the values were normalised to the concentrations of chlorophyll (~15 µg/ml) except for acetate. This is to show the consumption of acetate by the algal cells. Samples were also treated with 10 mM sodium hypophosphite (HP) to inhibit PFL1.

### 3.2.2.10 Gas analysis of *ldh*-KD mutants under sulphur deprivation

The gases that were produced by the sulphur-deprived culture were analysed using gas chromatography (GC). The GC successfully detected hydrogen and carbon dioxide gas in the headspace sample. However, the effects of *D-LDH* knockdown and/or PFL1 inhibition were unclear as the *ldh*-KD mutants did not show similar patterns of production (Figure 3.20). The productions of these gases were negatively affected in both *ldh*-KD3 and *ldh*-KD4 but no effect was observed on the other knockdown mutants. These could be due to biological variability. It could be observed that hydrogen production mostly occurred between 24 to 48 hours after post sulphur starvation, and slowed down after 72 hours.

**A**

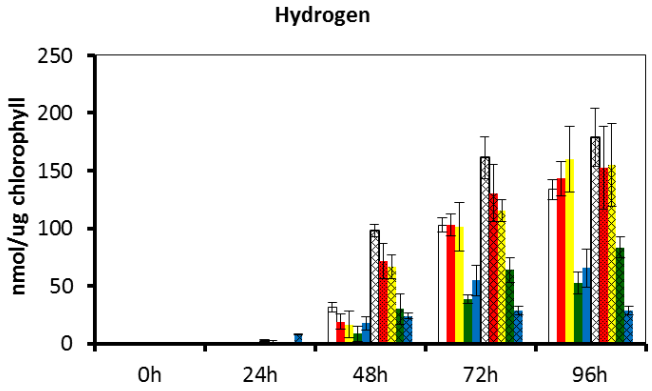


**B**

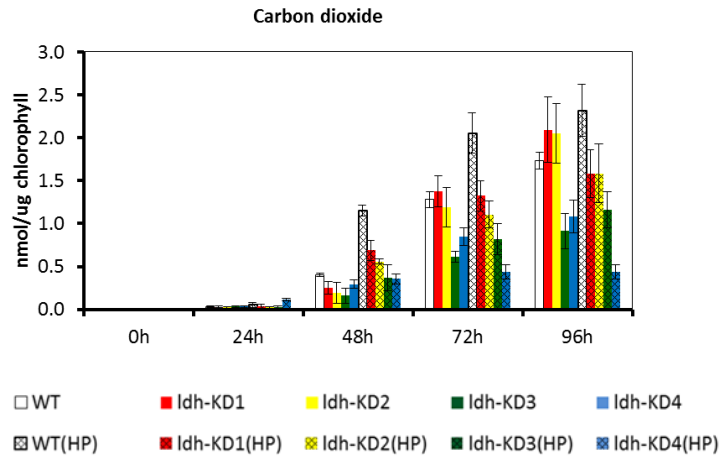


**Figure 3.20 GC analysis of gas accumulation under sulphur deprivation.**

Average values (±SE) were based on three independent replicates. Samples were also treated with 10 mM sodium hypophosphite (HP) to inhibit PFL1.

### 3.2.2.11 Determination of intracellular pyruvate concentrations

Our NMR and HPLC analyses showed that pyruvate was excreted by *C. reinhardtii*, and that the *D-LDH* knockdown seemed to increase the accumulation of pyruvate. Therefore, we were interested to confirm if this trend also applied to intracellular levels of pyruvate.

To determine the concentrations of intracellular pyruvate, we decided to use an enzyme assay approach. There are commercial pyruvate assay kits available to measure pyruvate concentration in a biological sample, which are based on the utilization of pyruvate oxidase. For example, Pyruvate Assay Kit (Abcam, UK) uses the enzyme to oxidise pyruvate for the generation of colour whose intensity can be quantified and is proportional to the pyruvate content. However, the kit has a sensitivity of >1 μM pyruvate, and thus it is not suitable to be used in this work because some of our samples had ~1 μM pyruvate. Therefore, we decided to employ *Lactobacillus leichmannii* $NAD^+$-dependent D-LDH for the measurement of pyruvate content in *C. reinhardtii*. The oxidation of NADH due to the D-LDH enzymatic reaction could be measured by the decrease in absorbance at 340 nm. The rate of NADH oxidation could be used to determine the pyruvate content by applying Michaelis-Menten kinetics.

To generate a pyruvate standard curve for the quantification of pyruvate content in our samples, we measured the rates of NADH oxidation by *L. leichmannii* D-LDH from a series of pyruvate solutions of differing concentrations (10,000 to 0.01 μM). It was found that the rate could still be effectively determined at 1 μM pyruvate but the sensitivity was lost at 0.01 μM pyruvate. A negative control was also performed by using 0 μM pyruvate, and as expected there was no change in the absorbance (data not shown). A Michaelis-Menten plot was plotted and showed the maximum rate was achieved at ~1000 μM pyruvate. The plot was converted to a Lineweaver-Burk plot to get a linear relationship between rate and pyruvate concentration that could be used as a pyruvate standard curve (Appendix 9).

As a first step to determine the intracellular concentration of pyruvate, we used the same samples described previously in section 3.3.5, in which intracellular D-LDH activity had been quantified. The assays were performed in a 1-ml mixture containing 25 mM sodium phosphate at pH 7.5, 250 mM sodium chloride, 300 μM NADH and 500 μl cell extract. The reaction was initiated by adding 1 μl *L. leichmannii* D-LDH (Sigma, UK) that was dissolved in the same buffer as the reaction buffer to a concentration of 0.66 mg/ml as determined using the Bio-Rad Protein Assay (Bio-Rad, UK). The decrease in absorbance at 340 nm was recorded (Appendix 9 for representative results). We also performed a control assay where we measured the oxidation rate of NADH without adding *L. leichmannii* D-LDH (Appendix 9

for representative results), and the values were found to be lower than when using *L. leichmannii* D-LDH. The value obtained from this control assay was used to deduct any value obtained from its corresponding D-LDH assay. We also did a negative control assay where we did not add any cell extract into the 1-ml assay mixture, and our results showed there was no decrease in the absorbance as expected (data not shown).

Our analysis of the intracellular levels of pyruvate showed the *D-LDH* knockdown had an effect in increasing the amounts of pyruvate (Figure 3.21). This is in agreement with our NMR analysis on the excreted pyruvate levels, as *ldh*-KD1 and *ldh*-KD3 were observed to accumulate pyruvate.

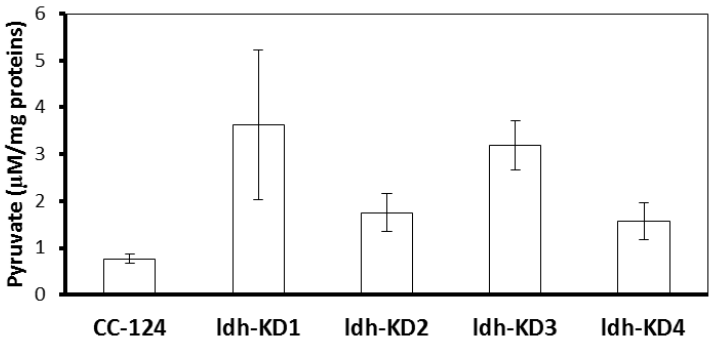


**Figure 3.21 Intracellular concentration of pyruvate.**

Average values (±SE) were based on three biological replicates. The values were normalized to the total protein content of the cell extract used in the 1-ml assay.

### 3.2.2.12 Determination of the stereospecific configuration of the lactate produced by *C. reinhardtii*

By using an enzyme-based assay, Husic and Tolbert (1985) found the lactate produced by *C. reinhardtii* under anaerobic conditions was of D-configuration. However, since the conditions that we used to generate lactate differed from this previous study, it was important to re-confirm the stereospecific configuration of the lactate produced in our samples. To do this, we used the same samples that were shown from NMR and HPLC analyses to produce higher levels of lactate (i.e. in the presence of HP; Section 3.3.7).

To determine the stereospecific configuration, we carried out lactate assays. We used commercially available D-LDH and L-LDH (Sigma, UK) from *L. leichmanii* and *E. coli*, respectively. These enzymes were confirmed to be only able to utilise lactate with similar stereospecific configuration (Appendix 10). The 1 ml reaction mixture contained 12.5 mM sodium phosphate at pH 7.5, 125 mM sodium chloride and 3 mM $NAD^+$. We used 500 µl of the sample which according to our HPLC analysis should contain ~0.1 µmole lactate. The reaction was initiated by adding an optimised amount of enzyme i.e. 0.2 and 0.02 unit of D-LDH and L-LDH, respectively (1 unit would reduce 1 µmole of pyruvate to lactate per min), and the absorbance at 340 nm was quickly recorded every 30 seconds until there was no further change in the absorbance. If there was an increase of absorbance, it would suggest that lactate was converted to pyruvate and $NAD^+$ was reduced to NADH. The increase in absorbance corresponded to the increase in the amount of NADH generated. We used WT (biological replicate #1 and 2), of which only the representative result (biological replicate #2) is presented here, *ldh*-KD3 (biological replicate #2) to represent all the *ldh*-KD mutants, and we also did controls in which no enzyme was added (Figure 3.22). The lactate assays showed there was no increase in the absorbance observed from the controls. Similarly, there was also no increase observed both in the HP-treated WT and *ldh*-KD mutant when L-LDH was used to initiate the reaction, indicating an undetectable level of L-lactate. However, when D-LDH was used, we observed an increase in the absorbance, indicating the presence of D-lactate. However, the increase was quite small, consistent with the low levels of lactate present in our samples.

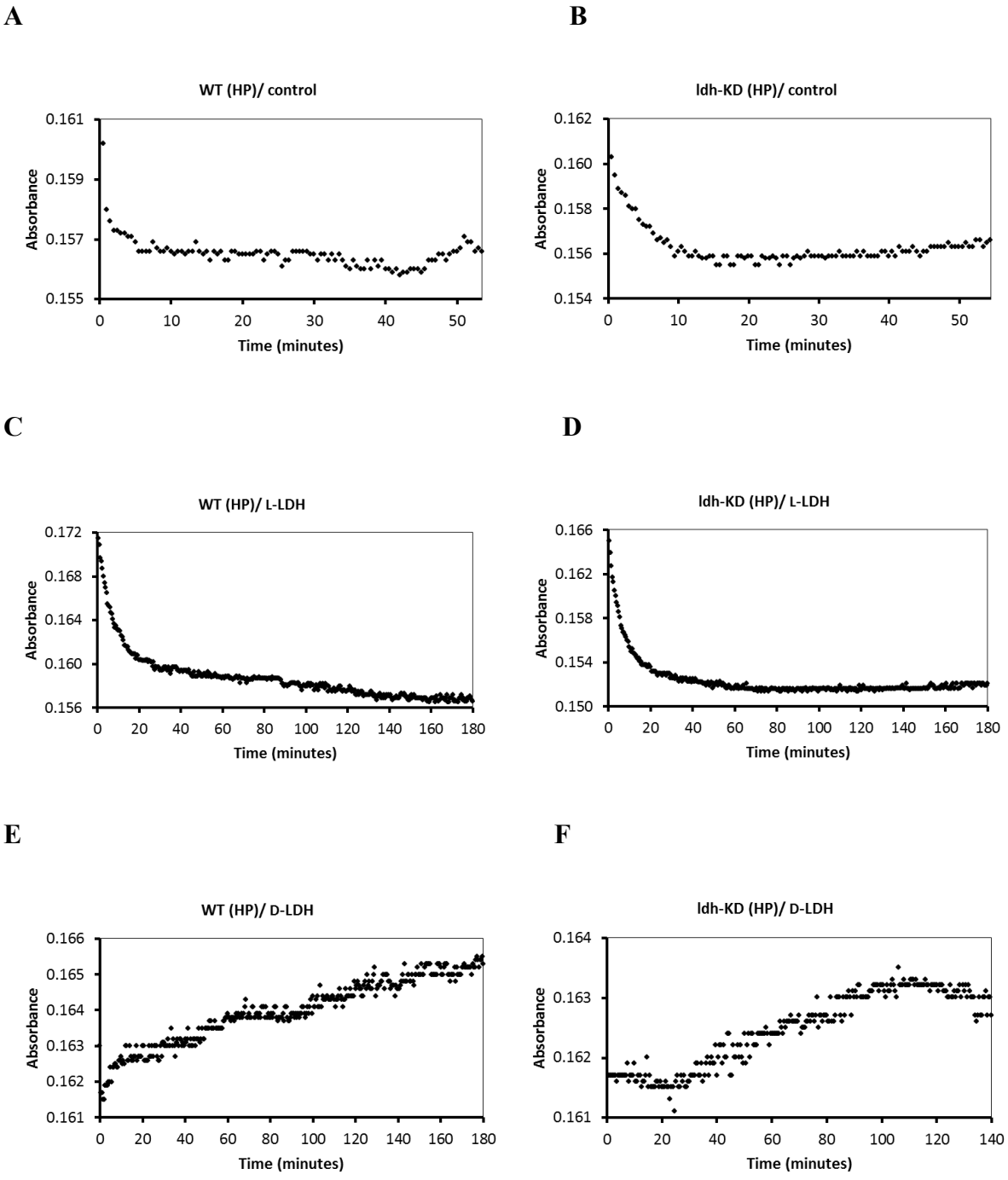


**Figure 3.22 Determination of stereoscopic configuration of lactate.**

Lactate assays were carried out by initiating the enzymatic reaction with either D-LDH or L-LDH (as labelled above) in the presence of $NAD^+$. Absorbance was measured at 340 nm. Controls (A & B) were also carried out whereby no enzyme was added into the reaction mixture. We used samples containing excreted lactate from the cells treated with sodium hypophosphite (HP). Two biological replicates were determined for WT but only the representative result is shown (C & E), and only one biological replicate for the *ldh*-KD mutant (i.e. *ldh*-KD3; D & F).

## 3.3 Discussion

### 3.3.1 D-LDH protein

Our bioinformatics analysis identified a candidate nucleus-encoded D-LDH (Cre07.g324550) that was predicted to be localised to the chloroplast. Current reports in the literature assume that the enzyme is localised in the cytoplasm (Atteia *et al*., 2013; Catalanotti *et al*., 2013). However, by using an immunochemical approach, our group has proved that the protein is targeted to the chloroplast (Burgess, 2011). Unfortunately, this protein has not been identified in previous proteomic analyses of *C. reinhardtii* chloroplast and mitochondria (Atteia *et al*, 2009; Terashima *et al*., 2010), which has presumably led to the previous speculation about its cytoplasmic localisation.

By using an immunochemical approach in tandem with native gel electrophoresis, previous work from our group found that the native D-LDH protein in *C.reinhardtiii* extracts was oligomeric with a molecular mass of approximately 160 kDa (Burgess, 2011). Based on the analysis of the *E. coli*-expressed D-LDH enzyme presented in this chapter, it appears likely that the enzyme is tetrameric. We also did protein crystallisation work on the D-LDH protein (data not shown), and have now successfully obtained a crystal structure with a resolution of 2.5 Å by X-ray crystallography, which is considered a suitable resolution for determining protein structure. We are yet to complete the refinement of the crystal structure but our preliminary analysis suggests that the protein is a tetramer. This is in agreement with the LDHs from other species, which were also found to be tetrameric (Buehner *et al*., 1974; Grau *et al*., 1981; Abad-Zapatero *et al*., 1987; Piontek *et al*., 1990; Wigley *et al*., 1992; Auerbach *et al*., 1998; Uchikoba *et al*., 2002; Antonyuk *et al*., 2009). Burgess (2011) also showed that the D-LDH is soluble and not associated with the thylakoid membrane.

We have confirmed that the protein acts as an $NAD^+$-dependent D-LDH, favouring the reduction of pyruvate rather than the stereospecific oxidation of D-lactate. This is in agreement with the early conclusions of Husic & Tolbert (1985) who worked on pyruvate reductase activity of crude extracts of *C. reinhardtii*. Here, we have managed to identify the gene encoding this pyruvate reductase. The Michaelis constant ($K_m$) was slightly higher (1.85 mM; Table 3.1) than the $K_m$ determined by this previous study (0.5 mM) but this could be due to the different assay conditions or the fact that a $His_6$-tagged derivative was analysed here. We also further showed that the enzyme could also consume glyoxylate, which has not been reported before in this green alga. However, the catalytic efficiency ($k_{cat}/K_m$) with glyoxylate as substrate was much less than that for pyruvate, indicating the enzyme is

preferentially a pyruvate reductase. Moreover, the inability of the enzyme to utilise phenylpyruvate suggests the enzyme displays high substrate specificity. However, to confirm this, more substrates should be tested. The enzyme database, BRENDA (http://www.brenda-enzymes.org/) showed the D-LDHs from other species could also utilise other substrates such as hydroxypyruvate, bromopyruvate and oxoglutarate.

We did not manage to confidently confirm the previous pH profile of the pyruvate reductase, whereby Husic & Tolbert (1985) found the pH optimum to be around pH 7.0. However, our preliminary analysis (data not shown) suggests the maximal activity was also observed at neutral pH. Replicates need to be carried out to confirm the preliminary analysis. For future work, the $K_m$ and $k_{cat}$ for NADH could also be determined.

It is interesting to note that certain bacterial LDHs are reported to be activated by fructose 1,6-biphosphate, which is one of the intermediates of glycolysis, but mammalian LDHs are not allosterically regulated by this metabolite (Garvie, 1980). As *C. reinhardtii* D-LDH was able to reduce pyruvate in the absence of fructose 1,6-biphosphate, with a low $K_m$ value, it indicates the enzyme was not allosterically activated by the compound. On the other hand, Tarmy & Kaplan (1968) showed the D-LDH of *E. coli* is allosterically regulated by pyruvate. However, the lack of a sigmoid curve observed in the plot of rate of enzymatic activity against pyruvate concentration (Figure 3.6) suggests this was not the case for the *C. reinhardtii* enzyme.

### 3.3.2 Physiological role of D-LDH pathway

The physiological role of lactate metabolism in green algae is not well understood. In *C. reinhardtii*, lactate is a minor product of dark fermentation (Gfeller & Gibbs, 1984; Kreuzberg, 1984). This dark fermentative production is to allow for regeneration of $NAD^+$ that is needed for the maintenance of redox balance and sustenance of glycolysis (Catalanotti *et al*., 2013). Interestingly, lactate has also been shown to be produced by light-acclimated *C. reinhardtii* cultures (Davis *et al*., 2013). Burgess (2011) also showed D-LDH protein was not only expressed when the cells were grown in the dark but also in the light under aerobic conditions with preliminary data showing that lactate could be produced during photoautotrophic growth.

This raises the question of its physiological role(s) under these conditions. For many bacteria, lactate is a major product of anaerobic metabolism and can be used as a carbon and energy source, whereby it can be fermented to other organic acids (Crow 1986; Duncan *et al*., 2004). However, lactate is only a minor product in *C. reinhardtii*. Lactate can also be used in

the biosynthesis of bacterial cell walls (Delcour *et al*., 1999; Goffin *et al*., 2005). LDHs from animals and plants have been shown to also catalyse the reduction (in the presence of NADH) or oxidation (in the presence of $NAD^+$) of glyoxylate, producing glycolate or oxalate, respectively (Sawaki *et al*., 1967; Asker & Davies, 1984). It has been reported that *C. reinhardtii* mitochondrial glycolate dehydrogenase can oxidise D-lactate (Nelson & Tolbert, 1970; Beezley *et al*., 1976). The data reported in this chapter (Figure 3.6) showed that D-LDH can reduce glyoxylate, suggesting a potential role in the photorespiratory glycolate pathway used to detoxify a toxic compound produced from the oxygenation reaction of ribulose-1,5-bisphosphate carboxylase/oxygenase (Rubisco) (Bruin *et al*., 1970; Eisenhut *et al*., 2008). However, this has to be further proven experimentally.

The occurrence of lactate-producing D-LDH and lactate-consuming cytochrome-dependent LDH in *C. reinhardtii* has led to the suggestion of a possible lactate valve (Gruber *et al*., 1974; Burgess, 2011), similar to the malate valve, for exporting excess reducing equivalents between the chloroplast and mitochondria, especially when plants are exposed to high light (Scheibe, 2004). However, our photoinhibition assays (Figure 3.15) and high light treatments (Figure 3.13) did not provide evidence for such a lactate valve. However, it is possible that the low levels of D-LDH present in the knockdown mutants still afforded protection. Consequently, it will be interesting in the future to examine photoprotection in a D-LDH knockout mutant. It should also be noted that in *A. thaliana*, an insertion mutant without NADP-dependent malate dehydrogenase, which is the key enzyme of the malate valve, also did not show any phenotypic differences relative to the WT when exposed to high light, possibly due to the occurrence of compensatory mechanisms for maintaining redox homeostasis (Hebbelmann *et al*., 2012). Similarly, this could also explain the lack of phenotype observed in this work as other compensatory mechanisms could be present in the green alga.

### 3.3.3 Lactate production

It was anticipated that the levels of excreted D-lactate would be reduced significantly when the D-LDH level was substantially reduced by the artificial microRNA technology. However, D-lactate was still produced at WT levels in the *ldh*-KD mutants (Figure 3.16). Surprisingly, when the knockdown was coupled with PFL1 inhibition, there was also no substantial difference in the D-lactate levels between the WT and the knockdown mutants (Figure 3.16).

Although the amount of D-LDH protein (Figure 3.11) and activity (Figure 3.12) was reduced in the knockdown mutants, we cannot rule out that the residual D-LDH could potentially be responsible for the WT level of D-lactate production. According to the Michaelis-Menten equation, the rate of enzymatic reaction is not only dependent on the concentrations of the enzyme but also on the concentrations of the enzyme's substrate. An increase in the substrate concentration will increase the enzymatic activity, leading to an increase production of the enzymatic product. This could potentially explain the observed WT levels of D-lactate, as pyruvate was observed to be elevated at the extracellular and intracellular levels (Figure 3.16; Figure 3.21). However, caution needs to be taken when interpreting the intracellular levels of pyruvate. This is because the sample preparation did not involve flash freezing in liquid nitrogen to prevent unwanted metabolic changes, as recommended by Bolling & Fiehn (2005).

Our bioinformatics analysis and the stereospecific configuration of the generated lactate rule out the production of L-lactate by any potential $NAD^+$-dependent L-LDH. However, the bioinformatics analysis suggests the occurrence of two putative gene products that could possess cytochrome-dependent D-LDH activity. It is not known if this particular enzyme could also reduce pyruvate into lactate, as the enzyme has only been reported in *C. reinhardtii* to oxidise D-lactate in the mitochondria under aerobic conditions (Husic & Tolbert, 1987), suggesting the enzyme would only be active under these conditions. Considering the dark anaerobic production of D-lactate, it is unlikely that lactate production could be explained by the putative cytochrome-dependent LDHs. Nevertheless, the possibility of the reverse reaction (producing lactate) cannot be ruled out entirely.

As there is only a single $NAD^+$-dependent D-LDH in *C. reinhardtii*, the production of D-lactate could potentially be carried out by a different metabolic pathway. Indeed this possibility has been overlooked in recent discussions of fermentative metabolism in *C. reinhardtii*. Lactate has been shown to be produced by the methylglyoxal pathway in many organisms such as *A. thaliana* (Engqvist *et al*., 2009), *E. coli* (Weber *et al*., 2005) and mammalian cells (Liu *et al*., 2013). Methylglyoxal is formed from dihydroxyacetone phosphate (DHAP), one of the intermediates of the glycolytic pathway (Figure 3.23). This formation is carried out by the enzyme methylglyoxal synthase (MGS) which involves the removal of phosphate ($P_i$) from DHAP. However, we could not find a clear homologue of MGS encoded in the *C. reinhardtii* genome. Alternatively, methylglyoxal can also be formed by spontaneous degradation of the glycolytic triose phosphates i.e. glyceraldehyde 3-phosphate (G3P) and DHAP, possibly via the enediolate phosphate intermediate. This

intermediate is susceptible to spontaneous phosphate elimination, resulting in the formation of methylglyoxal (Richard, 1993; Phillips & Thornalley, 1993). Triose phosphate isomerase is an enzyme responsible for the reversible interconversion of G3P and DHAP, an enzymatic reaction involving the formation of the enediolate phosphate intermediate. The enzyme favours the production of DHAP (Totemeyer *et al*., 1998). Therefore, in the presence of this enzyme an increase in the formation of methylglyoxal has also been reported (Phillips & Thornalley, 1993).

Methylglyoxal is highly toxic (Thornalley, 1990) and therefore needs to be converted to either L- or D-lactate. For the production of the former, methylglyoxal reductase converts methylglyoxal into lactaldehyde which is eventually converted to L-lactate by aldehyde dehydrogenase. On the other hand, for the production of the latter, methyglyoxal enters the glyoxalase (also known as glyoxylase) pathway, whereby it is converted into lactoylglutathione by glyoxalase 1 (GLO1), and further converted to D-lactate by glyoxalase 2 (GLO2) (Thornalley, 1990). The generated lactate could be further oxidised to pyruvate by cytochrome-dependent LDH (Engqvist *et al*., 2009) or potentially by mitochondrial glycolate dehydrogenase (Beezley *et al*., 1976). As the $NAD^+$-dependent D-LDH is in the chloroplast (Burgess, 2011) while the D-lactate-oxidising enzymes are in the mitochondria (Beezley *et al*., 1976; Husic & Tolbert, 1987), lactate metabolism potentially involves a lactate shuttle between these two organelles, and potentially plays a physiological role in maintaining cell viability and also energy conservation as pyruvate would be recaptured and not be lost.

As L-lactate was not observed under our experimental conditions (Figure 3.22), the production of D-lactate could potentially come from the glyoxalase pathway. Moreover, we could not find a homologue of methylglyoxal reductase in the *C. reinhardtii* genome, suggesting this L-lactate-producing pathway is absent in this alga. Interestingly, homologues of glyoxalase 1 (Cre04.g216100) and glyoxalase 2 (Cre12.g557700) have been reported to be found in the *C. reinhardtii* genome and EST database (Burgess, 2011). This provides strong support for D-lactate production by the methylglyoxal pathway.

Alternatively, the green alga genome contains nine putative aldehyde dehydrogenase (ALDH) genes (Wood & Duff, 2009; Brocker *et al*., 2013). It has been reported that ALDH from goat liver can oxidise lactaldehyde to lactate (Ray & Ray, 1984). Therefore, potentially lactate could be produced if there is a metabolic pathway that could generate lactaldehyde, assuming the putative *C. reinhardtii* ALDH could metabolise this particular substrate.

Methylglyoxal is mainly produced non-enzymically from the glycolytic triose phosphates or enzymically from DHAP by MGS (Thornalley, 1990). Other sources of

methylglyoxal are from aminoacetone (Ray & Ray, 1987) and acetone (Casazza *et al*., 1984) but these sources are considered as minor sources (Thornalley, 1990). Aminoacetone can be formed from the catabolism of threonine. Threonine can be converted to 2-aminoacetoacetate by threonine 3-dehydrogenase, and this generated metabolite can be further converted to aminoacetone by spontaneous decarboxylation. However, there is no homologue of the enzyme in the *C. reinhardtii* genome but there is a homologue of amine oxidase (Cre12.g560900) which could potentially convert aminoacetone to methyglyoxal. Due to the missing link, the production of methyglyoxal from threonine in the green alga is currently unclear. The production of acetone in *C. reinhardtii* is also unknown, and there are no homologues of acetone monooxygenase and acetol monooxygenase in the *C. reinhardtii* genome, which can convert acetone to acetol, and acetol to methylglyoxal, respectively.

The methylglyoxal pathway is considered an energetically unfavourable bypass to glycolysis as no ATP is generated (Cooper & Anderson, 1970). However, it is believed this pathway is activated to deal with the stress caused by an elevated level of glycolytic sugar phosphates as the accumulation of these sugars can inhibit cell growth (Kadner *et al*., 1992; Ferguson *et al*., 1998; Totemeyer *et al*., 1998). Therefore, it is not surprising that methylglyoxal is reported to be produced when cells are grown in the presence of glucose 6-phosphate and fructose 6-phosphate (Kadner *et al*., 1992), and that the synthesis of methyglyoxal is induced by high concentrations of DHAP (Hopper & Cooper, 1971). The production of methylglyoxal is also reported to increase when cells are incubated with increasing glucose concentrations (Weber *et al*., 2005), suggesting the increase was caused by an elevation in the glycolytic sugar phosphate levels.

The inhibition of *C. reinhardtii* PFL1 pathway, either alone or coupled with *D-LDH* knockdown, led to an increase in the glycerol levels. This suggests an increase in the sugar phosphate levels particularly DHAP. This increase should be due to the elimination of the major fermentative pathway, leading to poor utilisation of pyruvate and its accumulation. This is supported by the fact that there was an increase in the pyruvate levels. The excretion of pyruvate by *C. reinhardtii* observed in this work further suggests the importance of preventing the build-up of this three-carbon metabolite. As more starch and glucose are catabolised, the levels of sugars phosphates should also increase since the carbon flux was disrupted at the level of pyruvate. This build-up would lead to the activation of the methylglyoxal pathway. However, it is also possible for this pathway to be active in the WT since methylglyoxal can be formed by spontaneous degradation but the amounts of methylglyoxal and hence D-lactate should only be very small as there should not be a build-

up of either G3P or DHAP. We showed that the amount of D-lactate produced by the WT was very small but it is also possible that the observed lactate could solely come from the $NAD^+$-dependent pathway. When the amounts of the glycolytic triose phosphates increased, as assumed when the PFL1 pathway was blocked, more methylglyoxal should be formed. At high levels, this metabolite is toxic, so cells detoxify this metabolite into D-lactate through the glyoxalase pathway. Potentially, the cells could also excrete this metabolite as observed in *E. coli* (Kadner *et al*., 1992; Weber *et al*., 2005) but we did not detect this compound in our metabolite analysis, suggesting efficient detoxification by the glyoxalase pathway.

We did not measure the amount of sugar phosphates present in the cells. The increased amounts of glycerol provide an indication of an increased flux through the upper segment of glycolysis. However, in Chapter 4, interestingly, we detected glucose being excreted by *C. reinhardtii*. We observed that elevated glucose levels were always accompanied with elevated levels of D-lactate. This provides further evidence for D-lactate production by the methylglyoxal pathway. The accumulation and excretion of glucose suggest a disruption of the carbon source utilisation, leading to increasing levels of phosphorylated sugars which could be detrimental to the cells. Consequently, this could direct carbon flux towards the methylglyoxal pathway or the glycerol pathway. The advantage of using the former pathway is D-lactate could be oxidised to pyruvate, possibly when oxygen becomes available. This generated fuel could then potentially be used for cell growth and viability. On the other hand, the fate of the produced glycerol is currently unclear. Nevertheless, the production of glycerol is still beneficial for the cells since it helps in the re-oxidation of NADH for the maintenance of glycolysis.

To further prove the activation of the methylglyoxal pathway, transcript analysis by real-time PCR could be carried out to assess the induction of glyoxalase 1 and 2. I would expect the transcript levels of these two genes to increase with increasing dark anaerobic incubation period as more substrates would be available. However, it should be noted that there is no strict correlation between transcript levels and enzyme activity (Atteia *et al*., 2013). For example, the transcript levels of glycerol kinase (GK) and *sn*-glycerol-3-phosphate phosphatase (GPP), which are the putative enzymes thought to be involved in the formation of glycerol from DHAP, could not explain the observed glycerol production. Alternatively, to prove the occurence of the glyoxalase pathway, the enzymes could be inhibited with glyoxalase inhibitors (Thornalley, 1990) or mutants generated. If the pathway is successfully blocked, no lactate could be formed from this pathway but this would also lead to the toxic build-up of methylglyoxal. Hence, the cell growth and viability could be

determined in the presence of these inhibitors plus PFL1 inhibitor. The production of lactate could also be tested with *C. reinhardtii* incubated anaerobically in the dark with glucose or sugar phosphates, assuming the cells could consume these carbon sources from the medium.

### 3.3.4 Acetoin production

Acetoin was observed to be excreted by *C. reinhardtii* (Figure 3.16), and as far as we are aware, this is the first report of the excretion of this organic compound by *C. reinhardtii* under dark anaerobic conditions. The acetoin production described in this chapter was only for one specific time point i.e. 4 hours of dark anaerobic incubation. However, in Chapter 4, acetoin was detected after 4 and 8 hours of dark anaerobic incubation. We observed an increase in acetoin production from 4 to 8 hours of incubation, suggesting its production was anaerobically induced. To further confirm this, acetoin production should be analysed with more time points. The small amounts of acetoin produced by the WT suggest the metabolite is a minor end product of dark fermentation, similar to lactate and glycerol. Acetoin production was only noticeable when the fermentative pathway(s) is eliminated, suggesting a rearrangement of metabolic flux that included acetoin production.

Acetoin production occurs in different bacteria in response to stress such as low oxygen concentration, low pH or pyruvate accumulation (Goupil-Feuillerat *et al*., 1997). In lactic acid bacteria, the fermentative production of acetoin starts with pyruvate being converted to 2-acetolactate by acetolactate synthase, which is then converted to acetoin by acetolactate decarboxylase. However, in the presence of oxygen, 2-acetolactate can spontaneously be converted to diacetyl, which is then converted to acetoin by diacetyl-acetoin reductase (Goupil-Feuillerat *et al*., 1997). We found a homologue of acetolactate synthase (Cre01.g055453) in the *C. reinhardtii* genome. Unfortunately, we could not find homologues for acetolactate decarboxylase nor diacetyl-acetoin reductase. Alternatively, acetoin could potentially be formed by acetoin dehydrogenase (Opperman *et al*., 1991; Opperman & Steinbuchel, 1994), requiring acetaldehyde and acetyl-CoA as substrates. However, the presence of this homologue in the *C. reinhardtii* genome is also unclear.

Acetoin production has also been reported to be produced from acetaldehyde and catalysed by pyruvate decarboxylase in wheat (Singer & Pensky, 1952; Crout *et al*., 1986), yeast (Chen & Jordan, 1984; Stivers & Washabaugh, 1993), purple non-sulphur bacteria (Qadri & Hoare, 1973) and *Zymomonas mobilis* (Bruhn *et al*., 1995; Wu *et al*., 2000). There is only one putative pyruvate decarboxylase gene found in the *C. reinhardtii* genome (Burgess, 2011), which is annotated as *PDC3*. Although there are two genes also annotated as

*PDC1* and *PDC2*, these putative genes are found to encode pyruvate dehydrogenase E1 α components, and therefore are not a true pyruvate decarboxylase (Burgess, 2011). Given this, one possibility is that acetoin is produced in *C. reinhardtii* by the PDC3 pathway. Therefore, it might be expected that mutant strains lacking the PDC3 pathway should not be able to produce acetoin. This was true for most of the mutants lacking PDC3, which are described in Chapter 4. However, acetoin production was still observed for the quadruple (*ldh-pdc3-pfl1-adh1*) and *ldh-pdc3-pfl1* mutants. However, the amounts of acetoin produced by these mutants were rather low. Nevertheless, it has been reported that pyruvate dehydrogenase from a rat tumor mitochondria can also synthesize acetoin (Baggetto&Lehninger, 1987). Consequently, *C. reinhardtii* pyruvate dehydrogenases might also contribute to acetoin synthesis.

The production of acetoin has been reported in lactic bacteria to be induced by high concentrations of intracellular pyruvate, whereby high pyruvate accumulation can cause a drop in internal pH, and therefore, the conversion of pyruvate to acetone would help in maintaining pH homeostasis (Tsau *et al*., 1992). Acetoin production was also reported to be enhanced when cells were grown in the presence of pyruvate (Monville *et al*., 1987, Tsau *et al*., 1992). To confirm the relationship between pyruvate and acetoin production, *C. reinhardtii* could be grown or incubated with pyruvate, assuming pyruvate could be taken up by *C. reinhardtii*. However, since we found a homologue (Cre01.g039950) of the pyruvate transporter (Sanchez, 2013), we expect this might be feasible. Alternatively, the production of acetoin could also be tested by incubating cells with acetaldehyde, assuming increasing the amount of the enzymatic substrate would increase acetoin production. In this work, apart from the D-LDH protein, we also attempted to overexpress *C. reinhardtii PDC3* in *E. coli* in order to understand its enzyme kinetics, and if it were able to produce acetoin. However, we could not manage to obtain soluble PDC3 protein under the conditions we tested (data not shown). A comparison between acetoin levels and pyruvate levels from our dark anaerobic metabolite analysis suggests there seems to be a good correlation between pyruvate and acetoin, whereby the higher the pyruvate level the higher the acetoin level. However, in Chapter 4, when we compared the production of acetoin and pyruvate levels among the various fermentative mutants, the correlation between acetoin and pyruvate was not clearly observed but this could be due the involvement of other metabolic pathways that could more efficiently consume pyruvate, and therefore pyruvate consumption by the PDC3 pathway was no longer essential to reduce the effect of pyruvate build-up.

It is also interesting to note that in wheat, it has been reported that cytoplasmic pH regulation is important for survival under hypoxia, with pH regulation triggered by cytoplasmic acidification, resulting in the formation of ethanol (Roberts *et al*., 1984). It has also been reported that the wheat pyruvate decarboxylase was more active at lower pH (Lee & Langston-Unkefer, 1985). This potentially means a drop in cytoplasmic pH, which can be caused the generation of glycolytic organic acids, would trigger the activation of the pyruvate decarboxylase, leading to the consumption of pyruvate and production of ethanol for pH homeostasis (Roberts *et al*., 1984; Lee & Langston-Unkefer, 1985). However, in *C. reinhardtii*, the pH profile of the PDC3 enzyme has not yet been studied.

### 3.3.5 Galactose production

*C. reinhardtii* has been reported to be able to secrete a large amount of exopolysaccharide containing galactose, glucose and other sugars (Bafana, 2013). Therefore, the excretion of galactose observed in this work is perhaps unsurprising. Although no significant effect was observed on galactose production in our mutant strains, the proposed metabolic pathways for galactose production is described here as no previous studies, as far as we are aware of, have described galactose production under dark anaerobic conditions.

Under our experimental conditions, we propose that galactose is produced as a side path to glycolysis. During glycolysis, glucose is broken down to glucose 6-phosphate. This sugar phosphate could be converted to glucose 1-phosphate by phosphoglucomutase (Cre01.g012600), which could be further converted to uridine diphosphate (UDP) glucose by uridine triphosphate(UTP):glucose-1-phosphate uridylyltransferase (Cre04.g229700; also known as UDP–glucose pyrophosphorylase). The generated UDP glucose could be converted to UDP galactose by UDP-glucose 4-epimerase (Cre09.g401022), and further converted to galactose 1-phosphate by UDP-galactose/glucose pyrophosphorylase (Cre14.g621750). Galactose 1-phosphate could finally be converted to galactose by galactokinase (Cre17.g732300). Alternatively, galactose and also glucose can be produced from the breakdown of lactose by β-galactosidase (Cre08.g379450). However, lactose production in *C. reinhardtii* has not been reported in any previous studies including that of Bafana (2013). Moreover, there seems to be no homologue of lactose permease for transporting lactose encoded by the *C. reinhardtii* genome. There is also no galactose permease for transporting galactose, which raise the question of how galactose is transported across the cell membrane in *C. reinhardtii*.

Another possibility is that galactose could potentially come from the breakdown of glycoproteins. It has been reported the outer wall glycoproteins of the green alga consist exclusively of arabinose and galactose (Bollig *et al*., 2007). However, we did not detect arabinose in the culture medium.

### 3.3.6 Effects of *D-LDH* knockdown on dark anaerobic metabolite production

*D-LDH* knockdown appeared to have little effect on dark metabolite production (Figure 3.23). The knockdown caused an increase in the accumulation of pyruvate, indicating the utilisation of pyruvate was affected by the elimination of this pyruvate-consuming pathway. This also provides evidence that the $NAD^+$-dependent D-LDH pathway is involved in pyruvate consumption under dark anaerobic conditions. If it was not involved, the pyruvate elevation should not be observed. However, the increase in pyruvate levels was only small, suggesting the pathway is only a minor fermentative pathway in *C. reinhardtii*. This is further supported by the non-substantial changes in the production of the other metabolites. Although the D-LDH pathway is involved in supplying $NAD^+$ for the maintenance of glycolysis, no metabolic flux was observed towards the other $NAD^+$-producing pathways such as the glycerol-producing pathway. The role of NADH re-oxidation could be sufficiently carried out by the major ethanol-producing fermentative pathway. The increase in pyruvate could also suggest a slight increase in the sugar phosphates from the upper segment of glycolysis. This would cause the increased formation of methylglyoxal and eventually D-lactate, as previously mentioned. However, even if there was no increase in the sugar phosphates, methylglyoxal could still be formed by spontaneous degradation of triose phosphates and thus explaining the minor presence of D-lactate. The fact that there was no substantial increase in glycerol suggests there was probably no substantial increase in the levels of sugar phosphates especially DHAP.

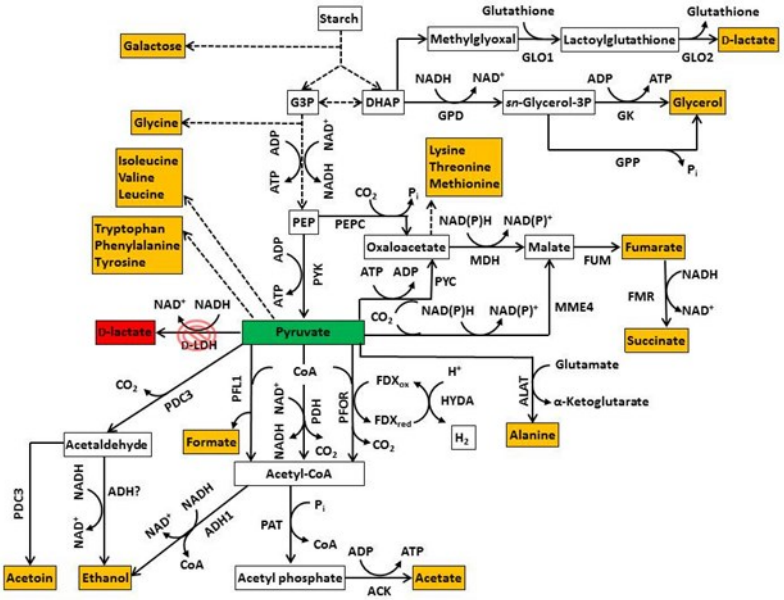


**Figure 3.23 Proposed model of dark fermentative metabolism in *ldh*-KDs.**

Metabolites which increased, decreased and unchanged relative to the WT's are highlighted in green, red and orange, respectively. For simplicity, some metabolic pathways (dash lines) are not described. Abbreviations: ACK (acetate kinase), ADH1 (bifunctional acetaldehyde/alcohol dehydrogenase 1), ADP (adenosine diphosphate) ALAT (alanine aminotransferase), ATP (adenosine triphosphate), $CO_2$ (carbon dioxide), CoA (coenzyme A), DHAP (dihydroxyacetone phosphate), $FDX_{ox}$ (oxidised ferredoxin), $FDX_{red}$ (reduced ferredoxin), FMR (fumarate reductase), FUM (fumarase), G3P (glyceraldehyde 3-phosphate), GK (glycerol kinase), GLO (glyoxalase), GPD (*sn*-glycerol-3 phosphate dehydrogenase), GPP (*sn*-glycerol-3-phosphate phosphatase), $H^+$ (hydrogen positive ion), $H_2$ (hydrogen gas), HYDA (hydrogenase), LDH (D-lactate dehydrogenase), MDH (malate dehydrogenase), MME4 (malic enzyme 4), $NAD^+$ (oxidised nicotinamide adenine dinucleotide), NADH (reduced nicotinamide adenine dinucleotide), $NADP^+$ (oxidised nicotinamide adenine dinucleotide phosphate), NADPH (reduced nicotinamide adenine dinucleotide phosphate), $P_i$ (inorganic phosphate), PAT (phosphotransacetylase), PDC3 (pyruvate decarboxylase 3), PDH (pyruvate dehydrogenase complex), PEPC (phosphoenolpyruvate carboxylase), PFL1 (pyruvate formate lyase 1), PFOR (pyruvate:ferredoxin oxidoreductase), PYC (pyruvate carboxylase), and PYK (pyruvate kinase).

### 3.3.7 Effects of PFL1 inhibition on dark anaerobic metabolite production

PFL1 inhibition with 10 mM HP showed considerable effects on dark anaerobic metabolite production (Figure 3.24). This is as expected since formate is a major fermentative end product. The inhibition of PFL1 by HP caused a substantial reduction in formate as expected. However, there was also a substantial reduction in acetate. This could be due to the

metabolic flux being directed towards the ADH1 pathway instead. Since the PFL1 pathway was eliminated, the pool of acetyl-CoA should be reduced. The cells probably had to feed most of the acetyl-CoA into the ADH1 pathway, presumably due to the needs for regenerating $NAD^+$ as 2 molecules of $NAD^+$ would be generated per molecule of acetyl-CoA. It would be more beneficial to generate ATP from glycolysis instead of from the acetate-producing pathway, as more ATP is produced by glycolysis than by this fermentative pathway. Therefore, cells could afford to reduce its acetate production. However, it is also possible for the ethanol to be contributed by the PDC3 pathway. Since there was an increase in the pyruvate level, more pyruvate could be decarboxylated to acetaldehyde by PDC3. The generated acetaldehyde could then be converted to ethanol by so far ill-defined alcohol dehydrogenase(s). Previous studies assumed this was carried out by ADH1 (Magneschi *et al*., 2012; Catalanotti *et al*., 2012) but there are still other potential alcohol dehydrogenases in the *C. reinhardtii* genome (Magneschi *et al*., 2012), which are yet to be characterised. Catalanotti *et al*. (2012) favour this PDC3/ADH route since this previous study observed an increase in the carbon dioxide level, which they assumed mostly due to the pyruvate decarboxylation by PDC3. However, in Chapter 4 we describe the dark anaerobic metabolite production of *pdc3-pfl1* mutant. If ethanol was mostly produced through the PDC3/ADH route, the ethanol level should be reduced. However, this was not observed in the *pdc3-pfl1* mutant, suggesting most of the ethanol came from acetyl-CoA. The elevated level of carbon dioxide observed by the previous study could potentially come from other pathways. To further confirm this hypothesis, the levels of carbon dioxide and hydrogen gas should be measured in this work. This would provide a clue if more pyruvate was re-routed towards the PFOR pathway, producing more hydrogen, carbon dioxide and acetyl CoA. The increased level of the latter would also nicely explain the observed level of ethanol, as more acetyl-CoA would be available to compensate the loss caused by the PFL1 inhibition. The PDH pathway is assumed to be active only under aerobic conditions (Grossman *et al*., 2007), and as it uses $NAD^+$, which is needed to sustain glycolysis, it is considered to be the least favoured pathway in generating acetyl-CoA (Catalanotti *et al*., 2013).

The PFL1 inhibition also caused an increase in D-lactate. We hypothesise that the generated D-lactate could come from both the D-LDH pathway and the methylglyoxal pathway as there were elevated levels of pyruvate and glycerol. We suspected most of the generated D-lactate came from the methylglyoxal pathway because when PFL1 inhibition was coupled to *D-LDH* knockdown, we generally observed no substantial difference in the amounts of excreted D-lactate. Therefore, the D-LDH pathway would not help in consuming

most of the pyruvate. This could cause a build-up of pyruvate. To prevent this, the cells had to excrete excess pyruvate and also had to switch on other pyruvate-consuming pathways. In this case, acetoin, ALAT pathway and the reverse TCA reactions were activated. The activation of the acetoin pathway is consistent with an increase in the intracellular pyruvate levels, and also suggests an increase in acetaldehyde levels as two molecules of acetaldehyde are needed to produce one molecule of four-carbon acetoin. If there is more acetaldehyde, more ethanol could also be produced from acetaldehyde but it is assumed the increase in the ethanol production from this pathway was only small as the increase in acetoin was only small.

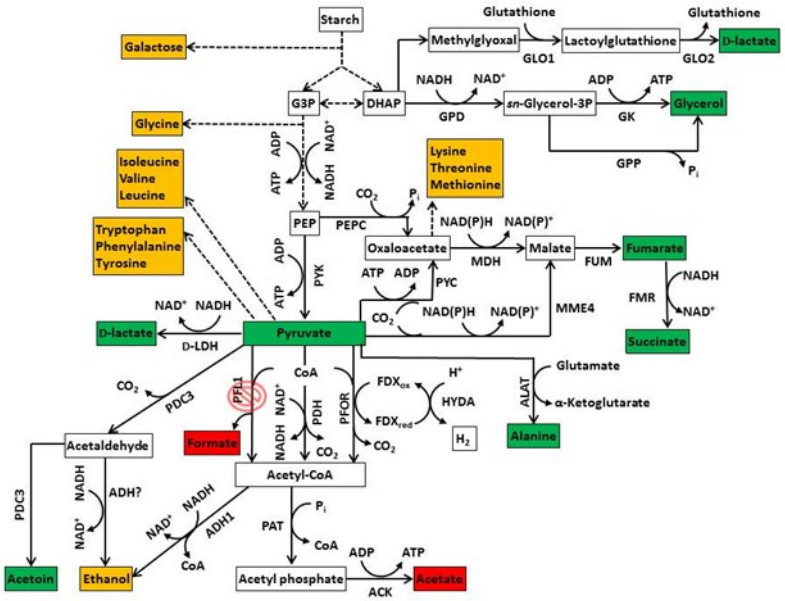


**Figure 3.24 Proposed model of dark fermentative metabolism in WT treated with 10 mM HP.**

Metabolites which increased, decreased and did not change relative to the WT's are highlighted in green, red and orange, respectively. See Figure 3.23 for designations of enzymes and metabolites.

### 3.3.8 Effects of *D-LDH* knockdown and PFL1 inhibition on dark anaerobic metabolite production

*D-LDH* knockdown coupled to PFL1 inhibition using 10 mM HP showed similar effects to that observed with PFL1 inhibition alone except there was slightly more metabolic flux towards glycerol (Figure 3.25). This should probably be due to the presence of more

glycolytic sugar phosphates, as their downstream utilisation was more affected by the elimination of more than one metabolic pathway. This is suggested by the potentially higher amounts of pyruvate and acetoin. Arguably, the predicted increase in the sugar phosphate levels should also increase the amounts of D-lactate produced by the methylglyoxal pathway but this was not observed here, whereby the D-lactate production was similar to the production observed with the PFL1 inhibition. This could be due to the production of glycerol was carried out by enzymes whereas the production of methylglyoxal was proposed to be by spontaneous degradation. Therefore, metabolite production by an enzymatic means should be more efficient than by a non-enzymatic means. Nevertheless, the increase in glycerol levels was only small. As the effects on metabolite production were mostly similar to the effect observed with the PFL1 inhibition, it further provides suggestion that the D-LDH pathway is only a minor fermentative pathway in *C. reinhardtii*.

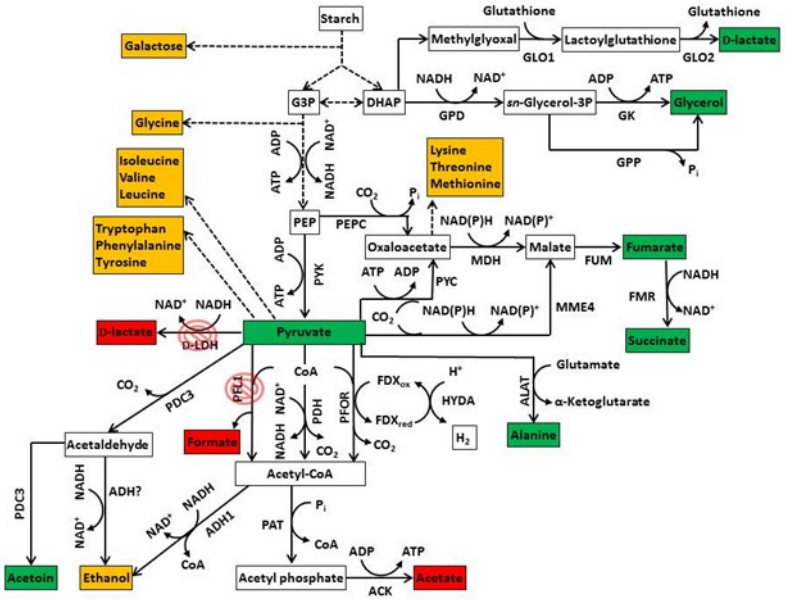


**Figure 3.25 Proposed model of dark fermentative metabolism in *ldh*-KDs treated with 10 mM HP.**

Metabolites which increased, decreased and did not change relative to the WT's are highlighted in green, red and orange, respectively. See Figure 3.23 for designations of enzymes and metabolites.

### 3.3.9 Effects of *D-LDH* knockdown and/or PFL1 inhibition on sulphur-deprived metabolite production

The sulphur-deprived metabolite production of *LDH* knockdown mutants showed no drastic differences relative to the WT. This was similar to the observation made with the dark anaerobic conditions, further suggesting the minor role of the D-LDH pathway. During the first 24 hours of sulphur starvation, the cells did not yet become anoxic and were expected at this stage to accumulate its starch reserves (Melis, 2007). However, after 24 hours the cells became anaerobic, and this would activate fermentative metabolism, which leads to the gradual production of D-lactate, formate, ethanol, alanine, hydrogen gas and carbon dioxide (Kosourov *et al*., 2003; Burgess *et al*., 2012). There was also a gradual accumulation of pyruvate, which could be due to continuous degradation of starch and glucose for maintaining cell viability. However, the pyruvate amounts were only small. Acetate levels stabilised after 24 hours. However, this could be due the natural production of acetate by the alga. Glycolate was also produced after 24 hours, potentially due to photorespiration.

PFL1 inhibition with 10 mM HP showed as expected the dramatic reduction in formate production, in agreement with previous studies (Hemschemeier *et al*., 2008; Burgess *et al*., 2012). Some of the carbon flux was re-directed towards D-lactate production, which is in agreement with the dark anaerobic metabolite production described above and also with a previous study (Burgess *et al*., 2012). However, it is unclear whether the generated D-lactate mostly came from the D-LDH or the methylglyoxal pathway. Since pyruvate and not glycerol was detected, it could potentially mean the metabolic flux was re-routed towards the D-LDH pathway. Unlike the dark anaerobic metabolite production, there was no substantial increase observed in the pyruvate levels. This could be due to the occurrence of many other metabolic pathways that could consume the excess pyruvate, which was possible under these conditions. There was only a slight increase in hydrogen and carbon dioxide production, which might not be significant, as previous studies found no effect on hydrogen production (Burgess *et al*., 2012; Hemschemeier *et al*., 2008).

The *D-LDH* knockdown coupled to PFL1 inhibition with 10 mM HP showed as expected the substantial reduction of formate, which could potentially lead to the re-routing of the carbon flux towards the methylglyoxal pathway. The total amounts of D-lactate generated were lower than the amount observed with the PFL1 inhibition alone, as there was potentially no contribution of D-lactate from the downregulated D-LDH pathway. Nevertheless, it still could not be ruled out that D-lactate could be produced by the residual D-LDH. There seemed to be no effect on the hydrogen and carbon dioxide production.

# Chapter 4: Isolation and characterisation of quadruple and triple mutants

## 4.1 Introduction

As a means to produce energy for survival, pyruvate is produced from the glycolytic breakdown of starch reserves when cells are experiencing anaerobic conditions (Atteia *et al*., 2013). In unicellular *C. reinhardtii*, the generated pyruvate can be further metabolised through the activation of multiple fermentative pathways that are catalysed by several enzymes including pyruvate formate lyase (PFL1), bifunctional acetaldehyde/alcohol dehydrogenase (ADH1), pyruvate:ferredoxin oxidoreductase (PFOR) and possibly pyruvate decarboxylase (PDC3) (Grossman *et al*., 2007; Catalanotti *et al*., 2013).

PFL1 (Phytozome ID Cre01.g044800) is an enzyme found mainly in prokaryotes so it is considered rather unusual for eukaryotes such as *C. reinhardtii* to possess this protein (Atteia *et al*., 2006). The production of formate as a major end product of dark fermentation in *C. reinhardtii* has been observed in numerous studies (Gfeller & Gibbs, 1984; Kreuzberg, 1984; Ohta *et al*., 1987; Mus *et al*., 2007; Hemschemeier *et al*., 2008; Philipps *et al*., 2011; Burgess *et al*., 2012; Catalanotti *et al*., 2012). Similarly, formate has also been observed to be generated under sulphur-deprived conditions (Winkler *et al*., 2002; Kosourov *et al*., 2003; Hemschemeier *et al*., 2008; Burgess *et al*., 2012).

The role of PFL1 in catalysing the dark fermentative production of formate was confirmed after production was significantly affected when the PFL1 pathway was blocked by using different strategies i.e. through the use of a PFL1 inhibitor (Ohta *et al*., 1987; Hemschemeier *et al*., 2008; Philipps *et al*., 2011; Burgess *et al*., 2012) and the isolation and analyses of both PFL1 knockout (Philipps *et al*., 2011; Catalanotti *et al*., 2012) and knockdown mutants (Burgess *et al*., 2012). When the PFL1 pathway was inactivated, *C. reinhardtii* was found to re-direct its metabolic flux to other fermentative pathways, producing lactate, alanine, and products of the reverse TCA reactions, indicative of metabolic flexibility (Philipps *et al*., 2011; Burgess *et al*., 2012; Catalanotti *et al*., 2012).

*C. reinhardtii* is believed to possess three iron-containing alcohol dehydrogenases that could be involved in the production of ethanol (Posewitz *et al*., 2009; Magneschi *et al*., 2012). ADH1 (Phytozome ID Cre17.g746997) has been predicted to be a bifunctional alcohol dehydrogenase/acetaldehyde dehydrogenase, and is capable in converting acetyl-CoA into acetaldehyde and subsequently into ethanol in a two-step enzymatic reaction, resulting in the oxidation of two molecules of NADH per molecule of acetyl-CoA (Atteia *et al*., 2003; Hemschemeier & Happe, 2005; Atteia *et al*., 2006; Grossman *et al*., 2007; Mus *et al*., 2007).

Meanwhile, the other two alcohol dehydrogenases, designated as ADH2 (JGI version 4.0 protein identifier 121409) and ADH3 (JGI version 4.0 protein identifier 82021) by Magneschi *et al*. (2012), are not well understood yet. These two enzymes are thought to be monofunctional as the protein would only convert acetaldehyde into ethanol, resulting in the oxidation of only one molecule of NADH per molecule of acetaldehyde (Posewitz *et al*., 2009). However, the analysis of protein domains by InterProScan suggests ADH2 could also have a bifunctional role due to the existence of both alcohol and acetaldehyde dehydrogenase domains but this has yet to be verified as there are alterations on the conserved sequences of the acetaldehyde dehydrogenase domains which might impair this activity (Magneschi *et al*., 2012). Alcohol dehydrogenase activity but not acetaldehyde dehydrogenase activity was still detected when the acetaldehyde dehydrogenase domain was removed from the bifunctional ADH of *Entamoeba histolytica* but no activity at all was observed when the alcohol dehydrogenase domain was removed instead (Espinosa *et al*., 2001). However, it is unclear if this also applies to the *C. reinhardtii* ADH2.

A rerouting of *C. reinhardtii* fermentative metabolism has been observed when the ADH1 pathway was eliminated (Magneschi *et al*., 2012). Interestingly, there was no dark fermentative production of ethanol in the *adh1* knockout mutant, as the metabolite was undetected by HPLC analysis, indicating only ADH1 was involved in ethanol production (Magneschi *et al*., 2012). However, this result does not entirely rule out the participation of the other two alcohol dehydrogenases as culturing and induction conditions could also influence the end products of dark fermentation (Posewitz *et al*., 2009). In addition to the effect on ethanol production, the levels of formate and carbon dioxide were also reduced but no effect was observed on hydrogen evolution because the metabolic flux was rerouted instead towards acetate, lactate and glycerol production (Magneschi *et al*., 2012).When the elimination of the ADH1 pathway was coupled to the elimination of PFL1, a similar metabolic restructuring was observed (Catalanotti *et al*., 2012). The double *pfl1-adh1* knockout mutant showed no formation of both formate and ethanol and a decrease in acetate, hydrogen and carbon dioxide production but showed an increase in the formation of lactate and glycerol with an elevated reverse TCA activity (Catalanotti *et al*., 2012). Furthermore, there was also an increase in the intracellular levels of several sugars but the opposite was observed for various amino acids (Catalanotti *et al*., 2012).

PDC3 (Phytozome ID Cre03.g165700), which was previously referred as PDC1 (Mus et al., 2007), is predicted to decarboxylate pyruvate into acetaldehyde and carbon dioxide. Two other putative proteins exist in the *C. reinhardtii* genome that are also annotated as

PDC1 and PDC2 but these protein are believed to be the E1 alpha component of pyruvate dehydrogenase (PDH) complex, and therefore should not have PDC activity (Burgess, 2011). The knockdown of the PDC3 pathway in *C. reinhardtii* through the isolation of a *pdc3*-KD (knockdown) mutant by artificial microRNA technology resulted in no observable effects on the dark fermentative metabolite production (formate, acetate, ethanol and lactate), suggesting the PDC3 pathway only has a minor role in dark fermentation or could be inactive under the conditions tested (Burgess, 2011). However, when the *PDC3* knockdown was coupled to inhibition of PFL1 pathway with hypophosphite, apart from the reduction in formate and acetate, there was a distinctive increase in ethanol production and a marked accumulation of lactate (Burgess, 2011). The effect on dark fermentative hydrogen production was not determined in this previous study as the analytical equipment used was not sensitive enough to detect the gas.

Under sulphur-derived conditions, the *pdc3*-KD mutant showed an increase in formate and ethanol accumulation but showed a negative effect on the hydrogen photoproduction, and no change in the evolution of carbon dioxide (Burgess, 2011). This previous study also showed that when the *pdc3*-KD mutant was treated with PFL1 inhibitor, formate production was significantly decreased but lactate and alanine were significantly increased. No change in ethanol and hydrogen photoproduction was observed but the amount of carbon dioxide was found to be lower than the WT. However, caution needs to be taken when interpreting these previous results as no additional line of *PDC3* knockdown mutant has yet been isolated (Burgess, 2011).

The overall aim of this thesis is to try to manipulate metabolism to favour the production of biohydrogen. Given the observed metabolic flexibility of *C. reinhardtii*, we hypothesised that several fermentative pathways would have to be inactivated before an effect on biohydrogen would be observed. As a first step, I describe in this chapter the isolation and characterisation of single, double, triple and quadruple mutants affected in the expression of the D-LDH, PDC3, PFL1 and ADH1 enzymes.

## 4.2 Results

### 4.2.1 Generation and isolation of quadruple and triple mutants

Fermentative mutants were generated using a cell mating approach. We were kindly given the double mutant, *pfl1-adh1* (Catalanotti *et al*., 2012) by Prof. Arthur Grossman (Standford University, USA). This double mutant was generated by crossing a *pfl1* knockout mutant (Catalanotti *et al*., 2012) with the *adh1* knockout mutant (Magneschi *et al*., 2012). Prior to the crossing of these two single strains, the *pfl1* and *adh1* mutants were backcrossed four times with CC-125 and CC-124, respectively. To generate a triple mutant with reduced levels of PDC3, I decided to cross this *pfl1-adh1* double mutant with the *PDC3* knockdown mutant, *pdc3*-KD, which was generated previously from CC-124 by Steven J. Burgess in the Nixon group (Burgess, 2011).

*C. reinhardtii* cells can only be mated together if they are of the opposite mating type. The cells can either be of a mating type *plus* ($mt^+$) or *minus* ($mt^-$). CC-124 ($mt^-$) and CC-125 ($mt^+$) are of the opposite mating type, and therefore, can be crossed together. The *pdc3*-KD mutant should be $mt^-$ due to its CC-124 genetic background. However, the mating type of *pfl1-adh1* was unknown. Therefore, its mating type had to be determined before the triple mutant could be generated.

To determine cell mating type, cells of unknown mating type were tested by crossing with strains of known mating type (CC-124 and CC-125) and the resulting mating reaction analysed. The cells had to be first prepared for gametogenesis by incubating them in modified TAP medium that was deficient in nitrogen (Section 2.14). The gametes were mixed together to form zygotes and left unstirred overnight under strong light. If mating was efficient, the zygotes could be seen as a big clump of cells that would adhere to the flask. This clump of cells would remain clustered together even if the medium was agitated. If mating was inefficient, no clumps of cells would be seen (Appendix 11).

Our tests showed the mating reaction *pfl1-adh1* x CC-125 produced a positive result (mating occurred) while *pfl1-adh1* x CC-124 produced a negative result (mating did not occur). We did several negative controls (CC-124 x CC-124, CC-125 x CC-125 and *pfl1-adh1* x *pfl1-adh1*), and as expected, the reactions were all negative. We also did a positive control (CC-124 x CC-125), and the reaction was positive as expected. Our results showed that the *pfl1-adh1* mutant was $mt^-$. To confirm *pdc3*-KD was also $mt^-$, we also carried out mating reactions with the gametes of this mutant. A positive reaction was observed for *pdc3*-KD x CC-125 but negative with *pdc3*-KD x CC-124. No reaction was observed in the

negative control (*pdc3*-KD x *pdc3*-KD) as expected. This means it would not be possible for *pdc3*-KD and *pfl1-adh1* to be crossed together. To confirm this, we did cross the gametes together but no zygotes were observed. In light of this situation, the mating type of one of the strains had to be changed to the other type before any mating could take place.

We decided to backcross *pdc3*-KD with the WT strain (CC-125) in order to obtain a $mt^+$ strain. The 4-hour mating reaction mixture was spotted onto a 3% TAP agar plate. After allowing the zygotes to mature, they were germinated overnight to produce four daughter cells per zygote. We also did negative controls (CC-125 x CC-125 and *pdc3*-KD x *pdc3*-KD) and as expected, we did not observe any zygotes on the 3% TAP agar plate. However, the positive control (CC-124 x CC-125) produced the zygote and daughter cells as expected. The matured zygote could be identified using a compound microscope by its larger size and thicker wall, and they also stuck better to the agar compared to the vegetative cells which could be scraped off easily (Jiang & Stern, 2009; Harris, 2009). The daughter cells from the *pdc3*-KD backcross were plated onto TAP plates and TAP agar plates containing 10 μg/ml paromomycin ($TAP_{P10}$), and were allowed to grow until green colonies could be picked for screening.

A total of 50 antibiotic-resistant colonies were picked from the $TAP_{P10}$ agar plate. By growing the progenies in the selective medium, any antibiotic-sensitive cells would be eliminated including the parental WT strain that could be introduced as a contaminant during the cell plating. However, the paromomycin would not eliminate any contaminating parental *pdc3*-KD which is paromomycin-resistant. However, any contaminating *pdc3*-KD would be $mt^-$ whereas I wished to isolate $mt^+$ dervatives. We determined the mating types of the 50 antibiotic-resistant colonies, and found 19 of them to be $mt^+$. This was almost a 1:1 segregation of $mt^+$ to $mt^-$ progenies. The 19 colonies were grown in TAP medium to late log phase for the collection of protein samples. We assessed the PDC3 protein level from the samples by immunoblotting. Our blots showed that all 19 samples had no observable PDC3 band when compared to the WT. This was expected as the parental *pdc3*-KD also did not produce any observable PDC3 band. Coomassie Brilliant Blue staining of gel confirmed equal loading of samples (representative results are shown in Figure 4.1.A). For future work, progeny #1 was randomly chosen and designated as *pdc3*-1st.

The original *pdc3*-KD strain was generated by Burgess (2011) by transforming CC-124 with a ~6 kbp plasmid that contained a paromomycin-resistance cassette and a DNA construct designed to synthesise an artificial microRNA targeting the *PDC3* transcript. It is possible that the plasmid integrated into a single chromosome as an intact construct.

However, it is also possible for the construct to be fragmented so that the DNA fragments encoding the artificial microRNA and paromoycin-resistance cassette were integrated into different chromosomes. If this were true, it would be possible to isolate a progeny that shows a *PDC3* knockdown phenotype but is sensitive to the antibiotic. To test this, we analysed the daughter cells that were plated onto the TAP agar plate. A total of 67 colonies were picked and re-grown on $TAP_{P10}$ agar plates. We found 40 out of the 67 colonies were paromomycin-sensitive. We assessed the PDC3 protein level from these 40 cell lines by immunoblotting, and found all of them to express the PDC3 protein at a comparable level to the WT strains (representative results are shown in Figure 4.1.B). These results indicated that the *PDC3* knockdown was tightly linked to the paromomycin-resistance casette but did not rule out the possibility of multiple integrations of DNA fragments into a single chromosome.

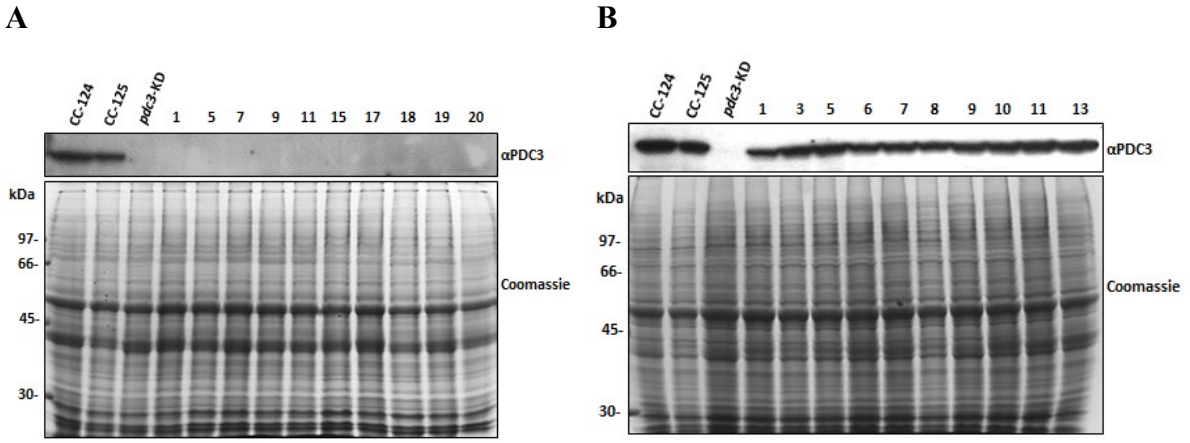


**Figure 4.1 First backcross of *pdc3*-KD.**

PDC3 protein (61 kDa) levels were evaluated by immunoblotting. Coomassie Brilliant Blue staining served as a loading control. A number of progenies obtained from the first backcross of *pdc3*-KD were evaluated but only representative results are shown. (A) Paromomycin-resistant and $mt^+$ progenies. (B) Paromomycin-sensitive progenies.

The success from generating the first backcross of *pdc3*-KD led us to the decision of backcrossing the knockdown mutant several times with the WT strains in order to get a cleaner genetic background. The *PDC3* knockdown mutation was induced by inserting a DNA construct into the *C. reinhardtii* genome but there was a possibility of additional mutations. Backcrossing could get rid or dilute out these background mutations. However, since the site of insertion in the genome was random, there was also a possibility that the insertion could occur within a gene or promoter. Backcrossing will not be able to get rid of

this secondary mutation. Therefore, in this case, it was also important to get at least a second line of the same mutant to establish that any phenotype observed would be due to the result of a single gene mutation and not several genes. However, we have so far been unsuccessful in our attempts to get a second *pdc3*-KD mutant (data not shown) and so we had to settle with backcrossing.

The second backcrossing of *pdc3*-KD involved the crossing between the chosen first backcross with the WT of the opposite mating type. We did several mating controls as described previously, and one of the controls was crossing the first backcross with itself. The resulting mating reaction was negative, indicating there was no contamination of the culture with cells of the opposite mating type. We picked a total of 50 daughter colonies for screening. As described previously, the screening first involved the assessment of the mating types, as we would only be interested in $mt^-$. We found 32 out the 50 progenies to be a $mt^-$ strain. Ten of them were randomly chosen for protein sample collection. Evaluation of the PDC3 protein level of these ten samples was carried out by immunoblotting. It was found all the samples did not show any observable PDC3 band in comparison to the WT strains, and the Coomassie Brilliant Blue staining of the gel confirmed equal loading of samples (Figure 4.2). Progeny #30 (designated as *pdc3*-2nd) was randomly chosen for future work.

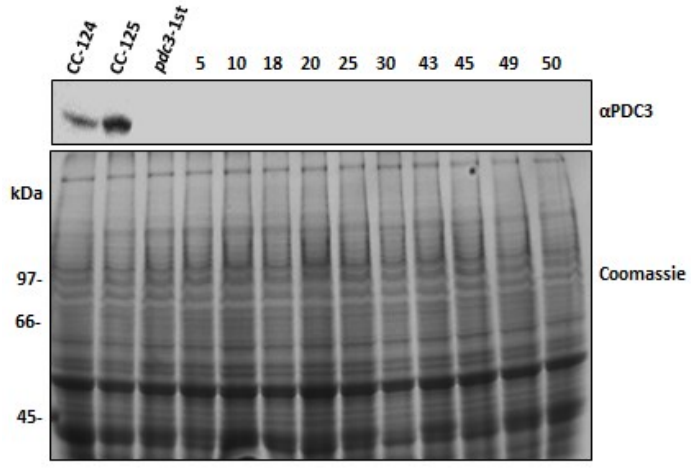


**Figure 4.2 Second backcross of *pdc3*-KD.**

PDC3 protein (61 kDa) levels were evaluated by immunoblotting. Coomassie Brilliant Blue staining served as a loading control. The first backcross of *pdc3*-KD (labelled as *pdc3*-1st) served as a positive control.

To get the third backcross of *pdc3*-KD, the chosen second backcross was crossed with CC-125. One of the mating controls involved crossing the second backcross with itself, and the resulting mating reaction was appropriately negative. A total of 25 daughter colonies were screened for their mating types, and we only obtained 5 progenies with $mt^{+}$. These 5 progenies were sampled and blotted for the assessment of their PDC3 protein level. It was found all 5 samples did not show any noticeable PDC3band (Figure 4.3). The progeny labelled as 'h' was randomly selected for future work and designated *pdc3*-3rd.

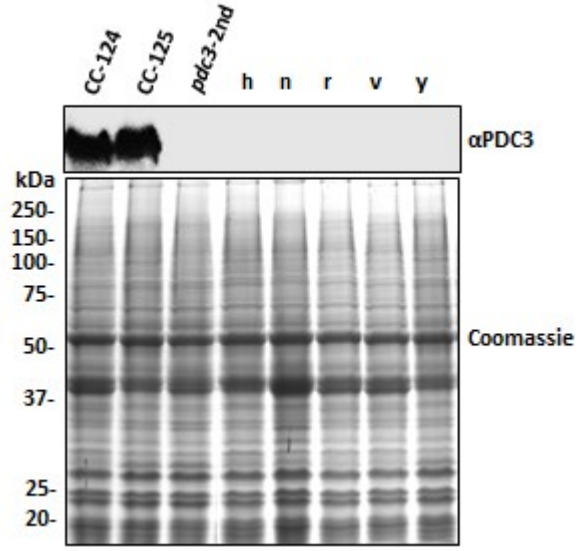


**Figure 4.3. Third backcross of *pdc3*-KD.**

PDC3 protein (61 kDa) levels were evaluated by immunoblotting. Coomassie Brilliant Blue staining served as a loading control. The second backcross of *pdc3*-KD (labelled as *pdc3*-2nd) served as a positive control.

The fourth and final backcrossing of *pdc3*-KD involved the crossing between the selected third backcross and CC-124. As one of the several mating controls, there was no mating reaction observed when the third backcross was crossed to itself, suggesting a pure culture. A total of 25 daughter colonies were screened to isolate progenies with $mt^{-}$. It was found only 4 progenies had the required mating type. The assessment of the PDC3 protein level of these progenies by immunoblotting showed no visible PDC3 band was observed (Figure 4.4).The progeny labelled as 'a' was randomly selected for future work. This fourth backcross of *pdc3*-KD is hereafter labelled as *pdc3*.

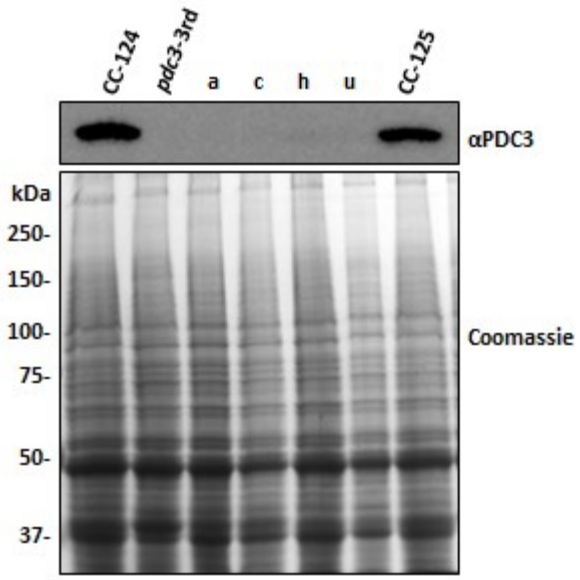


**Figure 4.4 Fourth backcross of *pdc3*-KD.**

PDC3 protein (61 kDa) levels were evaluated by immunoblotting. Coomassie Brilliant Blue staining served as a loading control. The third backcross of *pdc3*-KD (labelled as *pdc3*-3rd) served as a positive control.

We were kindly given the double mutant, *pfl1-adh1* but did not request the single mutants, *pfl1* and *adh1*. Although works on these single and double mutants had been published, we felt it was important to include them in our future analyses. It would be expected for similar findings to be obtained if similar analyses were performed. However, it was also possible for the outcomes to be different due to variations in experimental conditions and techniques used. Thus, it was of great interest to obtain both *pfl1* and *adh1*. To do this, the double mutant was crossed with the WT of the opposite mating type (CC-125). We picked a total of 24 daughter colonies for screening by immunoblotting. We identified a total of 7 cell lines of *pfl1*, 10 lines of *adh1* and 7 lines of *pfl1-adh1* (data not shown). To further confirm these results, we selected only 3 lines each for *pfl1* and *adh1*, and re-grew them mixotrophically for protein sample collection and immunoblotting. The repeated immunoblots confirmed we had successfully isolated *pfl1* and *adh1* single mutants (Figure 4.5). For future work, we randomly selected progeny #2 for *pfl1* and #3 for *adh1*.

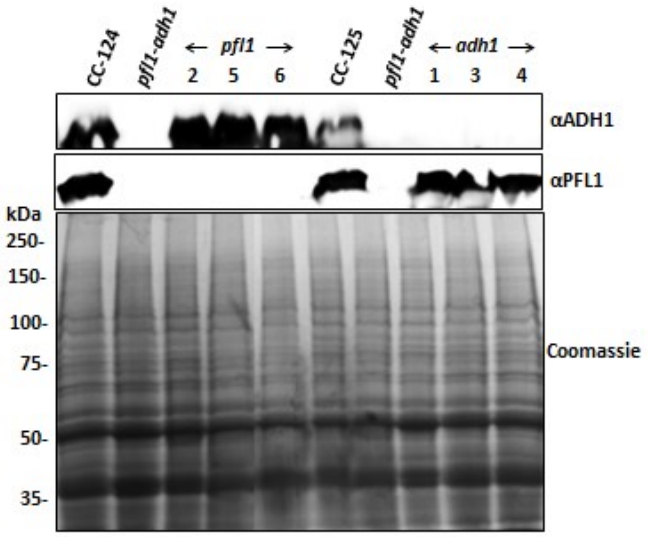


**Figure 4.5 Single mutants obtained from crossing *pfl1-adh1* with CC-125.**

ADH1 (102 kDa) and PFL1 protein (91 kDa) levels were evaluated by immunoblotting. Coomassie Brilliant Blue staining served as a loading control.

To get the *pdc3-pfl1-adh1* mutant (hereafter known as triple mutant), we crossed *pfl1-adh1* with the first backcross of *pdc3*-KD which had the opposite mating type to the double mutant. Ideally, any crosses that involve a single mutant should be performed with the fourth backcross of the mutant. However, this strain was not available when the triple mutant was made. The generation of all the backcross lines required an extensive period of time to complete, and time was one of the constraints in this work. We picked a total of 100 daughter colonies in order to increase the chance of getting the triple mutant. Protein samples were collected from these selected progenies which were grown mixotrophically to late log phase. We screened the protein samples by immunoblotting. We identified a total of 18 cell lines of triple mutant, 18 lines of *pdc3-pfl1* and 14 lines of *pdc3-adh1* (data not shown). To further confirm these results, we randomly selected 10 lines each from the double mutants, *pdc3-pfl1* and *pdc3-adh1* and re-grew them for immunoblotting. The repeated immunoblots confirmed our results (Figure 4.6.A and B). There was a need to use the triple mutant for future cell mating, and so the mating type had to be determined. It was found 6 lines were $mt^+$ and the other 12 lines were $mt^-$. We randomly selected only 4 and 5 lines of the $mt^+$and $mt^-$ strains, respectively. These cell lines were re-grown for the repeated immunoblotting to confirm our earlier results. Our blots confirmed our results (Figure 4.6.C). For future work, we randomly selected progeny #43 for *pdc3-pfl1*, #52 for *pdc3-adh1* and #35 for triple mutant.

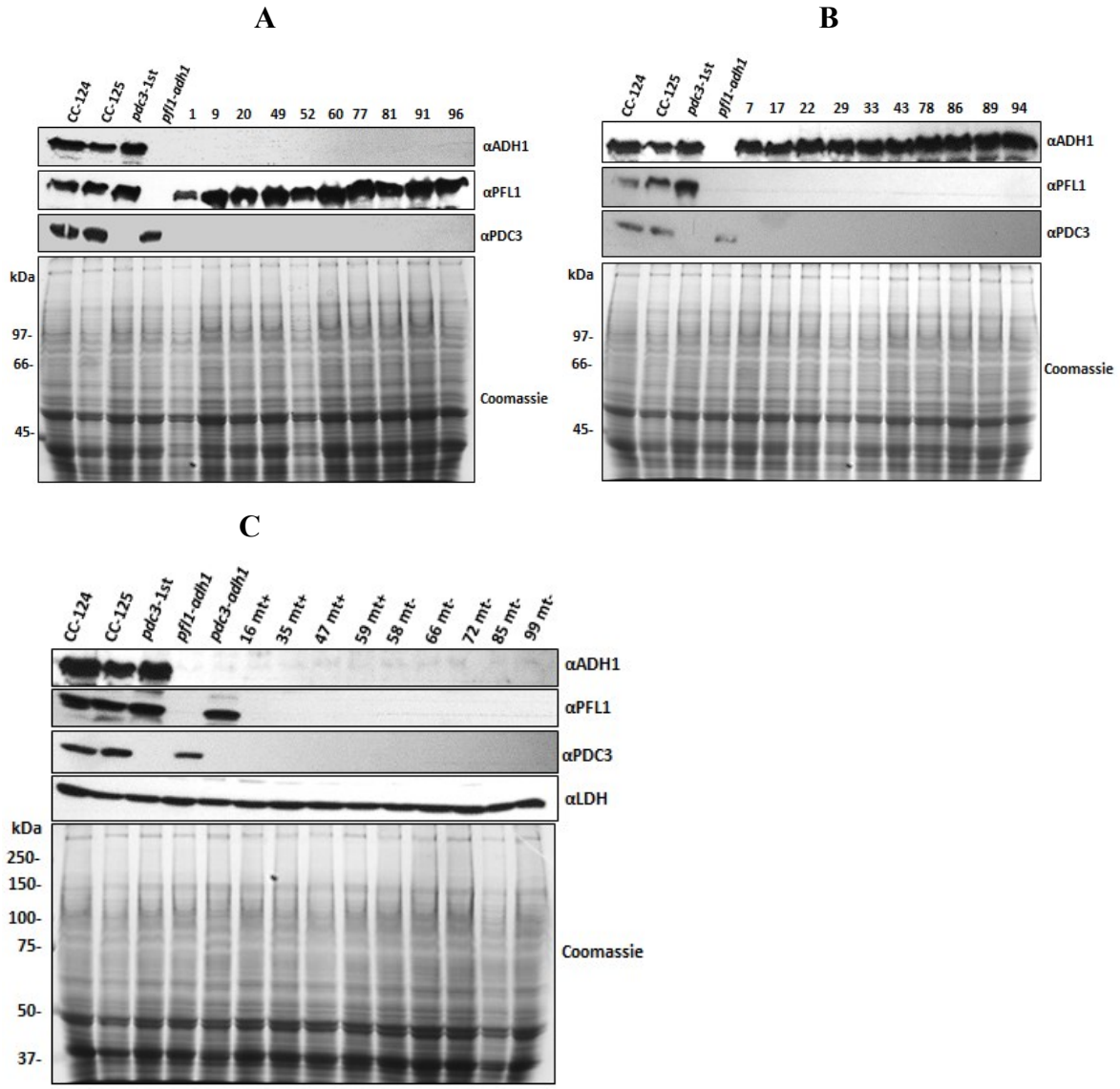


**Figure 4.6 Mutants obtained from crossing *pdc3*-1st with *pfl1-adh1*.**

Protein levels of ADH1 (102 kDa), PFL1 (91 kDa), PDC3 (61 kDa) and D-LDH (45 kDa) were assessed by immunoblotting. Coomassie Brilliant Blue staining served as a loading control. (A) *pdc3-adh1*. (B) *pdc3-pfl1*. (C) Triple mutants with their designated mating types.

Apart from the triple mutant, we were also interested to obtain the *ldh-pdc3-pfl1-adh1* mutant (hereafter known as the quadruple mutant). To do this, an *ldh*-KD mutant was crossed with the selected triple mutant, and we chose *ldh*-KD1 that we had previously isolated for this purpose (Section 3.3.3). The resulting mating reaction was positive, and so were the positive controls (CC-124 x CC-125, *ldh*-KD1 x CC-125 and triple x CC-124). The negative controls (CC-124 x CC-124, CC-125 x CC-125, *ldh*-KD1 x CC-124, triple x CC-125, *ldh*-KD1 x *ldh*-KD1 and triple x triple) produced negative mating reactions as expected. We picked a total of 100 daughter colonies in order to increase the chance of getting the quadruple mutant. Protein samples were collected from these selected progenies which were grown mixotrophically to late log phase. We screened the protein samples by immunoblotting. We identified a total of 18 cell lines of triple mutant, 18 lines of *pdc3-pfl1* and 14 lines of *pdc3-adh1* (data not shown). We identified a total of 6 cell lines of quadruple mutant, 5 lines of *ldh-pfl1-adh1*, 6 lines of *ldh-pdc3-adh1*, 3lines of *ldh-pdc3-pfl1*, 4 lines of *ldh-pdc3*, 7 lines of *ldh-pfl1* and 3 lines of *ldh-adh1* (data not shown). To further confirm these results, the progenies were re-grown and re-sampled for immunoblotting. The repeated blots confirmed our results, and representative blots showing all combinations of the fermentative mutation are shown in Figure 4.7. For future analyses, we selected progeny #84 for quadruple, #59 for *ldh-pfl1-adh1*, #57 for *ldh-pdc3-adh1*, #26 for *ldh-pdc3-pfl1*, #40 for *ldh-pdc3*, #68 for *ldh-pfl1* and #43 for *ldh-adh1*. As expected all these progenies had a considerably reduced amount of D-LDH protein when compared to the WT strains (Appendix 13).

**A**

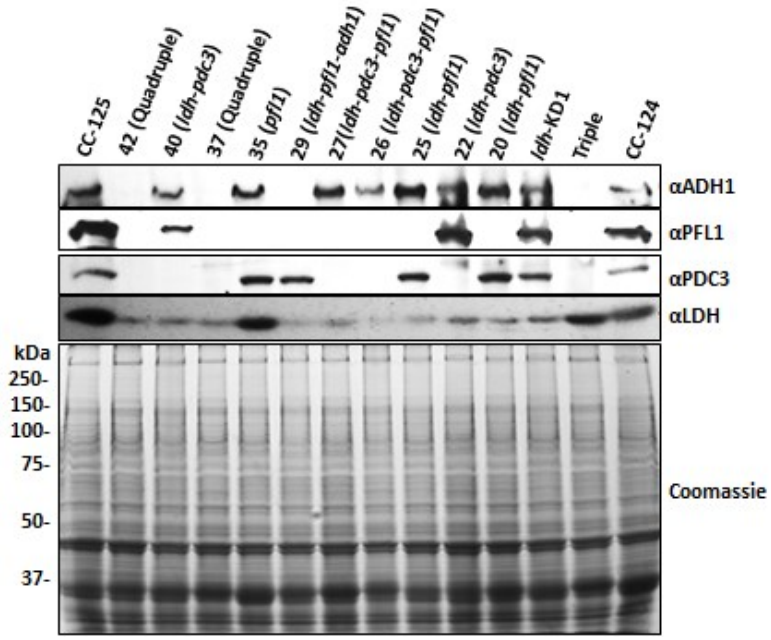


**B**

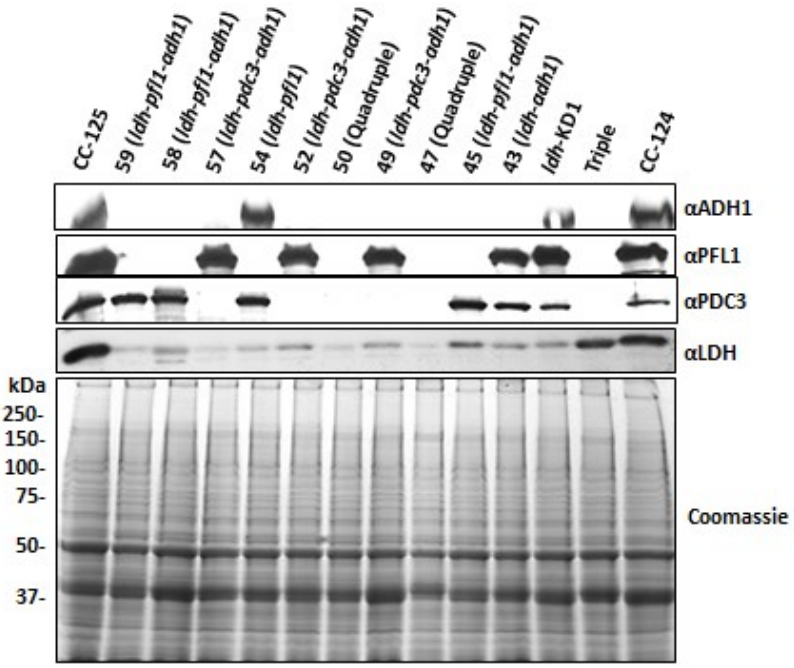


**Figure 4.7 Mutants obtained from crossing triple mutant with *ldh*-KD1.**

Protein levels of ADH1 (102 kDa), PFL1 (91 kDa), PDC3 (61 kDa) and D-LDH (45 kDa) were assessed by immunoblotting. Coomassie Brilliant Blue staining served as a loading control. A number of progenies were assessed but only representative results are shown above in A and B.

### 4.2.2 Characterisation of quadruple and triple mutants

We had successfully generated and isolated a series of *C. reinhardtii* fermentative mutants. However, due to time constraints we were not able to test all of these mutants in all of our analyses. Therefore, it was decided for the work to focus mainly on the triple and quadruple mutants that we thought would be more interesting. The other mutants were only analysed when time permitted. To analyse the quadruple and triple mutants, the analyses should involve comparison with both of the WT strains. This was because the mutants were derived from the CC-124 and CC-125 genetic backgrounds. When this work was first started it was assumed both of the WT strains would produce similar results due to their common origin from the 137c wild type strain (Harris, 2009; Proschold *et al*., 2005). However, it was found later on that they behaved differently in some analyses. Apart from the comparison with the WT strains, we also decided to compare them with the *pdc3* mutant and also the parental strains i.e. *ldh*-KD1, *pfl1*, *adh1* and *pfl1-adh1*with the anticipation to pinpoint the gene mutation responsible for any phenotype observed if there was any. All of these strains had both CC-124 and CC-125 genetic background except for *ldh*-KD1 which had a CC-124 genetic background.

#### 4.2.2.1 Analysis of protein level and D-LDH activity

To quantify the knockdown level of D-LDH in the quadruple mutant, algal cells were grown photoautotrophically with aeration to late log phase in HSM. The starting cultures used for inoculation were also grown in HSM instead of TAP medium to ensure photoautotrophic growth. Proteins were extracted and immunoblotting was performed. We did two independent replicates, and a representative result is shown in Figure 4.8. Our results showed for *ldh*-KD1, the D-LDH band for this mutant was of similar intensity to that found in 12.5% of CC-124. This was as expected as *ldh*-KD1 should have a reduction of ~80% relative to the WT as previously quantified (Section 3.3.4). Interestingly, the quadruple mutant had a stronger reduction in its D-LDH level in comparison with *ldh*-KD1. There was no noticeable D-LDH band for this quadruple mutant under the conditions used. The 6.25% WT sample hardly showed any observable D-LDH band. However, an overexposed blot showed the 6.25% WT sample revealed a faint band with a roughly similar intensity to the quadruple mutant (data not shown). This confirmed the quadruple mutant had ~90% reduction in its D-LDH level compared to the WT strains. Our loading controls (Coomassie Brilliant Blue staining, αPDC1 and αPDC2) confirmed the differences observed were not due

to unequal loading of samples. The D-LDH levels for the other fermentative mutants (*pfl1*, *adh1*, *pfl1-adh1*, *pdc3* and triple) were as expected. Their levels were similar to both of the WT strains. We also checked the levels of oxygen-sensitive PFOR and hydrogenases to confirm the cells were aerobically induced. The reason for this was to confirm the fermentative enzymes of interest were expressed under aerobic conditions (and not just under anaerobic conditions as shown in Appendix 13). This would validate any of our future analyses that involved assessment of the mutants under aerobic conditions. Our blots showed PFOR and hydrogenases were hardly being expressed in these cells, indicating the aerobic nature of the samples. There were some faint bands observed from some of the samples. This could be due to the centrifugation effect. When the cells were harvested by centrifugation (2000g, 2 minutes, room temperature) for protein extraction, the centrifugal force could make the cells became slightly anaerobic. Alternatively, these faint bands could be non-specific cross-reactions as previously suggested (Burgess, 2011).

The *pdc3*-KD mutant was previously quantified by immunoblotting to have over 90% reduction in the PDC3 protein compared to the WT (Burgess, 2011). The fourth backcross of *pdc3*-KD named *pdc3* was found to also have similar reduction. A very faint band was observed from *pdc3* which was equivalent to the 6.25% WT sample, indicating ~90% PDC3 reduction (Figure 4.8). Similarly, the triple and quadruple mutants also showed ~90% reduction in their PDC3 level. These results were confirmed with an overexposed blot where the faint band was more noticeable (data not shown). Interestingly, the PDC3 level of *pfl1* was reduced to ~25% of WT level and this observation was consistent in both independent replicates (data not shown). However, the reason behind this reduction is unclear.

The PFL1 band was not observed in the expected fermentative mutants (*pfl1*, *pfl1-adh1*, triple and quadruple) under the conditions used (Figure 4.8). Similarly, the band was also not observed from the overexposed blot, indicating the protein was below detection limit (data not shown). This was consistent with the immunoblot analyses of the original *pfl1* mutant by Catalanotti *et al*. (2012) who could not detect PFL1 protein under dark anoxic conditions consistent with it being a knockout mutant. Also as expected, all the other mutants (*adh1*, *pdc3* and *ldh*-KD1) showed a WT level of PFL1.

Similarly, there was no ADH1 band observed in the expected fermentative mutants (*adh1*, *pfl1-adh1*, triple and quadruple) (Figure 4.8). This is consistent with the original *adh1* knockout mutant, in which ADH1 protein was not detected both under oxic and anoxic conditions (Magneschi *et al*., 2012).

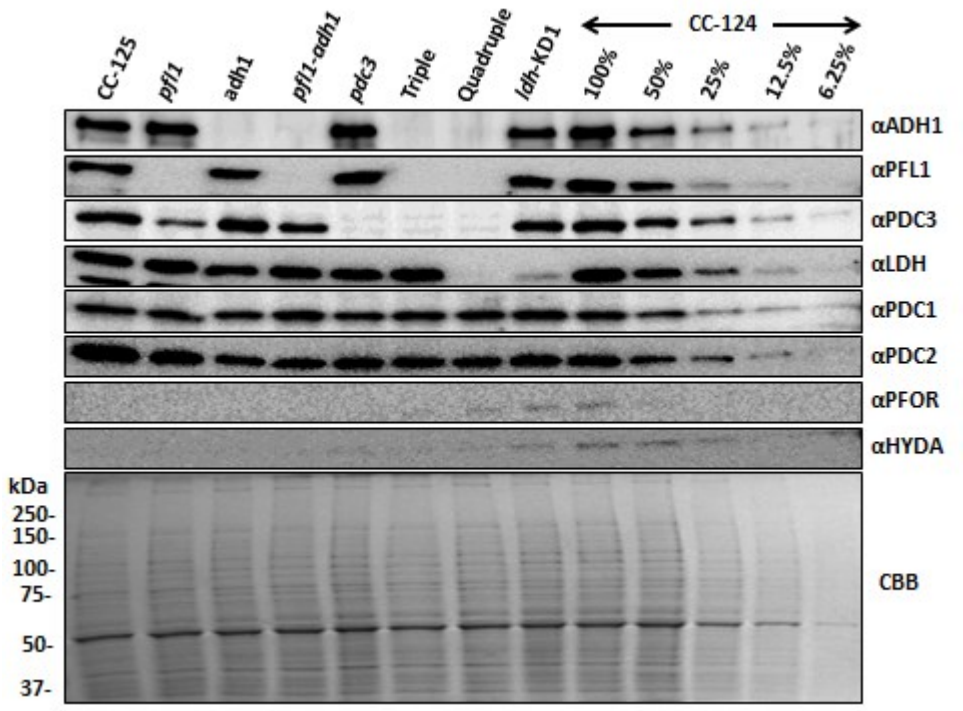


**Figure 4.8 Protein quantitative analyses of HSM-grown fermentative mutants.**

Proteins levels were measured by immunoblotting. Loading controls were provided by gel staining with Coomassie Brilliant Blue (CBB), αPDC1 and αPDC2 (43 kDa). Aerobic/anaerobic induction controls were provided by αPFOR and αHYDA (recognising both HYDA1 and HYDA2; 53 kDa).

The protein analysis showed the quadruple mutant had ~90% reduction in its D-LDH level relative to the WT. To further confirm the D-LDH pathway was affected by this knockdown, we did an enzymatic activity assay by using the intracellular materials extracted from the cells, as described earlier in Chapter 3 (section 3.3.5). Our D-LDH activity assays showed there was a faster drop in the absorbance values at 340 nm (indicating the utilisation of NADH by the enzyme) in both of the WT strains compared to the quadruple mutant when similar amount of extracted proteins were used. The faster drop in absorbance should indicate the presence of higher amount of the enzyme. As a control, we also measured the D-LDH activity of the triple mutant which had a WT level of D-LDH protein. As expected, the drop in absorbance was also quicker compared to the quadruple mutant (representative results are shown in Appendix 4 ). The rates of NADH oxidation by other enzymes (background rates of NADH oxidation in absence of added pyruvate) were also measured, and were found to be lower than by the D-LDH enzyme (representative results are shown in Appendix 4).

We calculated the rate of NADH oxidation by D-LDH (which should be equivalent to the rate of pyruvate reduction) by subtracting the calculated background rate of NADH

oxidation from the overall rate of NADH oxidation (Figure 4.9). We found the rates of NADH oxidation by D-LDH from CC-124, CC-125 and the triple mutant were similar. This was as expected due the similar levels of D-LDH proteins found in these strains as determined earlier by immunoblotting. The D-LDH activity of the quadruple mutant was quite low, indicating the D-LDH pathway in this mutant was affected by the knockdown mutation. On average, the quadruple only showed 7% of D-LDH enzymatic activity relative to both of the WT strains. In comparison with the D-LDH activity of *ldh*-KD1 that we did earlier (Section 3.3.5), the rate of NADH oxidation by the quadruple (0.4 ± 0.3 nmol/min/mg protein) was similar to the *ldh*-KD1 (0.5 ± 0.2 nmol/min/mg protein) although the immunoblot analyses showed the quadruple had a lower level of D-LDH protein compared to the *ldh*-KD1. This close correlation between D-LDH levels and activity indicate that D-LDH is the main route for pyruvate reduction in the triple mutant.

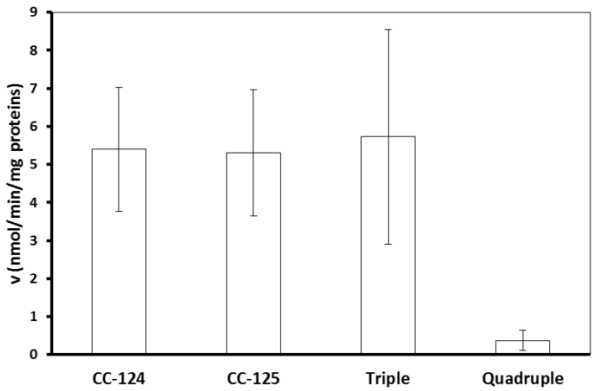


**Figure 4.9 Rates of NADH oxidized/ pyruvate reduced by *C. reinhardtii* D-LDH.**

Average values (±SE) were based on three biological replicates. The units of enzymatic activity (v) were calculated as nmol of NADH oxidized (or pyruvate reduced) per minute per mg of total protein assayed.

Due to time constraints, we could not manage to determine the enzymatic activity of ADH1 and PDC3 by measuring the changes in absorbance at 340 nm. The PFL1 activity could not be determined by using this method because the PFL1 pathway does not utilize NADH. However, the ADH1 (or PDC3) protein is involved directly (or indirectly) with the conversion of acetaldehyde to ethanol, and this particular reaction involves NADH that could possibly be measured. To do this, the conditions for the enzyme assays might need to be optimised first. Nevertheless, Catalanotti *et al*. (2012) found that the *pfl1-adh1* mutant could not synthesize both formate and ethanol. This should mean both of the PFL1 and ADH1

pathways were highly affected. Although not measured, it was expected for the PDC3 activity to also be affected by the high knockdown level of *PDC3*. As we had demonstrated with our D-LDH activity assay, a high reduction in the total amount of a particular enzyme would reduce the activity of that metabolic pathway.

#### 4.2.2.2 Analysis of cell growth under different conditions

We were interested to determine if cell growth under different light intensities was affected when the fermentative pathways were blocked. As a first test, we spotted an equal number of cells on both TAP and HSM agar plates, and grew them under different light intensities (400, 150 and 30 $\mu Em^{-2}s^{-1}$). We also grew the cells in the dark but the growth was very poor, and therefore the data are not shown. The starting cells (inoculum) that were spotted on the agar plates were initially grown either in HSM or TAP medium to late log phase. We observed similar results between HSM- and TAP-starting cultures, and therefore only the results from the HSM-starting cultures are shown here (Figure 4.10). The qualitative analysis of cell growth under the different light intensities showed, as expected, that cells tend to grow better on TAP agar plates than HSM agar plates.

We also determined quantitatively the effect of eliminating fermentative pathway(s) on cell growth. This was quantified by measuring the optical density of the cell culture at 750 nm. We only tested two different light settings which were 30 (light) and 0 (dark) $\mu Em^{-2}s^{-1}$ (Section 2.2). The starting cells (inoculum) were grown in HSM to late log phase before being diluted to $OD_{750}$ of 0.05, either in 30 ml HSM or TAP medium. The culture was grown in Corning 25 $cm^2$ Cell Culture Flask with continuous shaking, and the $OD_{750}$ was measured at specific time points for a total of 96 hours (Figure 4.11). When we grew the cells in HSM and without light, we observed no cell growth as expected, and therefore, the data are not shown here. When the cells were grown in either HSM or TAP medium with light exposure, we did not observe any differences among all the strains. This is in agreement with the qualitative analysis that was described above.

Surprisingly, when we tested cell growth in the dark (Figure 4.11), we observed that CC-124 and CC-125 showed different growth rates, which was unexpected given that these strains originated from the 137c strain. CC-125 did not grow very well in the dark in comparison with CC-124. Moreover, we observed that the CC-125 culture became yellow while the CC-124 culture remained green in colour throughout the experiment. Similarly, when grown in the dark on TAP agar plate CC-125 became yellow (Appendix 12). In order to rule out any spontaneous mutations in our CC-125 as it have been kept and grown in our lab

for almost a year, we bought a new CC-125 strain from the *Chlamydomonas* Resource Centre (University of Minnesota). Similarly, the newly bought strain also showed poor growth in the dark with yellowish appearance. This means that we were unable to assess the effect of eliminating fermentative pathway(s) on cell growth in the dark as all of the mutants except *ldh*-KD1 had CC-125 genetic background.

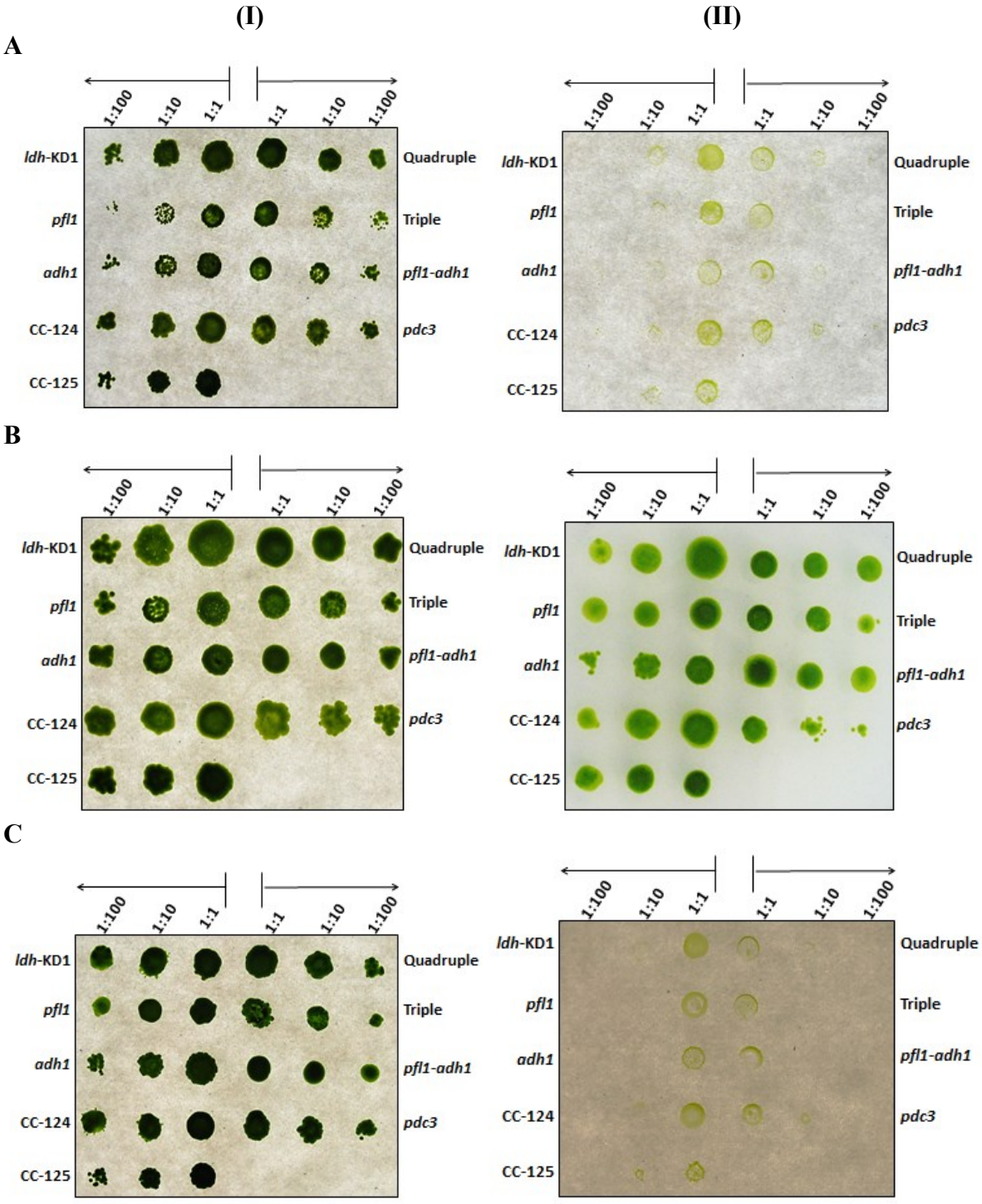


**Figure 4.10 Cell growth on agar plates under different light intensities.**

Cells were grown in HSM to late log phase ($OD_{750}$ 1.0), and 5 µl of the culture was spotted onto either TAP (I) or HSM (II) agar plate. Two serial 1:10 dilutions of the culture were also spotted. The cells were grown under different light intensities i.e. 400 (A), 150 (B) and 30 (C) $\mu Em^{-2}s^{-1}$ for 1 to 2 weeks before photos were taken. It should be noted the *pdc3* mutant refers to the 4$^{th}$ backcross of *pdc3*-KD.

**A**

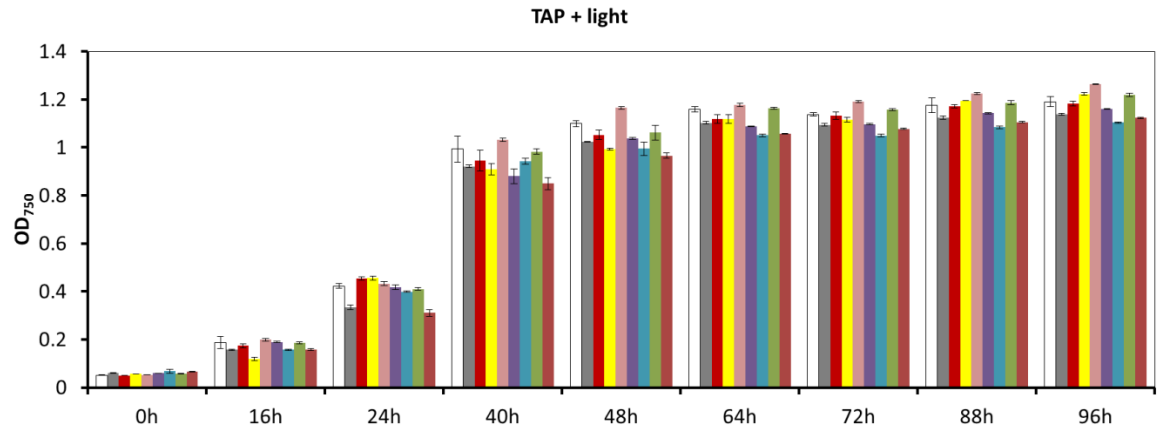


**B**

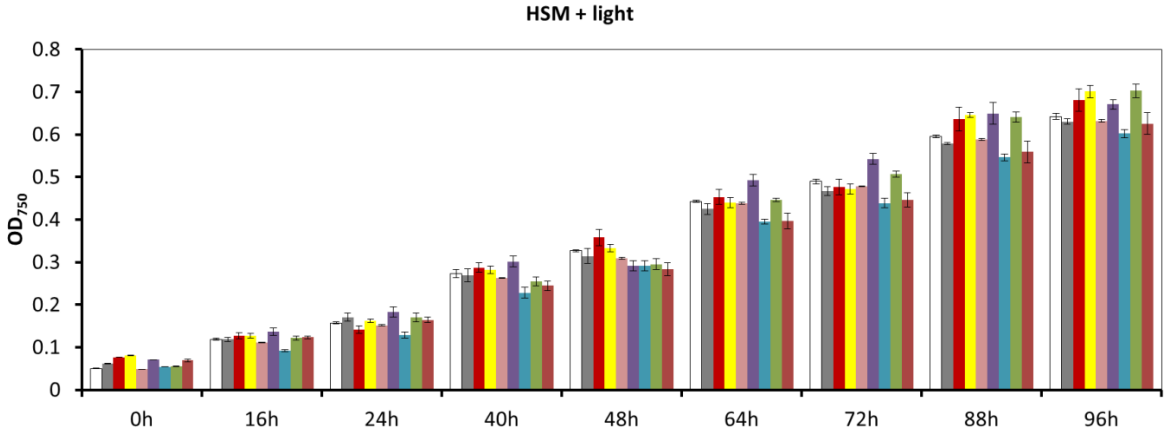


**C**

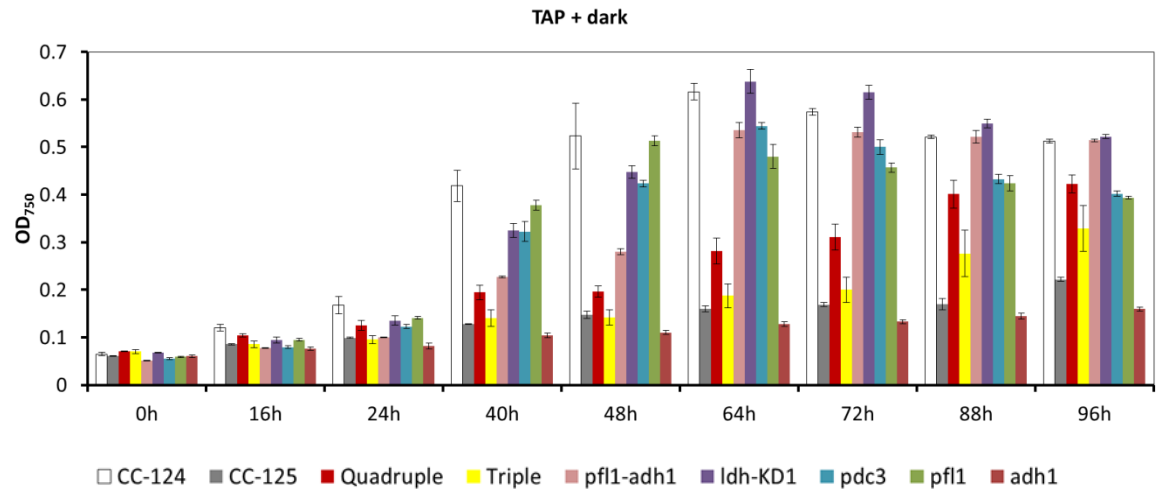


**Figure 4.11 Cell growth in growth medium under light and dark conditions.**

Average values (±SE) were based on three replicates. Cells were grown either in HSM or TAP medium, and grown either exposed to light (30 $\mu Em^{-2}s^{-1}$) or in the dark. Optical density ($OD_{750}$) was measured at 750 nm. It should be noted the *pdc3* mutant refers to the 4$^{th}$ backcross of *pdc3*-KD.

#### 4.2.2.3 Analysis of cell viability

To assess the effect of eliminating fermentative pathway(s) on cell viability under certain conditions, the cell viability was determined quantitatively and qualitatively (Section 2.30). We were interested to determine if the cells were affected when incubated under dark conditions and also under sulphur-deprived conditions. As a control, the cells were also incubated under normal conditions (grown in the light in TAP medium). Cells were incubated at the specified condition for a total of 96 hours, and a sample was taken every 24 hours. This sample was spotted for qualitative analysis (Figure 4.12) and also spread onto a TAP agar plate for viable cell counting (Figure 4.13).

The qualitative analysis of cell viability (Figure 4.12) showed that the cell viability of CC-124 did not seem to be considerably affected when the cells were incubated either under dark conditions or sulphur-deprived conditions, as compared to the control i.e. cells incubated in the light in TAP medium. However, the cell viability of CC-125 was negatively affected in both dark and sulphur-deprived conditions with the cells from the dark incubation seeming to be more badly affected than the ones from the sulphur-deprived conditions. This is in agreement with the optical density measurements of CC-125 cell growth in the dark. We did not anticipate these differences between these two WT strains when we did this experiment. These results mean we could not confidently assess the effect of eliminating fermentative pathway(s) on cell viability. The only mutant that could be assessed properly was *ldh*-KD1 mutant which only had the CC-124 genetic background. Our analysis showed the cell viability of this knockdown mutant seemed not to be considerably affected under the experimental conditions tested.

The quantitative analysis of cell viability (Figure 4.13) supported the qualitative analysis of cell viability (Figure 4.12) described above. The viable cell count for CC-125 showed that more than half of the cells were no longer viable after 48 hours of dark incubation, and after 96 hours most of the cells were found dead. Similarly, the incubation under sulphur-deprived conditions also showed the cell viability was affected but no as much as observed with the dark incubation. The viable cell counts for *ldh*-KD1 showed when the cells were incubated in the dark, the cell viability was not considerably affected within the 48 hours of incubation but only started to be slightly affected towards the end of the incubation period. However, when the cells were incubated under sulphur-deprived conditions, ~40% of the cells were found dead after 48 hours of incubation but no further change was observed afterwards.

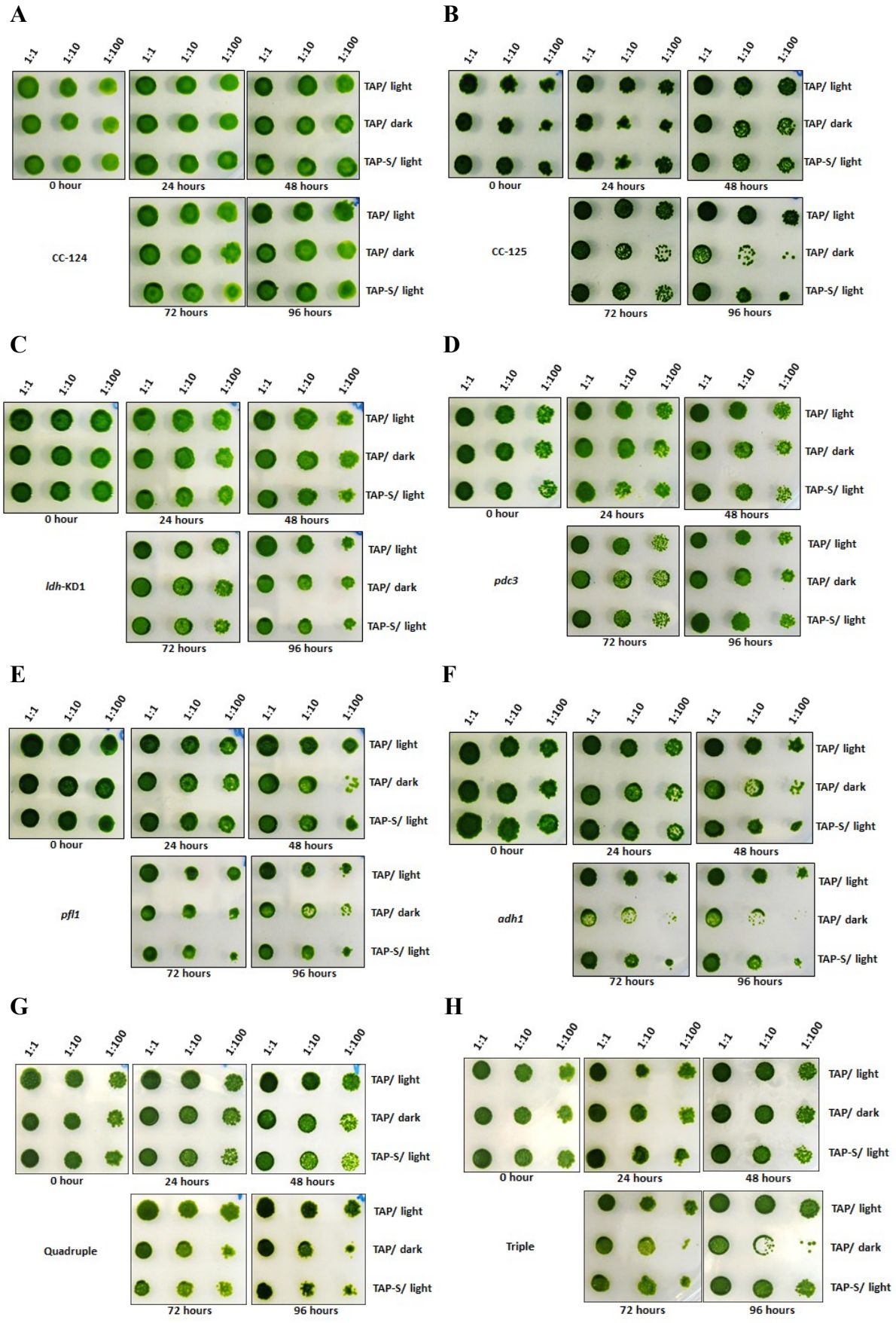
A
B
C
D
E
F
G
H
1:1
1:10
1:100
TAP/ light
TAP/ dark
TAP-S/ light
0 hour
24 hours
48 hours
72 hours
96 hours
CC-124
CC-125
ldh-KD1
pdc3
pfl1
adh1
Quadruple
Triple

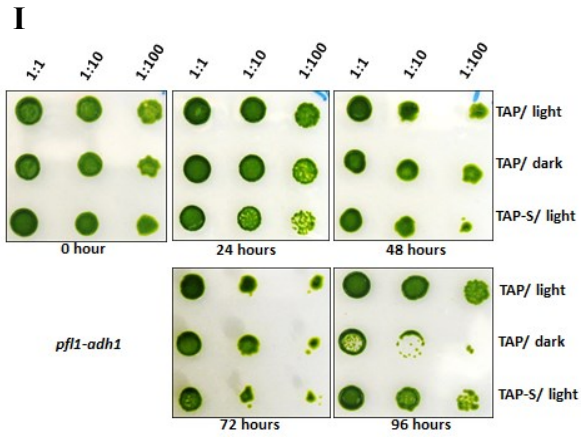


**Figure 4.12 Qualitative analysis of cell viability.**

Cells were incubated for a total of 96 hours either in TAP or TAP-S medium, and were either exposed or not exposed to high light (150 $\mu Em^{-2}s^{-1}$). Every 24 hours, a 5 µl culture sample was taken and spotted onto a TAP agar plate. Two 1:10 serial dilutions of the sample were also spotted. The cells were grown at 28°C and ~30 $\mu Em^{-2}s^{-1}$ for 1 to 2 weeks before photos were taken. It should be noted the *pdc3* mutant refers to the 4$^{th}$ backcross of *pdc3*-KD.

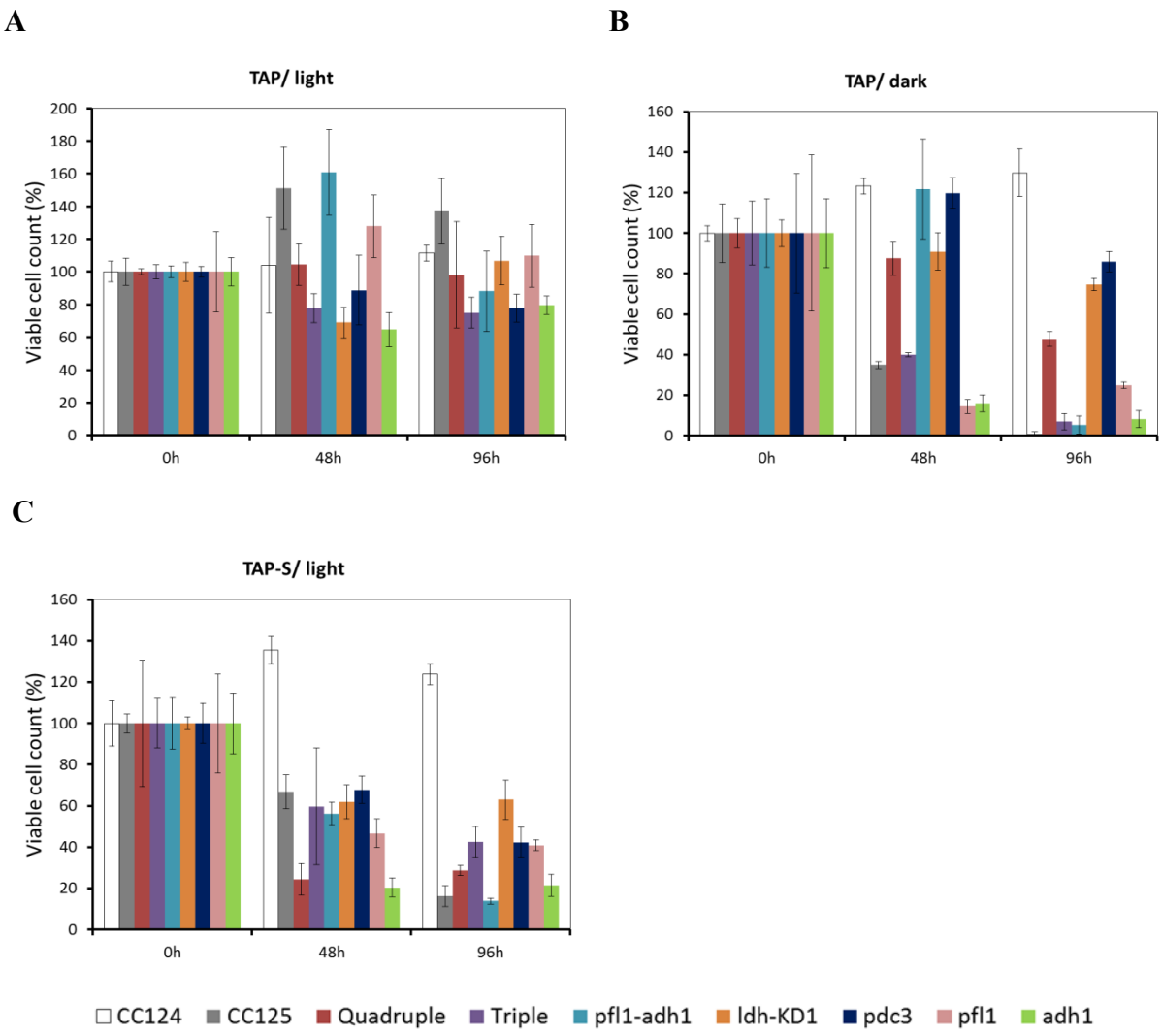


**Figure 4.13 Quantitative analysis of cell viability.**

Average values (±SE) were based on three replicates. Cells were incubated for a total of 96 hours either in TAP or TAP-S medium, and were either exposed or not exposed to high light (150 $\mu Em^{-2}s^{-1}$). Every 48 hours, a 5 µl culture sample was taken, diluted to 1:100 with TAP medium, and only 5 µl of this diluted sample was spread onto a TAP agar plate. The cells were grown for 2 to 3 weeks at 28°C and ~30 $\mu Em^{-2}s^{-1}$ before the number of viable colonies was counted. The cell count was expressed as percentage of the initial cell count (in the range of 100 to 300 colonies). It should be noted the *pdc3* mutant refers to the 4$^{th}$ backcross of *pdc3*-KD.

#### 4.2.2.4 Metabolite analysis of fermentative mutants under dark anaerobic condition

To assess if the elimination of one or more fermentative pathway(s) had an effect on dark anaerobic metabolite production, we analysed the metabolites secreted by *C. reinhardtii* cells after 4 and 8 hours of dark anaerobic incubation in HSM. The excreted metabolites were collected and quantified by using NMR and/or HPLC analyses. Apart from the metabolite analysis, the cells were also collected for immunoblot analysis in order to confirm that the protein(s) of interest (D-LDH, PDC3, PFL1 and ADH1) was eliminated or reduced in the fermentative mutant. Our immunoblot analysis (Appendix 13) confirmed the absence of PFL1 and ADH1, and the continued suppressed expression of D-LDH and PDC3. The immunoblot analysis also confirmed that the cells were in an anoxic condition as anticipated, as expression of the oxygen-sensitive hydrogenases was now induced. The levels of metabolites accumulated under dark anaerobic conditions in CC-124, *ldh*-KD1, *pdc3*, *pfl1* and *adh1* are given in Figure 4.14. For these experiments we were only able to analyse these fermentative mutants by using HPLC, as NMR spectroscopy was not available.

In a later experiment, NMR spectroscopy was used to measure the accumulation of metabolites in the dark under anoxic conditions in CC-124 and the quadruple, triple, *ldh-pfl1-adh1*, *ldh-pdc3-pfl1*, *ldh-pdc3-adh1*, *ldh-pdc3*, *ldh-pfl1*, *ldh-adh1*, *pdc3-pfl1*, *pdc3-adh1* and *pfl1-adh1* mutants (Figure 4.15). We only managed to repeat the metabolite analysis using HPLC with only four fermentative mutants i.e. triple, *pdc3-pfl1*, *pdc3-adh1* and *pfl1-adh1* mutant (Appendix 13). The HPLC analysis is generally in agreement with the NMR analysis, and therefore only the NMR data are discussed.

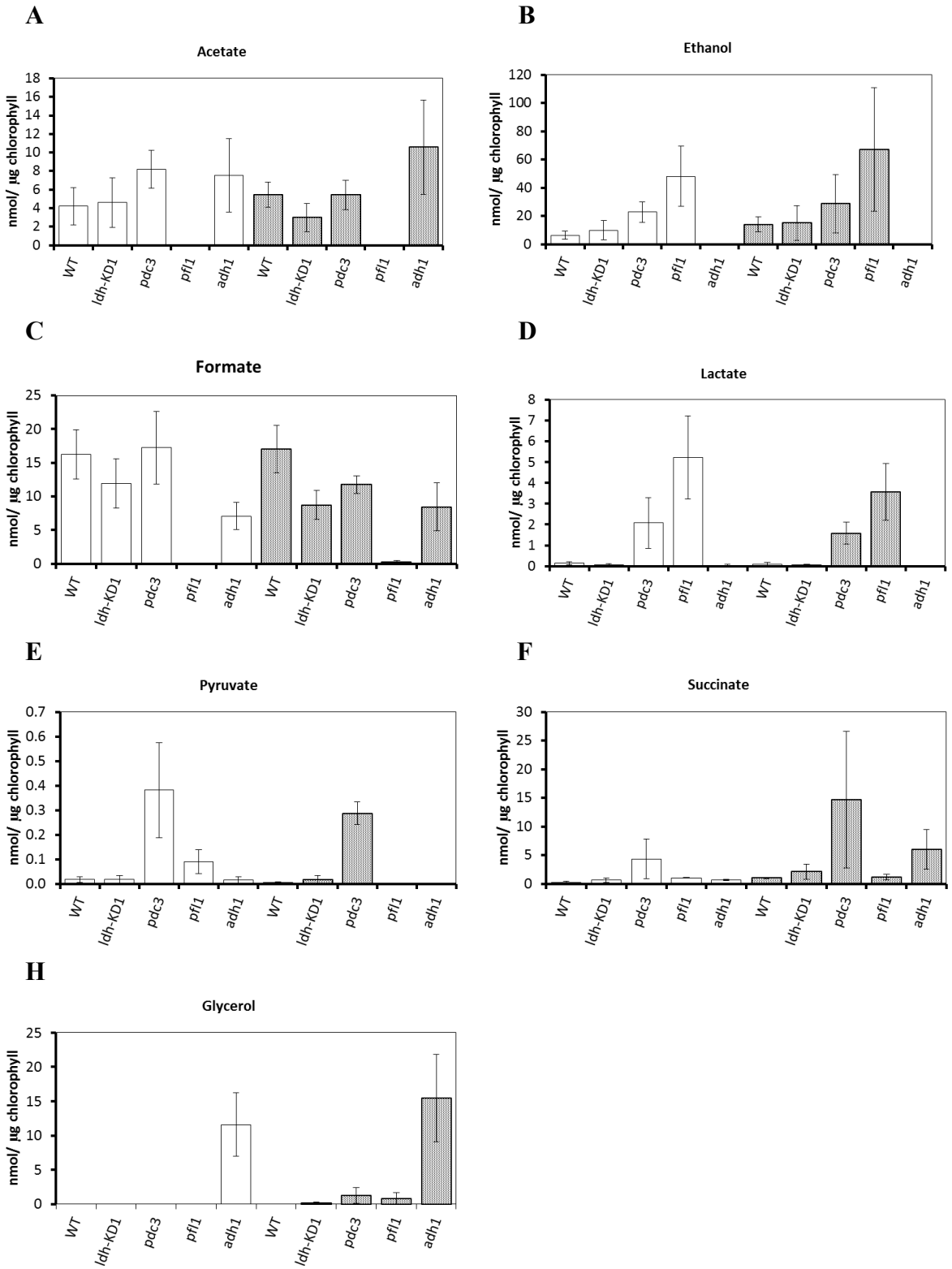


**Figure 4.14 HPLC analysis of dark fermentative metabolites.**

Average values (±SE) were based on three independent replicates. The excreted metabolites were quantified after 4 hours (white bars) and 8 hours (grey bars) of dark anaerobic incubation in HSM. The values obtained were normalized to the amount of total chlorophyll (~150 µg/ml). The WT strain used was CC-124.

**1**

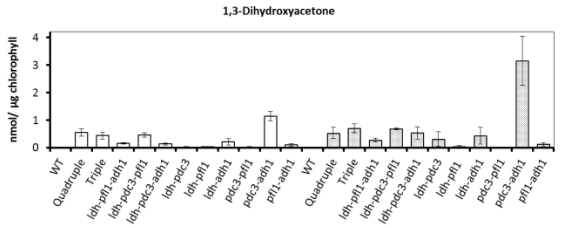


**2**

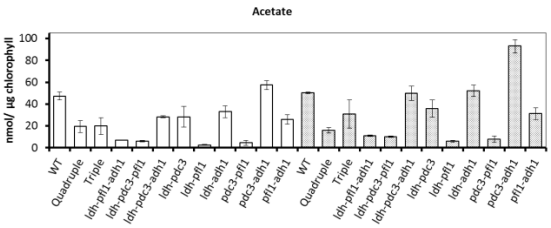


**3**

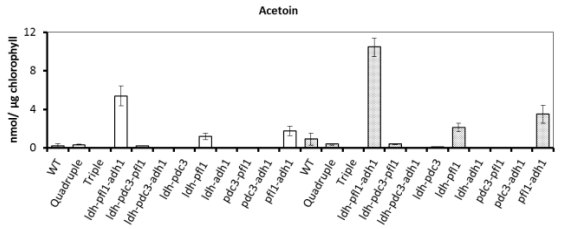


**4**

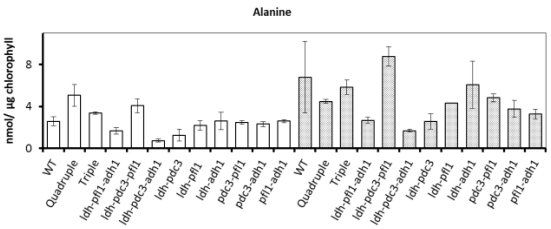


**5**

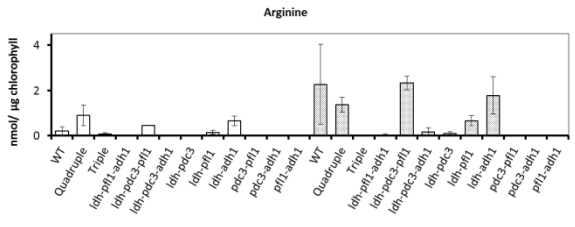


**6**

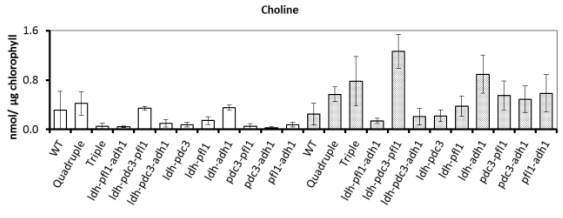


**7**

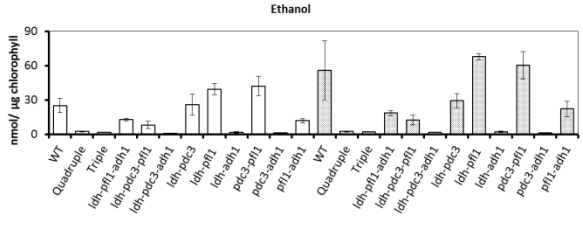


**8**

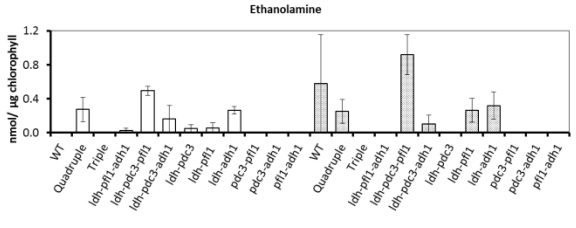


**9**

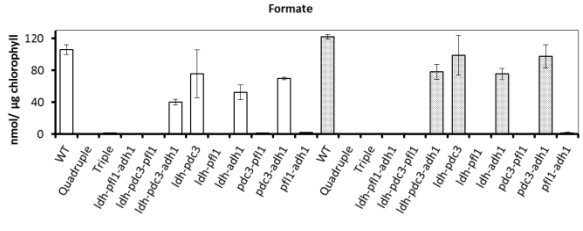


**10**

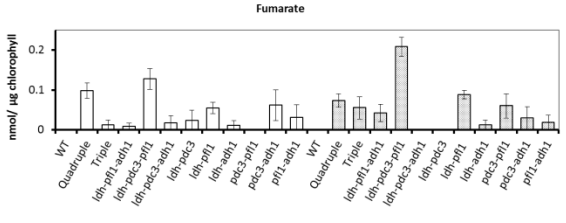


**11**

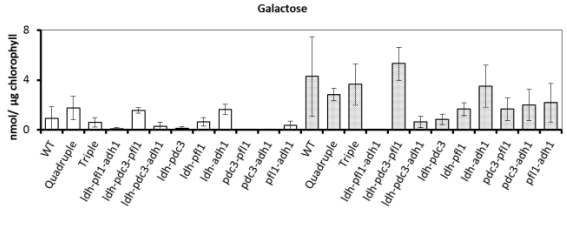


**12**

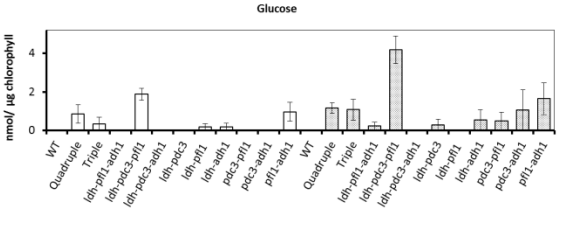

**13**

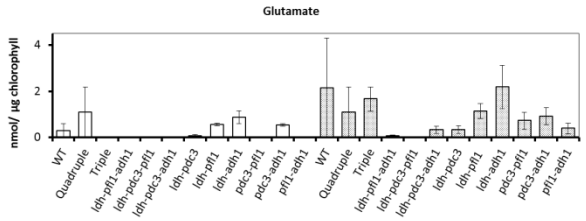


**14**

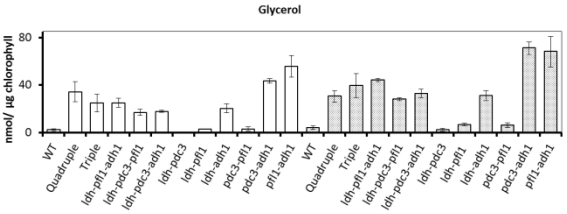


**15**

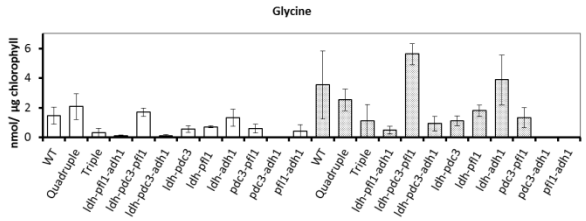


**16**

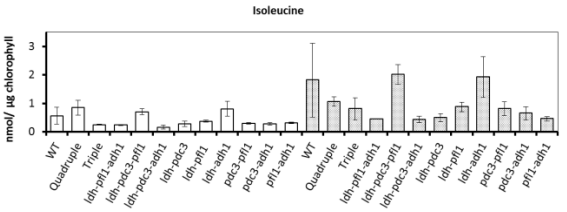


**17**

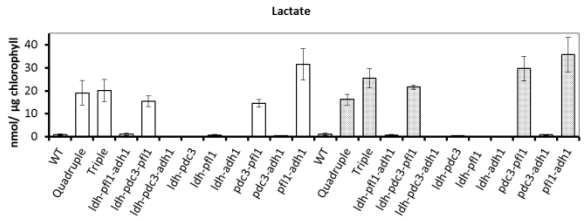


**18**

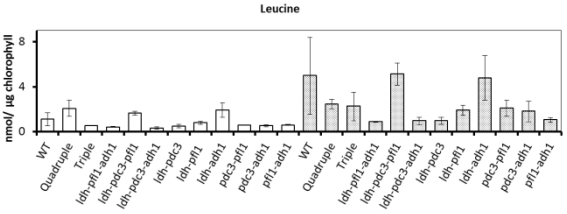


**19**

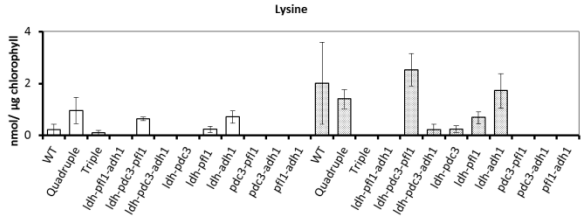


**20**

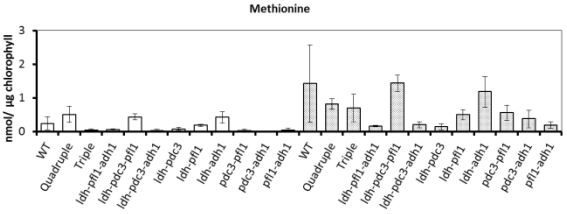


**21**

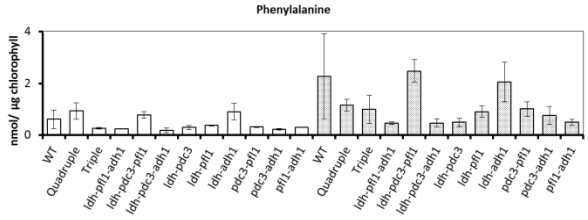


**22**

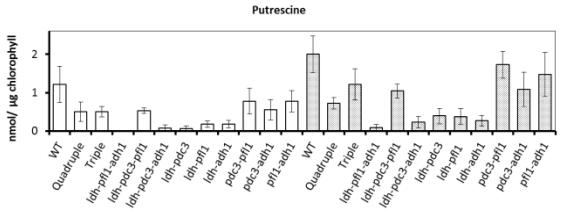


**23**

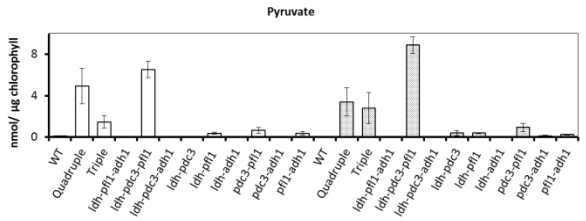


**24**

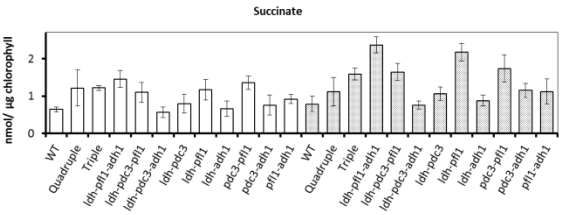

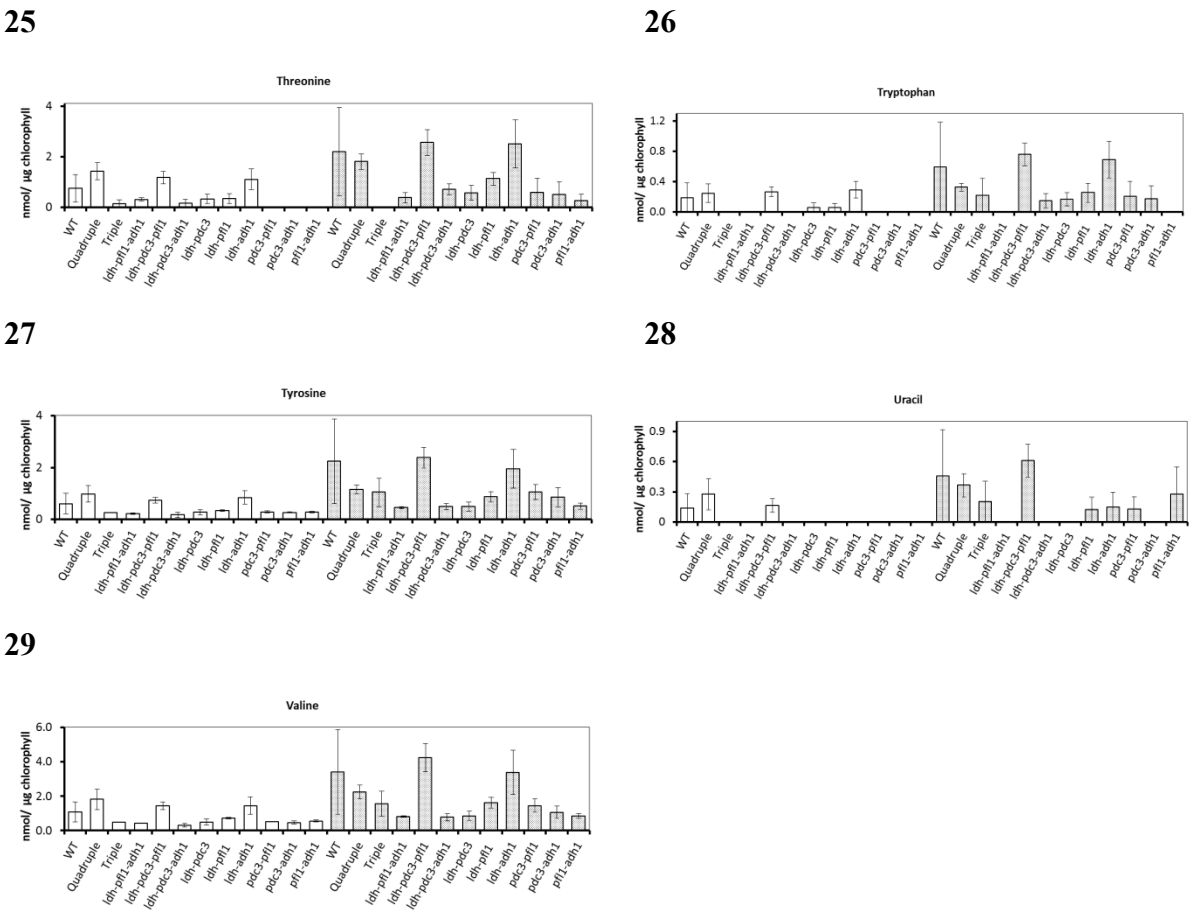


**Figure 4.15 NMR analysis of dark fermentative metabolites.**

Average values (±SE) were based on three independent replicates, and were normalised to the chlorophyll concentrations (~150 µg/ml). The excreted metabolites were quantified after 4 hours (white bars) and 8 hours (grey bars) of dark anaerobic incubation in HSM. The metabolite concentrations were quantified relative to the NMR standard (DSS). The WT strain used was CC-124.

#### 4.2.2.4.1 *ldh*-KD1 metabolite production

The metabolite production for the four *ldh*-KD mutants after 4 hours of dark fermentation has already been described in Chapter 3. However, in order to analyse a 4- and 8-hour metabolite production for this current chapter, the dark anaerobic incubation was repeated again. Our HPLC analysis showed the results are in agreement with the previous chapter (Section 3.3.7). There was no difference relative to the WT with regard to the production of acetate, ethanol, formate, D-lactate, succinate and glycerol. Similarly, there was also no difference in the excreted pyruvate levels as observed before. However, it should be noted that in the previous chapter we also had shown that the intracellular pyruvate levels were slightly higher in the knockdown mutants than the WT. Although at minor amounts, D-lactate was also detected in the knockdown mutant.

#### 4.2.2.4.2 *pfl1* metabolite production

Although the *pfl1* metabolite production had previously been described (Philipps *et al*., 2011; Burgess *et al*., 2012; Catalanotti *et al*., 2012), the analysis of PFL1 knockout mutation was carried out again in order to rule out the potential effects of different experimental conditions on metabolite analysis. Moreover, our *pfl1* mutant was obtained by crossing with our WT (CC-125). Therefore, this would also rule out the potential effects of different laboratory strains. Our HPLC analysis showed the results are in agreement with the results described in Chapter 3 (Section 3.3.7), whereby the WT was treated with 10 mM of the PFL1 inhibitor. Both formate and acetate were reduced to an undetected level. Ethanol, D-lactate, pyruvate and succinate levels were elevated. However, there were no substantial changes in glycerol although there was a tendency for increased production with increasing incubation time. These results are in agreement with previous studies (Philipps *et al*., 2011; Burgess *et al*., 2012; Catalanotti *et al*., 2012).

#### 4.2.2.4.3 *adh1* metabolite production

The *adh1* metabolite production has also been previously described (Magneschi *et al*., 2012) but we repeated it again to rule out different experimental conditions and laboratory strains. Our HPLC analysis showed ethanol was undetected, formate was reduced, and glycerol was remarkably increased. These results are in agreement with the previous study. However, Magneschi *et al*. (2012) found, after 4 hours of dark anaerobic incubation, the acetate level doubled relative to the WT. We did not observe substantial differences between our WT and *adh1*, as the error bars overlapped each other. Nevertheless, there was a tendency for increased production of acetate. By using the average values, there was an approximate 1.8x increase in acetate level after 4 hours of dark anaerobic incubation, which was almost double the WT amount. Similarly, we did not observe any significant changes in D-lactate production but Magneschi *et al*. (2012) observed an increase in lactate level. These differences could be due to the different experimental conditions or laboratory strains. The previous study did not analyse succinate, presumably due to analytical limitations. We found the succinate levels to be elevated especially after 8 hours of dark anaerobic incubation.

#### 4.2.2.4.4 *pdc3* metabolite production

The *pdc3*-KD metabolite production was previously described by Burgess (2011) with no substantial changes in acetate, formate, ethanol and D-lactate levels observed. We repeated the analysis with the fourth backcross of *pdc3*-KD to rule out any potential

background mutations. Our HPLC analysis showed acetate, formate and ethanol levels remained unaffected although there were variations between the 4 hours and 8 hours. These variations suggest different production rates of ethanol or consumption of excreted metabolites (acetate and formate). The levels of D-lactate on the other hand were elevated by 15x, and this is in disagreement with the previous study. Pyruvate, succinate and glycerol were not analysed by Burgess (2011). We found pyruvate and succinate were increased. There were no substantial changes in glycerol levels although there was a tendency for higher production relative to the WT.

#### 4.2.2.4.5 *ldh-pfl1* metabolite production

As described in Chapter 3 (Section 3.3.7), we have already analysed *ldh*- KD mutants treated with the PFL1 inhibitor (HP). Here, we repeated our analysis on a *bona fide pfl1-ldh* mutant to confirm the previous analysis. Our NMR analysis showed formate was undetected in this strain due to the *PFL1* knockout mutation. This was unlike the HP-treated samples, whereby formate was still detected as the PFL1 inhibitor is a competitive inhibitor (Knappe *et al*., 1984). Our NMR analysis is in agreement with the results described in Chapter 3 (Section 3.3.7). There was no substantial difference in ethanol, a reduction in acetate, and an increase in fumarate, succinate and glycerol. There were also no substantial changes in galactose, the aromatic amino acids (phenylalanine, tryptophan and tyrosine), the branched-chain amino acids (isoleucine, valine and leucine), the aspartate-derived amino acids (lysine, methionine and threonine) and glycine. However, we did not observe any increase in alanine production as observed with the PFL1 inhibitor. This is perhaps unsurprising as the previous increase was only small. We also did not observe any increase in D-lactate in this mutant as observed with the PFL1 inhibitor. The D-lactate excreted was hardly at a detectable level. Our NMR analysis also detected glucose being excreted by *C. reinhardtii*. However, there were no substantial changes in the glucose levels relative to the WT. Interestingly, an increase in acetoin was also observed, which is in agreement with the previous results described in Chapter 3 (Section 3.3.7).

There were no substantial changes in 1,3-dihydroxyacetone, arginine, choline, glutamate, ethanolamine and uracil. However, there was a reduction in putrescine.

#### 4.2.2.4.6 *pfl1-adh1* metabolite production

We also repeated the metabolite analysis of *pfl1-adh1* mutant. There was a reduction in formate and acetate, and an elevation in D-lactate and glycerol. These changes are in

agreement with a previous study (Catalanotti *et al*., 2012). There were no substantial changes in alanine. This is also in agreement with the previous study, whereby significant increase in the intracellular alanine was only observed after 24 hours of dark anaerobic incubation but not at 4 hours or earlier. We observed no substantial changes in fumarate and succinate, as the error bars overlapped each other, but there seemed to be a tendency for these metabolites to have higher production relative to the WT, as the average values were higher. Catalanotti *et al*. (2012) showed there was a significant increase in both fumarate and succinate levels but these were measured at an intracellular level. We also observed an increase in pyruvate, glucose and acetoin. However, there were no substantial changes in galactose and aromatic amino acids (phenylalanine, tryptophan and tyrosine). The branched-chain amino acids, isoleucine and valine were unaffected but leucine was reduced. The aspartate-derived amino acids, methionine and threonine were also unaffected but lysine was reduced. Similarly, glycine was also negatively affected.

There were no substantial changes in 1,3-dihydroxyacetone, choline, ethanolamine, glutamate, putrescine and uracil. However, there was a reduction in arginine.

Surprisingly, we observed that ethanol was still produced at about 40% of WT levels, in contrast to the earlier study. The representative NMR spectrum showing the ethanol signals is given in Appendix 13. To test whether the different observations could be explained by the use of different media, as the earlier study used anaerobic induction buffer (AIB), we repeated our experiment by using both HSM and AIB. Due to the unavailability of NMR and HPLC, we used an ethanol assay kit (R-Biopharm, UK) according to the manufacturer's instructions to quantify ethanol production. Our analysis (based on one biological replicate; Appendix 13) showed similar results as before. The ethanol produced by the *pfl1-adh1* mutant in both HSM and AIB were 30-40% the amount observed in the WT. These results confirmed ethanol was produced by the *pfl1-adh1* mutant, and the different media did not appear to significantly affect ethanol production.

#### 4.2.2.4.7 *pdc3-adh1* metabolite production

Ethanol was substantially reduced while formate was only slightly reduced. Acetate and glycerol were increased. There were no substantial changes in D-lactate, pyruvate, glucose, fumarate, succinate, alanine, acetoin, galactose, the aromatic amino acids and the branched-chain amino acids. There were also no substantial changes in the aspartate-derived amino acids except for lysine, whereby its production was reduced. Similarly, glycine was also reduced.

There were no substantial changes in choline, ethanolamine, glutamate, putrescine and uracil. However, there was a substantial increase in 1,3-dihydroxyacetone but a reduction in arginine.

#### 4.2.2.4.8 *pdc3-pfl1* metabolite production

Formate and acetate were reduced but there was no substantial change in ethanol. D-lactate, pyruvate, glycerol, fumarate and succinate were all increased. There were no substantial changes in glucose, alanine, acetoin, glycine, the branched-chain amino acids and the aromatic amino acids. The aspartate-derived amino acids were also unchanged except for lysine which was reduced.

There were no substantial changes in 1,3-dihydroxyacetone, choline, ethanolamine, glutamate, putrescine and uracil. However, arginine was reduced.

#### 4.2.2.4.9 *ldh-adh1* metabolite production

The *ldh-adh1* metabolite analysis by using NMR showed a substantial reduction in ethanol (~0.04x of WT levels) while formate was slightly reduced. There was an elevation of glycerol. There was no substantial change in D-lactate, acetate, pyruvate, fumarate, succinate, alanine, acetoin, glucose, glycine, the branched-chain amino acids, the aromatic amino acids and the aspartate-derived amino acids.

There were no substantial changes in arginine, ethanolamine, glutamate and uracil. There was a reduction in putrescine while 1,3-dihydroxyacetone and choline had a slight increase.

#### 4.2.2.4.10 *ldh-pdc3* metabolite production

The *ldh-pdc3* metabolite analysis by using NMR showed acetate was slightly reduced. There were no substantial difference between the WT and the mutant in ethanol, formate, D-lactate, fumarate, succinate, alanine, glycerol, acetoin, glucose, galactose, glycine and the aromatic amino acids. There was also no difference in the branched-chain amino acids except for leucine which was reduced. The aspartate-derived amino acids were also reduced except for threonine, which was not unaffected.

There were no substantial changes in 1,3-dihydroxyacetone, choline, ethanolamine, glutamate and uracil. However, there was a reduction in arginine and putrescine.

#### 4.2.2.4.11 *ldh-pdc3-adh1* metabolite production

The NMR analysis of *ldh-pdc3-adh1* metabolite production showed a substantial reduction (~0.03x of WT levels) in ethanol and alanine and only a slight reduction in formate. On the other hand, glycerol was increased. There was no substantial change in acetate, D-lactate, pyruvate, fumarate, succinate, acetoin, glucose, galactose, glycine, the aromatic amino acids and the aspartate-derived amino acids. There was also no substantial change in the branched-chain amino acids except leucine which experienced a reduction.

There were no substantial changes in choline, ethanolamine, glutamate and uracil. However, there was an increase in 1,3-dihydroxyacetone but a decrease in arginine and putrescine.

#### 4.2.2.4.12 *ldh-pdc3-pfl1* metabolite production

The NMR analysis of *ldh-pdc3-pfl* metabolite production showed a reduction in formate, ethanol and acetate. There was an increase in D-lactate, glycerol, pyruvate, glucose, fumarate and succinate. There were no substantial changes in alanine, acetoin, galactose, glycine, the branched-chain amino acids, the aromatic amino acids and the aspartate-derived amino acids.

There were no substantial changes in arginine, ethanolamine, glutamate and uracil. However, there was an increase in 1,3-dihydroxyacetone and choline but a decrease in putrescine.

#### 4.2.2.4.13 *ldh-pfl1-adh1* metabolite production

The NMR analysis of *ldh-pfl1-adh1*metabolite production showed a reduction in formate, acetate and alanine. Like in the *pfl1-adh1* mutant, ethanol was detected at about 34% of WT levels. The representative NMR spectrum showing the ethanol signals is given in Appendix 13. As described earlier (Section 4.3.4.6), we repeated our experiment to confirm the surprising production of ethanol observed in this mutant strain. Our repeat analysis confirmed the production of ethanol by this mutant strain (Appendix 13). There was an increase in acetoin, glycerol, fumarate and succinate. However, there were no substantial changes in pyruvate and glucose. Interestingly, there were many metabolite reductions observed in this mutant strain i.e. alanine, galactose, glycine, the branched-chain amino acids, the aromatic amino acids (except tryptophan), and the aspartate-derived amino acids (except threonine).

There were no substantial changes in 1.3-dihydroxyacetone, choline, ethanolamine, glutamate and uracil. However, there was a reduction in arginine and putrescine.

#### 4.2.2.4.14 Triple mutant metabolite production

There was a substantial reduction in formate and ethanol but only a slight reduction in acetate. There was an increase in D-lactate, glycerol, pyruvate, glucose, fumarate and succinate. There were no substantial changes in alanine, acetoin, galacatose, glycine, the branched-chain amino acids and the aromatic amino acids. There was a reduction in the aspartate-derive amino acids except methionine.

There were no substantial changes in choline, ethanolamine, glutamate, putescine and uracil. However, there was an increase in 1,3-dihydroxyacetone but a decrease in arginine.

#### 4.2.2.4.15 Quadruple mutant metabolite production

The NMR analysis of the quadruple mutant metabolite production showed that there was a reduction in formate, ethanol and acetate (0.01x, 0.04x and 0.32x of WT levels, respectively). There was an increase in D-lactate, glycerol, pyruvate and glucose. The observed increase in fumarate was not accompanied by any substantial increase in succinate but there was a tendency for increased production of this organic acid. There were no substantial changes in alanine, acetoin, galacatose, glycine, the branched-chain amino acids, the aromatic amino acids and the aspartate-derived amino acids

There were no substantial changes in arginine, choline, ethanolamine, glutamate and uracil. However, there was an increase in 1,3-dihydroxyacetone but a decrease in putrescine.

### 4.2.2.5 Hydrogen gas analysis of fermentative mutants under sulphur deprivation

The effect of eliminating one or more fermentative pathway(s) on hydrogen production in sulphur-deprived cultures was assessed by GC (Figure 4.16). Our immunoblot analysis confirmed the absence of PFL1 and ADH1, and the continued suppressed expression of D-LDH and PDC3 (Appendix 14). The GC analysis showed the elimination of two or more fermentative pathways did not improve hydrogen production under sulphur-deprived conditions. The quadruple and triple mutants produced negligible amounts of hydrogen gas with the average total accumulation found to be 0.5 ± 0.5 and 0.5 ± 0.4 (±SE) nmole/µg chlorophyll, respectively. The hydrogen production by *pdc3-adh1* mutant was not affected at all. However, the rest of the fermentative mutants (*pdc3-pfl1*, *pfl1-adh1*, *ldh-pfl1-adh1*, *ldh-*

*pfl1* and *ldh-adh1*) were negatively affected but not as much as the quadruple and triple mutants.

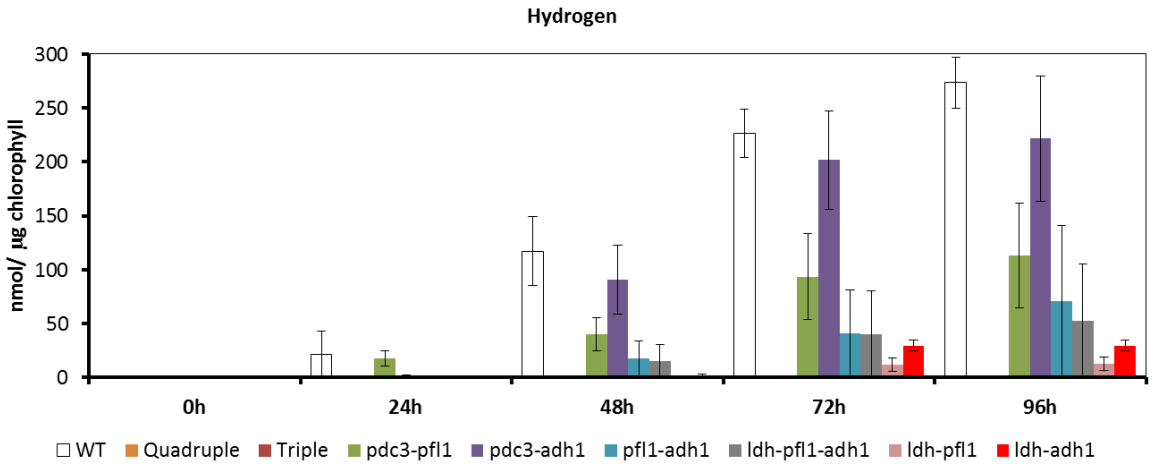


**Figure 4.16 GC analysis of gas accumulation under sulphur deprivation.**

Average values (±SE) were based on three independent replicates. The values obtained were normalized to the amount of total chlorophyll (~15 µg/ml). The WT strain used was CC-124.

### 4.2.2.6 Determination of intracellular pyruvate concentrations

Our NMR analysis showed that the amounts of excreted pyruvate were higher in the quadruple and triple mutants relative to the WT (CC-124). To assess if this could also be observed at the intracellular level, we did pyruvate assays on the same samples described previously in section 4.3.1, whereby the intracellular D-LDH activity had been quantified. The concentration of pyruvate was determined by first measuring the rate of NADH oxidation (Appendix 9 for representative results), and the concentration of pyruvate could then be approximated by using a standard curve (Appendix 9). Our pyruvate assays showed the intracellular levels of pyruvate for both strains of WT were similar, and the levels were relatively higher in the triple and especially quadruple (Figure 4.17). This is in agreement with the NMR analysis of the excreted pyruvate levels.

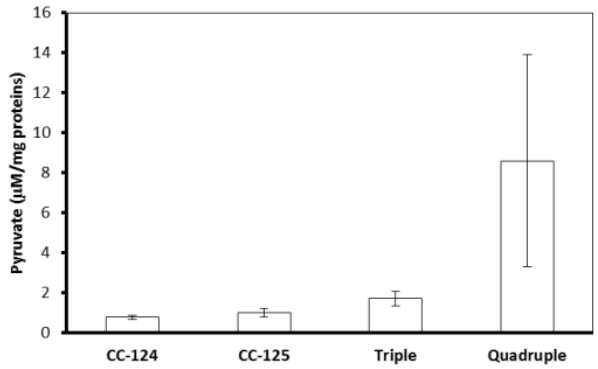


**Figure 4.17 Intracellular concentration of pyruvate.**

Average values (±SE) were based on three biological replicates. The values were normalized to the total protein content of the cell extract used in the 1-ml assay.

## 4.3 Discussion

### 4.3.1 Metabolite analysis

Our metabolic study is a starting point for studying the *C. reinhardtii* dark fermentative metabolism, as we detected several metabolites that have never been described before. These excreted metabolites were unlikely to be produced due to cell lysis, as increased production was observed with increasing period of dark anaerobic incubation. Therefore, future work has to involve quantifying intracellular levels of metabolites produced under dark anaerobic conditions to confirm the present results and provide more insight into the green algal fermentative metabolism.

### 4.3.2 Ethanol production

A striking result presented in this chapter is the observation that ethanol was produced by the *pfl1-adh1* and *ldh-pfl1-adh1* mutants. This is in contrast to a previous study (Catalanotti *et al*., 2012) that failed to detect ethanol production from the same *pfl-adh1* mutant analysed here. This led to the earlier study to conclude that only ADH1 was involved in ethanol production under their experimental conditions. In contrast, the amounts of ethanol produced by both the *pfl1-adh1* and *ldh-pfl1-adh1* mutants were ~40% of the amounts produced by the WT (Figure 4.15.7). Initially, we assumed the ethanol produced in our work could be due to the differences in the experimental conditions used between our work and the earlier study, as culturing and induction conditions could also influence the end products of dark fermentation (Posewitz *et al*., 2009). Our work used HSM with 5 minutes of argon

purging whereas Catalanotti *et al*. (2012) used AIB and 30 minutes of argon purging. However, our repeat analysis (based on one biological replicate) by comparing these different media also confirmed the ethanol production by these mutant strains (Appendix 13). However, we did not manage to test the effect of purging time on metabolite production. Nevertheless, our immunoblot analysis (Appendix 13) showed the conditions were anaerobic. Catalanotti *et al*. (2012) incubated their samples at room temperature whereas we did our work at 28ºC, and therefore, the observed differences could probably due to the possible differences in temperatures.

Another possible reason to explain the discrepancy could be differences in the amounts of starch accumulated by the mutant. Neither the previous study nor ours quantified the starch content. If there was less starch in the cells, less pyruvate and hence ethanol could potentially be produced during fermentation. The amount of starch accumulated by the *C. reinhardtii* is also potentially affected by how the green alga is grown. There were significant differences between how we grew our cells compared with the previous study. The most notable difference was that the previous study bubbled the algal cultures with air enriched with 3% carbon dioxide while we did not bubble our cultures. Therefore, our cultures were expected to be exposed to lower levels of carbon dioxide especially when the growth reached a late log phase, as more cells would be competing for carbon dioxide. It has been reported that pyrenoid starch rapidly accumulates in *C. reinhardtii* when the extracellular concentrations of carbon dioxide are lowered (Kuchitsu *et al*., 1988). Reduced starch accumulation in the previous study is also consistent with differences in the amounts of metabolites produced. For example, based on our HPLC analysis, our WT produced ~15 nmol/µg chlorophyll of formate whereas the formate production after 4 hours of dark anaerobic induction in the previous study was estimated to be between ~6 to 9 nmol/µg chlorophyll (assuming their 10x concentrated samples contained 160 to 240 µg/ml of chlorophyll).

Although starch content was a possibility, we still could not rule out other differences in the experimental conditions used could also contribute to the different observations.

To explain the ethanol production observed in the *pfl1-adh1* and *ldh-pfl1-adh1*mutants, we proposed that the ethanol production observed in these mutants was carried out by one or more alcohol dehydrogenase(s) that are yet to be characterised, with the most likely candidates ADH2 and ADH3 (Magneschi *et al*., 2012). However, given that little ethanol was produced in some of the other fermentative mutants lacking ADH1 (i.e. quadruple, triple, *ldh-pdc3-adh1*, *ldh-adh1*, *pdc3-adh1* and *adh1*), ADH1 does appear to play

a major role in ethanol production under certain conditions. Based on our metabolite analysis, ethanol production by the unknown ADH appears to be associated with the PDC3 pathway. Pyruvate would be decarboxylated by PDC3 to acetaldehyde. This would be further converted to acetoin and ethanol by PDC3 and the unknown ADH, respectively. We observed higher amounts of acetoin in *pfl1-adh1* and *ldh-pfl1-adh1*, suggesting the association between PDC3 and the unknown ADH. High amounts of acetoin should mean high amounts of available acetaldehyde, and if the amount of acetaldehyde was high, there should also be more carbon flux towards the unknown ADH. Therefore, high concentrations of acetaldehyde could potentially regulate the activity of this ADH, and as the amounts of acetaldehyde are dependent on the amounts of available pyruvate, the ADH could also be activated by high concentrations of pyruvate, possibly by cytoplasmic acidification. In hypoxic maize root tips, ethanol production was triggered by a drop in cytoplasmic pH (Roberts *et al*., 1984). It should not be surprising if the unknown ADH was activated by high concentrations of acetaldehyde as this metabolite is highly toxic (Lieber, 1988). The metabolite analysis of *ldh-pfl1-adh1* suggests acetaldehyde toxicity as the production of many amino acids was severely affected, possibly due to enzyme interference by acetaldehyde (Lieber, 1988). Therefore, the ADH pathway could potentially serve as a regulatory mechanism to detoxify excess acetaldehyde produced by PDC3.

Our bioinformatics analysis managed to find the potential genes responsible for the putative ADH2 (Cre16.g669125) and ADH3 (Cre16.g669150) proteins described by Magneschi *et al*. (2012). No experimental work so far has been carried out on ADH3. However, a transcript analysis has been carried out on ADH2 (Whitney *et al*., 2012) but we found the primers used in this particular study for amplifying the cDNA of ADH2 could also possibly amplify ADH1. The forward primer could anneal to both ADH1 and ADH2, and the reverse primer only had two mismatches when aligned to the cDNA of ADH1 and therefore might be able to anneal to the *ADH1* transcript as well. This means it is currently still unclear if ADH2 is expressed. However, the EST of ADH3 has been previously reported (Posewitz *et al*., 2009; Burgess 2011), suggesting it could play a role in ethanol production. Burgess (2011) also identified eight putative medium-chain dehydrogenase/reductase (MDR) genes in the *C. reinhardtii* genome, which possess cinnamyl alcohol dehydrogenase (CAD) domains. It has been reported CAD could utilise a wide range of substrates including acetaldehyde, and therefore was proposed to have a role in aldehyde detoxification (Mee *et al*., 2005).

### 4.4.3 Proposed regulatory mechanisms of fermentative pathways

We propose the D-LDH and PDC3 pathways have a regulatory role in preventing the potentially toxic accumulation of pyruvate (Magneschi *et al*., 2012). In this work, the accumulation of pyruvate was speculated to be caused by the elimination of PFL1 which formed the major fermentative pathway in *C. reinhardtii*. It is speculated the D-LDH pathway is the favoured choice for pyruvate detoxification compared to the PDC3 pathway. Firstly, apart from reducing pyruvate, the D-LDH pathway could also contribute to NADH reoxidation for sustaining glycolysis. Secondly, D-LDH is conveniently localised to the chloroplast (Burgess, 2011) where pyruvate accumulation is expected to take place. Thirdly, the product of this pathway is D-lactate which is a weaker acid (p$K_a$ = 3.86) compared to pyruvate (p$K_a$ = 2.50). Therefore, it could probably help in preventing cytoplasmic acidification by pyruvate. Moreover, based on the amounts of excreted pyruvate and D-lactate observed in this work, it seems to appear that D-lactate was more favourably excreted by the cells compared to pyruvate. The ease of excretion could further help in preventing cytoplasmic acidification.

It is perhaps a better strategy to put the PDC3 pathway as a second defence mechanism against pyruvate elevation. This is because the immediate product of this pathway is acetaldehyde. However, the advantage of this pathway is the generation of $NAD^+$ through the conversion of acetaldehyde to ethanol. This conversion could be carried out by the bifunctional ADH1. However, if this is the case, the generated acetaldehyde has to travel from the cytoplasm into the chloroplast as ADH1 is located in the chloroplast (Atteia *et al*., 2009; Terashima *et al*., 2010) and PDC3 in the cytoplasm (Burgess, 2011). Alternatively, the acetaldehyde could be converted to ethanol by other alcohol dehydrogenase(s) but perhaps not as effectively as ADH1, based on the observed amounts of ethanol. Nevertheless, since the production of ethanol by this pathway is coupled to the production of acetoin, the effectiveness of acetaldehyde and pyruvate detoxification could be made possible. In fact, it has been reported that pyruvate decarboxylase plays an important role in maintaining pH homeostasis (Tsau *et al*., 1992).

Another potential reason for PDC3 to be the second defence mechanism for pyruvate accumulation is the enzyme might only be active under low pH as reported in wheat (Lee & Langston-Unkefer, 1985). *C. reinhardtii* D-LDH works best at neutral pH (Husic & Tolbert, 1985). Therefore, I speculate that during the early stage of pyruvate accumulation, the low amounts of pyruvate do not drastically affect the pH of the cytoplasm but as the concentrations of pyruvate increase, the cytoplasmic pH starts to drop and consequently this

increases the activity of PDC3 while decreasing the activity of D-LDH. It is speculated for the PDC3 to only convert acetaldehyde into acetoin when the amounts of this compound are high since two molecules of acetaldehyde are needed to produce one molecule of acetoin.

Although NADH reoxidation can be carried out by the D-LDH pathway, most of the $NAD^+$ needed for sustaining glycolysis is hypothesised to be supplied by the ADH1 pathway. Moreover, the D-LDH pathway is only active when there is a build-up of pyruvate. More $NAD^+$ is expected to be generated from the conversion of acetyl-CoA to ethanol compared to the D-LDH pathway. NADH reoxidation can also be performed by the reverse TCA reactions. However, based on the observed tiny amounts of excreted succinate and fumarate, we speculated this pathway is activated not for the purpose of NADH reoxidation but mainly to help in preventing pyruvate accumulation. As the TCA intermediates are weaker acids ($pK_a$ = >3) compared to pyruvate, it would help in slowing down cytoplasmic acidification. If the main role for the reverse TCA was to compensate for the loss in NADH reoxidation, any fermentative mutants that lacked ADH1 should show highly elevated levels of succinate but this was not observed in this work. The activation of reverse TCA reactions was first reported in *HydEF* mutant (Dubini *et al*., 2009). I speculated the elimination of the hydrogen-producing pathway in this mutant resulted in pyruvate accumulation as its consumption by PFOR was affected.

As the major producer of $NAD^+$, the elimination of ADH1 pathway should affect the availability of $NAD^+$ for maintaining glycolysis. To cope with this, I hypothesise that *C. reinhardtii* activates the glycerol-producing pathway. Glycerol production plays an important role in osmoregulation and redox balancing in yeasts (Wang *et al*., 2001). The activation in *C. reinhardtii* could be brought about by the lack of $NAD^+$. When there is not enough $NAD^+$ to convert glyceraldehyde 3-phosphate (G3P) into pyruvate, this glycolytic sugar phosphate accumulates and consequently is converted to DHAP as the formation of this triose phosphate is favoured more by triose phosphate isomerase (Totemeyer *et al*., 1998). Consequently, the increase in DHAP could lead to the increased production of glycerol. However, one issue with this proposed mechanism is that it is not supported by our metabolite data. We assumed the observed increase in excreted glucose reflects increased levels of sugar phosphates. An increase in glucose excretion should be accompanied by an increase in the glycerol production. However, this is not observed in a few of the fermentative mutants (*ldh-pdc3-adh1*, *ldh-adh1* and *pdc3-adh1*) but observed in some (triple, quadruple and *pfl1-adh1*). This suggests that regulation of the glycerol-producing pathway is not exclusively controlled by the sugar-phosphate levels but could also involve other mechanism. This mechanism could

possibly be through the regulation of the enzymes involved in the glycerol production, particularly *sn*-glycerol-3 phosphate dehydrogenase (GPD). It has been reported the expression of this enzyme in yeast is regulated by a wide variety of stresses including oxidative stress (Godon *et al*., 1998; Jung *et al*., 2010). However, in the absence of oxygen it is difficult to imagine how reactive oxygen species (ROS) can be formed to create oxidative stress. Nevertheless, in *A. thaliana* it has been reported oxygen deprivation can be accompanied by ROS and reactive nitrogen species (RNS) (Blokhina & Fagerstedt (2010), and the former is capable to trigger the expression of many genes (Pucciariello *et al*., 2012).

As described above, the activation of the glycerol-producing pathway could be mainly regulated at the enzyme level and not just dependent of the levels of sugar phosphates. We hypothesized the activation of the methylglyoxal pathway is highly dependent on the levels of sugar phosphates. In Chapter 3, we proposed the production of methylglyoxal from the glycolytic triose phosphates is by spontaneous degradation. Therefore, it should be expected for this pathway to increase in activity when the levels of sugar phosphates are elevated. Based on the observed levels of glucose, when the levels of sugar phosphates were high (as observed in the quadruple mutant) we observed an elevation of D-lactate. However, when the levels of sugar phosphates were low (as observed in *ldh-adh1*, *ldh-pfl1*, *ldh-pdc3* and *ldh-pdc3-adh1*) there was no elevation of D-lactate observed. These observations provide evidence for our hypothesis. However, the detoxification of sugar phosphates could also be carried out together with the glycerol-producing pathway.

We observed there was a reduction in the production of formate when the ADH1 pathway was eliminated, indicating the link between the two pathways. However, the regulatory mechanism behind this is not clear. Nevertheless, the PFL of *Streptococcus mutans* has been reported to be strongly inhibited by glyceraldehyde 3-phosphate and dihydroxyacetone phosphate (Takahashi *et al*., 1982). Therefore, when the ADH1 pathway was eliminated, more triose phosphates were accumulated due to the unavailability of $NAD^+$, which was needed to convert glyceraldehyde 3-phosphate to pyruvate. Eventually, the high levels of the triose phosphates led to the inhibition of the PFL1 enzyme. Alternatively, formate reduction could be due to the need to prevent the accumulation of acetyl-CoA but the toxicity of this metabolite is not well documented. There could probably be a negative feedback inhibition imposed by acetyl-CoA on the PFL1 enzyme, whereby an initial increase in the concentrations of acetyl-CoA would later reduce its rates of production. Pyruvate formate lyase can be deactivated by bifunctional alcohol dehydrogenase in some bacteria (Kessler *et al*., 1992; Asanuma *et al*., 2004). It is not known if *C. reinhardtii* ADH1 could

deactivate PFL1 but if it did, the elimination of ADH1 should not be expected to reduce the formation of formate. Another alternative is the reduction in the formation of formate could be due to a rearrangement in the metabolic flux. The carbon flow could be re-routed from the PFL1 pathway to the PFOR pathway, presumably to generate more reducing equivalents. Therefore, the hydrogen gas needs to be quantified to give more understanding of the metabolic rearrangement. Under dark fermentation, hydrogen gas is generally produced at minor amounts. Due to the minor amounts, it is tempting to assume the carbon flux towards this pathway is less significant compared to the PFL1 pathway as formate is a major end product of dark fermentation. However, the amounts of hydrogen produced might not truly reflect the metabolic significance of the PFOR pathway. This is because hydrogen gas is produced via ferredoxin, and *C. reinhardtii* encodes six differently regulated ferredoxins (Terauchi *et al*., 2009). Therefore, it is possible for the generated ferredoxins, which in this case could possibly be FDX2 and FDX5 (Mus *et al*., 2007), to be re-routed towards other metabolic pathways instead of towards hydrogenases.

In summary, it is speculated that:

1. the D-LDH pathway is a first defense mechanism against pyruvate accumulation;
2. the PDC3 pathway is a second defense mechanism against pyruvate accumulation, and is possibly activated when there is a drop in cytoplasmic pH;
3. the ADH1 pathway is a major pathway for NADH reoxidation;
4. in the absence of the ADH1 pathway, the glycerol-producing pathway is activated and the PFL1 pathway is downregulated, suggesting the existence of a regulatory mechanism;
5. the methylglyoxal pathway is influenced by high levels of sugar phosphates.

### 4.3.4 Effects of D-LDH elimination on dark anaerobic metabolite production

The repeat analysis of *D-LDH* knockdown (using *ldh*-KD1 mutant) as a control for the current metabolite analysis showed similar patterns of metabolic flux as previously described in Chapter 3, indicating reproducibility.

### 4.3.5 Effects of PFL1 elimination on dark anaerobic metabolite production

The effects of PFL1 elimination on dark anaerobic metabolite production (Figure 4.18) are in agreement with a previous study (Catalanotti *et al*., 2012). When the PFL1 pathway was eliminated, formate production was remarkably affected. The elimination of this major fermentative pathway resulted in the metabolic flux being re-directed towards ethanol production instead of acetate. In Chapter 3, we described the treatment of WT with the PFL1 inhibitor (HP). However, we did not observed a substantial increase in the ethanol production as observed here. This could be explained by the complete elimination of the pathway compared to the incomplete elimination using the PFL1 inhibitor. I speculate that when less pyruvate is converted to formate, it could lead to more accumulation of pyruvate, causing a slight drop in cytoplasmic pH. Under the acidic conditions, the PDC3 pathway could become active, leading to the formation of more acetaldehyde. The acetaldehyde could be converted to ethanol by ADH1 or other alcohol dehydrogenases. The accumulation of pyruvate also led to the production of D-lactate through the D-LDH pathway. It is unclear if there was more carbon flux through the PFOR pathway. Catalanotti *et al*. (2012) did not observe any increase in the levels of hydrogen gas, suggesting no increase in carbon flux towards the PFOR pathway. Nevertheless, the acetyl-CoA produced by this pathway was mostly re-routed to the ADH1 pathway for NADH reoxidation. No acetyl-CoA was assumed to be produced by the PDH pathway. It is unclear if the observed increase in D-lactate was mostly contributed by the D-LDH pathway or the methylglyoxal pathway as the glucose level was not measured. However, it is suspected most of the generated D-lactate could potentially come from the reduction of pyruvate by D-LDH since the increase in pyruvate was high. To prevent the build-up of pyruvate, the cells also activated the reverse TCA reactions, and this also led to the reoxidation of NADH.

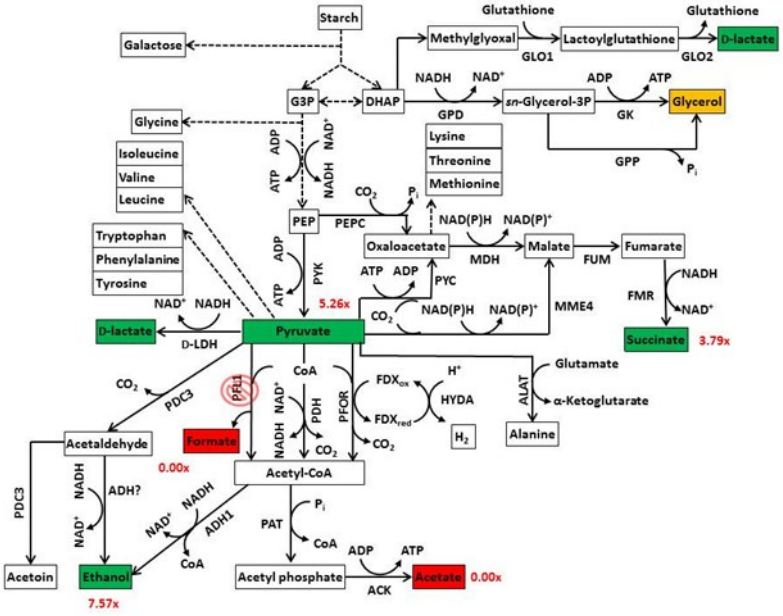


**Figure 4.18 Proposed model of dark fermentative metabolism in *pfl1*.**

Metabolites which increased, decreased and unchanged relative to the WT's are highlighted in green, red and orange, respectively. The approximate level relative to the WT is shown in red. The relative level of total D-lactate was 38.47x. If the metabolite was undetected in the WT, the average concentration was shown instead. See Figure 3.23 for designations of enzymes and metabolites.

### 4.3.6 Effects of ADH1 elimination on dark anaerobic metabolite production

The effects of ADH1 elimination on dark anaerobic metabolic production (Figure 4.19) are almost in agreement with a previous study (Magneschi *et al*., 2012). The slight difference in acetate and lactate could be due to different experimental conditions or laboratory strains used. When the ADH1 pathway was eliminated, ethanol was not produced and the metabolic flux towards the PFL1 pathway was reduced. The mechanism for this effect on PFL1 reduction is unclear but could be due to an elevation in the levels of triose phosphates, which subsequently inhibited the enzymatic activity of PFL1. This increase in the triose phosphates could also lead to the production of glycerol. As the production of acetyl-CoA was substantially reduced due to the reduction of PFL1 activity, this would explain the lack of substantial increase in the acetate level, which was in contrast to Magneschi *et al*. (2012). There was no noticeable elevation in the pyruvate levels because it was mostly metabolised to acetate and formate. The lack of excess pyruvate would probably explain the lack of increase in D-lactate production through the D-LDH pathway. However, there was an increase in the amounts of glycerol and succinate. The production of these metabolites was

probably to compensate for the loss of the ADH1 pathway which has a major role in NADH reoxidation.

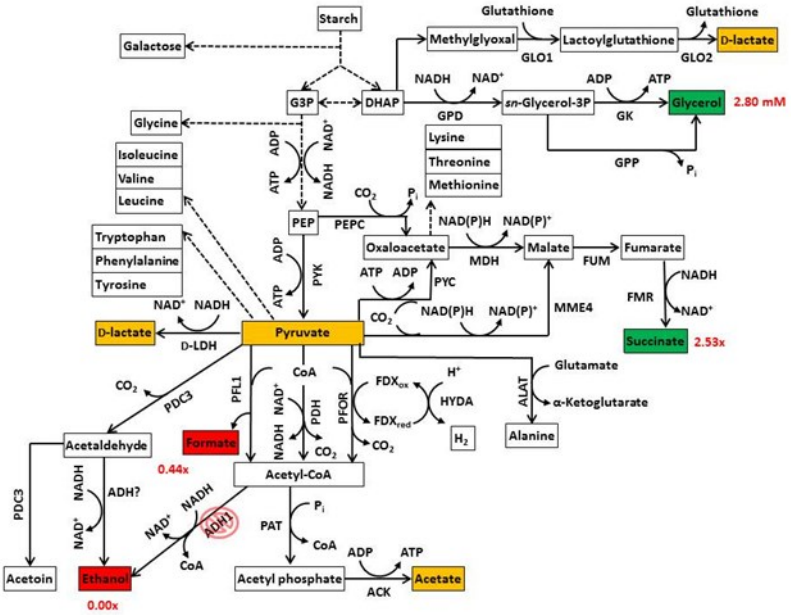


**Figure 4.19 Proposed model of dark fermentative metabolism in *adh1*.**

Metabolites which increased, decreased and unchanged relative to the WT's are highlighted in green, red and orange, respectively. The approximate level relative to the WT is shown in red. If the metabolite was undetected in the WT, the average concentration was shown instead. See Figure 3.23 for designations of enzymes and metabolites.

### 4.3.7 Effects of PDC3 elimination on dark anaerobic metabolite production

The effects of PDC3 elimination on dark anaerobic metabolic production (Figure 4.20) are largely in agreement with previous study (Burgess, 2011). The previous study did not observe any change in the production of lactate as observed in this work. This could be due to background mutations. In this work, the previous mutant (Burgess, 2011) was backcrossed four times with WT strains in order to obtain a cleaner genetic background. We showed the elimination of the PDC3 pathway did not affect the production of the major fermentative end products i.e. formate, acetate and ethanol. However, there was an increase in the amounts of pyruvate, indicating the PDC3 pathway did have a role in pyruvate metabolism. The unchanged level of ethanol suggests the PDC3 pathway does not have a major role in ethanol production under these conditions. It is speculated to play a significant role only when the pyruvate levels are sufficiently high to cause a drop in the cytoplasmic

pH. Under normal physiological conditions, it would only have a minor role in consuming pyruvate, similar to the D-LDH pathway. Most pyruvate was assumed to be consumed by the PFL1 pathway. I speculate that when the PDC3 levels are reduced, this leads to increased accumulation of pyruvate. This might activate the D-LDH pathway to reduce the build-up of pyruvate. The increase in D-lactate production could also be contributed by the methylglyoxal pathway. However, since the glucose level was not measured, the contribution of the methylglyoxal pathway is unclear. Nevertheless, I suspect the D-lactate production was mainly carried out by the D-LDH pathway due to the increase in pyruvate. The pyruvate build-up could also be responsible in activating the reverse TCA reactions, possibly in this case to prevent the build-up of pyruvate. However, it is also possible for it be activated in order to compensate for the loss of $NAD^+$ caused by the elimination of ethanol production through the PDC3 pathway.

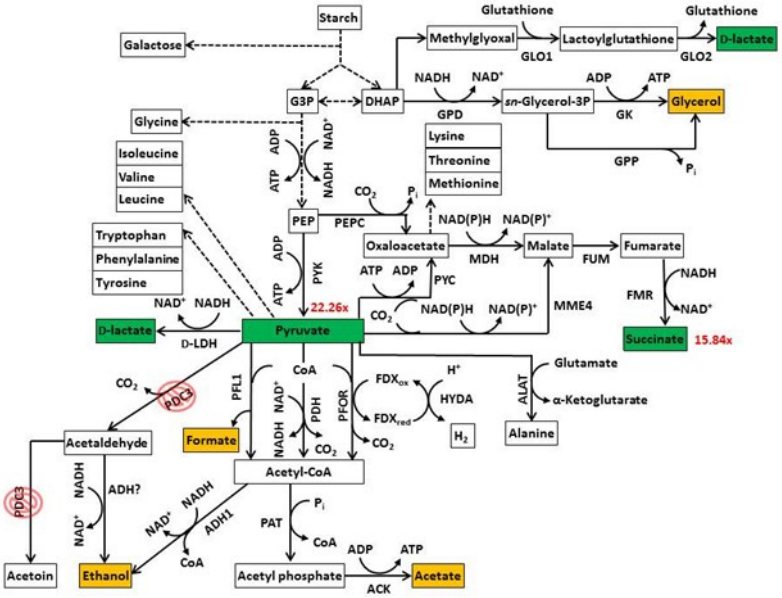


**Figure 4.20 Proposed model of dark fermentative metabolism in *pdc3*.**

Metabolites which increased, decreased and unchanged relative to the WT's are highlighted in green, red and orange, respectively. The approximate level relative to the WT is shown in red. The relative level of total D-lactate was 15.25x. If the metabolite was undetected in the WT, the average concentration was shown instead. See Figure 3.23 for designations of enzymes and metabolites.

### 4.3.8 Effects of D-LDH and PFL1 elimination on dark anaerobic metabolite production

The effects of D-LDH and PFL1 elimination on dark anaerobic metabolic production (Figure 4.21) are almost in agreement with the one described in Chapter 3, whereby the D-

LDH knockdown was coupled to the PFL1 inhibition with HP. However, an increase in D-lactate production, which was speculated to be associated with the methylglyoxal pathway, was not observed here. This lack of D-lactate production could potentially be explained by the observed glucose level. There was no elevation in the glucose level which suggests no increase in the levels of sugar phosphates. As the methyglyoxal pathway is speculated to be more active in the presence of more sugar phosphates, this could explain the observed D-lactate level. It is not clear why there was no increase in the glucose level but could potentially be due to poor starch reserve. The amount of starch had to be analysed to provide further understanding of the metabolic flux. Alternatively, there could be a regulatory mechanism that controls the degradation of starch into glucose, which could be affected under these conditions. The elimination of PFL1 resulted in hardly any formation of formate, and this means a reduction in the level of acetyl-CoA. As the cells needed $NAD^+$ to sustain glycolysis, most of the generated acetyl-CoA was speculated to be fed into the ADH1 pathway instead of the acetate-producing pathway. As PFL1 was no longer able to metabolise pyruvate, this also led to the build-up of pyruvate. In the absence of the D-LDH pathway, pyruvate detoxification had to be carried out by the PDC3 pathway, leading to the production of acetoin and possibly ethanol through ADH1 or other alcohol dehydrogenase(s). It is tempting to speculate the generated ethanol observed in this mutant could probably be contributed by both the ADH1 (from acetyl-CoA) and PDC3 pathways. A comparison of ethanol production between the *ldh-pfl1-adh1* and *ldh-pdc3-pfl1* mutants suggests both the PDC3 and ADH1 pathways contributed equally in the production of ethanol when the PFL1 and D-LDH pathways were both downregulated. If this was true, it means the metabolic flux from acetyl-CoA to ethanol was reduced, which consequently also reduced the generation of $NAD^+$ to maintain glycolysis. To compensate this, the cells had to activate its glycerol production and also the reverse TCA reactions. However, the activation of the reverse TCA reactions could also be due to the effect of high pyruvate concentrations.

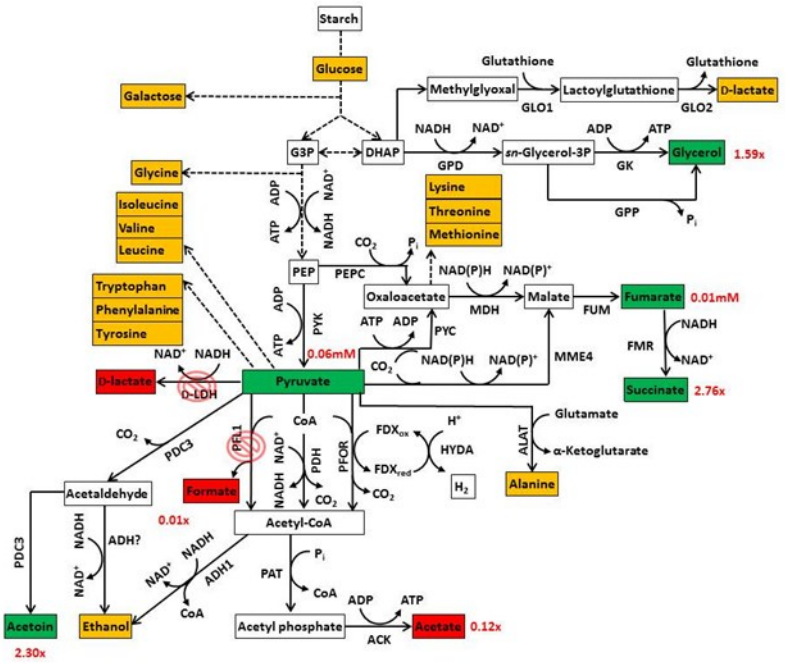


**Figure 4.21 Proposed model of dark fermentative metabolism in *ldh-pfl1*.**

Metabolites which increased, decreased and unchanged relative to the WT's are highlighted in green, red and orange, respectively. The approximate level relative to the WT is shown in red. If the metabolite was undetected in the WT, the average concentration was shown instead. See Figure 3.23 for designations of enzymes and metabolites.

### 4.3.9 Effects of PFL1 and ADH1 elimination on dark anaerobic metabolite production

The effects of PFL1 and ADH1 elimination on dark anaerobic metabolic production (Figure 4.22) are in agreement with previous study (Catalanotti *et al*., 2012) except for the ethanol production as explained above. The elimination of PFL1 resulted in hardly any formation of formate, and this would reduce the pool of acetyl-CoA. Since the ADH1 pathway was eliminated, the consumption of acetyl-CoA had to be carried out by the acetate-producing pathway. The elimination of the PFL1 pathway also resulted in the elevation of pyruvate. This activated the D-LDH pathway in order to detoxify excess pyruvate and also to reoxidise NADH. The elevation of pyruvate also caused an upsurge in the activity of the PDC3 pathway, possibly due to the acidification of the cytoplasm. Pyruvate was decarboxylated to acetaldehyde which was assumed to be rapidly converted to acetoin and ethanol as the intermediate is toxic. The high amount of generated acetoin provides evidence for the activation of the PDC3 pathway. The pyruvate-induced acidic conditions could activate alcohol dehydrogenase(s) to detoxify the generated acetaldehyde. Alternatively, the high concentrations of generated acetaldehyde could induce the activity of the alcohol

dehydrogenase(s). The loss of $NAD^+$ source due to the elimination of the ADH1 pathway was also compensated by the activation of the glycerol-producing pathway. However, the increase in glycerol production could also be associated with the observed increase in glucose level, suggesting an elevation of sugar phosphates especially DHAP. Similarly, the increased amounts of sugar phosphates could also possibly increase D-lactate production by the methylglyoxal pathway. This could explain the high total amount of D-lactate observed in this mutant strain.

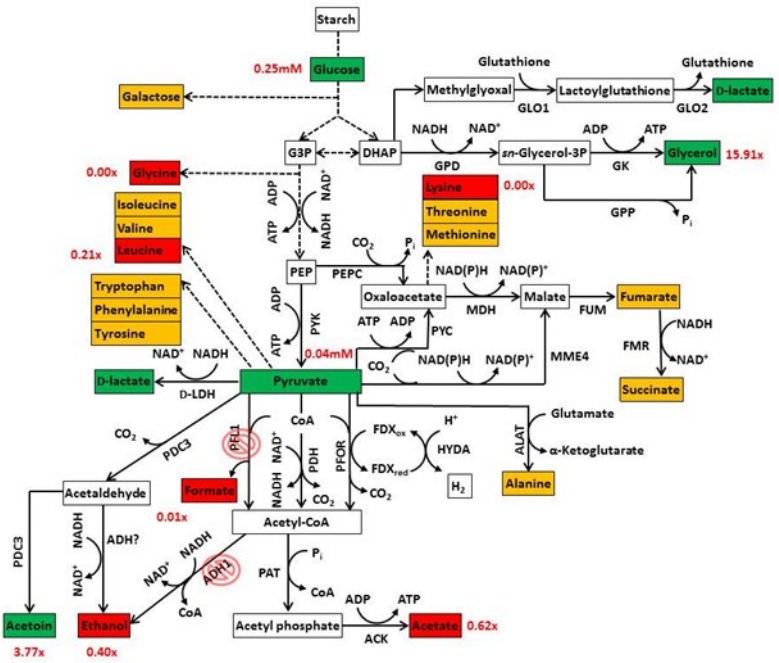


**Figure 4.22 Proposed model of dark fermentative metabolism in *pfl1-adh1*.**

Metabolites which increased, decreased and unchanged relative to the WT's are highlighted in green, red and orange, respectively. The approximate level relative to the WT is shown in red. The relative level of total D-lactate was 31.53x. If the metabolite was undetected in the WT, the average concentration was shown instead. See Figure 3.23 for designations of enzymes and metabolites.

### 4.3.10 Effects of PDC3 and ADH1 elimination on dark anaerobic metabolite production

The effects of PDC3 and ADH1 elimination on dark anaerobic metabolite production (Figure 4.23) seem to resemble the effects shown by the *adh1* mutant, suggesting the PDC3 pathway played a minor role under these conditions. This should not be surprising as there was no elevation in the pyruvate level (which was found to be mainly caused by the elimination of PFL1). No elevation of pyruvate could be due to efficient conversion into formate and acetate as these pathways were not remarkably affected. Therefore, as there was

no excess pyruvate, there was no activation in the D-LDH pathway and the reverse TCA reactions. The elimination of ADH1 hardly resulted in any production of ethanol. Similarly, the ADH1 elimination also caused a reduction in the carbon flux towards the PFL1 pathway. However, the reduction was not as severe as observed in the *adh1* mutant. This could potentially be due to lower levels of triose phosphates, and therefore less enzymatic inhibition of PFL1. As ethanol production was significantly affected, the reoxidation of NADH was also affected. To compensate for this loss, the cells activated the glycerol-producing pathway.

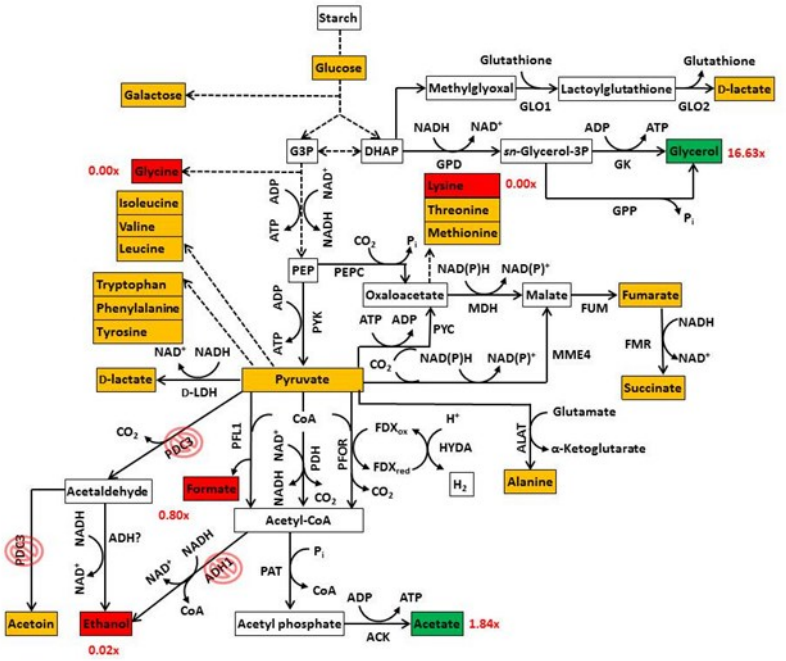


**Figure 4.23 Proposed model of dark fermentative metabolism in *pdc3-adh1*.**

Metabolites which increased, decreased and unchanged relative to the WT's are highlighted in green, red and orange, respectively. The approximate level relative to the WT is shown in red. If the metabolite was undetected in the WT, the average concentration was shown instead. See Figure 3.23 for designations of enzymes and metabolites.

### 4.3.11 Effects of PDC3 and PFL1 elimination on dark anaerobic metabolite production

The effects of PDC3 and PFL1 elimination on dark anaerobic metabolite production (Figure 4.24) seem to resemble the effects observed in the *pfl1* mutant. The elimination of the PFL1 pathway reduced the pool of acetyl-CoA. The generated acetyl-CoA was favourably directed towards the ADH1 pathway instead of the acetate-producing pathway in order to sustain glycolysis. Since the ADH1 pathway appeared to operate normally in producing $NAD^+$, it was speculated for the glycerol-producing pathway not to be activated. However, it

was still activated but only producing a slightly higher amount of glycerol compared to the WT, suggesting the reoxidation of NADH was efficiently carried out by the ADH1 pathway. Nevertheless, it could also be to compensate for the loss of $NAD^+$ that could be generated from the PDC3 pathway. The elevation of pyruvate caused by the PFL1 elimination stimulated the production of D-lactate. Due to the lack of increase in the glucose level, it was speculated the generated D-lactate could mostly come from the D-LDH pathway instead of the methylglyoxal pathway. Apart from the D-LDH pathway, the detoxification of pyruvate accumulation was also carried out by the reverse TCA reactions.

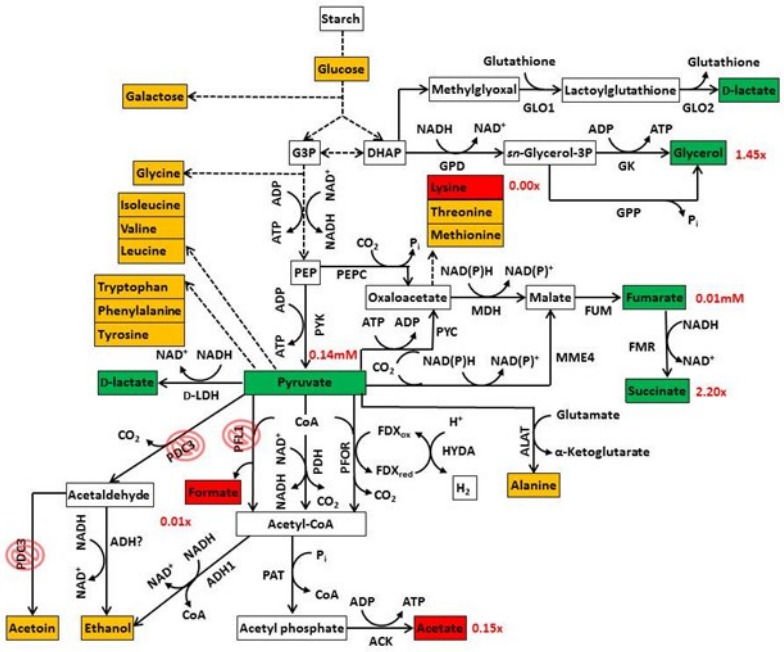


**Figure 4.24 Proposed model of dark fermentative metabolism in *pdc3-pfl1*.**

Metabolites which increased, decreased and unchanged relative to the WT's are highlighted in green, red and orange, respectively. The approximate level relative to the WT is shown in red. The relative level of total D-lactate was 26.16x. If the metabolite was undetected in the WT, the average concentration was shown instead. See Figure 3.23 for designations of enzymes and metabolites.

### 4.3.12 Effects of D-LDH and ADH1 elimination on dark anaerobic metabolite production

The effects of D-LDH and ADH1 elimination on dark anaerobic metabolite production (Figure 4.25) were broadly similar to the effects shown by the *adh1* mutant. The elimination of ADH1 caused the consumption of acetyl-CoA to be carried out by the acetate-producing pathway. Since the ADH1 pathway could no longer regenerate $NAD^+$, the

glycerol-producing pathway was activated to reoxidise NADH. This pathway could also potentially produce phosphate ($P_i$) that was needed by the acetate-producing pathway. As the production of acetyl-CoA by the PFL1 pathway was reduced, there was no excess acetyl-CoA available to increase the production of acetate. This explains the observed level of acetate. There was also no increase in the pyruvate level possibly due to its efficient conversion into formate and acetate. Therefore, there was no activation of the reverse TCA reactions. Since there was no production of acetoin and ethanol, it was also assumed no carbon flux was re-diverted towards the PDC3 pathway. The inactivation of the PDC3 pathway could be the result of the low pyruvate level that did not cause any drop in the cytoplasmic pH.

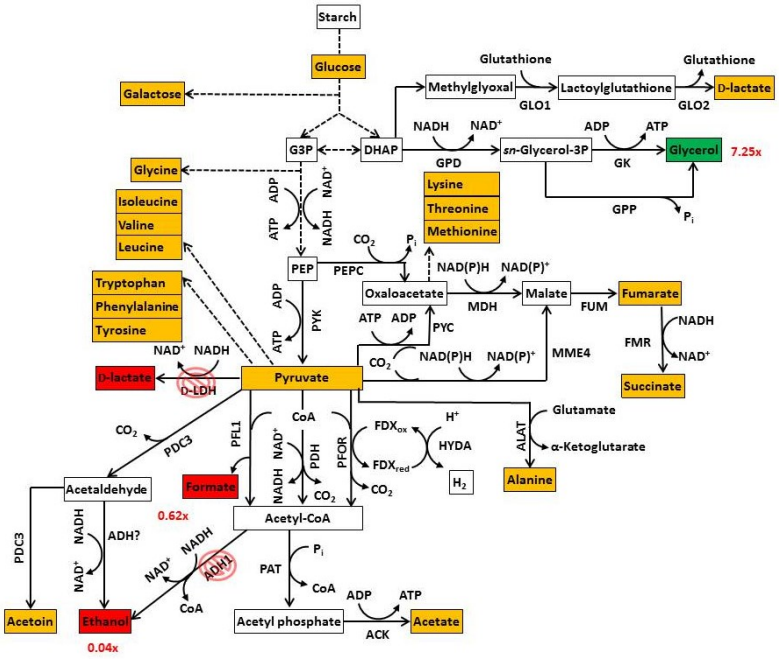


**Figure 4.25 Proposed model of dark fermentative metabolism in *ldh-adh1*.**

Metabolites which increased, decreased and unchanged relative to the WT's are highlighted in green, red and orange, respectively. The approximate level relative to the WT is shown in red. If the metabolite was undetected in the WT, the average concentration was shown instead. See Figure 3.23 for designations of enzymes and metabolites.

### 4.3.13 Effects of D-LDH and PDC3 elimination on dark anaerobic metabolite production

The effects of LDH and PDC3 elimination on dark anaerobic metabolite production (Figure 4.26) were perhaps surprising. Based on the effects observed in the *ldh-KD1* and *pdc3* mutants, the elimination of these two pathways should slightly increase the

accumulation of pyruvate. However, this was not observed in this mutant. Moreover, it was also expected for the acetate production not to be reduced as observed in both of the single mutants. Nevertheless, the reduction in acetate was only small. This could be due to poor starch reserve in this mutant strain, resulting in the poor availability of glucose and hence pyruvate. Therefore, when the PDC3 and D-LDH pathways were eliminated, the accumulation of pyruvate was not easily observed. The lower pyruvate level could also potentially explain the reduced production of acetate. Less acetyl-CoA would be generated from lower amounts of pyruvate. Since the production of formate was not affected, it could mean that less acetyl-CoA was produced by the PFOR pathway. To maintain glycolysis, the generated acetyl-CoA should be preferentially directed towards the ADH1 pathway instead of the acetate-producing pathway. Therefore, this would result in lower production of acetate. Alternatively, the slight reduction in acetate could also be due to other factors such as poor availability of $P_i$ and ADP, which are needed in the production. To confirm this, the starch content and hydrogen gas need to be quantified (assuming the hydrogen level reflects the metabolic flux of the PFOR pathway).

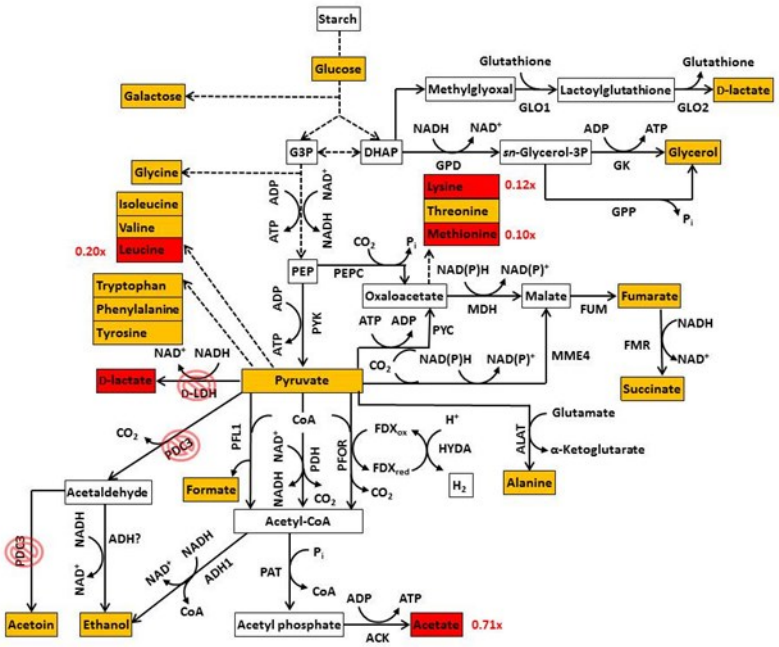


**Figure 4.26 Proposed model of dark fermentative metabolism in *ldh-pdc3*.**

Metabolites which increased, decreased and unchanged relative to the WT's are highlighted in green, red and orange, respectively. The approximate level relative to the WT is shown in red. If the metabolite was undetected in the WT, the average concentration was shown instead. See Figure 3.23 for designations of enzymes and metabolites.

### 4.3.14 Effects of D-LDH, PDC3 and ADH1 elimination on dark anaerobic metabolite production

The effects of LDH, PDC3 and ADH1 elimination on dark anaerobic metabolite production (Figure 4.27) were broadly similar to the effects observed in the *adh1* mutant. When the ADH1 pathway was eliminated, a reduction in the activity of the PFL1 pathway was similarly observed. Likewise, there was also no accumulation of pyruvate as it was mostly converted to formate and acetate. Therefore, it was unnecessary to activate the reverse TCA reactions to detoxify excess pyruvate. The surprising reduction in the alanine level could be due to poor availability of glutamate that was needed in the transamination reaction. However, how glutamate was reduced is not clear. The glycerol-producing pathway was activated to generate $NAD^+$ to compensate for the loss of ADH1. The activation of this pathway could probably be linked to the inhibition of the PFL1 pathway, as it means more glyceraldehyde 3-phosphate and DHAP would be present as potential inhibitors.

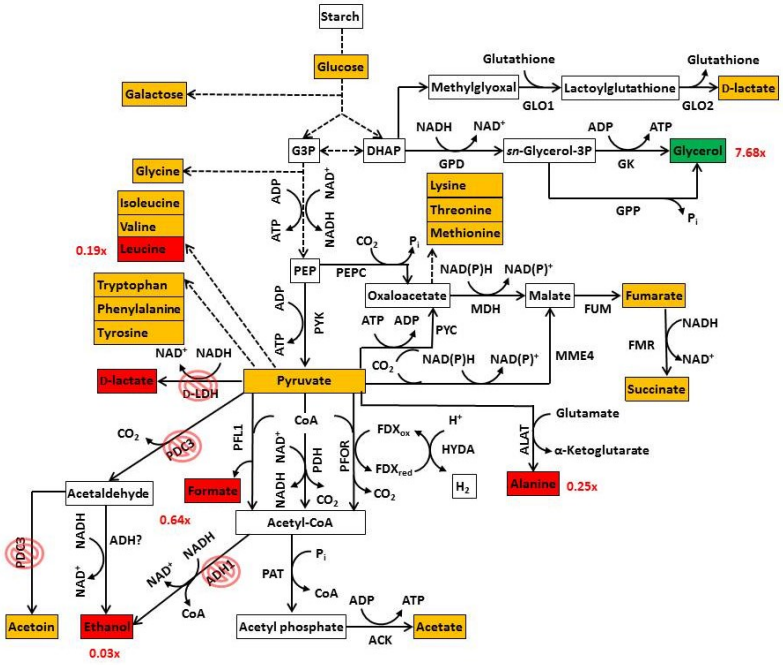


**Figure 4.27 Proposed model of dark fermentative metabolism in *ldh-pdc3-adh1*.**

Metabolites which increased, decreased and unchanged relative to the WT's are highlighted in green, red and orange, respectively. The approximate level relative to the WT is shown in red. If the metabolite was undetected in the WT, the average concentration was shown instead. See Figure 3.23 for designations of enzymes and metabolites.

### 4.3.15 Effects of D-LDH, PDC3 and PFL1 elimination on dark anaerobic metabolite production

The effects of D-LDH, PDC3 and PFL1 elimination on dark anaerobic metabolite production (Figure 4.28) were interesting. In the *pdc3-pfl1* mutant, there was a normal production of ethanol and also reduced acetate due to the diversion of the acetyl-CoA towards the ADH1 pathway instead of the acetate-producing pathway. However, in the *ldh-pdc3-pfl1* mutant, there was a remarkable reduction in ethanol as well as acetate. This suggests that there was a reduction in the carbon flow from pyruvate to acetyl-CoA. This reduction could be due to cytoplasmic acidification that inactivated the downstream fermentative pathways. The acidification was brought about by the PFL1 elimination which elevated the level of pyruvate. Since there were no D-LDH and PDC3 pathways to efficiently consume excess pyruvate, I speculate that the accumulated pyruvate level became high enough to inactivate the ADH1, PFOR and PAT/ACK pathways through acidification. In fact, a noticeable feature of this fermentative mutant was it excreted the highest amount of pyruvate compared to the other mutant strains. Arguably, the detoxification of pyruvate could also be carried out by the reverse TCA reactions. However, since the amount of generated succinate was observed to be very low, it means this pathway only played a minor in pyruvate detoxification. There was no upsurge of activity by the ALAT pathway to help with pyruvate consumption, possibly due to the lack of available glutamate. As there was a poor production of $NAD^+$, it caused the build-up of the glycolytic sugar phosphates since the conversion of glyceraldehyde 3-phosphate to pyruvate required $NAD^+$. The elevation of the sugar phosphates activated the methylglyoxal pathway and also the glycerol-producing pathway. The lack of NADH reoxidation by the ADH1 pathway could also regulate the glycerol production but this regulatory mechanism is currently unknown.

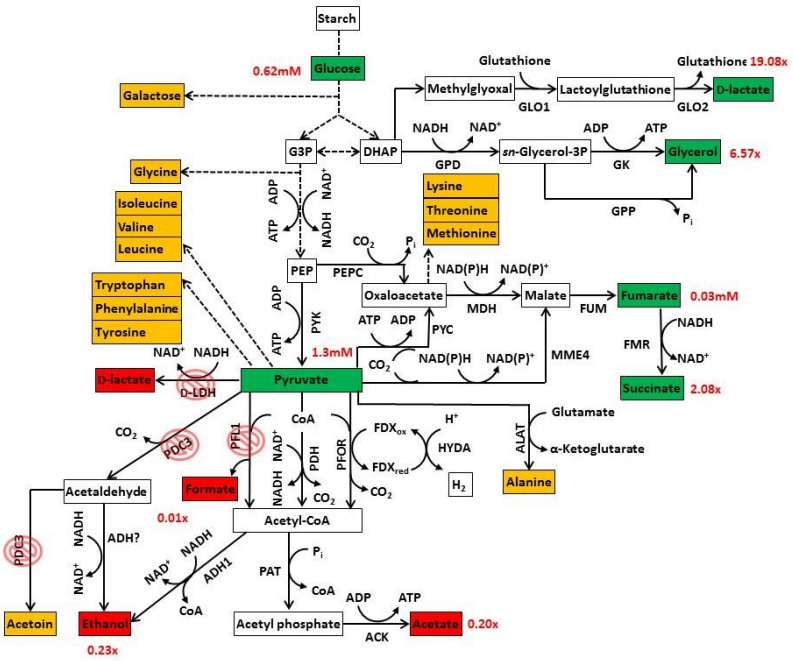


**Figure 4.28 Proposed model of dark fermentative metabolism in *ldh-pdc3-pfl1*.**

Metabolites which increased, decreased and unchanged relative to the WT's are highlighted in green, red and orange, respectively. The approximate level relative to the WT is shown in red. If the metabolite was undetected in the WT, the average concentration was shown instead. See Figure 3.23 for designations of enzymes and metabolites.

### 4.3.16 Effects of D-LDH, PFL1 and ADH1 elimination on dark anaerobic metabolite production

The effects of D-LDH, PFL1 and ADH1 elimination on dark anaerobic metabolite production (Figure 4.29) were also interesting and provided a clue to the physiological role of the PDC3 pathway. The elimination of the PFL1 pathway should elevate the pyruvate level. The build-up of pyruvate could be prevented by the activity of the D-LDH pathway. However, in this mutant the D-LDH pathway was eliminated and therefore, pyruvate detoxification had to be mainly carried out by the PDC3 pathway. This resulted in the increased production of acetaldehdye, leading to the production of acetoin and ethanol. The high amount of acetoin observed in this mutant strain provides evidence for the activation of the PDC3 pathway. Due to the rapid decarboxylation activity potentially caused by a drop in the cytoplasmic pH, less pyruvate became available that could be used in the production of amino acids. This could potentially explain the reduction in many amino acids. Alternatively, the increase production of toxic acetaldehyde could also be responsible in affecting the production of those amino acids as acetaldehyde can interfere with some enzyme activities

(Lieber, 1988). Acetaldehyde can also covalently bind to proteins and can impair protein secretion (Lieber, 1988). This could also explain the observed levels of excreted amino acids as their secretion was affected by acetaldehyde.

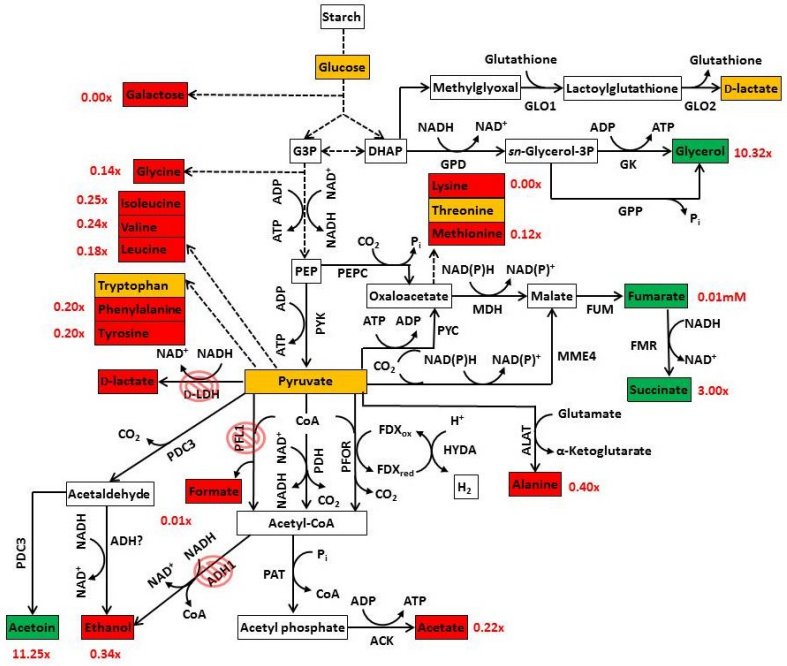


**Figure 4.29 Proposed model of dark fermentative metabolism in *ldh-pfl1-adh1*.**

Metabolites which increased, decreased and unchanged relative to the WT's are highlighted in green, red and orange, respectively. The approximate level relative to the WT is shown in red. If the metabolite was undetected in the WT, the average concentration was shown instead. See Figure 3.23 for designations of enzymes and metabolites.

### 4.3.17 Effects of PDC3, PFL1 and ADH1 elimination on dark anaerobic metabolite production

The triple mutant showed considerable effects in its dark anaerobic metabolite production (Figure 4.30). The elimination of the PFL1 pathway elevated the pyruvate level but the build-up of pyruvate was prevented by the reduction of pyruvate to D-lactate through the D-LDH pathway. The activation of the reverse TCA reactions could also help in lowering the pyruvate level apart from supplying $NAD^+$ to sustain glycolysis. The elimination of the PFL1 pathway should also reduce the pool of acetyl-CoA, and consequently this led to the reduction in the amount of generated acetate. The elimination of the ADH1 pathway reduced the regeneration of $NAD^+$. This would lead to the potentially toxic build-up of sugar

phosphates as $NAD^+$ was needed to convert glyceraldehyde 3-phosphate to pyruvate. To prevent the potentially toxic build-up of these sugar phosphates, the methylglyoxal pathway would be activated. The glycerol-producing pathway was also activated to supply $NAD^+$ and also to prevent the accumulation of sugar phosphates.

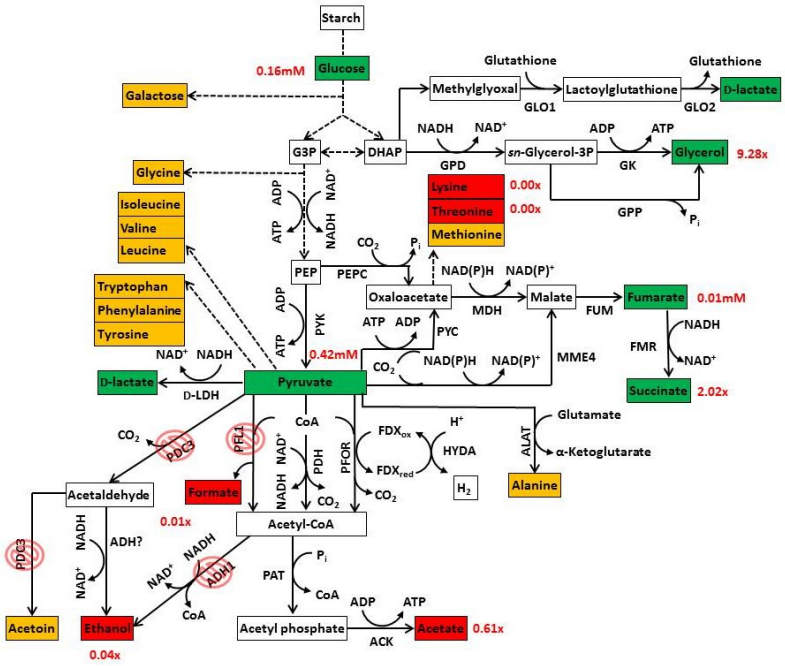


**Figure 4.30 Proposed model of dark fermentative metabolism in triple mutant.**

Metabolites which increased, decreased and unchanged relative to the WT's are highlighted in green, red and orange, respectively. The approximate level relative to the WT is shown in red. The relative level of total D-lactate was 22.46x. If the metabolite was undetected in the WT, the average concentration was shown instead. See Figure 3.23 for designations of enzymes and metabolites.

### 4.3.18 Effects of D-LDH, PDC3, PFL1 and ADH1 elimination on dark anaerobic metabolite production

The quadruple mutant showed considerable effects in its dark anaerobic metabolite production (Figure 4.31). The elimination of the PFL1 pathway elevated the pyruvate level. Since the D-LDH pathway was downregulated to prevent its accumulation, the pyruvate level should eventually become high and cause the cytoplasmic pH to become acidic. This resulted in the deactivation of the downstream fermentative pathways through the inactivation of pH-dependent enzymes. This could potentially explain the dramatic reduction observed in the production of acetate compared to the production observed in the triple mutant. The elimination of the downstream fermentative pathways resulted in the activation of the upper segment of the glycolytic pathways. This was mainly brought about by the low levels of

$NAD^+$ due to the elimination of ADH1. The unavailability of $NAD^+$ resulted in the accumulation of the glycolytic sugar phosphates, and this should cause the activation of the methylglyoxal pathway to detoxify the excess phosphorylated sugars. Similarly, the glycerol-producing pathway was also activated due to the elimination of the ADH1 pathway.

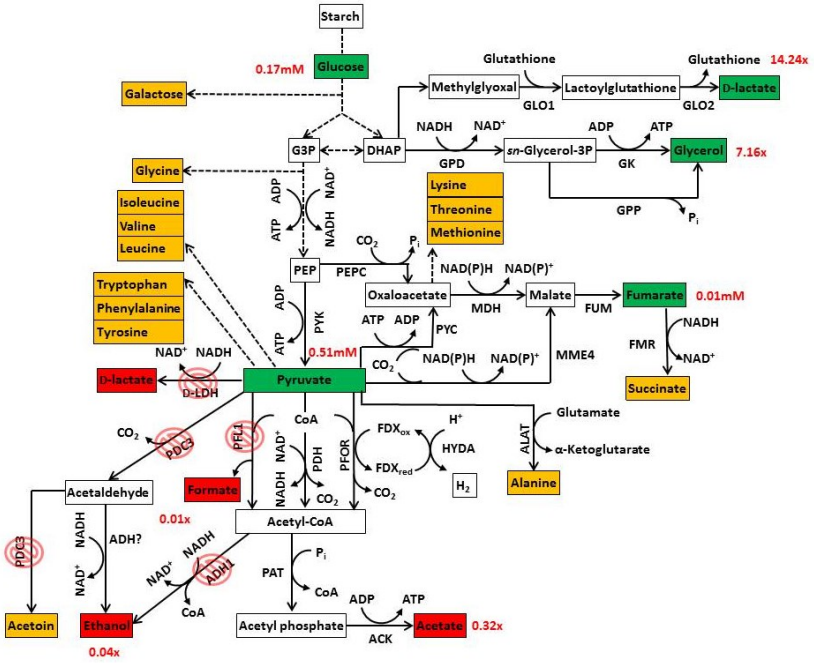


**Figure 4.31 Proposed model of dark fermentative metabolism in quadruple mutant.**

Metabolites which increased, decreased and unchanged relative to the WT's are highlighted in green, red and orange, respectively. The approximate level relative to the WT is shown in red. If the metabolite was undetected in the WT, the average concentration was shown instead. See Figure 3.23 for designations of enzymes and metabolites.

### 4.3.19 Hydrogen production under sulphur-deprived conditions

We could not manage to analyse the metabolite production under sulphur-deprived conditions due to the unavailability of analytical equipment. Nevertheless, we managed to analyse hydrogen production by some of the fermentative mutants. Unfortunately, the elimination of fermentative pathways did not result in the increased production of hydrogen gas. In fact, the production appeared to be negatively affected in most of the analysed mutants. We hypothesised this reduction in hydrogen production could be linked to the reduced cell viability under the conditions tested, as we have shown the cell viability of the quadruple and triple mutants were dramatically affected. However, we could not conclude if the reduced cell viability was due to the elimination of the fermentative pathway(s) or due to the genetic background of CC-125.

# Chapter 5: Conclusions and future work

## 5.1 Summary of results

Hydrogen gas produced by *C. reinhardtii* is an attractive fuel as it is a clean and renewable fuel. Moreover, the production of this fuel can also be coupled to other processes such as bioremediation and production of other high values products. However, for hydrogen gas to become an economically viable alternative fuel, it is necessary to improve its production in the green alga. One approach is to improve the conversion efficiency of light energy to hydrogen gas, which has been estimated to be currently low. It is believed that this low conversion efficiency is due to the existence of competing pathways that compete with the hydrogen-producing pathways for reductant. The photosynthetic production of hydrogen gas is contributed by PSII-dependent and PSII-independent pathways, and several competing pathways have been speculated. In this work, we described our efforts to improve hydrogen production by eliminating the competing pathways associated with the PSII-independent pathways, specifically the dark fermentative pathways. It has been previously hypothesised that the elimination of these competing pathways might improve hydrogen yields (Burgess *et al.*, 2012). To begin to test this hypothesis, we need to refine the current model of metabolism to include knowledge of all various competing pathways and their locations.

In Chapter 3, we identified the elusive pyruvate reductase (D-LDH) whose activity was originally detected by Husic & Tolbert (1985). Bioinformatics analysis of the algal genome revealed the occurrence of only one putative $NAD^+$-dependent D-LDH gene product, which was predicted to be localised to the chloroplast (Figure 5). The predicted chloroplast localisation had been previously confirmed by our group (Burgess, 2011). To further verify this *in silico* analysis, we overexpressed the putative protein in *E. coli* (without the predicted chloroplast transit peptide) and carried out enzyme assays. Our assays confirmed the gene did indeed encode a $NAD^+$-dependent D-LDH, favourably reducing pyruvate to D-lactate instead of oxidising D-lactate to pyruvate. Furthermore, we also found the enzyme was capable of utilising glyoxylate although with a higher $K_m$ compared to pyruvate. Therefore, this suggests the enzyme might also play a role in glyoxylate metabolism. This could be the direction for future work with regard to the enzyme physiological role(s). However, to add further understanding on the kinetics of the D-LDH enzyme, future work could also extend on the pH profile of the enzyme, $K_m$ for NADH and effects of possible inhibitors such as ATP. This could provide a clue if the regulatory mechanism of the D-LDH pathway could be associated with change in pH or change in the concentrations of NADH and ATP.

Apart from determining the enzyme kinetics, efforts were also made to determine the crystal structure of the D-LDH protein. To date, we managed to estimate the molecular mass of $His_6$-tagged D-LDH using size-exclusion chromatography, which was about 202 kDa, suggesting it was a tetrameric protein. This was in line with the previous study of native D-LDH carried out by our group (Burgess, 2011). Our preliminary crystal structure obtained by X-ray crystallography, which is currently under refinement, also suggests tetrameric protein structure. This should not be surprising as many LDHs from other species are also found to be a tetramer. Future work on the crystal structure will identify the potential substrate binding sites.

To assess the impact of the D-LDH pathway on metabolism and physiology, we successfully isolated four *LDH* knockdown mutants by using artificial microRNA technology as a *LDH* knockout mutant is not yet available from the *C. reinhardtii* mutant library. The ~80% knockdown levels of LDH were verified by quantifying the D-LDH protein and transcript levels by using protein immunoblots and RT-PCR, respectively. We also confirmed by enzyme activity assays that the observed reduction in the protein and transcript levels resulted in the reduction of D-LDH activity in the knockdown mutants.

Our efforts to predict the physiological role(s) of the D-LDH pathway have so far not been fruitful. Based on our cell growth analysis and photoinhibition assays, we did not observe any observable phenotypic difference to WT. This could be because the pathway was inactive under aerobic conditions. Alternatively, it could be because the residual D-LDH activity in the knockdown mutants was sufficient to compensate the knockdown or that compensating pathways were operational. Therefore, it is necessary for future work to verify the activity of this pathway under the specified conditions. Alternatively, it could also mean it only played a minor role. On the assumption that the pathway was active, more experimental parameters could be tested, such as growing the knockdown mutants under 2000 $\mu Em^{-2}s^{-1}$ or under rapid fluctuating light, to increase the possibility of observing a phenotypic difference to WT. On the other hand, our dark growth and cell viability analysis seem to indicate the D-LDH pathway was only a minor pathway under the conditions tested. However, the experiments could be repeated by trying an extended time period as the phenotype might require more time to show up if the pathway only played a minor role under the conditions tested.

By using $^{1}$H NMR and verified by HPLC, we found the impact of *LDH* knockdown on dark anaerobic metabolite production was interesting. We detected several metabolites excreted by *C. reinhardtii*, which have not been previously reported, indicating NMR analysis is an excellent approach for metabolite analysis. Unfortunately, hydrogen gas was at undetectable levels using our current experimental system and requires sensitive analytical equipment for future quantification. Interestingly, although the D-LDH pathway was severely affected, we still observed that the amount of excreted lactate was unaffected, which was enzymatically confirmed to have stereoscopic D-configuration. This led us to hypothesise the possible existence of a methylglyoxal pathway in the green alga (Figure 5). It has been previously reported the methylglyoxal pathway is a regulatory mechanism to prevent toxic accumulation of glycolytic sugar phosphates. We also discovered the excretion of acetoin, which led us to hypothesise that its production could potentially be carried out by PDC3 (Figure 5). The production of acetoin and ethanol through this enzyme has been previously reported to sustain pH homeostasis. Future work should mainly focus on verifying these hypotheses as it will give us more understanding of the fermentative metabolism and its regulation in *C. reinhardtii*. We also have attempted to overexpress PDC3 in *E. coli*. However, so far our attempts have been unsuccessful. Therefore, for future work, more conditions and different approaches need to be tested in order to successfully express the protein.

Similarly, we also assessed the impact of *LDH* knockdown on metabolite production under sulphur-deprived conditions, as the conditions are previously suggested for the industrial production of hydrogen gas. However, the metabolite data were not as interesting as the ones obtained from the dark anaerobic conditions due to the low concentrations of many metabolites. Therefore, it is suggested for future analysis, samples need to be concentrated before analysis to allow for the detection of various metabolites. Nevertheless, the impact of *LDH* knockdown on hydrogen production was found to be disappointing as no improvement was observed, indicating no re-routing of metabolic flux towards hydrogen production.

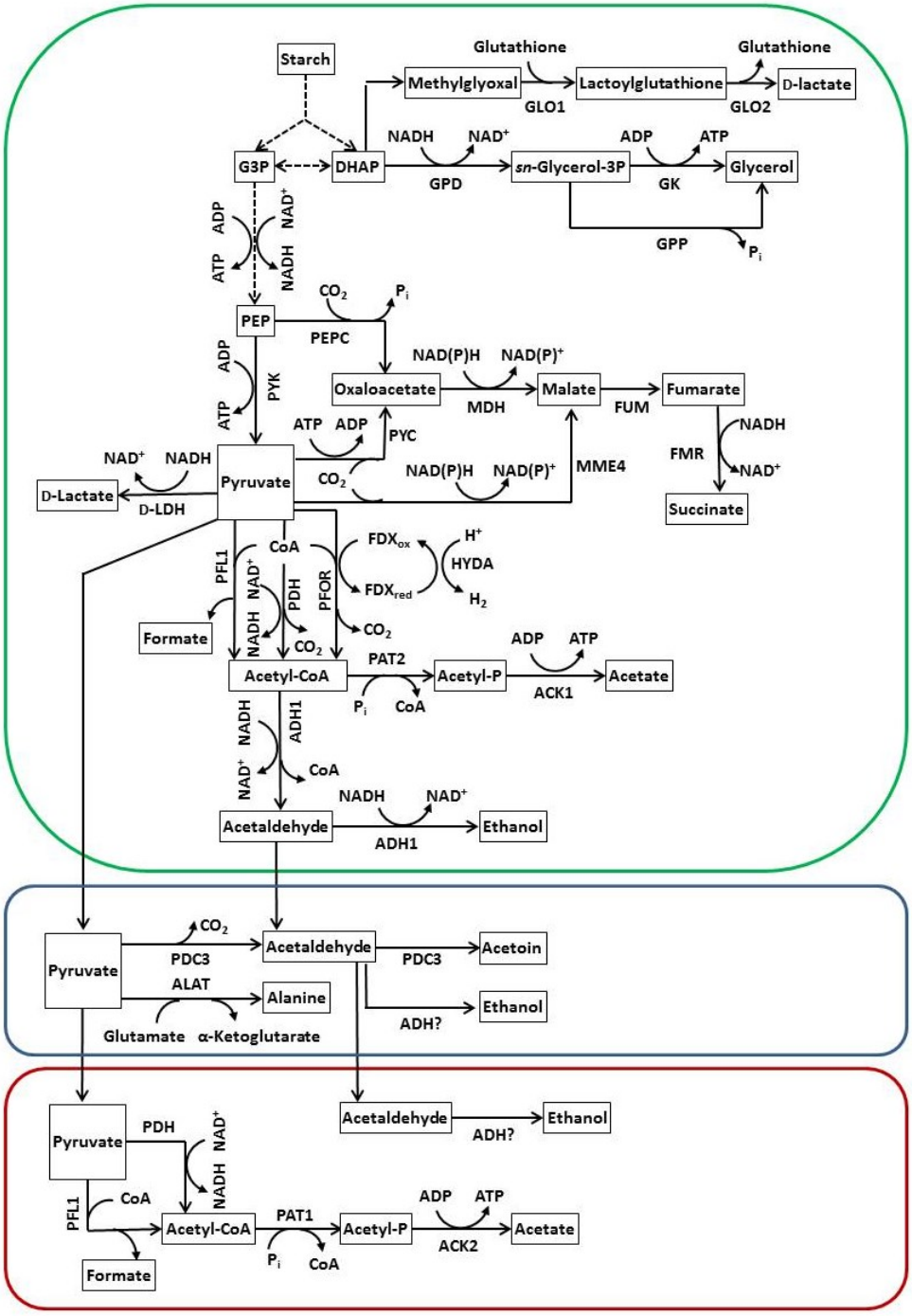


**Figure 5 Proposed fermentative pathways in *C. reinhardtii*.**

The map is adapted from Catalanotti *et al*. (2013). Green, blue and red boxes represent chloroplast, cytoplasm and mitochondrion, respectively. The subcellular locations of many enzymes are putative. For simplicity, some glycolysis pathways (dash lines) are not described. See Figure 3.23 for designations of enzymes and metabolites.

As it has been previously suggested the down regulation of the fermentative pathways could possibly improve hydrogen yields (Burgess *et al*., 2012), we isolated a quadruple mutant through cell mating in which two of the pathways were down-regulated and two inactivated. We successfully crossed *pdc3*-KD mutant with *pfl1-adh1* mutant, resulting in the isolation of triple mutant. Subsequently, we crossed the triple mutant with an *ldh-KD1* mutant, resulting in the successful isolation of the quadruple mutant. The crosses also concurrently resulted in the isolation of other fermentative mutants. However, due to time constraints, we focused our analysis mostly on the triple and quadruple mutants. However, our analysis was hampered by the discovery of phenotypic differences between the two WT strains i.e. CC-124 and CC-125. The inability of CC-125 to grow or survive under certain conditions has never been reported before, and the *Chlamydomonas* Resource Centre from whom we obtained the strains was also unaware of it. We assumed there was background mutation(s) in the CC-125 strain. Therefore, to verify our metabolite analysis, we are currently isolating independent lines of quadruple mutants in order to rule out the observed results were due to CC-125. Future work will involve repeating the metabolite analysis using at least one of the isolated independent lines. Work is also currently ongoing with our collaborators to extend the current metabolite analysis of the quadruple mutant to include intracellular metabolite analysis. This possibly will also involve lipid analysis to assess the impact of the downregulation of the fermentative pathways on lipid production, as algal biodiesel has currently received more interests than hydrogen fuel (Scott *et al*., 2010).

On the assumption that the CC-125 mutation(s) did not have significant effects on metabolite production after 4 and 8 hours of dark anaerobic treatment, we found the metabolite production to be interesting and we feel it provided an insight into the regulation of fermentative metabolism in *C. reinhardtii*. This assumption should be validated by comparing the metabolite production between CC-124 and CC-125. Due to time constraints and unavailability of analytical equipment, I did not manage to do this. Nevertheless, our qualitative analysis of cell viability suggests the viability of CC-125 was not affected in the first 24 hours of dark incubation. Our metabolite analysis showed a link between pyruvate elevations and the elimination of one of these pathways: D-LDH, PDC3 and especially PFL1. This provided evidence that these pathways were involved in pyruvate consumption as expected. It appeared that PFL1 was the main consumer of pyruvate, and this should be as expected as formate is the major end product of dark fermentation. It also appeared that when this pathway was eliminated the carbon flux from pyruvate was diverted towards the D-LDH and PDC3 pathway. The diversion towards the PFOR pathway was unclear as we did not

measure the hydrogen production. We also observed that acetyl-CoA was preferentially re-routed towards the ADH1 pathway instead of the acetate-producing pathway, which was unsurprising as this metabolic re-arrangement would sustain glycolysis. Interestingly, we also observed there was an association between the elimination of ADH1 and the activity of PFL1. In the absence of ADH1, the production of formate was downregulated, suggesting the existence of a regulatory mechanism. Moreover, we also observed a link between the elimination of ADH1 and the glycerol-producing pathway, further suggesting the existence of a regulatory mechanism that could potentially be related to the PFL1 pathway. There also seems to be a link between the glucose level and the activation of the proposed methylglyoxal pathway, suggesting the activation could be dependent on the levels of sugar phosphates as previously expected for this pathway. To rule out the observed effects could be due to different starch contents, it is also necessary for future work to confirm starch contents were not significantly different among the strains.

The metabolite assessment of the quadruple and triple mutants showed when the fermentative metabolism was downregulated, a metabolic rearrangement occurred that activated the upper segment of glycolysis. The glycerol-producing pathway and potentially the methylglyoxal pathway were activated. This was probably to cope with the speculated increase in the sugar phosphate and/or NADH levels. The elimination of the fermentative pathways also led to pyruvate elevation, both at the intracellular and extracellular levels. Excess pyruvate appeared to be re-routed towards the D-LDH pathway (in the case of the triple mutant), and we also observed the activation of the reverse TCA reactions. Interestingly, the production of acetate was more negatively affected compared to the triple mutant, suggesting reduced carbon flux from pruvate to acetyl-CoA through the PFOR pathway. However, this needs to be confirmed by assessing the dark anaerobic hydrogen production.

Interestingly, the hydrogen production by the quadruple and triple under sulphur-deprived conditions seemed to be highly affected by the downregulation of the fermentative metabolism. Hardly any hydrogen gas was produced. However, the results were inconclusive as the observed effects could be due to the mutation(s) found in CC-125 that reduced cell viability. Nevertheless, the observed results could also be jointly contributed by CC-125 mutation(s) and the downregulation of the fermentative metabolism as our dark anaerobic metabolite analysis suggests the lack of carbon flux towards the PFOR pathway. To confirm this, the hydrogen production by CC-125 under sulphur-deprived conditions needs to be assessed as well.

## 5.2 Evaluation of research project

The goal of the research project was to improve the production of hydrogen from *C. reinhardtii*, as the current production under the sulphur-deprived conditions is not economically feasible. To improve the hydrogen yields, it has been hypothesised that several competing metabolic pathways need to be eliminated in order to re-direct the metabolic flow from these competing pathways towards the hydrogen-producing pathway (Burgess *et al*., 2012). This forms the basis of this research project. In order to test the hypothesis, the research project was designed to consist of two main aims.

The first aim of the project was to refine and validate the current model of fermentative metabolism to include knowledge of the various competing pathways. We focused specifically on LDH pathway as this potential competing pathway has been previously suggested to be involved in the green algal fermentative metabolism (Grossman *et al*., 2007). Our research successfully managed to complete this aim, whereby we identified and characterised the D-LDH activity responsible for D-lactate production in *C. reinhardtii*. We effectively identified a nucleus-encoded gene (Cre07.g324550) that produced an enzyme with a molecular mass of approximately 202 kDa. We also confirmed it was an $NAD^+$-dependent D-LDH, favouring the reduction of pyruvate to D-lactate. Therefore, we have validated this elusive pathway to be one of the many competing fermentative pathways in *C. reinhardtii*. Apart from contributing to the existing knowledge in algal fermentation, it also justified our attempt to eliminate this metabolic pathway for improving biohydrogen production.

As we had validated the D-LDH pathway while several previous studies had carried out research and validation on the other competing fermentative pathways in *C. reinhardtii* (Phillips *et al*., 2011; Burgess, 2011; Magneschi *et al*., 2012; Catalanotti *et al*., 2012), this led to the second aim of the project which was to generate a quadruple *C. reinhardtii* mutant affected in fermentation, targeting the enzymes D-LDH, PDC3, PFL1 and ADH1, and to assess the impact of these mutations on physiology and metabolism. We successfully isolated a quadruple mutant affected in the specified fermentative pathways. Although the impact of these mutations on physiology and metabolism disappointingly could not be assessed with confidence due to the mutation(s) observed in one of the WTs used in this study, our metabolic profiling excitingly led to the proposal of methylglyoxal and acetoin production. This is considered as a very interesting finding as these metabolites have never been reported before in *C. reinhardtii*, further confirming the complexity of the algal fermentative metabolism. This new finding could form a basis for future research as more studies are still

needed to validate this proposal. Moreover, our metabolic profiling also showed the occurrence of metabolic rearrangement, confirming the well-known metabolic flexibility of the green alga. Interestingly, the metabolic profiling also suggests the possible occurrence of regulatory mechanisms that could regulate the metabolic rearrangement. This is another exciting direction for future research.

The research project unfortunately has not managed to achieve its goal in improving hydrogen production in *C. reinhardtii*, as we could not observe any improvement in the hydrogen photoproduction under the sulphur-deprived conditions. However, the results observed could be due the mutation(s) that are present in one of the WTs used in this study and therefore, the current hypothesis to improve hydrogen yields by eliminating competing pathways cannot be entirely ruled out yet. Nevertheless, this research project has contributed substantially to the fundamental understanding of *C. reinhardtii* fermentative metabolism.

### 5.3. Future directions

For hydrogen production from *C. reinhardtii* to be economically feasible, it is necessary to improve the hydrogen yields. This could be attempted through genetic engineering as carried out in this study. Apart from genetically manipulating the algal fermentative metabolism, there are various other methods that could be attempted to improve hydrogen production (Burgess *et al*., 2011). It is probably best for genetic manipulation to focus on the PSII-dependent pathways by eliminating any competing pathways, as the PSII-dependent pathways contribute significantly towards the hydrogen photoproduction. Another attractive method is to engineer an oxygen-tolerant hydrogenase, as the current production is greatly hampered by the extreme sensitivity of the enzyme towards oxygen.

Apart from improving biohydrogen yields, it is also perhaps necessary to couple the hydrogen production with the production of biodiesel or other high value products. This potentially could guarantee a commercial viability. Although currently algal biofuels could not compete with fossil fuels, the depletion of fuel reserves and increasing fuel prices has created a huge pressure to develop renewable energy. Moreover, the impacts of these biofuels to the environment should also be taken into account when assessing their economic feasibility. Indeed more works are still needed before algal biofuels could be a commercial success as our biological knowledge on this area is still new and limited. Therefore, more research into microalgae should be carried out to increase our fundamental understanding on microalgae with the goal to identify steps in improving biofuel production.

# Appendices

## Appendix 1. Protein standard curve

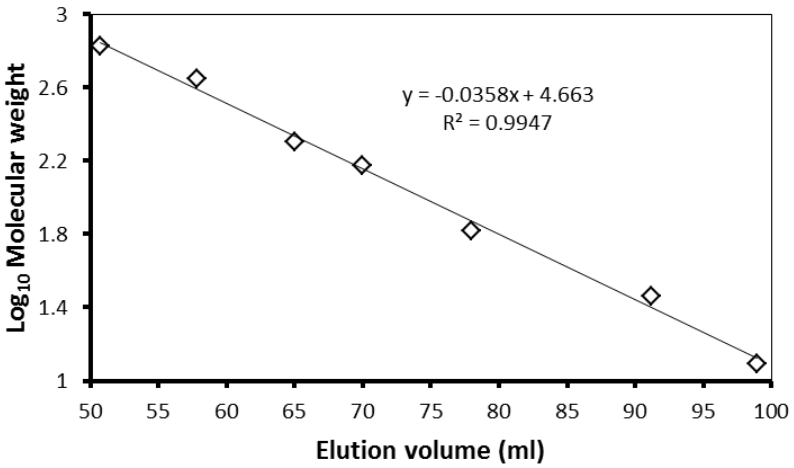


**Figure 6.1.1.Protein standard curve for gel filtration chromatography.**

Seven protein standards (Sigma-Aldrich, UK) were used i.e. cytochrome c (12.4 kDa), carbonic anhydrase from bovine erythrocytes (29 kDa), BSA (66 kDa), yeast alcohol dehydrogenase (150 kDa), β-amylase from sweet potato (200 kDa), apoferritin from horse spleen (443 kDa), and bovine thyroglobulin (669 kDa). Standard curve was generated by Dr. Wojciech J. Bialek (Imperial College London).

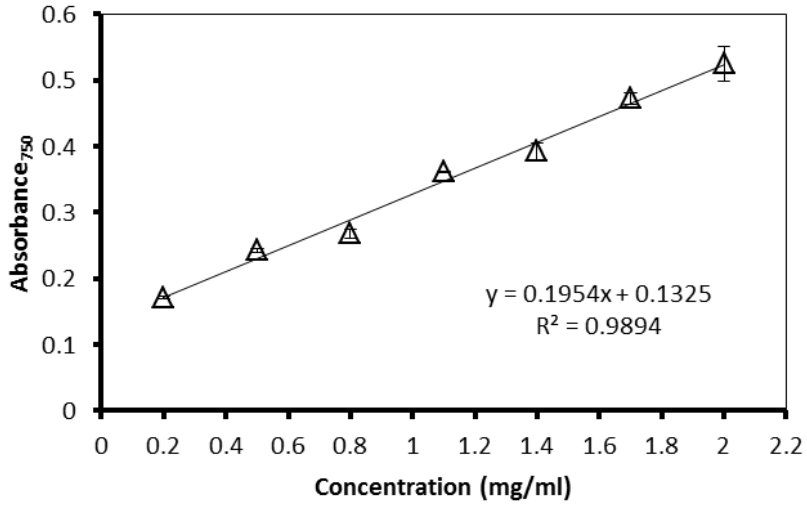


**Figure 6.1.2. Standard curve of bovine serum albumin.**

Error bars represent standard error of three technical replicates.

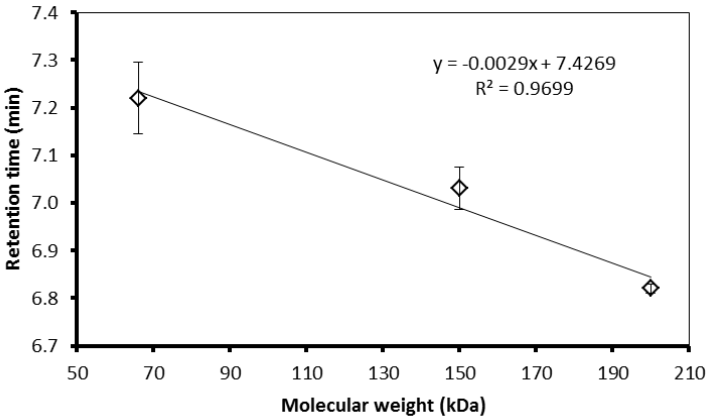


**Figure 6.1.3. Protein standard curve for size exclusion chromatography.**

Error bars represent standard error of three technical replicates. Three protein standards (Sigma-Aldrich, UK) were used i.e. bovine serum albumin (66 kDa), yeast alcohol dehydrogenase (150 kDa) and β-amylase from sweet potato (200 kDa).

## Appendix 2. Screening for *ldh*-KD mutants

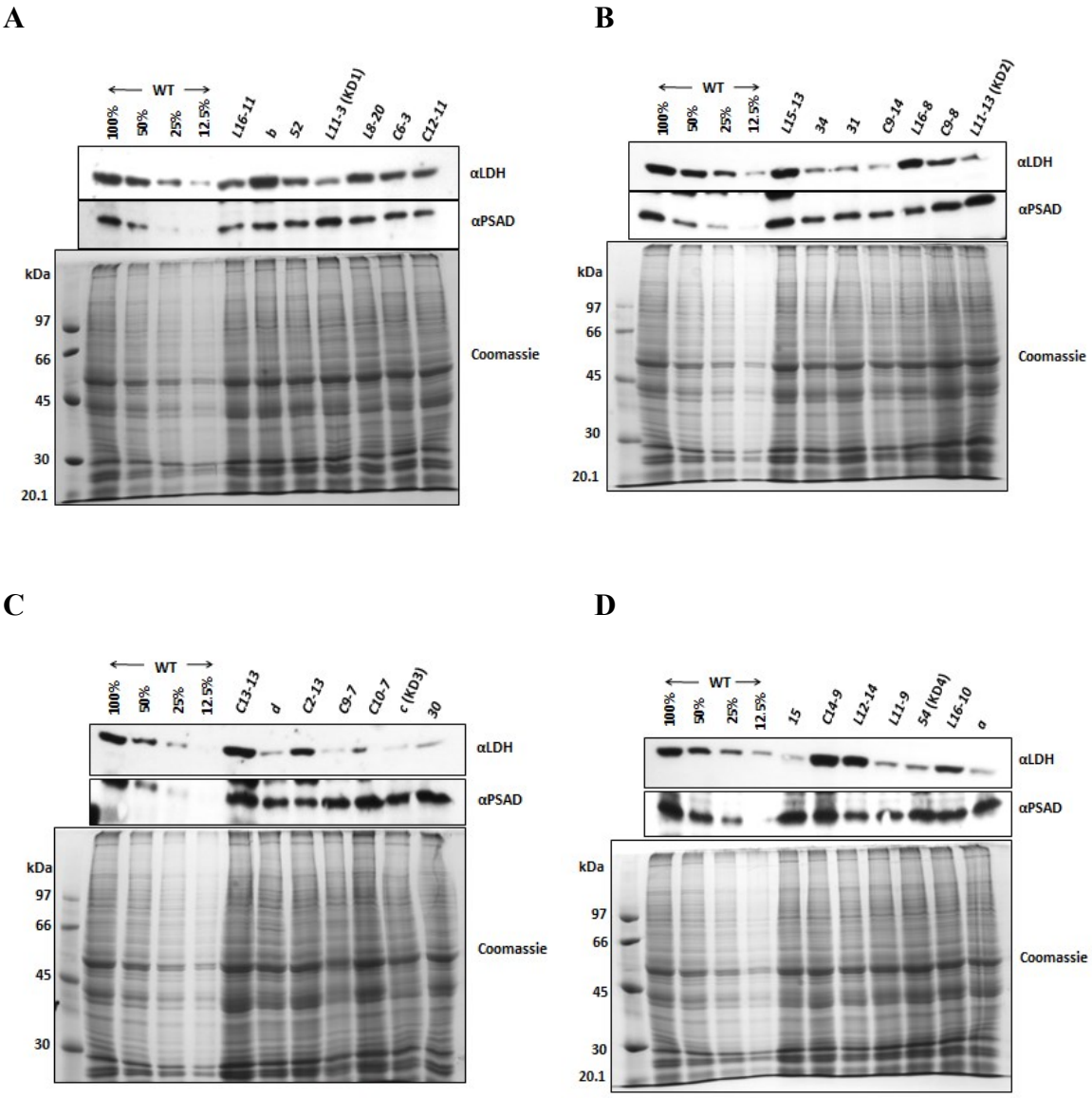


**Figure 6.2. Screening for *ldh*-KD mutants.**

Cells were grown mixotrophically to late log phase and their D-LDH protein levels were screened by immunoblotting. Coomassie Brilliant Blue staining and αPSAD served as loading controls. Four knockdown mutants were chosen for future analyses i.e. *L11-3*, *L11-13*, *c* and *54* (later re-named as *ldh*-KD1, *ldh*-KD2, *ldh*-KD3 and *ldh*-KD4, respectively).

## Appendix 3. Relative efficiency plots and standard curves

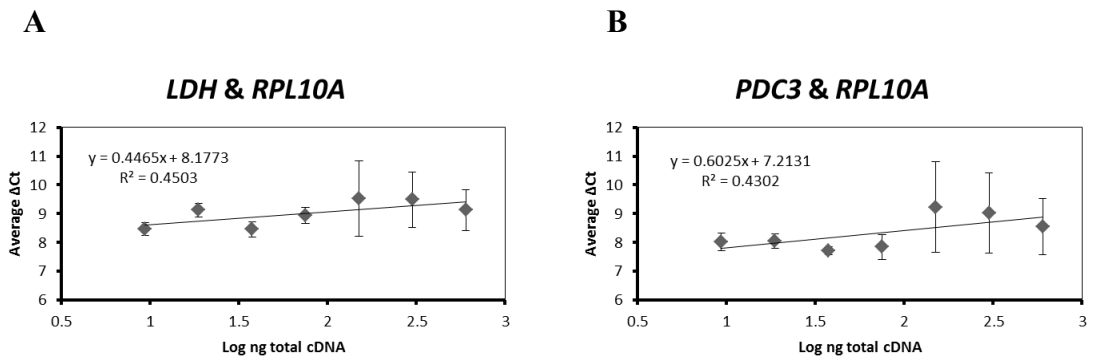


**Figure 6.3.1. Relative efficiency plots for *LDH* and *PDC3* against *RPL10A*.**

Error bars represent standard error of three biological replicates (each with two technical replicates).

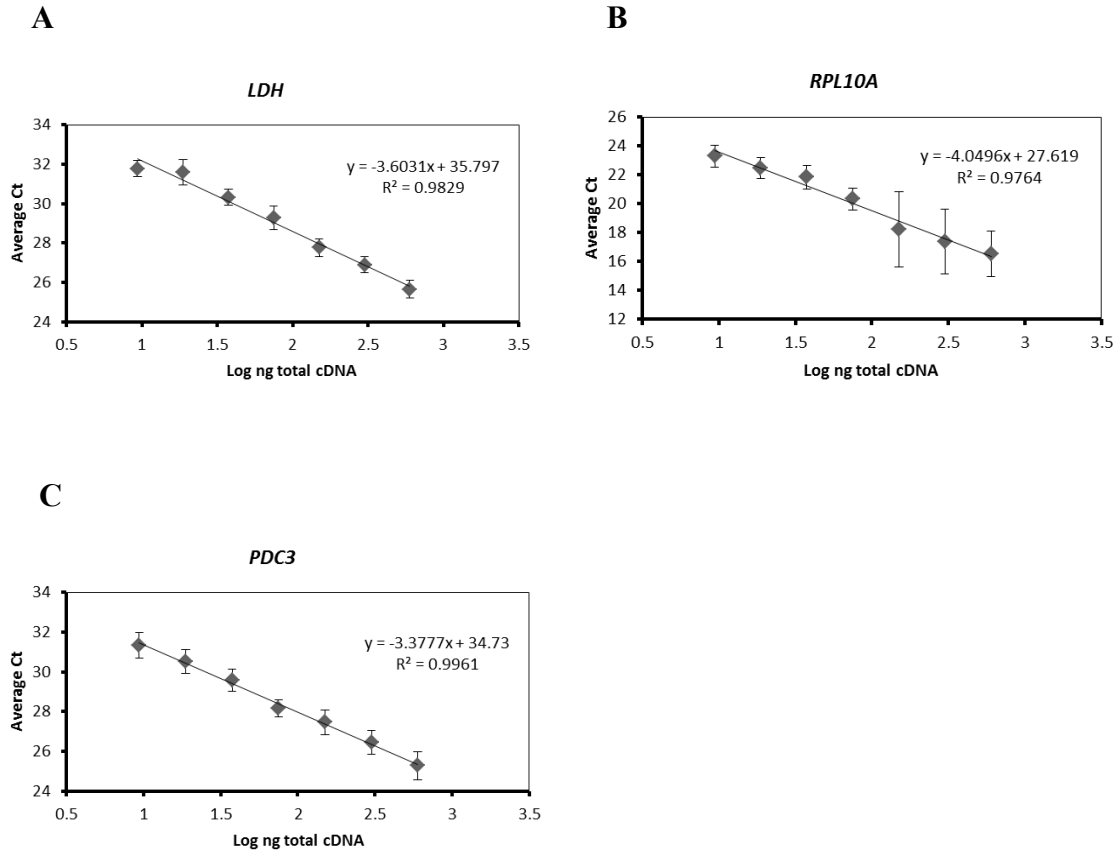


**Figure 6.3.2. Standard curves for *LDH*, *RPL10A* and *PDC3*.**

Error bars represent standard error of three biological replicates (each with two technical replicates).

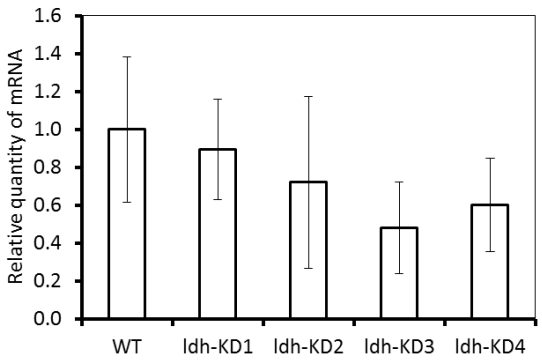


**Figure 6.3.3. *PDC3* transcript level of *ldh*-KD mutants.**

Transcript levels were measured by using qRT-PCR. Average values (±SE) were based on three biological replicates with two technical replicates each.

## Appendix 4. D-LDH activity assays

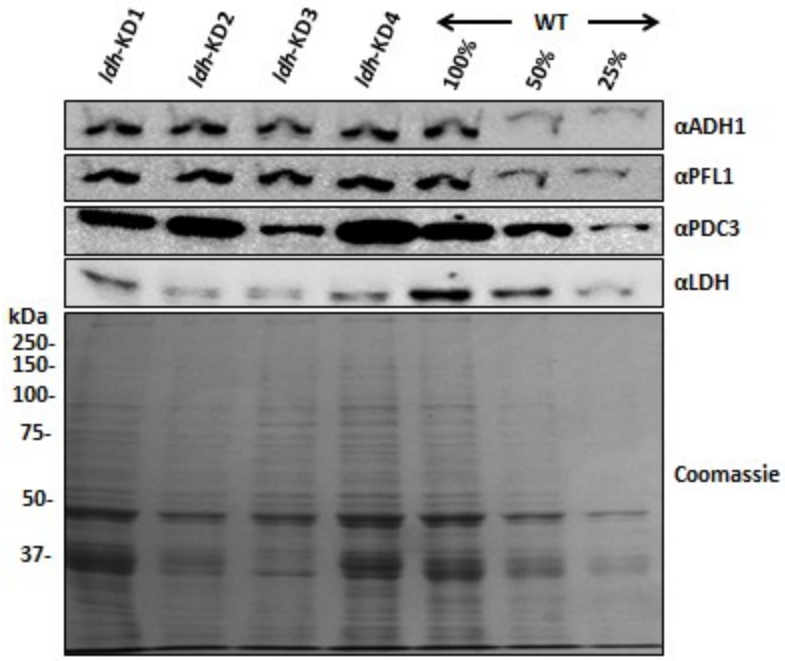


**Figure 6.4.1. Protein quantitative analyses of cell-free extracts.**

Cells were grown in TAP medium to late log phase and concentrated to one tenth of the original volume. The cells were lysed with ultrasonicator, and the protein-containing supernatants were collected after removing the unbroken cells and cellular debris by centrifugation. Protein samples were analysed by immunoblotting. Loading controls were provided by Coomassie Brilliant Blue staining, αPDC3, αPFL1 and αADH1.

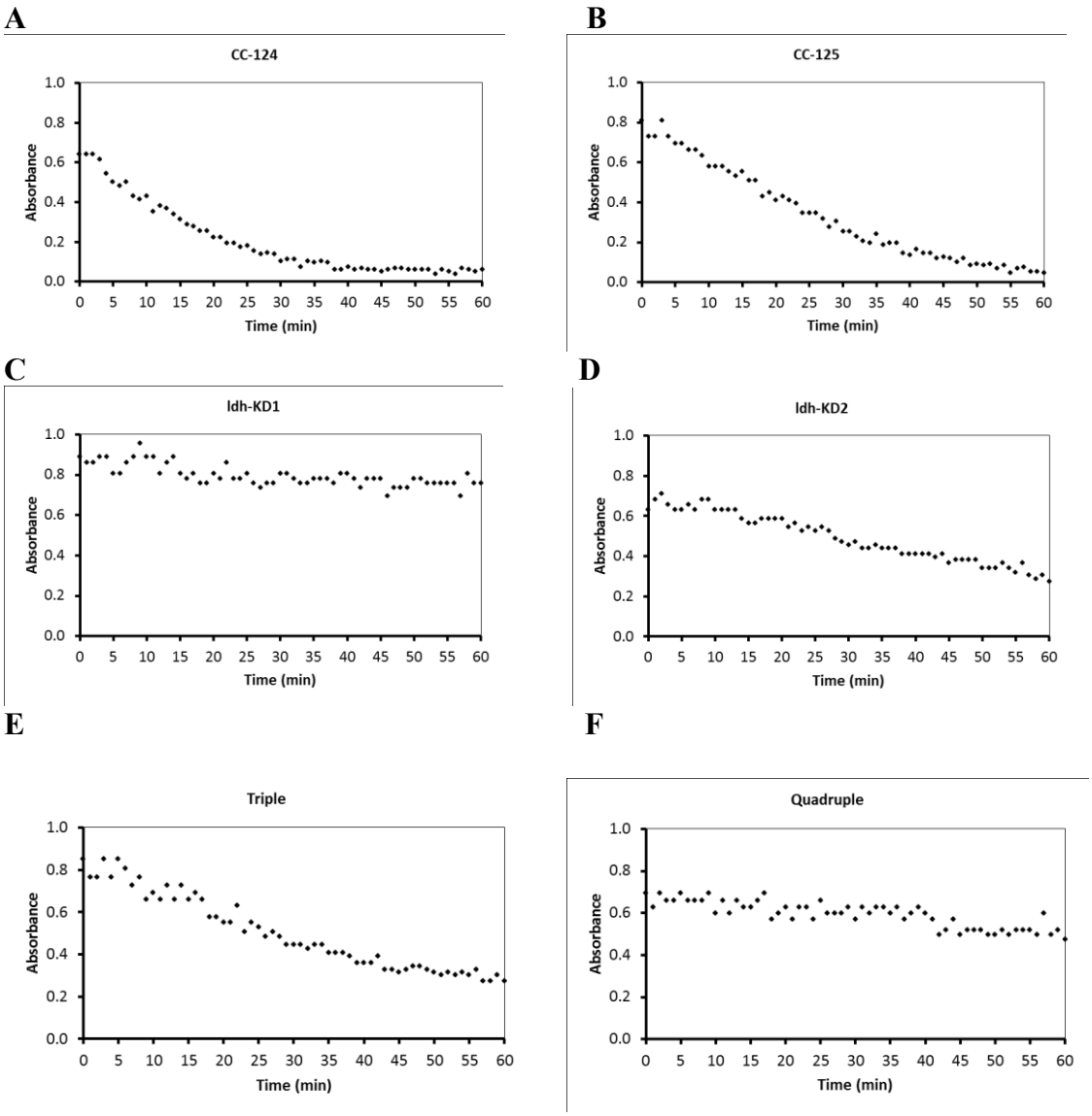


**Figure 6.4.2. NAD$^+$-dependent *C. reinhardtii* D-LDH activity assays.**

The *C. reinhardtii* D-LDH enzymatic activity in the presence of 300 μM NADH and 10 mM sodium pyruvate was determined by measuring the changes in absorbance at 340 nm. All assays were performed in three biological replicates, and only representative result is shown. Total amounts of proteins used for the 1-ml assay mixture were (A) 0.272, (B) 0.283, (C) 0.224, (D) 0.265, (E) 0.342, and (F) 0.230 mg.

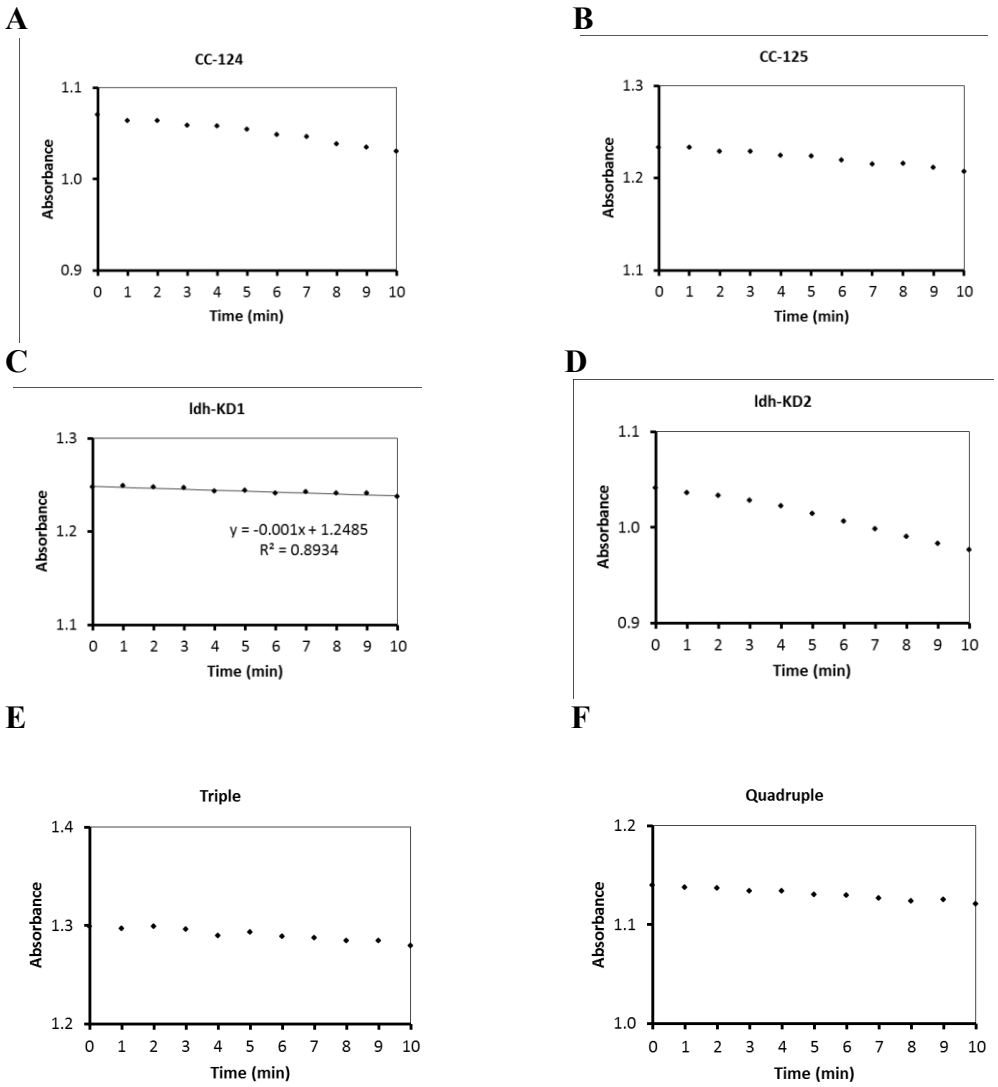


**Figure 6.4.3. NADH assays.**

The rates of NADH oxidised was measured without adding pyruvate into the 1-ml assay mixture. All assays were performed in three biological replicates, and only representative result is shown. The rates for the above reactions were calculated to be (A) 2.30, (B) 1.48, (C) 1.26, (D) 3.15, (E) 0.89, and (F) 1.19 nmol/min/mg proteins. Total amounts of proteins used for the 1-ml assay mixture were as above.

## Appendix 5. Quantification of D-LDH from cells grown under low and high light

### A) Low light

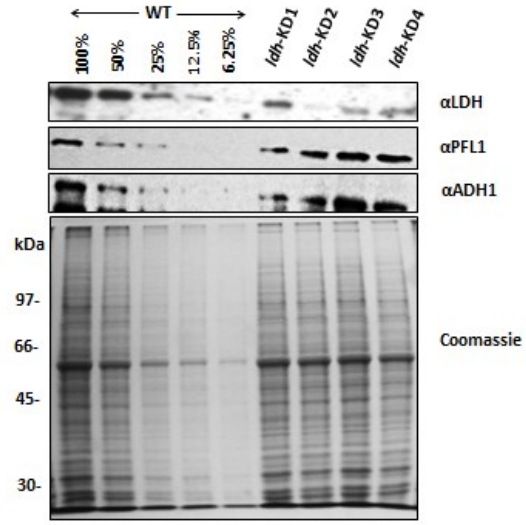


### B) High light

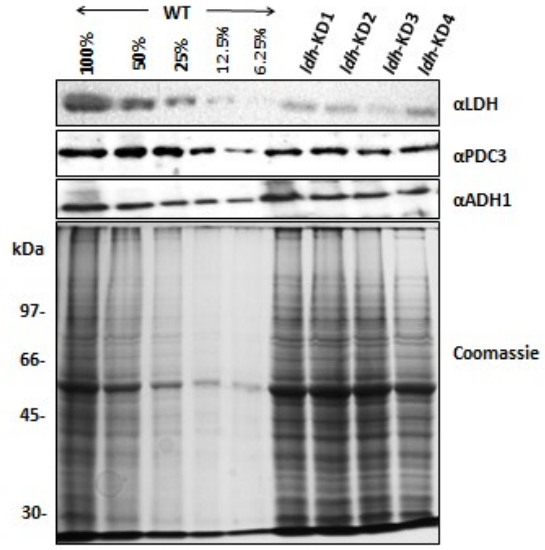


**Figure 6.5. Protein quantitative analyses of cells grown under low and high light.**
WT (CC-124) and *ldh*-KD mutants were grown to late log phase in HSM which was constantly stirred and bubbled with air. The cells were exposed either to low (30 $\mu Em^{-2}s^{-1}$) or high light (150 $\mu Em^{-2}s^{-1}$). The proteins were quantified using immunoblotting. Loading controls were provided by Coomassie Brilliant Blue staining, αPDC3, αPFL1 and αADH1.

## Appendix 6. Optimisation of chlorophyll amount for photoinhibition assays

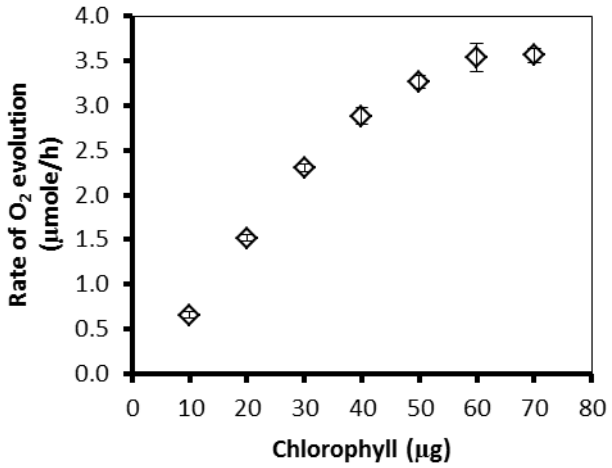


**Figure 6.6. Rate of oxygen evolution with different amounts of chlorophyll.**

A dilution series of HSM-grown *C. reinhardtii* cells was prepared and the chlorophyll concentrations were determined. Oxygen measurements were determined for these dilution series in the presence of DCBQ and KFeCN. Average values (±SE) were based on three technical replicates. The result showed at 50 µg of chlorophyll and above, light was a limiting factor under the conditions tested. Therefore, for the determination of light-saturated rate of oxygen evolution, the working chlorophyll amounts had to be less than 50 µg under similar conditions.

## Appendix 7. Cells treated under dark anaerobic conditions

### A) No PFL1 inhibitor added

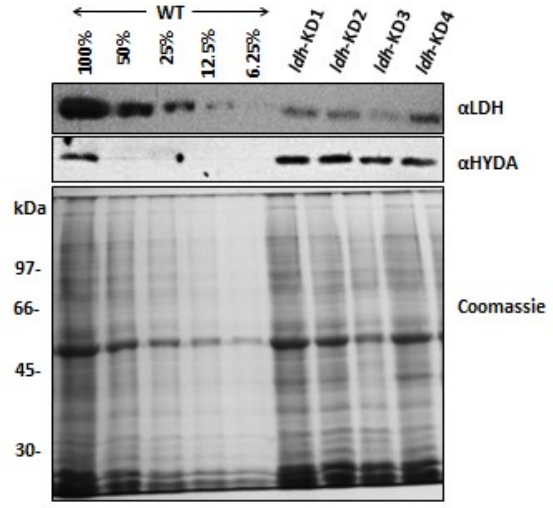


### B) PFL1 inhibitor added

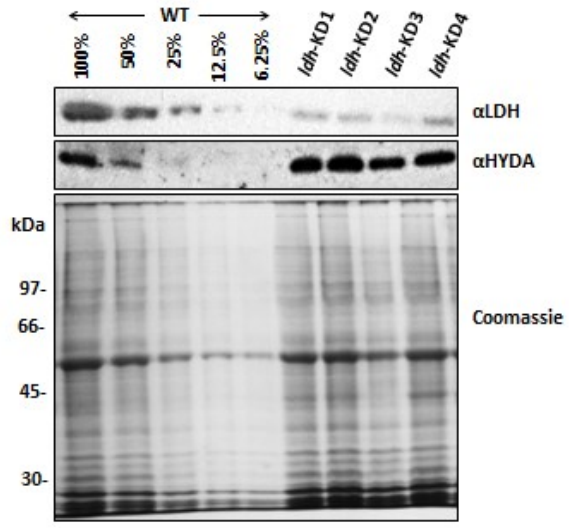


**Figure 6.7.1. Protein quantitative analyses of cells treated under dark anaerobic conditions.**

Cells grown in TAP medium to late log phase were resuspended in HSM to a chlorophyll concentration of ~150 µg/ml. PFL1 inhibitor (sodium hypophosphite) was either not added or added into the cell suspension. After purging with argon, the cells were left in an air-tight vial in the dark. Protein samples were collected after 4 hours, and analysed by using immunoblotting. Loading controls were provided by Coomassie Brilliant Blue staining and αPFL1. αHYDA (recognising both HYDA1 and HYDA2) was used to confirm cells were anaerobic.

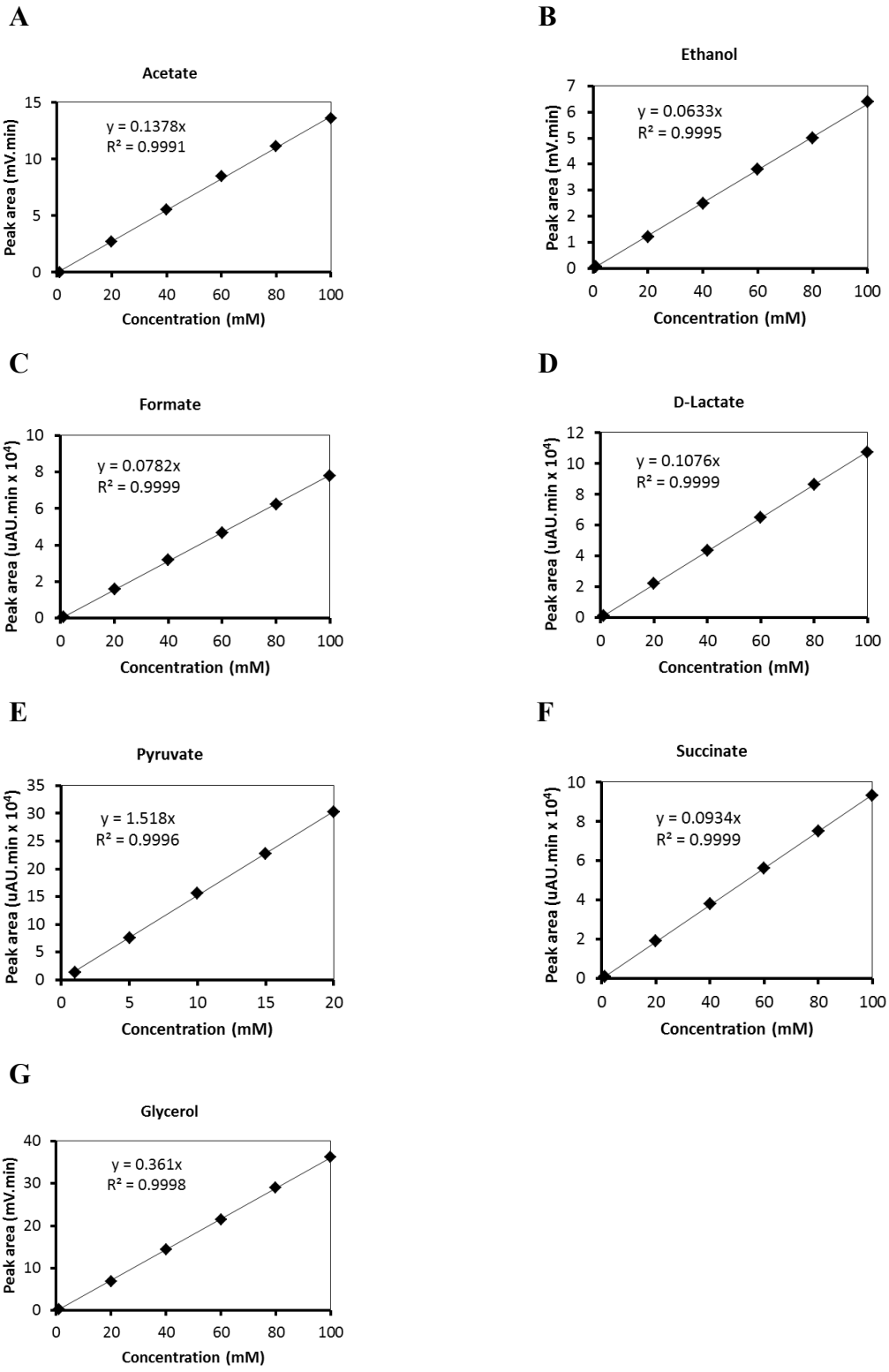


**Figure 6.7.2. Standard curves for HPLC analysis.**

A dilution series for each standard was prepared and run on a HPLC. Each standard produced a distinctive peak, and the peak area was quantified. The standard curves for acetate, ethanol and glycerol were generated by using the data obtained from the refractive index (RI) detector while the other metabolites from the UV/Vis spectrophotometer.

**A**

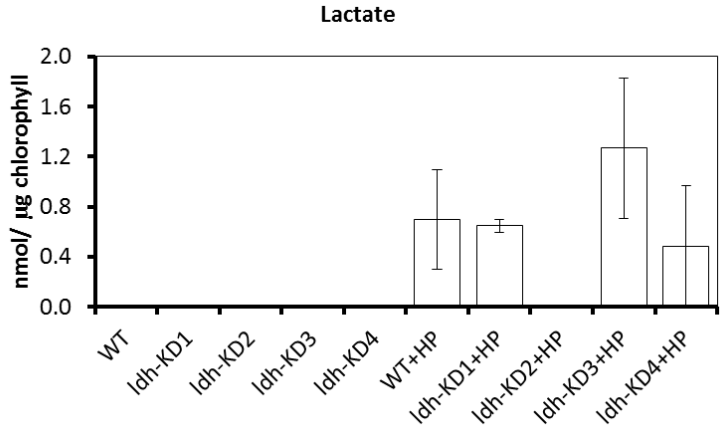


**B**

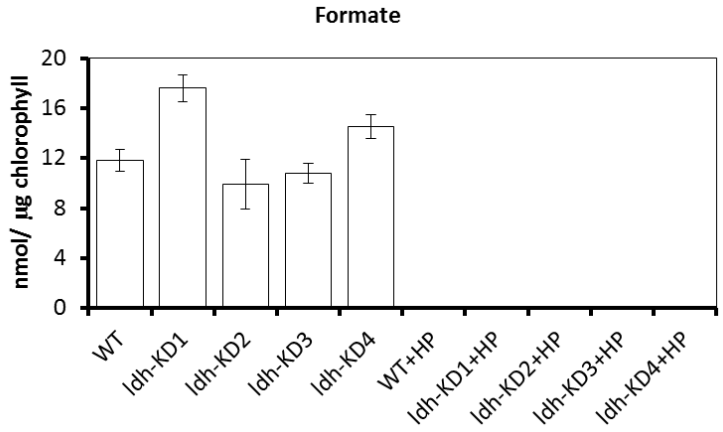


**Figure 6.7.3. HPLC analysis of *ldh*-KD mutants by using RI.**

When a sample was run on a HPLC, it could be analysed either by UV/Vis spectrophotometer or refractive index (RI) detector. This appendix is to re-confirm the HPLC analysis using the UV/Vis absorbance, as discussed in Chapter 3. The excreted metabolites were quantified after 4 hours of dark anaerobic incubation in HSM. Average values (±SE) were based on three biological replicates, and the values were normalized to the amount of total chlorophyll. Samples were also treated with 10 mM sodium hypophosphite (HP) to inhibit PFL1.

## Appendix 8. Cells incubated in TAP-S medium

**(I)** **(II)**

**A**

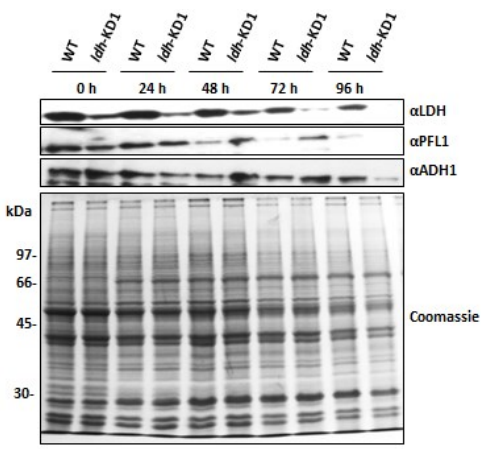


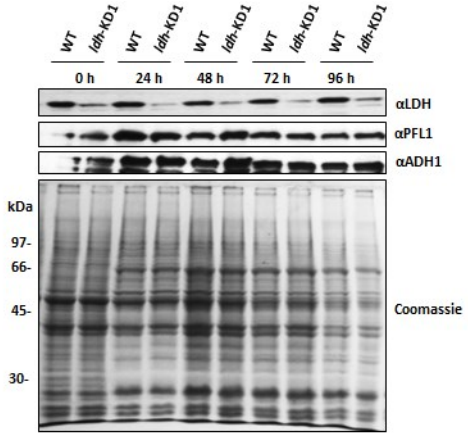


**B**

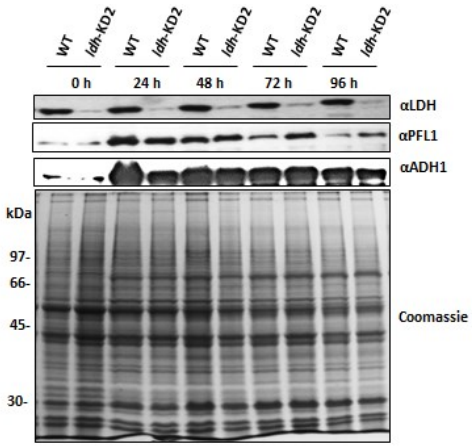


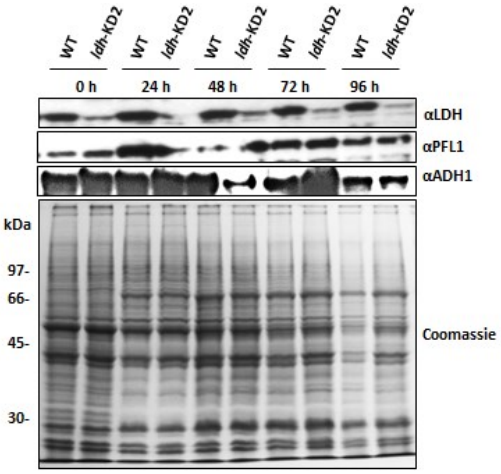


**C**

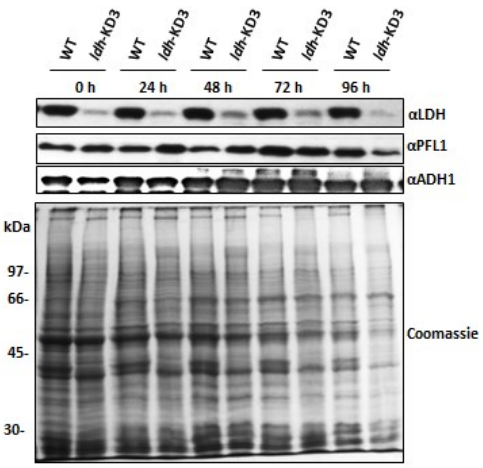


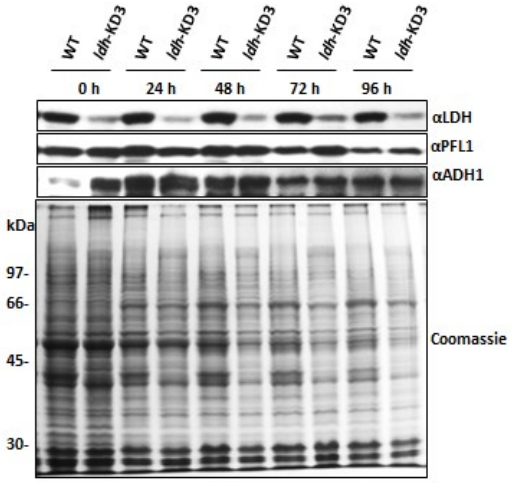

**D**

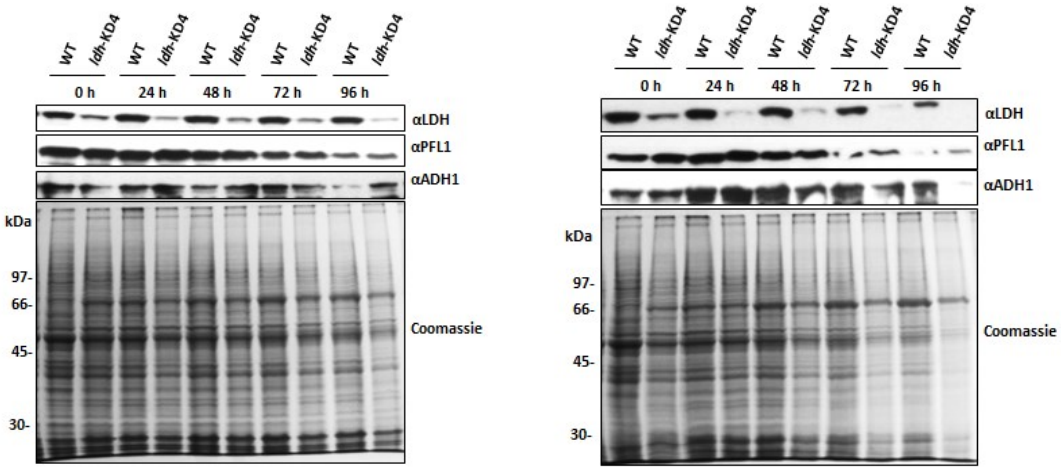


**Figure 6.8. Protein quantitative analyses of cells incubated in TAP-S medium.**

Cells grown in TAP medium to late log phase were harvested and resuspended in TAP-S medium to a chlorophyll concentration of ~15 μg/ml. PFL1 inhibitor (sodium hypophosphite) was either not added (I) or added (II) into the cell suspension. The cells were incubated in an air-tight bioreactor under high light (150 $\mu Em^{-2}s^{-1}$). Protein samples were collected every 24 hour, and analysed by immunoblotting. Loading controls were provided by Coomassie Brilliant Blue staining, αPFL1 and αADH1.

## Appendix 9. Determination of intracellular pyruvate concentrations

**(I)**

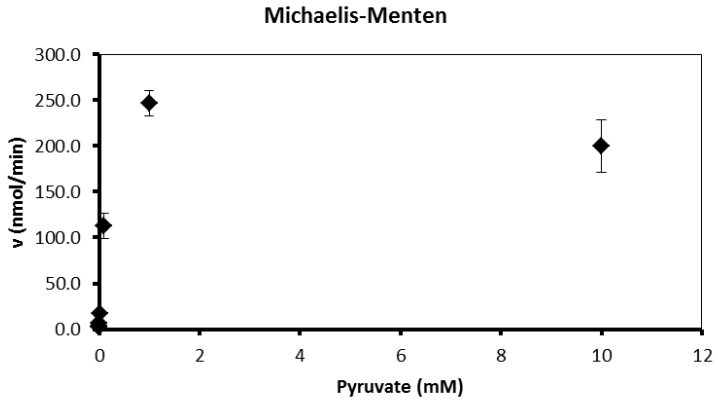


**(II)**

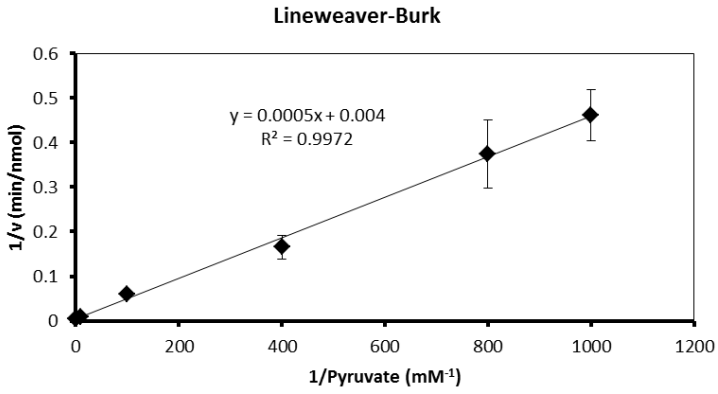


**Figure 6.9.1. Pyruvate standard curve.**

The rates of NADH oxidation by *L. leichmannii* D-LDH were measured by using pyruvate solutions of differing concentrations i.e. 0.001, 0.00125, 0.0250, 0.01, 0.1, 1 and 10 mM. All assays were performed in triplicate. Michaelis-Menten plot (I) was plotted using the average values (±SE) and the reciprocal of this plot, Lineweaver-Burk plot (II) was used as the standard curve.

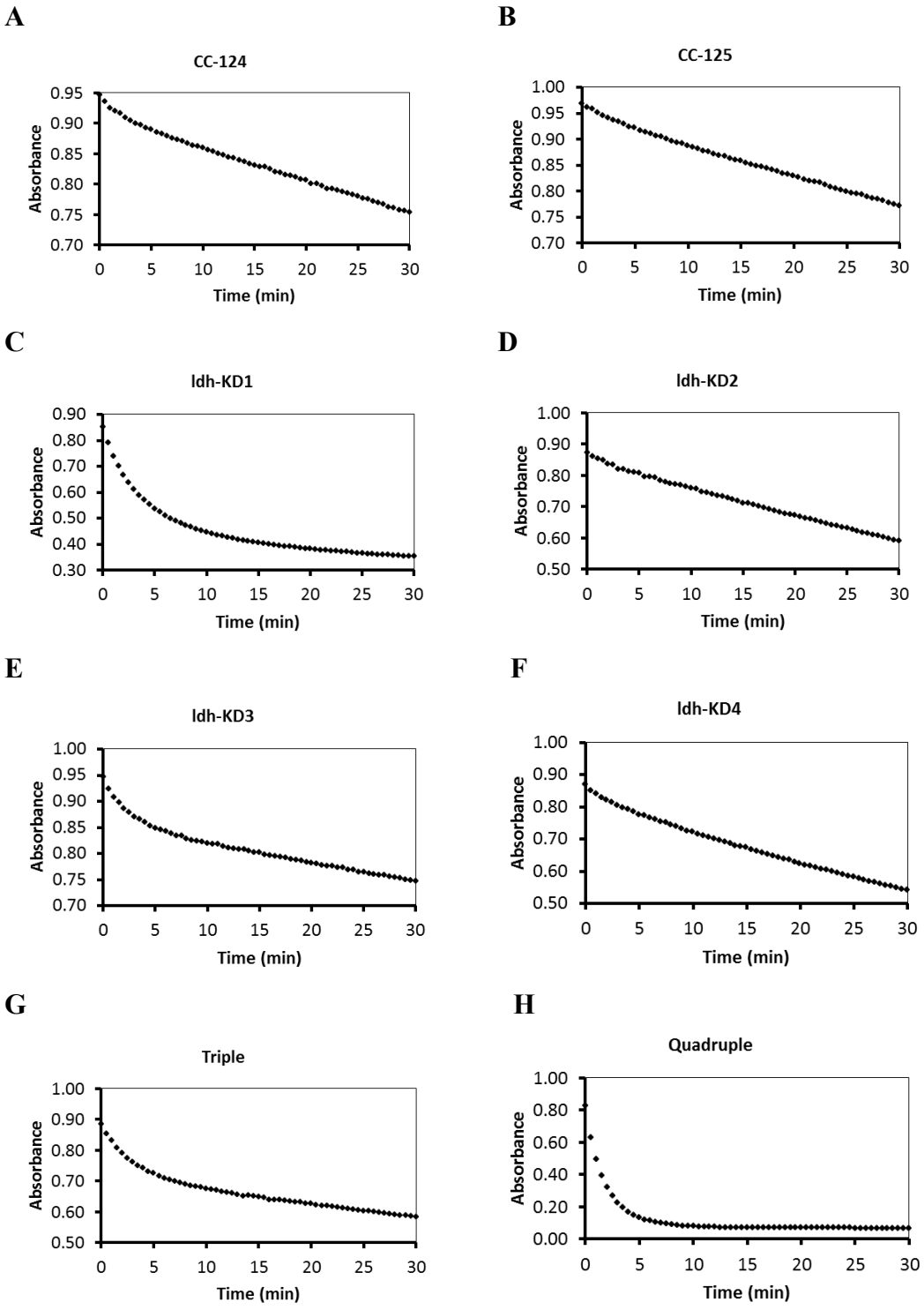


**Figure 6.9.2. $NAD^+$-dependent *L. leichmannii* LDH activity assays.**

The *L. leichmannii* D-LDH enzymatic activity in the presence of 300 μM NADH was determined by measuring the changes in absorbance at 340 nm. All assays were performed in three biological replicates, and only representative result is shown. Total amounts of proteins used for the 1-ml assay mixture were (A) 1.31, (B) 0.76, (C) 1.12, (D) 1.33, (E) 0.73, (F) 1.32, (G) 1.71 , and (H) 1.19 mg.

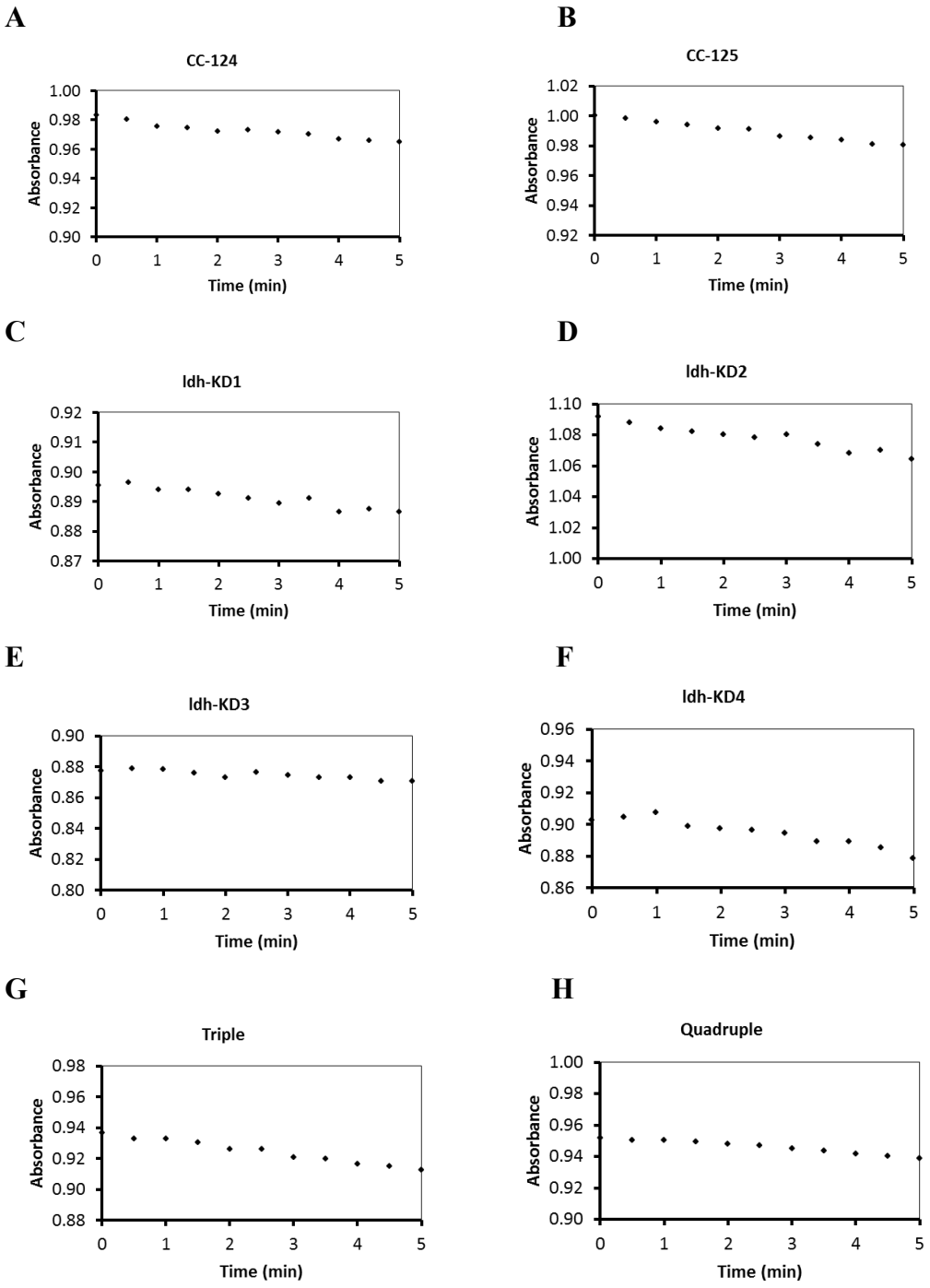


**Figure 6.9.3. NADH assays.**

The rates of NADH oxidised was measured without adding *L. leichmannii* D-LDH enzyme into the 1-ml assay mixture. All assays were performed in three biological replicates, and only representative result is shown. The rates for the above reactions were calculated to be (A) 2.30, (B) 1.48, (C) 1.26, (D) 3.15, (E) 1.78, (F) 2.08, (G) 0.89, and (H) 1.19 nmol/min/mg proteins. Total amounts of proteins used for the 1-ml assay mixture were as above.

## Appendix 10. Stereospecific configuration specificity of LDHs

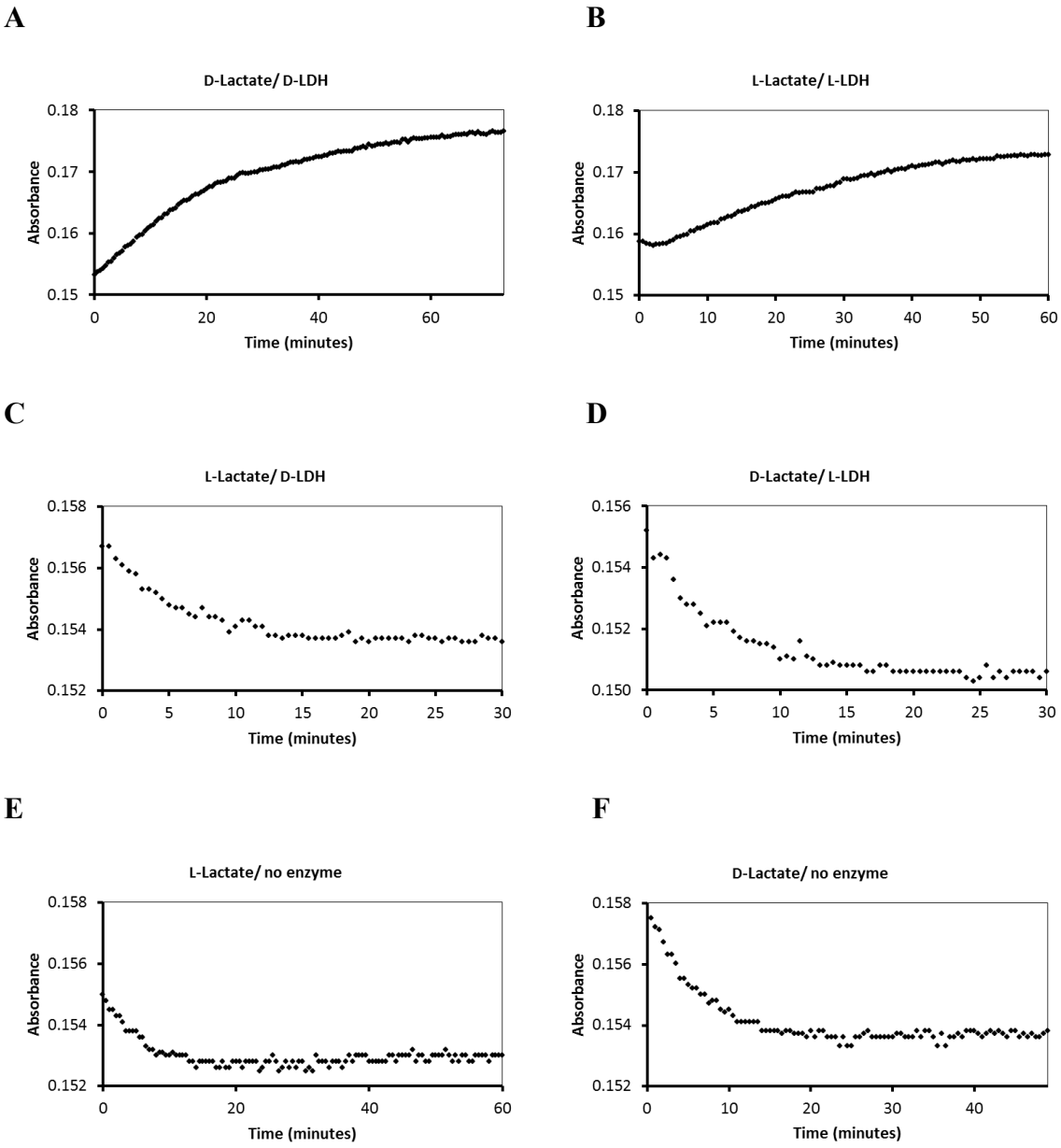


**Figure 6.10. Stereospecific configuration specificity of LDHs.**

To test the specificity of *L. leichmanii* D-LDH and *E. coli* L-LDH, lactate assays were carried out. The 1 ml reaction mixture contained 12.5 mM sodium phosphate at pH 7.5, 125 mM sodium chloride and 3 mM $NAD^+$. We added 500 µl of either sodium D-lactate or L-lactate solution (solution was prepared using HSM). This volume should contain 0.1 µmole of sodium lactate. The reaction was initiated by adding 0.2 and 0.02 unit of D-LDH and L-LDH, respectively (1 unit would reduce 1 µmole of pyruvate to lactate per min). Controls were also carried out whereby no enzyme was added into the reaction mixture. The absorbance was recorded at 340 nm.

## Appendix 11. Cell mating

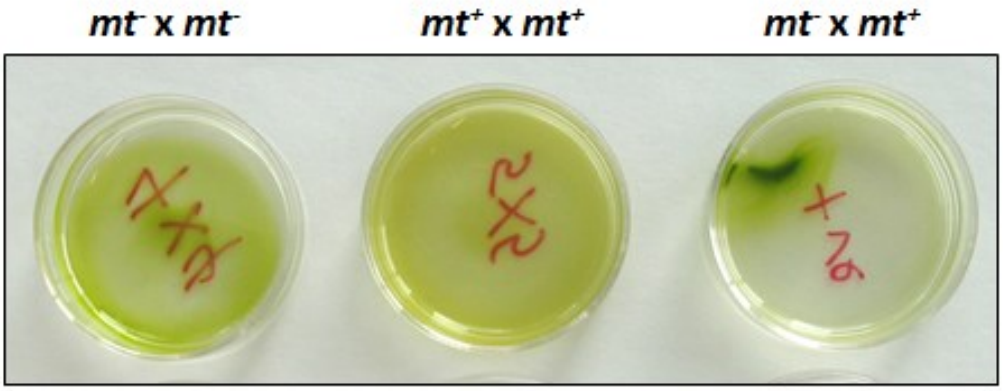


**Figure 6.11. Testing mating efficiency.**

*C. reinhardtii* cells can only be mated together if they are of the opposite mating types. The cells can either be of a mating type *plus* ($mt^+$) or *minus* ($mt^-$). Mated cells stick together while cells that have not mated easily resuspend after shaking.

**Appendix 12. Comparison of growth between CC-124 and CC-125**

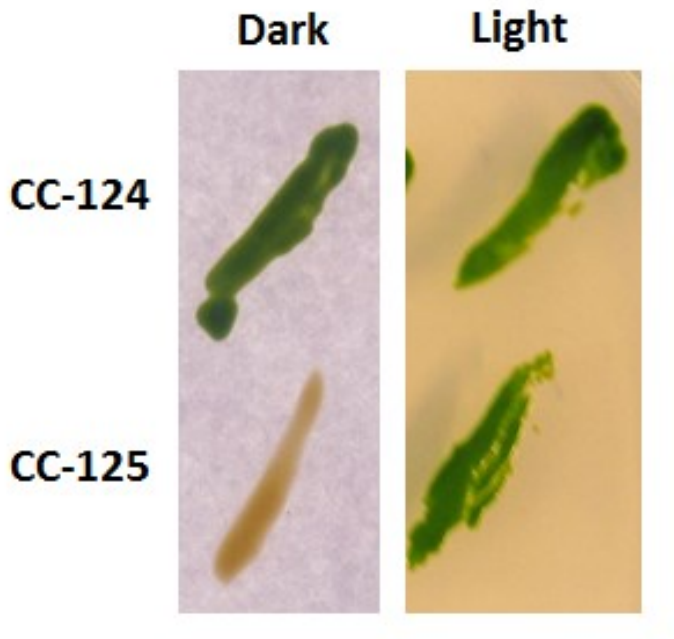


**Figure 6.12. Cell growth under dark and light conditions.**

WT cells were streaked onto TAP agar plates, and were left to grow either in the dark or under light (30 $\mu Em^{-2}s^{-1}$). Photos were taken after ten days of cell growth.

## Appendix 13. Cells treated under dark anaerobic conditions

### A) Quadruple

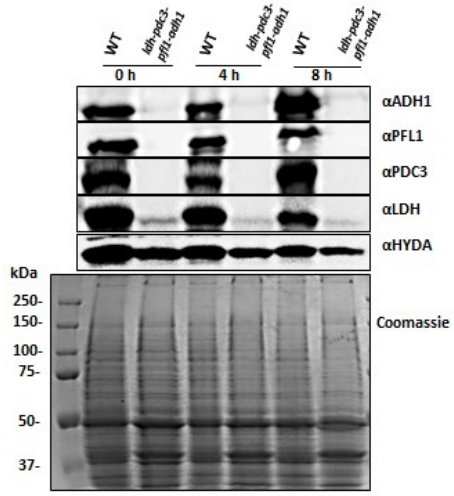


### B) Triple

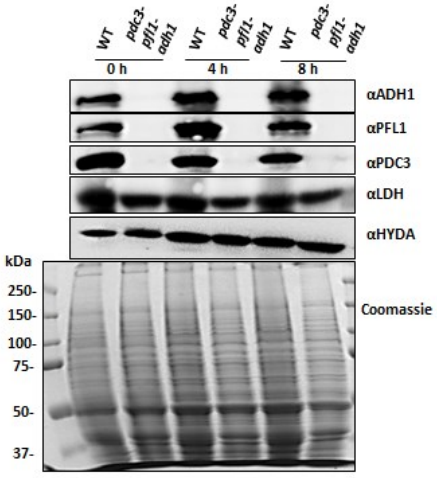


### C) *ldh-pfl1-adh1*

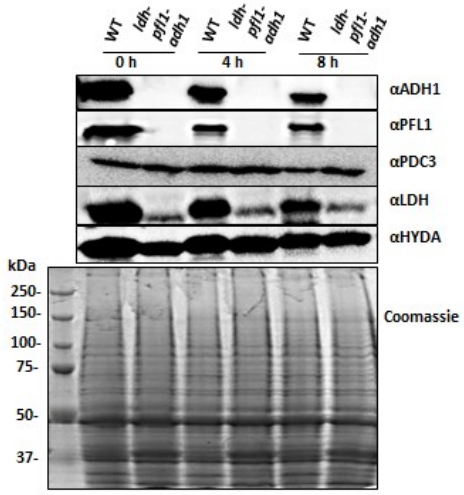


### D) *ldh-pdc3-adh1*

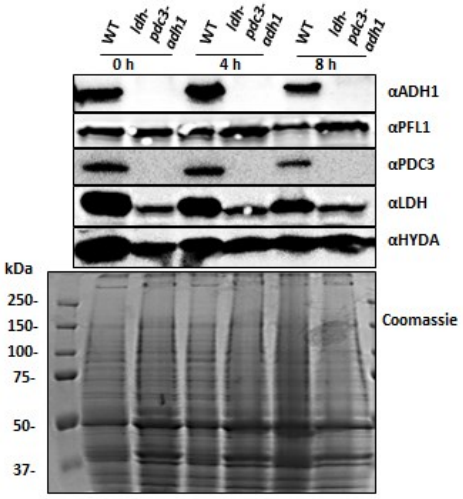


### E) *ldh-pdc3-pfl1*

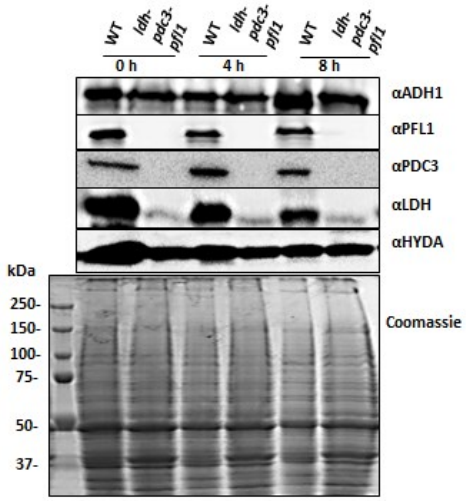


### F) *pfl1-adh1*

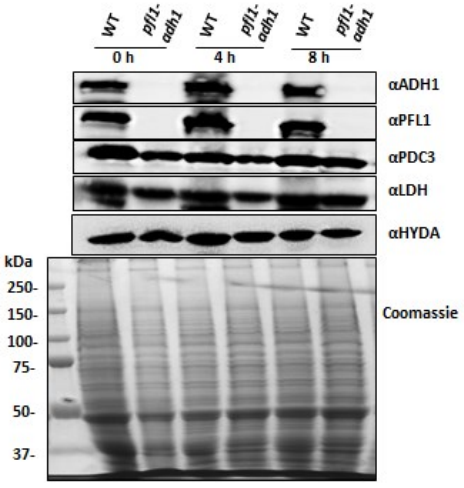


*adh1*

**G) *pdc3-pfl1***

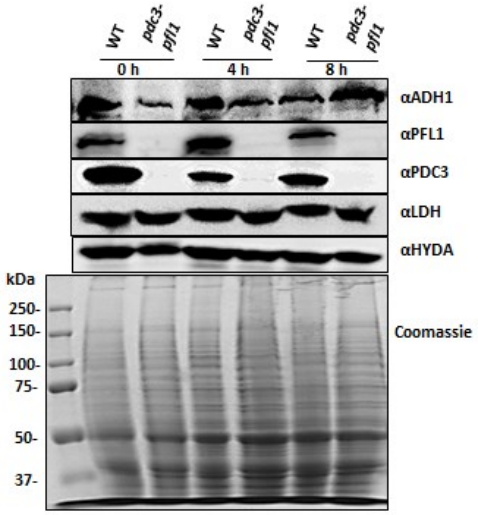


**H) *pdc3-adh1***

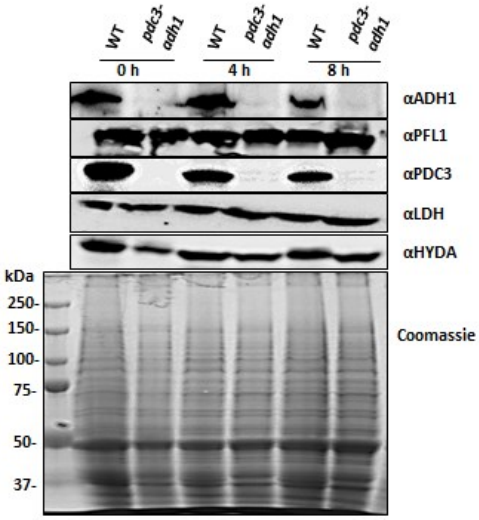


**I) *ldh-pdc3***

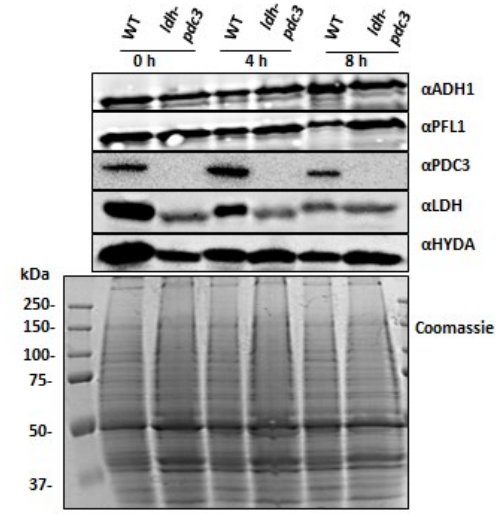


**J) *ldh-pfl1***

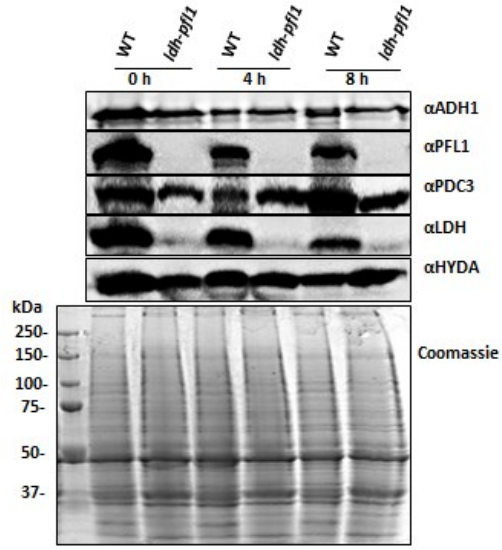


**K) *ldh-adh1***

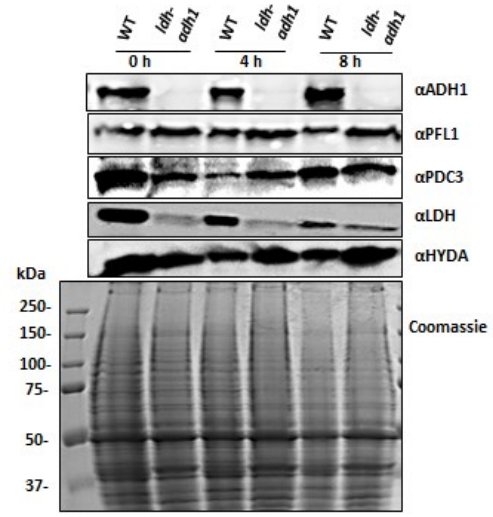


**L) *ldh*-KD1**

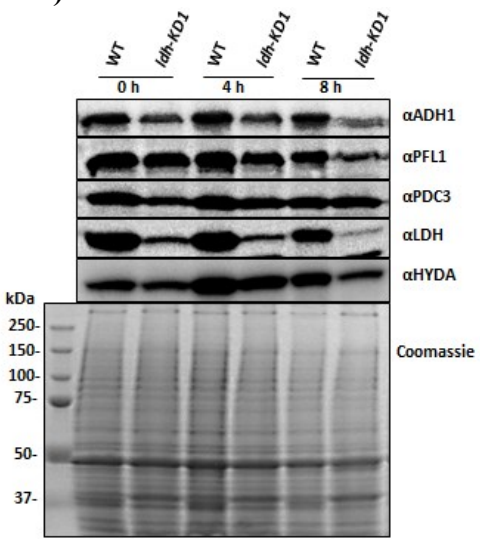

**M) *pdc3* (4th backcross)**

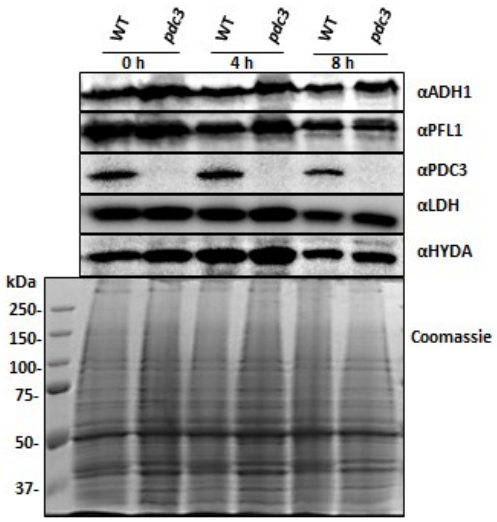


**N) *pfl1***

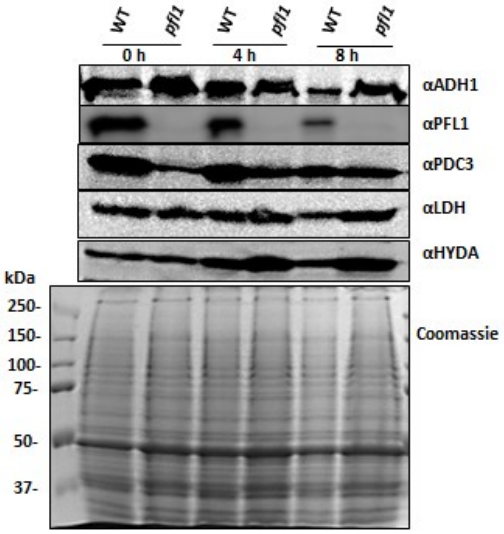


**O) *adh1***

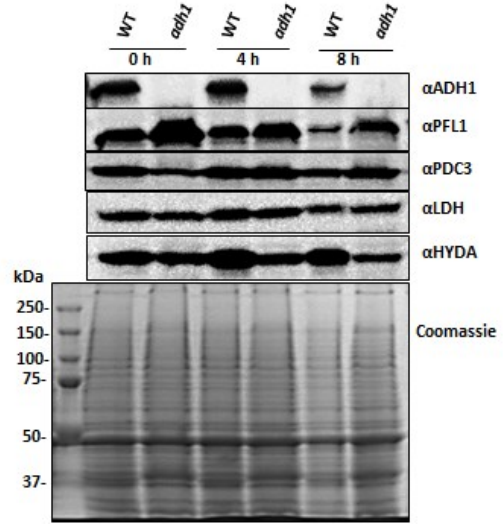


**Figure 6.13.1. Protein quantitative analyses of cells treated under dark anaerobic conditions.**

Cells grown in TAP medium to late log phase were harvested and resuspended in HSM to a chlorophyll concentration of ~150 µg/ml. After purging with argon, the cells were left in an air-tight vial in the dark. Protein samples were collected at different time points, and analysed by immunoblotting. Loading control was provided by Coomassie Brilliant Blue staining while αHYDA (recognising both HYDA1 and HYDA2) was used to confirm cells were anaerobic. The WT strain used was CC-124.

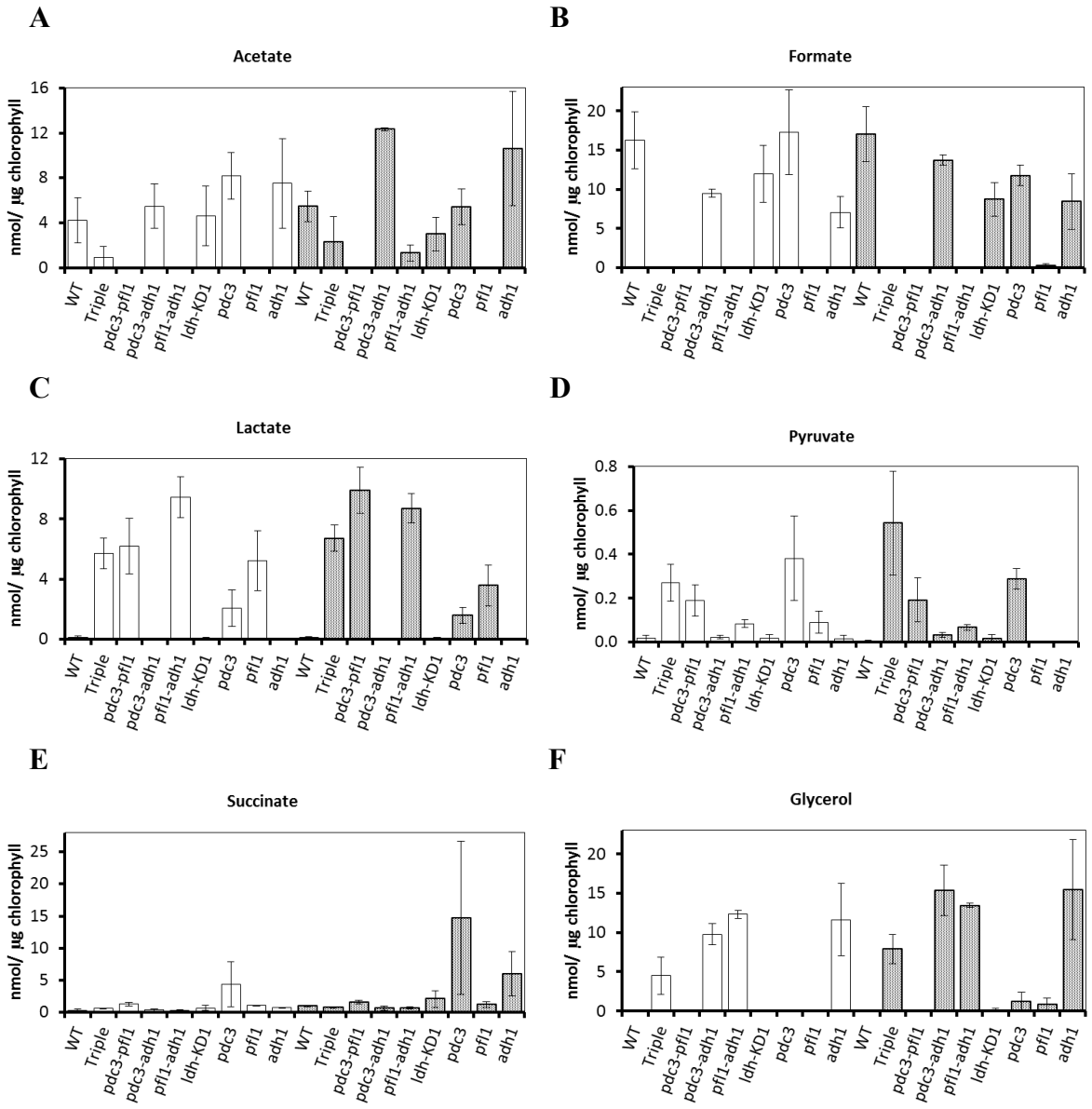


**Figure 6.13.2. HPLC analysis of dark fermentative metabolites.**

Average values (±SE) were based on three independent biological replicates. The excreted metabolites were quantified after 4 hours (white bars) and 8 hours (grey bars) of dark anaerobic incubation in HSM. The values obtained were normalized to the amounts of total chlorophyll. Ethanol (data not shown) could not be quantified for some samples because of the unavailability of the data processing software (Chrompass; Jasco, UK), as this metabolite had to be manually quantified unlike the other metabolites. The WT strain used was CC-124.

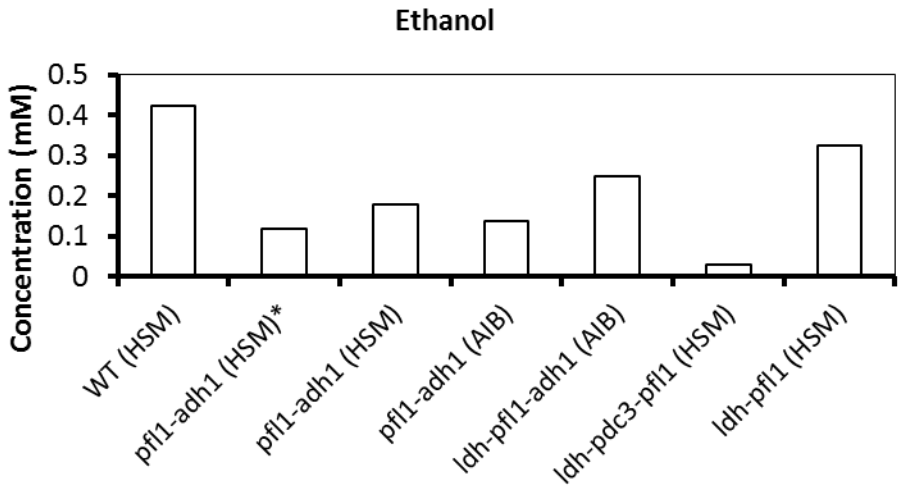


**Figure 6.13.3. Ethanol analysis.**

Ethanol produced under dark anaerobic conditions was quantified by using an enzyme-based assay kit (R-biopharm, UK). Preliminary analysis is based on one replicate. Cells were incubated in either AIB or HSM. Samples that had been previously quantified by NMR and HPLC were also re-analysed by using the kit i.e. pfl1-adh1 (HSM)*.

**A) CC-124**

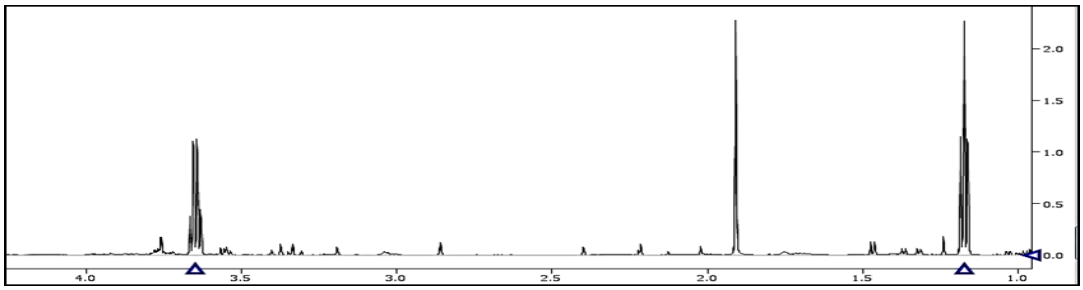


**B) *pfl1-adh1***

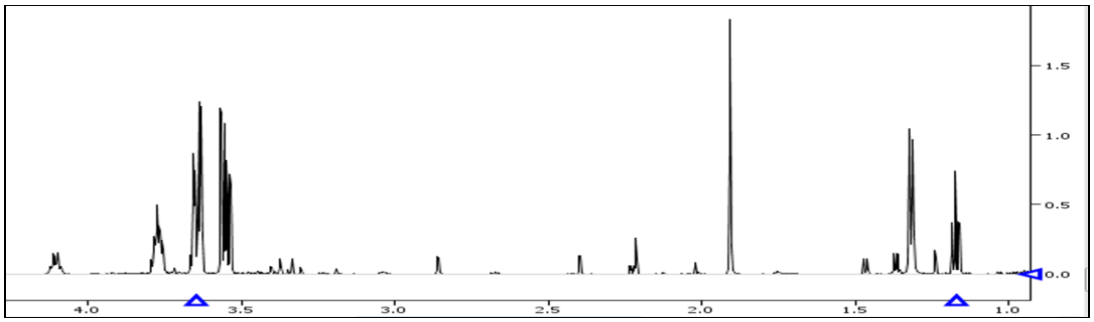


**C) *ldh-pfl1-adh1***

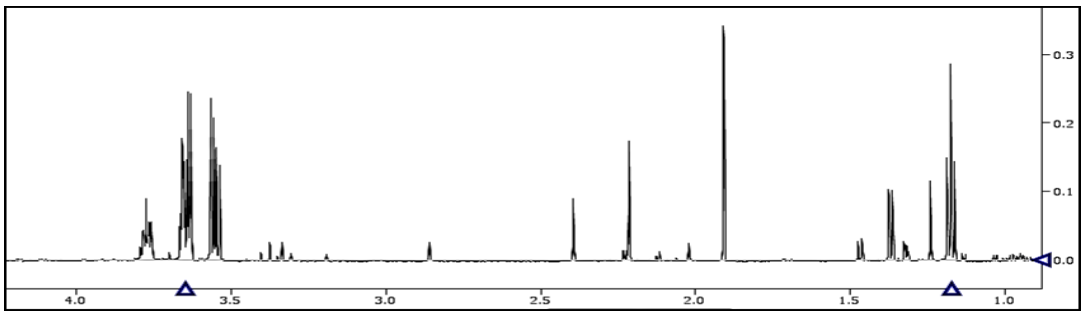


**D) Quadruple**

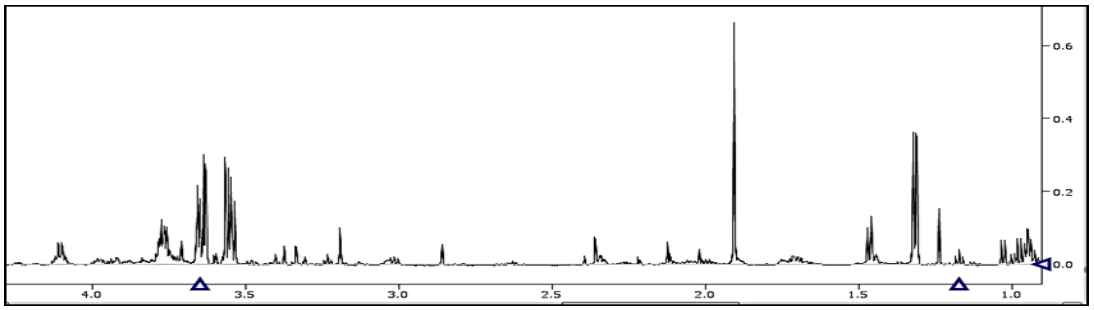


**Figure 6.13.4. Representative NMR spectra showing ethanol signals.**

Ethanol signals could be found at 3.6 and 1.2 ppm. Spectra were generated by using the Chenomx NMR Suite.

## Appendix 14. Cells incubated in TAP-S medium

### A) Quadruple

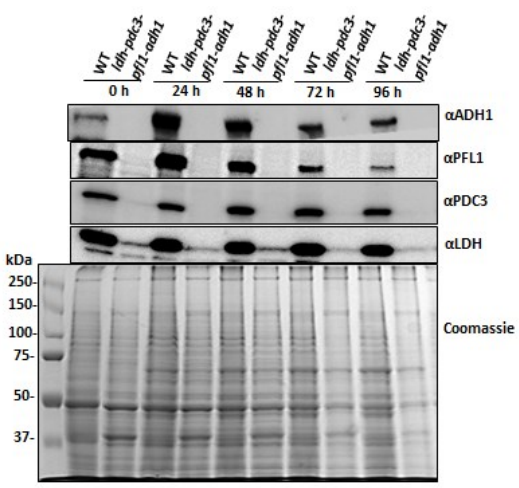


### B) Triple

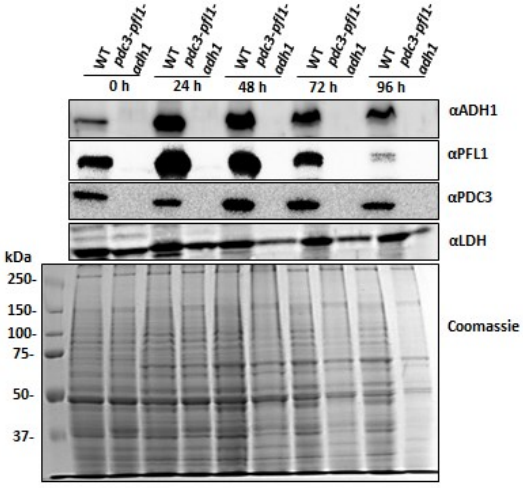


### C) *pdc3-pfl1*

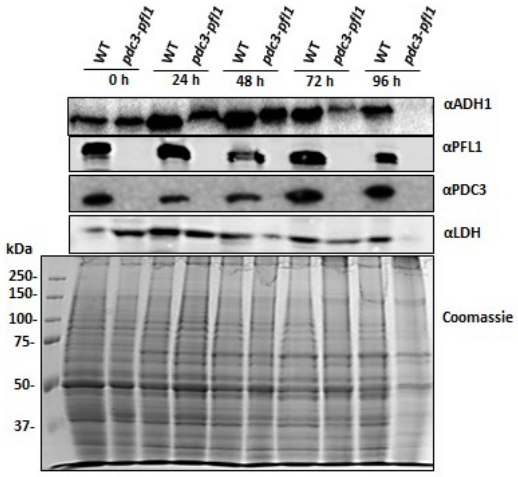


### D) *pdc3-adh1*

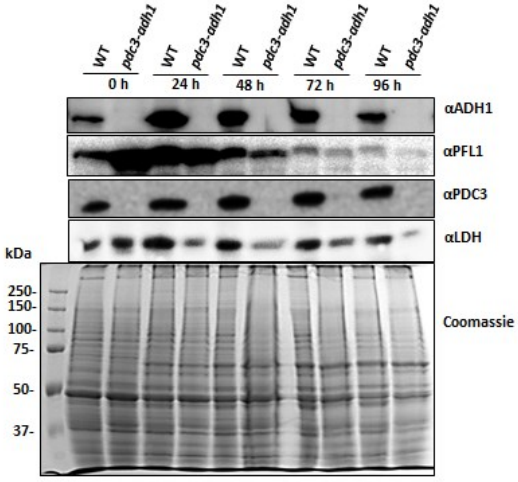

**E) *pfl1-adh1***

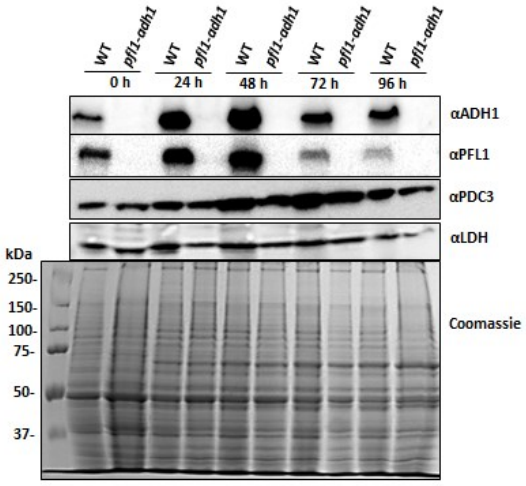


**Figure 6.14. Protein quantitative analyses of cells incubated in TAP-S medium.**

Cells grown in TAP medium to late log phase were harvested and resuspended in TAP-S medium to a chlorophyll concentration of ~15 µg/ml. The cells were incubated in an air-tight bioreactor and were exposed to high light (~150 $\mu Em^{-2}s^{-1}$). Protein samples were collected every 24 hour, and analysed by immunoblotting. Loading control was provided by Coomassie Brilliant Blue staining. The WT strain used was CC-124.

## References


Abad-Zapatero C, Griffith JP, Sussman JL, Rossmann MG (1987). Refined crystal structure of dogfish M4 apo-lactate dehydrogenase. *Journal of Molecular Biology* **198**: 445-467.

Adams MJ, Ford GC, Liljas A, Rossmann MG (1973). Atomic co-ordinates for dogfish M4 apo-lactate dehydrogenase. *Biochemical and Biophysical Research Communications* **53**: 46-51.

Akkerman I, Janssen M, Rocha J, Wijffels RH (2002). Photobiological hydrogen production: photochemical efficiency and bioreactor design. *International Journal of Hydrogen Energy* **27**: 1195-1208.

Antonyuk SV, Strange RW, Ellis MJ, Bessho Y, Kuramitsu S, Inoue Y *et al* (2009). Structure of d-lactate dehydrogenase from *Aquifex aeolicus* complexed with $NAD^+$ and lactic acid (or pyruvate). *Acta Crystallographica Section F* **65**: 1209-1213.

Asamizu E, Nakamura Y, Miura K, Fukuzawa H, Fujiwara S, Hirono M *et al* (2004). Establishment of publicly available cDNA material and information resource of *Chlamydomonas reinhardtii* (Chlorophyta) to facilitate gene function analysis. *Phycologia* **43**: 722-726.

Asanuma N, Yoshii T, Hino T (2004). Molecular characteristics and transcription of the gene encoding a multifunctional alcohol dehydrogenase in relation to the deactivation of pyruvate formate-lyase in the ruminal bacterium *Streptococcus bovis*. *Arch. Microbiol.* **181**: 122-128.

Asker H, Davies DD (1984). The physiological role of the isoenzymes of lactate dehydrogenase in potatoes. *Planta* **161**: 272-280.

Atteia A, van Lis R, Mendoza-Hernández G, Henze K, Martin W, Riveros-Rosas H *et al* (2003). Bifunctional aldehyde/alcohol dehydrogenase (ADHE) in chlorophyte algal mitochondria. *Plant Mol. Biol.* **53**: 175-188.

Atteia A, van Lis R, Gelius-Dietrich G, Adrait A, Garin J, Joyard J *et al* (2006). Pyruvate Formate-lyase and a Novel Route of Eukaryotic ATP Synthesis in *Chlamydomonas* Mitochondria. *Journal of Biological Chemistry* **281**: 9909-9918.

Atteia A, Adrait A, Brugière S, Tardif M, van Lis R, Deusch O *et al* (2009). A Proteomic Survey of *Chlamydomonas reinhardtii* Mitochondria Sheds New Light on the Metabolic Plasticity of the Organelle and on the Nature of the α-Proteobacterial Mitochondrial Ancestor. *Molecular Biology and Evolution* **26**: 1533-1548.

Atteia A, van Lis R, Tielens AGM, Martin WF (2013). Anaerobic energy metabolism in unicellular photosynthetic eukaryotes. *Biochimica et Biophysica Acta (BBA) - Bioenergetics* **1827**: 210-223.

Auerbach G, Ostendorp R, Prade L, Korndörfer I, Dams T, Huber R *et al* (1998). Lactate dehydrogenase from the hyperthermophilic bacterium *Thermotoga maritima*: the crystal structure at 2.1 Å resolution reveals strategies for intrinsic protein stabilization. *Structure* **6**: 769-781.

Axley MJ, Grahame DA, Stadtman TC (1990). *Escherichia coli* formate-hydrogen lyase. Purification and properties of the selenium-dependent formate dehydrogenase component. *Journal of Biological Chemistry* **265**: 18213-18218.

Bafana A (2013). Characterization and optimization of production of exopolysaccharide from *Chlamydomonas reinhardtii*. *Carbohydrate Polymers* **95**: 746-752.

Baggetto LG, Lehninger AL (1987). Isolated tumoral pyruvate dehydrogenase can synthesize acetoin which inhibits pyruvate oxidation as well as other aldehydes. *Biochemical and Biophysical Research Communications* **145**: 153-159.

Balzani V, Credi A, Venturi M (2008). Photochemical Conversion of Solar Energy. *ChemSusChem* **1**: 26-58.

Banerjee A, Sharma R, Chisti Y, Banerjee UC (2002). Botryococcus braunii: A Renewable Source of Hydrocarbons and Other Chemicals. *Critical Reviews in Biotechnology* **22**: 245-279.

Bartel DP (2004). MicroRNAs: Genomics, Biogenesis, Mechanism, and Function. *Cell* **116**: 281-297.

Bartels JR, Pate MB, Olson NK (2010). An economic survey of hydrogen production from conventional and alternative energy sources. *International Journal of Hydrogen Energy* **35**: 8371-8384.

Beezley BB, Gruber PJ, Frederick SE (1976). Cytochemical localization of glycolate dehydrogenase in mitochondria of *Chlamydomonas*. *Plant Physiology* **58**: 315-319.

Benemann J (1996). Hydrogen biotechnology: Progress and prospects. *Nat. Biotech.* **14**: 1101-1103.

Benemann J (2000). Hydrogen production by microalgae. *Journal of Applied Phycology* **12**: 291-300.

Benemann JR, Weare NM (1974). Nitrogen fixation by *Anabaena cylindrica*. *Arch Microbiol* **101**: 401-408.

BERR (2008). Meeting the energy challenge: a white paper on nuclear power. Department of Business, Enterprise & Regulatory Reform, UK.

Betsche T (1981). L-Lactate dehydrogenase from leaves of higher plants. Kinetics and regulation of the enzyme from lettuce (*Lactuca sativa*). *Biochem. J.* **195**: 615-622.

Bisaillon A, Turcot J, Hallenbeck PC (2006). The effect of nutrient limitation on hydrogen production by batch cultures of *Escherichia coli*. *International Journal of Hydrogen Energy* **31**: 1504-1508.

Blokhina O, Fagerstedt KV (2010). Oxidative metabolism, ROS and NO under oxygen deprivation. *Plant Physiology and Biochemistry* **48**: 359-373.

Bollig K, Lamshöft M, Schweimer K, Marner F-J, Budzikiewicz H, Waffenschmidt S (2007). Structural analysis of linear hydroxyproline-bound O-glycans of *Chlamydomonas reinhardtii* - conservation of the inner core in *Chlamydomonas* and land plants. *Carbohydrate Research* **342**: 2557-2566.

Bölling C, Fiehn O (2005). Metabolite Profiling of *Chlamydomonas reinhardtii* under Nutrient Deprivation. *Plant Physiology* **139**: 1995-2005.

Bothe H, Schmitz O, Yates MG, Newton WE (2010). Nitrogen Fixation and Hydrogen Metabolism in Cyanobacteria. *Microbiology and Molecular Biology Reviews* **74**: 529-551.

Boynton J, Gillham N, Harris E, Hosler J, Johnson A, Jones A *et al* (1988). Chloroplast transformation in *Chlamydomonas* with high velocity microprojectiles. *Science* **240**: 1534-1538.

Bringezu S, Schutz H, O' Brien M, Kauppi L, Howarth RW, McNeely J (2009). Towards sustainable production and use of resources: assessing biofuels. UNEP.

Brocker C, Vasiliou M, Carpenter S, Carpenter C, Zhang Y, Wang X *et al* (2013). Aldehyde dehydrogenase (ALDH) superfamily in plants: gene nomenclature and comparative genomics. *Planta* **237**: 189-210.

Broderick JB, Henshaw TF, Cheek J, Wojtuszewski K, Smith SR, Trojan MR *et al* (2000). Pyruvate Formate-Lyase-Activating Enzyme: Strictly Anaerobic Isolation Yields Active Enzyme Containing a [3Fe–4S] Cluster. *Biochemical and Biophysical Research Communications* **269**: 451-456.

Bruhn H, Pohl M, Grötzinger J, Kula MR (1995). The replacement of Trp392 by alanine influences the decarboxylase/carboligase activity and stability of pyruvate decarboxylase from *Zymomonas mobilis*. *European Journal of Biochemistry* **234**: 650-655.

Bruin W, Nelson EB, Tolbert N (1970). Glycolate pathway in green algae. *Plant Physiology* **46**: 386-391.

Buehner M, Hecht H-J, Hensel R, Mayr U (1982). Crystallization and preliminary crystallographic analysis at low resolution of the allosteric l-lactate dehydrogenase from *Lactobacillus casei*. *Journal of Molecular Biology* **162**: 819-838.

Buhrke T, Lenz O, Krauss N, Friedrich B (2005). Oxygen Tolerance of the $H_2$-sensing [NiFe] Hydrogenase from *Ralstonia eutropha* H16 Is Based on Limited Access of Oxygen to the Active Site. *Journal of Biological Chemistry* **280**: 23791-23796.

Burgess SJ (2011). Investigating the link between fermentation and hydrogen production in the green alga *Chlamydomonas reinhardtii*. PhD thesis, Imperial College London, UK.

Burgess SJ, Tamburic B, Zemichael F, Hellgardt K, Nixon PJ (2011). Solar-driven hydrogen production in green algae. *Advances in applied microbiology* **75**: 71-110.

Burgess SJ, Tredwell G, Molnàr A, Bundy JG, Nixon PJ (2012). Artificial microRNA-mediated knockdown of pyruvate formate lyase (PFL1) provides evidence for an active 3-

hydroxybutyrate production pathway in the green alga *Chlamydomonas reinhardtii*. *Journal of Biotechnology* **162**: 57-66.

Casazza JP, Felver M, Veech R (1984). The metabolism of acetone in rat. *Journal of Biological Chemistry* **259**: 231-236.

Catalanotti C, Dubini A, Subramanian V, Yang W, Magneschi L, Mus F *et al* (2012). Altered Fermentative Metabolism in *Chlamydomonas reinhardtii* Mutants Lacking Pyruvate Formate Lyase and Both Pyruvate Formate Lyase and Alcohol Dehydrogenase. *The Plant Cell Online* **24**: 692-707.

Catalanotti C, Yang W, Posewitz MC, Grossman AR (2013). Fermentation metabolism and its evolution in algae. *Frontiers in Plant Science* **4**: 1-17.

Chang FY, Lin CY (2004). Biohydrogen production using an up-flow anaerobic sludge blanket reactor. *International Journal of Hydrogen Energy* **29**: 33-39.

Chen GC, Jordan F (1984). Brewers' yeast pyruvate decarboxylase produces acetoin from acetaldehyde: a novel tool to study the mechanism of steps subsequent to carbon dioxide loss. *Biochemistry* **23**: 3576-3582.

Chochois V, Dauvillée D, Beyly A, Tolleter D, Cuiné S, Timpano H *et al* (2009). Hydrogen Production in *Chlamydomonas*: Photosystem II-Dependent and -Independent Pathways Differ in Their Requirement for Starch Metabolism. *Plant Physiology* **151**: 631-640.

Chochois V, Constans L, Dauvillée D, Beyly A, Solivérès M, Ball S *et al* (2010). Relationships between PSII-independent hydrogen bioproduction and starch metabolism as evidenced from isolation of starch catabolism mutants in the green alga *Chlamydomonas reinhardtii*. *International Journal of Hydrogen Energy* **35**: 10731-10740.

Chu C-F, Li Y-Y, Xu K-Q, Ebie Y, Inamori Y, Kong H-N (2008). A pH- and temperature-phased two-stage process for hydrogen and methane production from food waste. *International Journal of Hydrogen Energy* **33**: 4739-4746.

Claros MG, Vincens P (1996). Computational Method to Predict Mitochondrially Imported Proteins and their Targeting Sequences. *European Journal of Biochemistry* **241**: 779-786.

Collingridge P, Kelly S (2012). MergeAlign: improving multiple sequence alignment performance by dynamic reconstruction of consensus multiple sequence alignments. *BMC Bioinformatics* **13**: 117.

Cooper R, Anderson A (1970). The formation and catabolism of methylglyoxal during glycolysis in *Escherichia coli*. *FEBS Letters* **11**: 273-276.

Cristescu ME, Innes DJ, Stillman JH, Crease TJ (2008). D-and L-lactate dehydrogenases during invertebrate evolution. *BMC evolutionary biology* **8**: 268.

Crout DH, Littlechild J, Morrey SM (1986). Acetoin metabolism: stereochemistry of the acetoin produced by the pyruvate decarboxylase of wheat germ and by the α-acetolactate

decarboxylase of *Klebsiella aerogenes*. *Journal of the Chemical Society, Perkin Transactions* **1**: 105-108.

Crow VL (1986). Utilization of Lactate Isomers by *Propionibacterium freudenreichii* subsp. *shermanii*: Regulatory Role for Intracellular Pyruvate. *Applied and Environmental Microbiology* **52**: 352-358.

Davis MC, Fiehn O, Durnford DG (2013). Metabolic acclimation to excess light intensity in *Chlamydomonas reinhardtii*. *Plant, Cell & Environment* **36**: 1391-1405.

Debuchy R, Purton S, Rochaix JD (1989). The argininosuccinate lyase gene of *Chlamydomonas reinhardtii*: an important tool for nuclear transformation and for correlating the genetic and molecular maps of the ARG7 locus. *EMBO J* **8**: 2803-2809.

Delcour J, Ferain T, Deghorain M, Palumbo E, Hols P (1999). The biosynthesis and functionality of the cell-wall of lactic acid bacteria. *Antonie Van Leeuwenhoek* **76**: 159-184.

Dennis D, Kaplan NO (1960). d- and l-Lactic Acid Dehydrogenases in *Lactobacillus plantarum*. *Journal of Biological Chemistry* **235**: 810-818.

Dent RM, Haglund CM, Chin BL, Kobayashi MC, Niyogi KK (2005). Functional Genomics of Eukaryotic Photosynthesis Using Insertional Mutagenesis of *Chlamydomonas reinhardtii*. *Plant Physiology* **137**: 545-556.

Desplats C, Mus F, Cuiné S, Billon E, Cournac L, Peltier G (2009). Characterization of Nda2, a Plastoquinone-reducing Type II NAD(P)H Dehydrogenase in *Chlamydomonas* Chloroplasts. *Journal of Biological Chemistry* **284**: 4148-4157.

Doebbe A, Rupprecht J, Beckmann J, Mussgnug JH, Hallmann A, Hankamer B *et al* (2007). Functional integration of the HUP1 hexose symporter gene into the genome of *C. reinhardtii*: Impacts on biological $H_2$ production. *Journal of Biotechnology* **131**: 27-33.

Dorian JP, Franssen HT, Simbeck DR (2006). Global challenges in energy. *Energy Policy* **34**: 1984-1991.

Dubini A, Mus F, Seibert M, Grossman AR, Posewitz MC (2009). Flexibility in Anaerobic Metabolism as Revealed in a Mutant of *Chlamydomonas reinhardtii* Lacking Hydrogenase Activity. *Journal of Biological Chemistry* **284**: 7201-7213.

Duncan SH, Louis P, Flint HJ (2004). Lactate-Utilizing Bacteria, Isolated from Human Feces, That Produce Butyrate as a Major Fermentation Product. *Applied and Environmental Microbiology* **70**: 5810-5817.

Dürre P, Kuhn A, Gottschalk G (1986). Treatment with allyl alcohol selects specifically for mutants of *Clostridium acetobutylicum* defective in butanol synthesis. *FEMS Microbiology Letters* **36**: 77-81.

EIA (2013). International Energy Outlook 2013. U.S. Energy Information Administration, Washington.

Eisenhut M, Ruth W, Haimovich M, Bauwe H, Kaplan A, Hagemann M (2008). The photorespiratory glycolate metabolism is essential for cyanobacteria and might have been conveyed endosymbiontically to plants. *Proceedings of the National Academy of Sciences* **105**: 17199-17204.

Emanuelsson O, Nielsen H, Von Heijne G (1999). ChloroP, a neural network-based method for predicting chloroplast transit peptides and their cleavage sites. *PRS* **8**: 978-984.

Emanuelsson O, Brunak S, von Heijne G, Nielsen H (2007). Locating proteins in the cell using TargetP, SignalP and related tools. *Nat. Protocols* **2**: 953-971.

Engqvist M, Drincovich MF, Flügge U-I, Maurino VG (2009). Two d-2-Hydroxy-acid Dehydrogenases in *Arabidopsis thaliana* with Catalytic Capacities to Participate in the Last Reactions of the Methylglyoxal and β-Oxidation Pathways. *Journal of Biological Chemistry* **284**: 25026-25037.

Esper B, Badura A, Rögner M (2006). Photosynthesis as a power supply for (bio-)hydrogen production. *Trends in Plant Science* **11**: 543-549.

Espinosa A, Yan L, Zhang Z, Foster L, Clark D, Li E *et al* (2001). The Bifunctional *Entamoeba histolytica* Alcohol Dehydrogenase 2 (EhADH2) Protein Is Necessary for Amebic Growth and Survival and Requires an Intact C-terminal Domain for Both Alcohol Dehydrogenase and Acetaldehyde Dehydrogenase Activity. *Journal of Biological Chemistry* **276**: 20136-20143.

Faraloni C, Torzillo G (2010). Phenotypic characterization and hydrogen production in *Chlamydomonas reinhardtii* QB-binding D1-protein mutants under sulfur starvation: changes in chl fluorescence and pigment composition. *Journal of Phycology* **46**: 788-799.

Ferguson GP, Tötemeyer S, MacLean M, Booth I (1998). Methylglyoxal production in bacteria: suicide or survival? *Arch. Microbiol.* **170**: 209-218.

Fischer N, Rochaix JD (2001). The flanking regions of *PsaD* drive efficient gene expression in the nucleus of the green alga *Chlamydomonas reinhardtii*. *Molecular Genetics and Genomics* **265**: 888-894.

Forestier M, King P, Zhang L, Posewitz M, Schwarzer S, Happe T *et al* (2003). Expression of two [Fe]-hydrogenases in *Chlamydomonas reinhardtii* under anaerobic conditions. *European Journal of Biochemistry* **270**: 2750-2758.

Fuhrmann M, Oertel W, Hegemann P (1999). A synthetic gene coding for the green fluorescent protein (GFP) is a versatile reporter in *Chlamydomonas reinhardtii*. *The Plant Journal* **19**: 353-361.

Fuhrmann M, Hausherr A, Ferbitz L, Schödl T, Heitzer M, Hegemann P (2004). Monitoring dynamic expression of nuclear genes in *Chlamydomonas reinhardtii* by using a synthetic luciferase reporter gene. *Plant Mol. Biol.* **55**: 869-881.

Gaffron H (1939). Reduction of carbon dioxide with molecular hydrogen in green algae. *Nature* **143**: 204-205.

Gaffron H, Rubin J (1942). Fermentative and photochemical production of hydrogen in algae. *The Journal of General Physiology* **26**: 219-240.

Garvie EI (1980). Bacterial lactate dehydrogenases. *Microbiological reviews* **44**: 106.

Gasser F, Doudoroff M, Contopoulos R (1970). Purification and Properties of NAD-dependent Lactic Dehydrogenases of Different Species of *Lactobacillus*. *Journal of General Microbiology* **62**: 241-250.

Gfeller RP, Gibbs M (1984). Fermentative Metabolism of *Chlamydomonas reinhardtii*: I. Analysis of Fermentative Products from Starch in Dark and Light. *Plant Physiology* **75**: 212-218.

Ghirardi ML, Posewitz MC, Maness PC, Dubini A, Yu J, Seibert M (2007). Hydrogenases and hydrogen photoproduction in oxygenic photosynthetic organisms. *Annual review of plant biology* **58**: 71-91.

Gilchrist E, Haughn G (2010). Reverse genetics techniques: engineering loss and gain of gene function in plants. *Briefings in Functional Genomics* **9**: 103-110.

Godman JE, Molnár A, Baulcombe DC, Balk J (2010). RNA silencing of hydrogenase(-like) genes and investigation of their physiological roles in the green alga *Chlamydomonas reinhardtii*. *Biochemical journal* **431**: 345-351.

Godon C, Lagniel G, Lee J, Buhler J-M, Kieffer S, Perrot M *et al* (1998). The $H_2O_2$ Stimulon in *Saccharomyces cerevisiae*. *Journal of Biological Chemistry* **273**: 22480-22489.

Goffin P, Deghorain M, Mainardi J-L, Tytgat I, Champomier-Verges M-C, Kleerebezem M *et al* (2005). Lactate racemization as a rescue pathway for supplying D-lactate to the cell wall biosynthesis machinery in *Lactobacillus plantarum*. *Journal of Bacteriology* **187**: 6750-6761.

Goldschmidt-Clermont M (1991). Transgenic expression of aminoglycoside adenine transferase in the chloroplast: a selectable marker for site-directed transformation of *Chlamydomonas*. *Nucleic Acids Research* **19**: 4083-4089.

Gonzalez-Ballester D, Pootakham W, Mus F, Yang W, Catalanotti C, Magneschi L *et al* (2011). Reverse genetics in *Chlamydomonas*: a platform for isolating insertional mutants. *Plant Methods* **7**: 1-13.

González-Ballester D, de Montaigu A, Higuera JJ, Galván A, Fernández E (2005). Functional Genomics of the Regulation of the Nitrate Assimilation Pathway in *Chlamydomonas*. *Plant Physiology* **137**: 522-533.

Gorman DS, Levine RP (1965). Cytochrome f and plastocyanin: their sequence in the photosynthetic electron transport chain of *Chlamydomonas reinhardi*. *Proceedings of the National Academy of Sciences* **54**: 1665-1669.

Goupil-Feuillerat N, Cocaign-Bousquet M, Godon JJ, Ehrlich SD, Renault P (1997). Dual role of alpha-acetolactate decarboxylase in *Lactococcus lactis* subsp. *lactis*. *Journal of Bacteriology* **179**: 6285-6293.

Grau UM, Trommer WE, Rossmann MG (1981). Structure of the active ternary complex of pig heart lactate dehydrogenase with S-lac-NAD at 2.7 Å resolution. *Journal of Molecular Biology* **151**: 289-307.

Griebel T, Brinkmeyer M, Böcker S (2008). EPoS: a modular software framework for phylogenetic analysis. *Bioinformatics* **24**: 2399-2400.

Grossman AR (2000). *Chlamydomonas reinhardtii* and photosynthesis: genetics to genomics. *Current Opinion in Plant Biology* **3**: 132-137.

Grossman AR, Croft M, Gladyshev VN, Merchant SS, Posewitz MC, Prochnik S *et al* (2007). Novel metabolism in *Chlamydomonas* through the lens of genomics. *Current Opinion in Plant Biology* **10**: 190-198.

Gruber PJ, Frederick SE, Tolbert N (1974). Enzymes related to lactate metabolism in green algae and lower land plants. *Plant Physiology* **53**: 167-170.

Hallenbeck PC, Benemann JR (2002). Biological hydrogen production; fundamentals and limiting processes. *International Journal of Hydrogen Energy* **27**: 1185-1193.

Hallenbeck PC (2005). Fundamentals of the fermentative production of hydrogen. *Water Science & Technology* **52**: 21-29.

Hallenbeck PC, Ghosh D (2009). Advances in fermentative biohydrogen production: the way forward? *Trends in Biotechnology* **27**: 287-297.

Hambourger M, Moore GF, Kramer DM, Gust D, Moore AL, Moore TA (2009). Biology and technology for photochemical fuel production. *Chemical Society Reviews* **38**: 25-35.

Happe T, Naber JD (1993). Isolation, characterization and N-terminal amino acid sequence of hydrogenase from the green alga *Chlamydomonas reinhardtii*. *European Journal of Biochemistry* **214**: 475-481.

Happe T, Mosler B, Naber JD (1994). Induction, localization and metal content of hydrogenase in the green alga *Chlamydomonas reinhardtii*. *European Journal of Biochemistry* **222**: 769-774.

Happe T, Kaminski A (2002). Differential regulation of the Fe-hydrogenase during anaerobic adaptation in the green alga *Chlamydomonas reinhardtii*. *European Journal of Biochemistry* **269**: 1022-1032.

Harris EH (1989). The *Chlamydomonas* Sourcebook: a comprehensive guide to biology and laboratory use. Academic Press: San Diego.

Harris EH (2009). The *Chlamydomonas* Sourcebook, 2 edn. Academic Press, UK.

Hebbelmann I, Selinski J, Wehmeyer C, Goss T, Voss I, Mulo P *et al* (2012). Multiple strategies to prevent oxidative stress in *Arabidopsis* plants lacking the malate valve enzyme NADP-malate dehydrogenase. *J. Exp. Bot* **63**: 1445-1459.

Hemschemeier A, Happe T (2005). The exceptional photofermentative hydrogen metabolism of the green alga *Chlamydomonas reinhardtii*. *Biochemical Society transactions* **33**: 39-41.

Hemschemeier A, Jacobs J, Happe T (2008). Biochemical and Physiological Characterization of the Pyruvate Formate-Lyase Pfl1 of *Chlamydomonas reinhardtii*, a Typically Bacterial Enzyme in a Eukaryotic Alga. *Eukaryotic Cell* **7**: 518-526.

Hirsch RL, Bezdek R, Wendling R (2006). Peaking of World Oil Production and Its Mitigation. *AIChE Journal* **52**: 2-8.

Hirt G, Tanner W, Kandler O (1971). Effect of light on the rate of glycolysis in *Scenedesmus obliquus*. *Plant Physiology* **47**: 841-843.

Hopper DJ, Cooper RA (1971). The regulation of Escherichia coli methylglyoxal synthase; a new control site in glycolysis? *FEBS Letters* **13**: 213-216.

Husic DW, Tolbert NE (1985). Anaerobic Formation of d-Lactate and Partial Purification and Characterization of a Pyruvate Reductase from *Chlamydomonas reinhardtii*. *Plant Physiology* **78**: 277-284.

Husic DW, Tolbert NE (1987). Inhibition of glycolate and D-lactate metabolism in a *Chlamydomonas reinhardtii* mutant deficient in mitochondrial respiration. *Proceedings of the National Academy of Sciences* **84**: 1555-1559.

Hutner S, Provasoli L, Schatz A, Haskins C (1950). Some approaches to the study of the role of metals in the metabolism of microorganisms. *Proceedings of the American Philosophical Society* **94**: 152-170.

IEA (2008). Energy technology perspectives: scenarios and strategies to 2050. International Energy Agency, France.

IEA (2011). Key world energy statistics. International energy agency, France.

IEA (2012). Key world energy statistics. International Energy Agency, France.

IEA (2013). Key world energy statistics. International Energy Agency, France.

IEA (2014). Key world energy statistics. International Energy Agency, France.

IPCC (2007). Climate change 2007: synthesis report. Intergovernmental Panel on Climate Change, Switzerland.

Iwata S, Kamata K, Yoshida S, Minowa T, Ohta T (1994). T and R states in the crystals of bacterial L–lactate dehydrogenase reveal the mechanism for allosteric control. *Nature Structural & Molecular Biology* **1**: 176-185.

Jans F, Mignolet E, Houyoux P-A, Cardol P, Ghysels B, Cuiné S *et al* (2008). A type II NAD(P)H dehydrogenase mediates light-independent plastoquinone reduction in the chloroplast of *Chlamydomonas*. *Proceedings of the National Academy of Sciences* **105**: 20546-20551.

Jiang X, Stern D (2009). Mating and tetrad separation of *Chlamydomonas reinhardtii* for genetic analysis. *Journal of visualized experiments* **30**.

John RP, Anisha GS, Nampoothiri KM, Pandey A (2011). Micro and macroalgal biomass: A renewable source for bioethanol. *Bioresource Technology* **102**: 186-193.

Jones-Rhoades MW, Bartel DP, Bartel B (2006). MicroRNAs and their regulatory roles in plants. *Annual review of plant biology* **57**: 19.

Jung S, Marelli M, Rachubinski RA, Goodlett DR, Aitchison JD (2010). Dynamic Changes in the Subcellular Distribution of Gpd1p in Response to Cell Stress. *Journal of Biological Chemistry* **285**: 6739-6749.

Kadner RJ, Murphy GP, Stephens CM (1992). Two mechanisms for growth inhibition by elevated transport of sugar phosphates in *Escherichia coli*. *Journal of General Microbiology* **138**: 2007-2014.

Kessler D, Herth W, Knappe J (1992). Ultrastructure and pyruvate formate-lyase radical quenching property of the multienzymic AdhE protein of *Escherichia coli*. *Journal of Biological Chemistry* **267**: 18073-18079.

Kibbe WA (2007). OligoCalc: an online oligonucleotide properties calculator. *Nucleic Acids Research* **35**: W43-W46.

Kindle KL (1990). High-frequency nuclear transformation of *Chlamydomonas reinhardtii*. *Proceedings of the National Academy of Sciences* **87**: 1228-1232.

Klein U, Betz A (1978). Fermentative Metabolism of Hydrogen-evolving *Chlamydomonas moewusii*. *Plant Physiology* **61**: 953-956.

Knappe J, Neugebauer FA, Blaschkowski HP, Gänzler M (1984). Post-translational activation introduces a free radical into pyruvate formate-lyase. *Proceedings of the National Academy of Sciences* **81**: 1332-1335.

Kochhar S, Chuard N, Hottinger H (1992). Glutamate 264 modulates the pH dependence of the NAD(+)-dependent D-lactate dehydrogenase. *Journal of Biological Chemistry* **267**: 20298-20301.

Komenda J, Sobotka R, Nixon PJ (2012). Assembling and maintaining the Photosystem II complex in chloroplasts and cyanobacteria. *Current Opinion in Plant Biology* **15**: 245-251.

Kosourov S, Seibert M, Ghirardi ML (2003). Effects of Extracellular pH on the Metabolic Pathways in Sulfur-Deprived, $H_2$-Producing *Chlamydomonas reinhardtii* Cultures. *Plant and Cell Physiology* **44**: 146-155.

Kosourov SN, Ghirardi ML, Seibert M (2011). A truncated antenna mutant of *Chlamydomonas reinhardtii* can produce more hydrogen than the parental strain. *International Journal of Hydrogen Energy* **36**: 2044-2048.

Kreuzberg K (1984). Starch fermentation via a formate producing pathway in *Chlamydomonas reinhardii*, *Chlorogonium elongatum* and *Chlorella fusca*. *Physiologia Plantarum* **61**: 87-94.

Kruse O, Rupprecht J, Bader K-P, Thomas-Hall S, Schenk PM, Finazzi G *et al* (2005a). Improved Photobiological $H_2$ Production in Engineered Green Algal Cells. *Journal of Biological Chemistry* **280**: 34170-34177.

Kruse O, Rupprecht J, Mussgnug JH, Dismukes GC, Hankamer B (2005b). Photosynthesis: a blueprint for solar energy capture and biohydrogen production technologies. *Photochemical & Photobiological Sciences* **4**: 957-970.

Kuchitsu K, Tsuzuki M, Miyachi S (1988). Changes of Starch Localization within the Chloroplast Induced by Changes in $CO_2$ Concentration during Growth of *Chlamydomonas reinhardtii*: Independent Regulation of Pyrenoid Starch and Stroma Starch. *Plant and Cell Physiology* **29**: 1269-1278.

Kumar N, Ghosh A, Das D (2001). Redirection of biochemical pathways for the enhancement of $H_2$ production by Enterobacter cloacae. *Biotechnology Letters* **23**: 537-541.

Lapierre L, Germond J-E, Ott A, Delley M, Mollet B (1999). D-Lactate Dehydrogenase Gene (*ldhD*) Inactivation and Resulting Metabolic Effects in the *Lactobacillus johnsonii* Strains La1 and N312. *Applied and Environmental Microbiology* **65**: 4002-4007.

Lay JJ, Lee YJ, Noike T (1999). Feasibility of biological hydrogen production from organic fraction of municipal solid waste. *Water Research* **33**: 2579-2586.

Lee TC, Langston-Unkefer PJ (1985). Pyruvate decarboxylase from *Zea mays* LI Purification and partial characterization from mature kernels and anaerobically treated roots. *Plant Physiology* **79**: 242-247.

Liang J, Burris RH (1988). Hydrogen burst associated with nitrogenase-catalyzed reactions. *Proceedings of the National Academy of Sciences* **85**: 9446-9450.

Lieber C (1988). Metabolic effects of acetaldehyde. *Biochemical Society transactions* **16**: 241-247.

Liu H, Zhang T, Fang HHP (2003). Thermophilic $H_2$ production from a cellulose-containing wastewater. *Biotechnology Letters* **25**: 365-369.

Liu J, Desai K, Wang R, Wu L (2013). Up-regulation of aldolase A and methylglyoxal production in adipocytes. *British Journal of Pharmacology* **168**: 1639-1646.

Liu X, Zhu Y, Yang S-T (2006). Construction and Characterization of *ack* Deleted Mutant of *Clostridium tyrobutyricum* for Enhanced Butyric Acid and Hydrogen Production. *Biotechnology Progress* **22**: 1265-1275.

Lodi T, Ferrero I (1993). Isolation of the *DLD* gene of *Saccharomyces cerevisiae* encoding the mitochondrial enzyme D-lactate ferricytochrome c oxidoreductase. *Molec. Gen. Genet.* **238**: 315-324.

Lodi T, O'Connor D, Goffrini P, Ferrero I (1994). Carbon catabolite repression in *Kluyveromyces lactis*: isolation and characterization of the *KINLD* gene encoding the mitochondrial enzyme D-lactate ferricytochrome c oxidoreductase. *Molec. Gen. Genet.* **244**: 622-629.

Logan BE, Oh S-E, Kim IS, Van Ginkel S (2002). Biological Hydrogen Production Measured in Batch Anaerobic Respirometers. *Environmental Science & Technology* **36**: 2530-2535.

Long GL, Kaplan NO (1968). D-Lactate Specific Pyridine Nucleotide Lactate Dehydrogenase in Animals. *Science* **162**: 685-686.

Lubitz W, Reijerse EJ, Messinger J (2008). Solar water-splitting into $H_2$ and $O_2$: design principles of photosystem II and hydrogenases. *Energy & Environmental Science* **1**: 15-31.

Lubner CE, Knörzer P, Silva PJN, Vincent KA, Happe T, Bryant DA *et al* (2010). Wiring an [FeFe]-Hydrogenase with Photosystem I for Light-Induced Hydrogen Production. *Biochemistry* **49**: 10264-10266.

Lumbreras V, Stevens DR, Purton S (1998). Efficient foreign gene expression in *Chlamydomonas reinhardtii* mediated by an endogenous intron. *The Plant Journal* **14**: 441-447.

Maeda T, Sanchez-Torres V, Wood TK (2007). Enhanced hydrogen production from glucose by metabolically engineered *Escherichia coli*. *Appl. Microbiol. Biotechnol.* **77**: 879-890.

Maeda T, Sanchez-Torres V, Wood TK (2008). Metabolic engineering to enhance bacterial hydrogen production. *Microbial Biotechnology* **1**: 30-39.

Magneschi L, Catalanotti C, Subramanian V, Dubini A, Yang W, Mus F *et al* (2012). A Mutant in the *ADH1* Gene of *Chlamydomonas reinhardtii* Elicits Metabolic Restructuring during Anaerobiosis. *Plant Physiology* **158**: 1293-1305.

Markert CL (1984). Lactate dehydrogenase: Biochemistry and function of lactate dehydrogenase. *Cell Biochemistry and Function* **2**: 131-134.

Mata TM, Martins AA, Caetano NS (2010). Microalgae for biodiesel production and other applications: A review. *Renewable and Sustainable Energy Reviews* **14**: 217-232.

Maul JE, Lilly JW, Cui L, dePamphilis CW, Miller W, Harris EH *et al* (2002). The *Chlamydomonas reinhardtii* Plastid Chromosome: Islands of Genes in a Sea of Repeats. *The Plant Cell Online* **14**: 2659-2679.

Mee B, Kelleher D, Frias J, Malone R, Tipton KF, Henehan GTM *et al* (2005). Characterization of cinnamyl alcohol dehydrogenase of *Helicobacter pylori*. *FEBS Journal* **272**: 1255-1264.

Meher Kotay S, Das D (2008). Biohydrogen as a renewable energy resource - Prospects and potentials. *International Journal of Hydrogen Energy* **33**: 258-263.

Melchiorsen CR, Jokumsen KV, Villadsen J, Johnsen MG, Israelsen H, Arnau J (2000). Synthesis and Posttranslational Regulation of Pyruvate Formate-Lyase in *Lactococcus lactis*. *Journal of Bacteriology* **182**: 4783-4788.

Melis A, Zhang L, Forestier M, Ghirardi ML, Seibert M (2000). Sustained Photobiological Hydrogen Gas Production upon Reversible Inactivation of Oxygen Evolution in the Green Alga *Chlamydomonas reinhardtii*. *Plant Physiology* **122**: 127-136.

Melis A (2007). Photosynthetic hydrogen metabolism in *Chlamydomonas reinhardtii* (unicellular green algae). *Planta* **226**: 1075-1086.

Merchant SS, Prochnik SE, Vallon O, Harris EH, Karpowicz SJ, Witman GB *et al* (2007). The *Chlamydomonas* Genome Reveals the Evolution of Key Animal and Plant Functions. *Science* **318**: 245-250.

Meuser JE, D'Adamo S, Jinkerson RE, Mus F, Yang W, Ghirardi ML *et al* (2012). Genetic disruption of both *Chlamydomonas reinhardtii* [FeFe]-hydrogenases: Insight into the role of HYDA2 in $H_2$ production. *Biochemical and Biophysical Research Communications* **417**: 704-709.

Miyamoto K (1997). Renewable biological systems for alternative sustainable energy production, vol. 128. FAO of the United Nations, Italy.

Mizuno O, Dinsdale R, Hawkes FR, Hawkes DL, Noike T (2000). Enhancement of hydrogen production from glucose by nitrogen gas sparging. *Bioresource Technology* **73**: 59-65.

Molnar A, Bassett A, Thuenemann E, Schwach F, Karkare S, Ossowski S *et al* (2009). Highly specific gene silencing by artificial microRNAs in the unicellular alga *Chlamydomonas reinhardtii*. *The Plant Journal* **58**: 165-174.

Montville TJ, Hsu AH-M, Meyer ME (1987). High-efficiency conversion of pyruvate to acetoin by *Lactobacillus plantarum* during pH-controlled and fed-batch fermentations. *Applied and Environmental Microbiology* **53**: 1798-1802.

Morimoto K, Kimura T, Sakka K, Ohmiya K (2005). Overexpression of a hydrogenase gene in *Clostridium paraputrificum* to enhance hydrogen gas production. *FEMS Microbiology Letters* **246**: 229-234.

Mus F, Dubini A, Seibert M, Posewitz MC, Grossman AR (2007). Anaerobic acclimation in *Chlamydomonas reinhardtii*: anoxic gene expression, hydrogenase induction, and metabolic pathways. *Journal of Biological Chemistry* **282**: 25475-25486.

Nakayashiki H (2005). RNA silencing in fungi: Mechanisms and applications. *FEBS Letters* **579**: 5950-5957.

Nath K, Muthukumar M, Kumar A, Das D (2008). Kinetics of two-stage fermentation process for the production of hydrogen. *International Journal of Hydrogen Energy* **33**: 1195-1203.

Nelson EB, Tolbert NE (1970). Glycolate dehydrogenase in green algae. *Archives of Biochemistry and Biophysics* **141**: 102-110.

Nelson JA, Savereide PB, Lefebvre PA (1994). The *CRY1* gene in *Chlamydomonas reinhardtii*: structure and use as a dominant selectable marker for nuclear transformation. *Molecular and Cellular Biology* **14**: 4011-4019.

Nigam PS, Singh A (2011). Production of liquid biofuels from renewable resources. *Progress in Energy and Combustion Science* **37**: 52-68.

Nixon PJ, Michoux F, Yu J, Boehm M, Komenda J (2010). Recent advances in understanding the assembly and repair of photosystem II. *Annals of botany* **106**, 1-16.

Noda K, Zorin NA, Nakamura C, Miyake M, Gogotov IN, Asada Y *et al* (1998). Langmuir–Blodgett film of hydrogenase for electrochemical hydrogen production. *Thin Solid Films* **327**: 639-642.

Noth J, Krawietz D, Hemschemeier A, Happe T (2013). Pyruvate:Ferredoxin Oxidoreductase Is Coupled to Light-independent Hydrogen Production in *Chlamydomonas reinhardtii*. *Journal of Biological Chemistry* **288**: 4368-4377.

Oba K, Murakami S, Uritani I (1977). Partial Purification and Characterization of L-Lactate Dehydrogenase Isozymes from Sweet Potato Roots. *Journal of Biochemistry* **81**: 1193-1201.

Ohta S, Miyamoto K, Miura Y (1987). Hydrogen Evolution as a Consumption Mode of Reducing Equivalents in Green Algal Fermentation. *Plant Physiology* **83**: 1022-1026.

Oppermann FB, Schmidt B, Steinbüchel A (1991). Purification and characterization of acetoin: 2,6-dichlorophenolindophenol oxidoreductase, dihydrolipoamide dehydrogenase, and dihydrolipoamide acetyltransferase of the *Pelobacter carbinolicus* acetoin dehydrogenase enzyme system. *Journal of Bacteriology* **173**: 757-767.

Oppermann FB, Steinbüchel A (1994). Identification and molecular characterization of the *aco* genes encoding the *Pelobacter carbinolicus* acetoin dehydrogenase enzyme system. *Journal of Bacteriology* **176**: 469-485.

Ossowski S, Schwab R, Weigel D (2008). Gene silencing in plants using artificial microRNAs and other small RNAs. *The Plant Journal* **53**: 674-690.

Özgür E, Afsar N, de Vrije T, Yücel M, Gündüz U, Claassen PAM *et al* (2010). Potential use of thermophilic dark fermentation effluents in photofermentative hydrogen production by *Rhodobacter capsulatus*. *Journal of Cleaner Production* **18**: S23-S28.

Park MJ, Jo JH, Park D, Lee DS, Park JM (2010). Comprehensive study on a two-stage anaerobic digestion process for the sequential production of hydrogen and methane from cost-effective molasses. *International Journal of Hydrogen Energy* **35**: 6194-6202.
Peden EA, Boehm M, Mulder DW, Davis R, Old WM, King PW *et al* (2013). Identification of Global Ferredoxin Interaction Networks in *Chlamydomonas reinhardtii*. *Journal of Biological Chemistry* **288**: 35192-35209.

Penfold DW, Forster CF, Macaskie LE (2003). Increased hydrogen production by *Escherichia coli* strain HD701 in comparison with the wild-type parent strain MC4100. *Enzyme and Microbial Technology* **33**: 185-189.

Penfold DW, Sargent F, Macaskie LE (2006). Inactivation of the *Escherichia coli* K-12 twin-arginine translocation system promotes increased hydrogen production. *FEMS Microbiology Letters* **262**: 135-137.

Petersen TN, Brunak S, von Heijne G, Nielsen H (2011). SignalP 4.0: discriminating signal peptides from transmembrane regions. *Nat. Meth.* **8**: 785-786.

Philipps G, Krawietz D, Hemschemeier A, Happe T (2011). A pyruvate formate lyase-deficient *Chlamydomonas reinhardtii* strain provides evidence for a link between fermentation and hydrogen production in green algae. *The Plant Journal* **66**: 330-340.

Phillips SA, Thornalley PJ (1993). The formation of methylglyoxal from triose phosphates. *European Journal of Biochemistry* **212**: 101-105.

Piontek K, Chakrabarti P, Schär HP, Rossmann MG, Zuber H (1990). Structure determination and refinment of *Bacillus stearothermophilus* lactate dehydrogenase. *Proteins: Structure, Function, and Bioinformatics* **7**: 74-92.

Pollock S, Pootakham W, Shibagaki N, Moseley J, Grossman A (2005). Insights into the acclimation of *Chlamydomonas reinhardtii* to sulfur deprivation. *Photosynth. Res.* **86**: 475-489.

Pootakham W, Gonzalez-Ballester D, Grossman AR (2010). Identification and Regulation of Plasma Membrane Sulfate Transporters in *Chlamydomonas*. *Plant Physiol.* **153**: 1653-1668.

Porra RJ, Thompson WA, Kriedemann PE (1989). Determination of accurate extinction coefficients and simultaneous equations for assaying chlorophylls a and b extracted with four different solvents: verification of the concentration of chlorophyll standards by atomic absorption spectroscopy. *Biochimica et Biophysica Acta (BBA) - Bioenergetics* **975**: 384-394.

Posewitz MC, King PW, Smolinski SL, Smith RD, Ginley AR, Ghirardi ML *et al* (2005). Identification of genes required for hydrogenase activity in *Chlamydomonas reinhardtii*. *Biochemical Society transactions* **33**: 102-104.

Posewitz MC, Dubini A, Meuser JC, Seibert M, Ghirardi ML (2009). Hydrogenases, hydrogen production and anoxia. In: Stern DB (ed). The *Chlamydomonas* sourcebook, 2 edn. Academic Press, UK. pp 217-255.

Pregger T, Graf D, Krewitt W, Sattler C, Roeb M, Möller S (2009). Prospects of solar thermal hydrogen production processes. *International Journal of Hydrogen Energy* **34**: 4256-4267.

Promega (1996). Protocols and applications guide: the source for discovery, Third edn. Promega, USA.

Pucciariello C, Parlanti S, Banti V, Novi G, Perata P (2012). Reactive Oxygen Species-Driven Transcription in *Arabidopsis* under Oxygen Deprivation. *Plant Physiology* **159**: 184-196.

Qadri SH, Hoare D (1973). Pyruvic decarboxylase and acetoin formation in Athiorhodaceae. *Canadian Journal of microbiology* **19**: 1137-1143.

Rachman MA, Furutani Y, Nakashimada Y, Kakizono T, Nishio N (1997). Enhanced hydrogen production in altered mixed acid fermentation of glucose by *Enterobacter aerogenes*. *Journal of Fermentation and Bioengineering* **83**: 358-363.

Ramachandran R, Menon RK (1998). An overview of industrial uses of hydrogen. *International Journal of Hydrogen Energy* **23**: 593-598.

Randolph-Anderson B, Boynton J, Gillham N, Harris E, Johnson A, Dorthu M-P *et al* (1993). Further characterization of the respiratory deficient *dum-1* mutation of *Chlamydomonas reinhardtii* and its use as a recipient for mitochondrial transformation. *Molec. Gen. Genet.* **236**: 235-244.

Ray S, Ray M (1983). Formation of methylglyoxal from aminoacetone by amine oxidase from goat plasma. *Journal of Biological Chemistry* **258**: 3461-3462.

Ray S, Ray M (1984). Oxidation of lactaldehyde by cytosolic aldehyde dehydrogenase and inhibition of cytosolic and mitochondrial aldehyde dehydrogenase by metabolites. *Biochimica et Biophysica Acta (BBA) - General Subjects* **802**: 128-134.

Razeto A, Kochhar S, Hottinger H, Dauter M, Wilson KS, Lamzin VS (2002). Domain Closure, Substrate Specificity and Catalysis of d-Lactate Dehydrogenase from *Lactobacillus bulgaricus*. *Journal of Molecular Biology* **318**: 109-119.

REN21 (2013). Renewables 2013: Global status report. Renewable Energy Policy Network for the 21st Century Secretariat, Paris.

Richard J (1993). Mechanism for the formation of methylglyoxal from triosephosphates. *Biochemical Society Transactions* **21**: 549-553.

Roberts J, Callis J, Wemmer D, Walbot V, Jardetzky O (1984). Mechanisms of cytoplasmic pH regulation in hypoxic maize root tips and its role in survival under hypoxia. *Proceedings of the National Academy of Sciences* **81**: 3379-3383.

Rupprecht J (2009). From systems biology to fuel - *Chlamydomonas reinhardtii* as a model for a systems biology approach to improve biohydrogen production. *Journal of Biotechnology* **142**: 10-20.

Sanchez MA (2013). Molecular Identification and Characterization of an Essential Pyruvate Transporter from *Trypanosoma brucei*. *Journal of Biological Chemistry* **288**: 14428-14437.

Sawaki S, Hattori H, Yamada K (1967). Glyoxylate Dehydrogenase Activity of Lactate Dehydrogenase. *Journal of Biochemistry* **62**: 263-268.

Scheibe R (2004). Malate valves to balance cellular energy supply. *Physiologia Plantarum* **120**: 21-26.

Schenk P, Thomas-Hall S, Stephens E, Marx U, Mussgnug J, Posten C *et al* (2008). Second Generation Biofuels: High-Efficiency Microalgae for Biodiesel Production. *BioEnergy Research* **1**: 20-43.

Schroda M, Blöcker D, Beck CF (2000). The *HSP70A* promoter as a tool for the improved expression of transgenes in *Chlamydomonas*. *The Plant Journal* **21**: 121-131.

Schroda M (2006). RNA silencing in *Chlamydomonas*: mechanisms and tools. *Current Genetics* **49**: 69-84.

Schwab R, Palatnik JF, Riester M, Schommer C, Schmid M, Weigel D (2005). Specific Effects of MicroRNAs on the Plant Transcriptome. *Developmental Cell* **8**: 517-527.

Scott SA, Davey MP, Dennis JS, Horst I, Howe CJ, Lea-Smith DJ *et al* (2010). Biodiesel from algae: challenges and prospects. *Current Opinion in Biotechnology* **21**: 277-286.

Shimogawara K, Fujiwara S, Grossman A, Usuda H (1998). High-Efficiency Transformation of *Chlamydomonas reinhardtii* by Electroporation. *Genetics* **148**: 1821-1828.

Shinoda T, Arai K, Shigematsu-Iida M, Ishikura Y, Tanaka S, Yamada T *et al* (2005). Distinct Conformation-mediated Functions of an Active Site Loop in the Catalytic Reactions of NAD-dependent D-Lactate Dehydrogenase and Formate Dehydrogenase. *Journal of Biological Chemistry* **280**: 17068-17075.

Shrager J, Hauser C, Chang C-W, Harris EH, Davies J, McDermott J *et al* (2003). *Chlamydomonas reinhardtii* Genome Project. A Guide to the Generation and Use of the cDNA Information. *Plant Physiology* **131**: 401-408.

Singer TP, Pensky J (1952). Isolation and properties of the α-carboxylase of wheat germ. *Journal of Biological Chemistry* **196**: 375-388.

Singh J, Gu S (2010). Commercialization potential of microalgae for biofuels production. *Renewable and Sustainable Energy Reviews* **14**: 2596-2610.

Sizova I, Fuhrmann M, Hegemann P (2001). A *Streptomyces rimosus aphVIII* gene coding for a new type phosphotransferase provides stable antibiotic resistance to *Chlamydomonas reinhardtii*. *Gene* **277**: 221-229.

Sode K, Watanabe M, Makimoto H, Tnmiyama M (1999). Construction and characterization of fermentative lactate dehydrogenase mutant and its potential for bacterial hydrogen production. *Appl. Biochem. Biotech.* **77**: 317-323.

Sodeinde OA, Kindle KL (1993). Homologous recombination in the nuclear genome of *Chlamydomonas reinhardtii*. *Proceedings of the National Academy of Sciences* **90**: 9199-9203.

Spolaore P, Joannis-Cassan C, Duran E, Isambert A (2006). Commercial applications of microalgae. *Journal of Bioscience and Bioengineering* **101**: 87-96.

Stern N (2006). Stern review on the economics of climate change. HM Treasury, UK.

Stivers JT, Washabaugh MW (1993). Catalysis of acetoin formation by brewers' yeast pyruvate decarboxylase isoenzymes. *Biochemistry* **32**: 13472-13482.

Sueoka N (1960). Mitotic replication of deoxyribonucleic acid in *Chlamydomonas reinhardtii*. *Proceedings of the National Academy of Sciences* **46**: 83.

Taguchi H, Ohta T (1991). D-lactate dehydrogenase is a member of the D-isomer-specific 2-hydroxyacid dehydrogenase family. Cloning, sequencing, and expression in *Escherichia coli* of the D-lactate dehydrogenase gene of *Lactobacillus plantarum*. *Journal of Biological Chemistry* **266**: 12588-12594.

Takahashi S, Abbe K, Yamada T (1982). Purification of pyruvate formate-lyase from *Streptococcus mutans* and its regulatory properties. *Journal of Bacteriology* **149**: 1034-1040.

Tamagnini P, Axelsson R, Lindberg P, Oxelfelt F, Wünschiers R, Lindblad P (2002). Hydrogenases and Hydrogen Metabolism of Cyanobacteria. *Microbiology and Molecular Biology Reviews* **66**: 1-20.

Tamburic B, Zemichael FW, Crudge P, Maitland GC, Hellgardt K (2011). Design of a novel flat-plate photobioreactor system for green algal hydrogen production. *International Journal of Hydrogen Energy* **36**: 6578-6591.

Tarmy EM, Kaplan NO (1968). Kinetics of *Escherichia coli* B d-Lactate Dehydrogenase and Evidence for Pyruvate-controlled Change in Conformation. *Journal of Biological Chemistry* **243**: 2587-2596.

Terashima M, Specht M, Naumann B, Hippler M (2010). Characterizing the Anaerobic Response of *Chlamydomonas reinhardtii* by Quantitative Proteomics. *Molecular & Cellular Proteomics* **9**: 1514-1532.

Terauchi AM, Lu S-F, Zaffagnini M, Tappa S, Hirasawa M, Tripathy JN *et al* (2009). Pattern of Expression and Substrate Specificity of Chloroplast Ferredoxins from *Chlamydomonas reinhardtii*. *Journal of Biological Chemistry* **284**: 25867-25878.

Thompson JD, Higgins DG, Gibson TJ (1994). CLUSTAL W: improving the sensitivity of progressive multiple sequence alignment through sequence weighting, position-specific gap penalties and weight matrix choice. *Nucleic Acids Research* **22**: 4673-4680.

Thornalley PJ (1990). The glyoxalase system: new developments towards functional characterization of a metabolic pathway fundamental to biological life. *Biochemical journal* **269**: 1.

Timmins M, Thomas-Hall SR, Darling A, Zhang E, Hankamer B, Marx UC *et al* (2009a). Phylogenetic and molecular analysis of hydrogen-producing green algae. *J. Exp. Bot.* **60**: 1691-1702.

Timmins M, Zhou W, Rupprecht J, Lim L, Thomas-Hall SR, Doebbe A *et al* (2009b). The Metabolome of *Chlamydomonas reinhardtii* following Induction of Anaerobic $H_2$ Production by Sulfur Depletion. *Journal of Biological Chemistry* **284**: 23415-23425.

Toepel J, Albaum S, Arvidsson S, Goesmann A, la Russa M, Rogge K *et al* (2011). Construction and evaluation of a whole genome microarray of *Chlamydomonas reinhardtii*. *BMC Genomics* **12**: 579.

Tolleter D, Ghysels B, Alric J, Petroutsos D, Tolstygina I, Krawietz D *et al* (2011). Control of Hydrogen Photoproduction by the Proton Gradient Generated by Cyclic Electron Flow in *Chlamydomonas reinhardtii*. *The Plant Cell Online* **23**: 2619-2630.

Torzillo G, Scoma A, Faraloni C, Ena A, Johanningmeier U (2009). Increased hydrogen photoproduction by means of a sulfur-deprived *Chlamydomonas reinhardtii* D1 protein mutant. *International Journal of Hydrogen Energy* **34**: 4529-4536.

Tötemeyer S, Booth N, Nichols W, Dunbar B, Booth I (1998). From famine to feast: the role of methylglyoxal production in *Escherichia coli*. *Molecular microbiology* **27**: 553-562.

Tsau J-L, Guffanti AA, Montville TJ (1992). Conversion of pyruvate to acetoin helps to maintain pH homeostasis in *Lactobacillus plantarum*. *Applied and Environmental Microbiology* **58**: 891-894.

Uchikoba H, Fushinobu S, Wakagi T, Konno M, Taguchi H, Matsuzawa H (2002). Crystal structure of non-allosteric L-lactate dehydrogenase from *Lactobacillus pentosus* at 2.3 Å resolution: Specific interactions at subunit interfaces. *Proteins: Structure, Function, and Bioinformatics* **46**: 206-214.

Vahrenholz C, Riemen G, Pratje E, Dujon B, Michaelis G (1993). Mitochondrial DNA of *Chlamydomonas reinhardtii*: the structure of the ends of the linear 15.8-kb genome suggests mechanisms for DNA replication. *Current Genetics* **24**: 241-247.

Vallon O, Spalding MH (2009). Amino acid metabolism. In: Stern DB (ed). The *Chlamydomonas* sourcebook. Academic Press, UK. pp 115-158.

van Groenestijn JW, Hazewinkel JHO, Nienoord M, Bussmann PJT (2002). Energy aspects of biological hydrogen production in high rate bioreactors operated in the thermophilic temperature range. *International Journal of Hydrogen Energy* **27**: 1141-1147.

Vardar-Schara G, Maeda T, Wood TK (2008). Metabolically engineered bacteria for producing hydrogen via fermentation. *Microbial Biotechnology* **1**: 107-125.

Vignais PM, Billoud B (2007). Occurrence, Classification, and Biological Function of Hydrogenases: An Overview. *ChemInform* **38**: 4206-4272.

Volbeda A, Charon M-H, Piras C, Hatchikian EC, Frey M, Fontecilla-Camps JC (1995). Crystal structure of the nickel-iron hydrogenase from *Desulfovibrio gigas*. *Nature* **373**: 580-587.

Wagner A, Frey M, Neugebauer FA, Schäfer W, Knappe J (1992). The free radical in pyruvate formate-lyase is located on glycine-734. *Proceedings of the National Academy of Sciences* **89**: 996-1000.

Wang X, Zhao Y-c (2009). A bench scale study of fermentative hydrogen and methane production from food waste in integrated two-stage process. *International Journal of Hydrogen Energy* **34**: 245-254.

Wang Z, Zhuge J, Fang H, Prior BA (2001). Glycerol production by microbial fermentation: A review. *Biotechnology Advances* **19**: 201-223.

Weber J, Kayser A, Rinas U (2005). Metabolic flux analysis of *Escherichia coli* in glucose-limited continuous culture. II. Dynamic response to famine and feast, activation of the methylglyoxal pathway and oscillatory behaviour. *Microbiology* **151**: 707-716.

White AL, Melis A (2006). Biochemistry of hydrogen metabolism in *Chlamydomonas reinhardtii* wild type and a Rubisco-less mutant. *International Journal of Hydrogen Energy* **31**: 455-464.

White JL, Hackert ML, Buehner M, Adams MJ, Ford GC, Lentz Jr PJ *et al* (1976). A comparison of the structures of apo dogfish M4 lactate dehydrogenase and its ternary complexes. *Journal of Molecular Biology* **102**: 759-779.

Whitney LAS, Loreti E, Alpi A, Perata P (2011). Alcohol dehydrogenase and hydrogenase transcript fluctuations during a day–night cycle in *Chlamydomonas reinhardtii*: the role of anoxia. *New Phytologist* **190**: 488-498.

Whitney LAS, Novi G, Perata P, Loreti E (2012). Distinct mechanisms regulating gene expression coexist within the fermentative pathways in *Chlamydomonas reinhardtii*. *The Scientific World Journal* **2012**: 1-9.

Wigley DB, Gamblin SJ, Turkenburg JP, Dodson EJ, Piontek K, Muirhead H *et al* (1992). Structure of a ternary complex of an allosteric lactate dehydrogenase from *Bacillus stearothermophilus* at 2.5 Å resolution. *Journal of Molecular Biology* **223**: 317-335.

Wijffels RH, Barbosa MJ (2010). An outlook on microalgal biofuels. *Science* **329**: 796-799.

Winkelman JW, Clark DP (1984). Proton suicide: general method for direct selection of sugar transport- and fermentation-defective mutants. *Journal of Bacteriology* **160**: 687-690.

Winkler M, Hemschemeier A, Gotor C, Melis A, Happe T (2002). [Fe]-hydrogenases in green algae: photo-fermentation and hydrogen evolution under sulfur deprivation. *International Journal of Hydrogen Energy* **27**: 1431-1439.

Wood AJ, Duff RJ (2009). The aldehyde dehydrogenase (ALDH) gene superfamily of the moss *Physcomitrella patens* and the algae *Chlamydomonas reinhardtii* and *Ostreococcus tauri*. *The Bryologist* **112**: 1-11.

Wu S, Huang R, Xu L, Yan G, Wang Q (2010). Improved hydrogen production with expression of *hemH* and *lba* genes in chloroplast of *Chlamydomonas reinhardtii*. *Journal of Biotechnology* **146**: 120-125.

Wu S, Xu L, Huang R, Wang Q (2011). Improved biohydrogen production with an expression of codon-optimized *hemH* and *lba* genes in the chloroplast of *Chlamydomonas reinhardtii*. *Bioresource Technology* **102**: 2610-2616.

Wu YG, Chang AK, Nixon PF, Li W, Duggleby RG (2000). Mutagenesis at Asp27 of pyruvate decarboxylase from *Zymomonas mobilis*. *European Journal of Biochemistry* **267**: 6493-6500.

Wykoff DD, Davies JP, Melis A, Grossman AR (1998). The Regulation of Photosynthetic Electron Transport during Nutrient Deprivation in *Chlamydomonas reinhardtii*. *Plant Physiology* **117**: 129-139.

Yang W, Catalanotti C, D'Adamo S, Wittkopp TM, Ingram-Smith CJ, Mackinder L *et al* (2014). Alternative Acetate Production Pathways in *Chlamydomonas reinhardtii* during Dark Anoxia and the Dominant Role of Chloroplasts in Fermentative Acetate Production. *The Plant Cell Online*: tpc. 114.129965.

Yoshida A, Nishimura T, Kawaguchi H, Inui M, Yukawa H (2005). Enhanced Hydrogen Production from Formic Acid by Formate Hydrogen Lyase-Overexpressing *Escherichia coli* Strains. *Applied and Environmental Microbiology* **71**: 6762-6768.

Yoshida A, Nishimura T, Kawaguchi H, Inui M, Yukawa H (2006). Enhanced hydrogen production from glucose using *ldh*- and *frd*-inactivated *Escherichia coli* strains. *Appl. Microbiol. Biotechnol* **73**: 67-72.

Yu H, Zhu Z, Hu W, Zhang H (2002). Hydrogen production from rice winery wastewater in an upflow anaerobic reactor by using mixed anaerobic cultures. *International Journal of Hydrogen Energy* **27**: 1359-1365.

Zhang L, Melis A (2002). Probing green algal hydrogen production. *Philosophical Transactions of the Royal Society of London Series B: Biological Sciences* **357**: 1499-1509.

Zhang R, Patena W, Armbruster U, Gang SS, Blum SR, Jonikas MC (2014). High-Throughput Genotyping of Green Algal Mutants Reveals Random Distribution of Mutagenic Insertion Sites and Endonucleolytic Cleavage of Transforming DNA. *The Plant Cell Online* **26**: 1398-1409.

Zhang T, Liu H, Fang HHP (2003). Biohydrogen production from starch in wastewater under thermophilic condition. *Journal of Environmental Management* **69**: 149-156.

Zhang W, Wong KK, Magliozzo RS, Kozarich JW (2001). Inactivation of Pyruvate Formate-Lyase by Dioxygen: Defining the Mechanistic Interplay of Glycine 734 and Cysteine 419 by Rapid Freeze-Quench EPR. *Biochemistry* **40**: 4123-4130.

Zhao T, Wang W, Bai X, Qi Y (2009). Gene silencing by artificial microRNAs in Chlamydomonas. *The Plant Journal* **58**: 157-164.

Zhou L, Lim Q-E, Wan G, Too H-P (2010). Normalization with genes encoding ribosomal proteins but not GAPDH provides an accurate quantification of gene expressions in neuronal differentiation of PC12 cells. *BMC Genomics* **11**: 75.

Zhu H, Stadnyk A, Béland M, Seto P (2008). Co-production of hydrogen and methane from potato waste using a two-stage anaerobic digestion process. *Bioresource Technology* **99**: 5078-5084.

Zorin B, Hegemann P, Sizova I (2005). Nuclear-Gene Targeting by Using Single-Stranded DNA Avoids Illegitimate DNA Integration in *Chlamydomonas reinhardtii*. *Eukaryotic Cell* **4**: 1264-1272.

Zorin B, Lu Y, Sizova I, Hegemann P (2009). Nuclear gene targeting in *Chlamydomonas* as exemplified by disruption of the *PHOT* gene. *Gene* **432**: 91-96.